



Jaafar, Weaam (2015) *Laser decontamination and detection of bacteria and microalgae*. PhD thesis.

<https://theses.gla.ac.uk/6172/>

Copyright and moral rights for this work are retained by the author

A copy can be downloaded for personal non-commercial research or study, without prior permission or charge

This work cannot be reproduced or quoted extensively from without first obtaining permission in writing from the author

The content must not be changed in any way or sold commercially in any format or medium without the formal permission of the author

When referring to this work, full bibliographic details including the author, title, awarding institution and date of the thesis must be given

Enlighten: Theses

<https://theses.gla.ac.uk/>
research-enlighten@glasgow.ac.uk



University
of Glasgow

SCHOOL OF ENGINEERING

Laser decontamination and detection of bacteria and microalgae

By

Weaam Jaafar

A thesis presented in partial fulfilment of the requirements for the
degree of Doctor of Philosophy in the School of Engineering at the
University of Glasgow

December 2013

Abstract

There are many harmful airborne microorganisms which can be breathed in by animals or humans and lead to illness or even death. Such organisms can land on surfaces or in liquid leading to other opportunistic routes to infection such as touch and ingestion. Consequently, there is a need to develop novel forms of decontamination and detection of pathogens in air, on surfaces and in liquids. The present work investigates these areas and in particular assesses the impact of novel laser and plasma decontamination systems on inactivation of *Bacillus atropheaus* spores, an anthrax simulant, in aerosols and on surfaces. To further evaluate the performance of the methods, it was necessary to identify how the spores flowed through the systems. Experiments were devised to quantify the effect of flow shaping and the electrode's surface roughness, on the spore deposition.

The spatial distribution of *B. atropheaus* spores on the electrodes was determined by using two methods, either a membrane filter or an imprinting (pressing) technique. Rougher surfaces allowed a higher level of microorganisms adhesion compared to smooth surfaces. The angle of incidence of the flowshaping on the spore distribution was investigated by using two angles, 10° and 30°. The capture was quantified by the number of spores that were counted on agar plates following incubation. The number of colony forming unit CFU was greatest near the entry point, and generally reduced along the electrodes' length and was also greater for the 30° inlet angle. Computational Fluid Dynamics (CFD) techniques were applied to model the particular flow through the electrode geometry and for the laser decontamination system.

Methods of spatial detection of microorganisms on surface were further developed using microscopy methods. Three methods were used in this research: optical microscopy examination to find the minimum detectable level of *B. atropheaus* spores on surfaces, a fluorescence technique using LEDs was developed to investigate the spatial detection of spores and microalgae and a flow chamber system was developed that was used for cell counting of microalgae in liquid.

The effect of excimer laser radiation on *Escherichia coli* vegetative cells and *Bacillus atrophaeus* spores was investigated. *E. coli* or *B. atrophaeus* spores were lawned onto agar plates and treated with pulsed excimer laser radiation at 248 nm. The plates were incubated overnight at 37 °C and assessed for areas of clearing or inactivation. The applied pulse energy was 37 mJ, the pulse repetition frequency (PRF) was either 20 or 100 Hz, exposures were from 1-10 pulses, or up to 1 min. The range of applied energy densities was from 0.31 to 18500 Jcm⁻². Image processing techniques were developed to determine the cleared area, major and minor axis and fractional clearing away from the region directly exposed to the laser beam. The area of clearing was approximately linear for treatment against *E. coli*, and was non-linear against *B. atrophaeus*. Increasing the PRF increased the area of clearing, as did increasing the exposure time. Interestingly, these areas of clearing were much greater than the beam area (2 x 6 mm), suggesting that scattering of the radiation played a significant role in contributing towards inactivation away from the directly laser exposed region. The results showed that excimer lasers offer the potential for rapid decontamination of microorganisms and spores on surfaces. Simple protocols allow direct comparison of the inactivation efficacy of different laser sources and image processing techniques can be applied to accurately quantify these results.

Growing and harvesting microalgae is important for sustainable and secure biofuel and food production. There is a wide spread interest in growing and exploiting the microalgae. The lipid, protein, carbohydrate and vitamin content of microalgae are not only species dependent but are also a function of their growth parameters such as nutrient, light, temperature and CO₂. The importance of detection of microalgae on assessing optimal growth conditions was investigated, along with the impact of harvesting and lipid extraction. Image processing systems were developed to quantify the size distribution of microalgae as a determinant of growth efficiency.

Table of Contents

ABSTRACT	2
TABLE OF CONTENTS.....	4
ACKNOWLEDGEMENTS	7
AUTHOR'S DECLARATION	8
SUPERVISOR'S DECLARATION	8
NOMENCLATURE.....	9
CHAPTER 1	13
INTRODUCTION.....	13
1.1 SPATIAL DISTRIBUTION OF MICROORGANISMS.....	13
1.1.1 <i>Imprint</i>	16
1.1.2 <i>Filtration</i>	17
1.1.3 <i>Microscopic examination and counting</i>	19
1.1.4 <i>Culturing techniques</i>	21
1.1.5 <i>Fluorescence spectroscopy</i>	21
1.2 LASER DECONTAMINATION.....	23
1.2.1 <i>Introduction to the excimer laser</i>	24
1.2.2 <i>Laser marking system</i>	24
1.3 SURFACE ROUGHNESS.....	26
1.4 <i>BACILLUS ATROPHAEUS</i> SPORES.....	28
1.5 INTRODUCTION TO NI VISION	29
1.6 COMPUTATIONAL FLUID DYNAMICS (CFD) MODELLING.....	32
1.7 MICROALGAE	34
1.7.1 <i>Cultivation and harvesting systems</i>	35
1.7.2 <i>Photosynthesis</i>	36
1.7.3 <i>Decontamination protocols for microalgae</i>	37
1.8 THE SCOPE OF THE THESIS.....	37
CHAPTER 2	40
SPATIAL MAPPING OF MICROORGANISMS ON SURFACES.....	40
2.1 INTRODUCTION TO DEPOSITION OF MICROORGANISMS ONTO SURFACES AND THEIR RESULTING SPATIAL DISTRIBUTION	40
2.2 SAMPLE PREPARATION	41
2.2.1 <i>Grinding</i>	42
2.2.2 <i>Polishing</i>	43
2.3 LASER MARKING SYSTEM	43
2.4 SURFACE ROUGHNESS.....	44
2.5 INFLUENCE OF LASER MARKING ON THE SURFACE ROUGHNESS	44
2.5.1 <i>Electrode marking: varying scanning speed</i>	45
2.5.2 <i>Microscopic examination of surface texture</i>	46
2.5.3 <i>Overlap of laser pulses</i>	47
2.5.4 <i>Electrode marking: varying scanning speed and laser power</i>	49
2.5.5 <i>Electrode marking: varying scanning speed pulse repetition frequency</i>	51
2.5.6 <i>Laser marking of wire mesh</i>	51

2.6	SPATIAL MAPPING TECHNIQUES.....	52
2.6.1	<i>Inherent antibacterial activity of the metal disc (electrode)</i>	53
2.6.2	<i>Microorganism aerosol generator</i>	54
2.6.3	<i>Membrane filtration technique</i>	59
2.6.4	<i>Imprinting (pressing) technique</i>	68
2.6.5	<i>CFD modelling</i>	74
CHAPTER 3		79
SPATIAL DETECTION OF MICROORGANISMS ON SURFACES AND MICROALGAE IN LIQUID		79
3.1	PROBABILITY OF DETECTION <i>B. ATROPHAEUS</i> SPORES OVER AN AREA ON ROUGH ALUMINIUM SURFACE	80
3.1.1	<i>Results of B. atrophaeus spores over an area on rough aluminium surface</i>	82
3.1.2	<i>B. atrophaeus suspension of different densities</i>	84
3.1.3	<i>Detecting spores outside of the drop region</i>	85
3.1.4	<i>Alignment of B. atrophaeus on aluminium surface</i>	86
3.2	MICROSCOPIC DETECTION OF <i>B. ATROPHAEUS</i> SPORES OVER AN AREA ON POLISHED ALUMINIUM DISC	88
3.3	GLASS MICROSCOPE SLIDES	90
3.4	MICROSCOPE MODIFICATION FOR FLUORESCENCE	95
3.4.1	<i>Detection of aerosolized B. atrophaeus deposited onto glass microscope slide</i>	95
3.4.2	<i>Fluorescence microscope</i>	99
3.5	FLUORESCENCE SPECTRA MEASUREMENT.....	100
3.6	RESULTS OF THE FLUORESCENCE SPECTRA MEASUREMENT	102
3.7	CHLOROPHYLL FLUORESCENCE MEASUREMENTS	103
3.8	RESULTS OF CHLOROPHYLL FLUORESCENCE MEASUREMENTS	105
3.9	THE FLOW CHAMBER FOR CELL MICROSCOPY	108
CHAPTER 4		113
ANTIMICROBIAL EFFECTS OF EXCIMER LASER ON <i>E. COLI</i> AND <i>B. ATROPHAEUS</i>		113
4.1	EXCIMER IRRADIATION TREATMENT OF <i>E. COLI</i> ON AGAR SURFACES.....	113
4.1.1	<i>Culturing E. coli and optical density (OD) measurements</i>	113
4.1.2	<i>E. coli experimental test protocol and setup</i>	118
4.1.3	<i>Results from surface treatment using excimer laser of E. coli test</i>	119
4.1.4	<i>Surface treatment analysis using the NI Vision software</i>	121
4.2	KILLING OF <i>B. ATROPHAEUS</i> SPORES ON LB AGAR SURFACE WITH THE EXCIMER LASER EXPERIMENTS.....	125
4.2.1	<i>Results from increasing number of pulses</i>	126
4.2.2	<i>Results from fixed power exposure test</i>	127
4.2.3	<i>Results of varying the pulse repetition frequency</i>	128
4.3	THE BOOSTER SYSTEM FOR AIR DECONTAMINATION	129
4.3.1	<i>Introduction to the booster system</i>	129
4.3.2	<i>Glass booster system</i>	130
4.3.3	<i>Stainless steel booster system</i>	137
4.3.4	<i>Internal cell booster system</i>	141
4.3.5	<i>External and internal boosters comparison</i>	147
CHAPTER 5		148
DETECTION AND GROWTH OF MICROALGAE		148
5.1	ALGAL GROWTH	149
5.1.1	<i>Photobioreactors (PBR)</i>	149
5.1.2	<i>Sample preparation for microscopy</i>	151
5.2	ALGAL COUNTING	151
5.3	THE EFFECT OF SALINITY ON CELL DENSITY	152
5.3.1	<i>Salinity calibration curve</i>	152
5.3.2	<i>Ordinary salt and sea salt experiment</i>	154
5.3.3	<i>Results of salinity experiment</i>	155
5.3.4	<i>Growth with different salt concentrations, with/without an evaporation correction factor</i> . 156	
5.4	NUTRIENT CONCENTRATION EXPERIMENT	157
5.4.1	<i>Results of nutrient experiment</i>	158
5.5	AIR VELOCITY EFFECT	161
5.6	GLASS TANK EXPERIMENTS.....	163
5.6.1	<i>Fluorescent and grow light experiment</i>	164

5.6.2	<i>Results of fluorescent and grow light experiment</i>	164
5.6.3	<i>Grow light experiment</i>	165
5.7	<i>N. OCULATA GROWTH DEPENDENCY ON TEMPERATURE</i>	166
5.7.1	<i>Practical experiment</i>	166
5.7.2	<i>A Fluent model of PBR temperature distribution</i>	167
5.8	<i>CHLORELLA VULGARIS EXPERIMENTS</i>	170
5.8.1	<i>Cultivation</i>	170
5.8.2	<i>Nutrient concentration experiment for C. vulgaris</i>	171
5.8.3	<i>Results of nutrient concentration experiment for C. vulgaris</i>	172
5.9	<i>ALGAL DIAMETER DISTRIBUTION OF N. OCULATA</i>	173
5.10	<i>HARVESTING TECHNIQUES</i>	176
5.10.1	<i>Sedimentation</i>	176
5.10.2	<i>Chemical flocculation</i>	182
5.10.3	<i>Filtration</i>	183
5.10.4	<i>Centrifuging</i>	188
5.10.5	<i>Dewatering of algae</i>	192
5.10.6	<i>Laser marking</i>	194
5.11	<i>BIOFILM FORMATION</i>	196
5.12	<i>OIL EXTRACTION</i>	199
5.12.1	<i>Oil extraction with chemical solvents (methanol, isopropanol and ethanol)</i>	199
5.12.2	<i>Results of oil extraction using the chemical solvents</i>	201
5.12.3	<i>Oil extraction by pressing</i>	202
5.12.4	<i>Blending using a food mixer</i>	204
5.12.5	<i>Results of mechanical solid shear</i>	205
5.13	<i>OXYGEN BOMB CALORIMETER</i>	207
CHAPTER 6		209
CONCLUSIONS AND FUTURE WORK		209
APPENDICES		215
REFERENCES		221

Acknowledgements

This thesis would not have been possible without the support of many people. I wish to express my gratitude to my supervisor, Dr. Ian Watson who was abundantly helpful and offered invaluable assistance, support and guidance. My thanks also go to Dr. James Sharp for many helpful discussions on the research. My deepest gratitude to Dr. Roger Parton for his knowledge and assistance in the microbiological field. A special thanks also to Mr Ian Peden and all the staff at the School of Engineering and the University of Glasgow. Many thanks to Dr. Takashi Mine, Mr. Mehmood Ali, Mr. Jonathan McMillan, Mr. Robert Adam, and Ms. Susanna Drange for their assistance in this research.

I would also like to convey thanks to the Iraqi Ministry of Higher Education and Scientific Research and the Iraqi Embassy Cultural Attaché, London, for providing financial support.

I would like to thank my husband, parents and friends for supporting and encouraging me to pursue this degree.

Author's Declaration

I declare that the thesis embodies the results of my own research or advanced studies and that it has been composed by myself. Where appropriate, I have made acknowledgement to the work of others.

Signature

Date

Supervisor's Declaration

I certify that this thesis (**Laser decontamination and detection of bacteria and microalgae**) has been prepared under my supervision in the School of Engineering at the University of Glasgow, in partial fulfilment of the requirements for the degree of Doctor of Philosophy.

Signature

Date

Nomenclature

Symbol/Abbreviation	Meaning
A	Cross sectional area (m^2)
A_d	Drop area of culture (mm^2)
<i>AFM</i>	Atomic force microscope
<i>Al</i>	Aluminium
A_s	Surface area of deposition (mm^2)
<i>B. atrophaeus</i>	<i>Bacillus atrophaeus</i>
$^{\circ}C$	Degree Celsius
C_1	Initial culture concentration (cells/mL)
C_2	Final culture concentration (cells/mL)
c_3	Fuse wire length (mm)
<i>CAD</i>	Computer aided design
C_c	Culture concentration (CFU/mL)
<i>CCD</i>	Charge coupled device
C_f	Calibration factor ($\mu m/pixel$)
<i>CFD</i>	Computational fluid dynamics
<i>CFU</i>	Colony forming unit
<i>Chl</i>	Chlorophyll
<i>cm</i>	Centimetres
CO_2	Carbon dioxide
<i>CW</i>	Continuous wave
<i>C. vulgaris</i>	<i>Chlorella vulgaris</i>
C_{μ}	Turbulence model constant
d	Days of growth
D	Dark background intensity
D_h	Hydraulic diameter (m)
<i>DIC</i>	Differential interference contrast
<i>DNA</i>	Deoxyribonucleic acid
D_p	Particle density (particles/ mm^3)
<i>DPM</i>	Discrete phase model
e_3	Correction for combustion heat of fuse wire (calories)
<i>EC</i>	Electrical conductivity σ (mS/cm)

<i>E. coli</i>	<i>Escherichia coli</i>
<i>F</i>	Fluorescence intensity
<i>FAD</i>	Flavin adenine dinucleotide
<i>F_m</i>	Maximum fluorescence
<i>F_o</i>	Minimum fluorescence
<i>F_v</i>	Variable fluorescence
<i>g</i>	Gram
<i>G-force</i>	Centrifugal force
<i>H_g</i>	Heat of combustion (J/kg)
<i>hr</i>	Hour
<i>HEPA</i>	High efficiency particulate air
<i>Hz</i>	Hertz
<i>I_t</i>	Turbulent intensity
<i>IR</i>	Infra-red
<i>J</i>	Joules
<i>k</i>	Turbulent kinetic energy (m ² /s ²)
<i>K</i>	Kelvin
<i>kg</i>	Kilograms
<i>KrF</i>	Krypton flouride
<i>L</i>	Litre
<i>LB</i>	Lysogeny broth
<i>LCD</i>	Liquid crystal display
<i>LED</i>	Light emitting diode
<i>L_p</i>	Particle length (μm)
<i>l_t</i>	Turbulent length scale (m)
<i>m</i>	Metres
<i>min</i>	Minutes
<i>mm</i>	Millimeter
<i>m_s</i>	Sample mass (g)
<i>N₀</i>	Initial cell number (cells/mL)
<i>NA</i>	Numerical aperature
<i>NADH</i>	Nicotinamide adenine dinucleotide
<i>N_c</i>	Cell number in the observation field of the microscope
<i>Nd:YAG</i>	Neodymium-doped yttrium aluminium garnet
<i>Nd:YVO₄</i>	Neodymium-doped yttrium orthovanadate

N_f	Final cell number (cells/mL)
NI	National instrument
nm	Nanometres
$N. oculata$	<i>Nannochloropsis oculata</i>
N_t	Total number of cells (cells/mL)
OD	Optical density or absorbance
P	Sample spectrum
P_0	Reference spectrum
pa	Per annum
PBR	Photobioreactor
PC	Personal computer
pH	Measure of hydrogen ion activity
ppm	Parts per million
ppt	Parts per thousand
PRF	Pulse repetition frequency (Hz)
r	Growth rate (per day)
r_1	Rate of temperature rising before firing ($^{\circ}C/min$)
r_2	Rate of temperature rising after time t_c ($^{\circ}C/min$)
R_a	Surface roughness (μm)
R_e	Reynolds number
rpm	Revolutions per minute
s	Seconds
S	Siemens
SD	Standard deviation
SEM	Scanning electron microscopy
SPG	Small particle generator
t_a	Firing time (min)
T_a	Temperature at firing time ($^{\circ}C$)
T_{air}	Air temperature (K)
t_b	Time when the temperature is 60% (min)
t_c	Time after the temperature become constant (min)
T_c	Temperature at time t_c ($^{\circ}C$)
t_f	Frame or exposure time of camera (s)
T_i	Initial temperature ($^{\circ}C$)
$TNTC$	Too numerous to count

T_r	Temperature rise ($^{\circ}\text{C}$)
TTL	Transistor–transistor logic
UV	Ultraviolet
v	Inlet velocity (m/s)
V_c	Culture volume (mL)
V_p	Particle velocity (mm/s)
V_s	Slide channel volume (mm^3)
\dot{V}	Volumetric flow rate (m^3/s)
W	Watts
W_c	Calorimeter energy equivalent (calories/ $^{\circ}\text{C}$)
X	Width of microscopic image (pixel)
Y	Length of microscopic image (pixel)
z	Profile height
Z	Sample depth (μm)
ε	Turbulent dissipation (m^2/s^3)
μ	Fluid viscosity (Kg/m.s)
μm	Micrometers
ρ	Fluid density (Kg/m^3)
σ	Electrical conductivity (mS/cm)

Chapter 1

Introduction

1.1 Spatial distribution of microorganisms

A spatial distribution can be defined as the way in which some object or measurand is arranged within an environment. By assessing and analysing the spatial distribution important data can be gleaned about the surroundings or how the objects are affected by the environment; enabling greater understanding of the object, and allowing some prediction about what may occur in the future, what happened in the past or under some given circumstances. Identifying and analysing spatial distributions and their data is becoming increasingly important in many disciplines such as astronomy, sociology and the life sciences. For example, the cosmic microwave background radiation has been mapped, and produced evidence of the big bang, Figure 1.1.

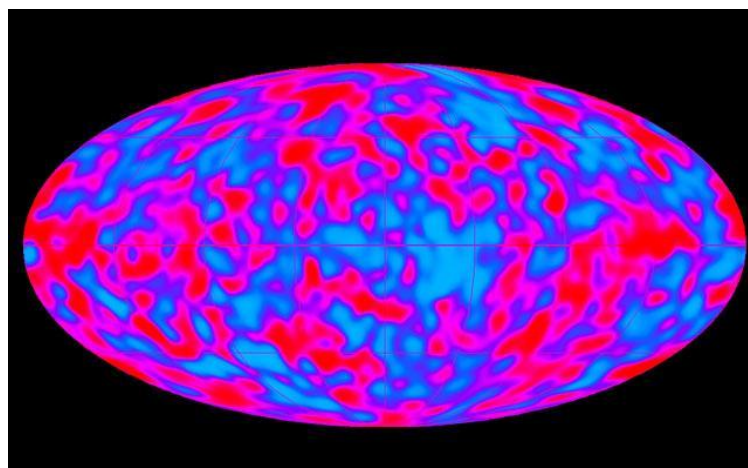


Figure 1.1 A map of the cosmic microwave background CMB from NASA's COBE satellite
(Schiller 2009)

The Planck mission was initiated in 2009 with the launch of a satellite to map the background radiation in more detail, as can be seen in Figure 1.2 (Malik 2013). The Planck space mission announced that the Universe is expanding more slowly than previously thought, and the new estimate for the Universe's age is 13.8 billion years. The most recent and best map ever of the universe can be seen in Figure 1.3 (Clavin & Harrington 2013). The glow is the cosmic microwave background remaining from the beginning of the cosmos, the colder areas are in blue and the hotter areas are in red (Buckwalter-Poza 2014).

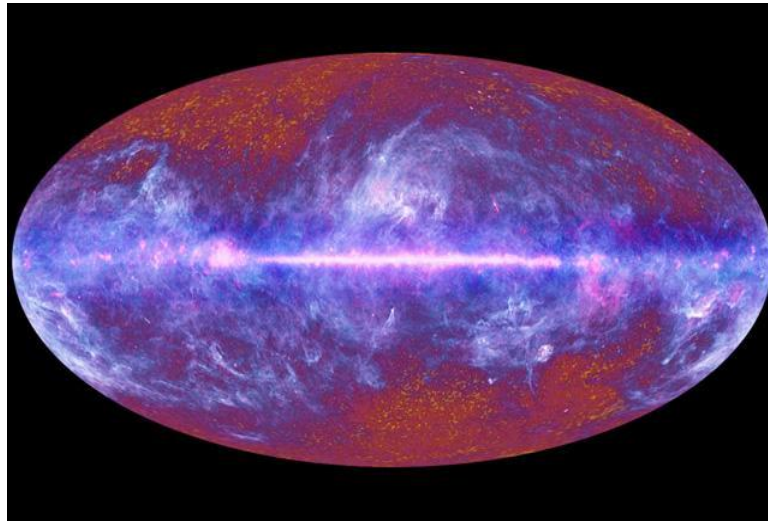


Figure 1.2 The microwave sky from Planck (Malik 2013)

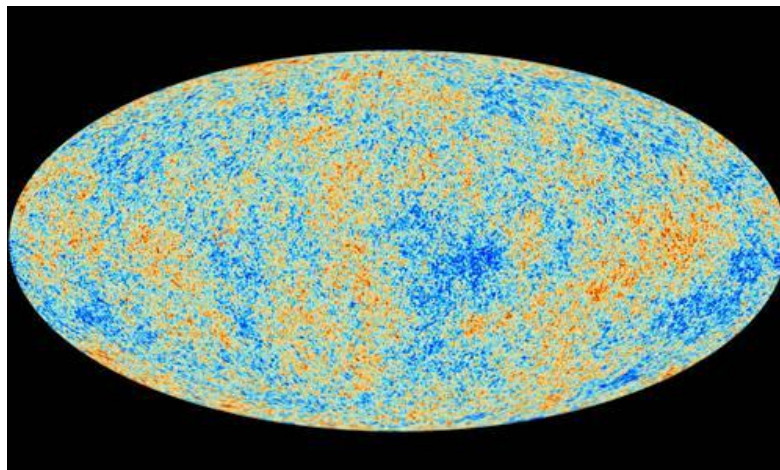


Figure 1.3 Best map to date of the Universe seen by the Planck satellite (credit: ESA and the Planck collaboration) (Clavin & Harrington 2013)

One example of an active area of research within sociology is mapping crime data onto geographical maps. This allows crime hot spots to be determined with intervention possible (Mayer-Schonberger & Cukier 2013). Recent work even predicts where crimes will happen, based on analysing enormous amount of data (Grill 2013). Cracolici & Uberti (2009) investigated the crime activities in Italy using exploratory spatial data analysis. Kitchens (2013) investigated the effects of changes in the spatial distribution of policing forces based on the data from the national football league (NFL) for crime detection.

Satellite images have been used to assess forest structures and growth (Shamsoddini *et al.*, 2013). Various spectral bands were used to provide data for forest inventory parameters. Such techniques over time allow the impact of environmental or man-made changes to be quantified, and if necessary remedial action taken. To reduce the use of drugs and the risk of later addiction, Lisita *et al.* (2013) used an object-based image analysis to detect the potential sites of illicit *C. sativa* drug cultivation. Cavalie *et al.* (2013) investigated the spatial distribution of water in Jupiter's stratosphere using the heterodyne instrument of the far infrared (HIFI) with the photodetector array camera and spectrometer (PACS). Chemical Imaging (CI) is combination between digital imaging and near infrared (NIR) spectroscopy used to obtain spatial and spectral data. CI techniques are used in pharmaceutical and medical fields (Gowen *et al.*, 2008). Amrania *et al.* (2011) used ultrafast chemical imaging systems (mid-infrared laser and micro-imaging) to investigate the fingerprint signatures of live cells and find the spatial distributions of chemical moieties in the cells.

Assessing distribution of microorganisms or infectious agents is highly desirable in public health control. This is particularly the case if there is an outbreak and mapping infections is usually the only method to trace the source of the outbreak, leading to its control and eradication. The risk of outbreaks of water pollution caused by *Cryptosporidium* sp. for example, can be reduced by assessing the spatial distribution of the relative risk of water becoming contaminated in the first instance. Samadder *et al.* (2010) developed a risk potential index (RPI) to identify locations where the risk of infection was potentially higher. These regions can be monitored, which is more cost effective and realistic than monitoring everywhere.

Within the context of the current research herein, the spatial distribution of microorganisms was assessed over different areas and on different substrates. The investigation of the distribution of microorganisms on surfaces is important in evaluating

the contamination level and aids in selecting an appropriate method of decontamination. Generally, the investigation of spatial mapping of microorganisms required a sampling process in the beginning, detecting and then quantifying the data with statistical analysis. Investigation of the spatial arrangement of microorganisms gives information about the density and number of adhering microorganism (Busscher *et al.*, 1991). Detection of microorganisms and analysing their distribution are essential in many fields in our life such as the food industry, health, environment and contamination control (Dickert *et al.*, 2003). There are various techniques to investigate the potential distribution of microorganisms which are: imprint (Cohen *et al.*, 2010), lithography (Zhao *et al.*, 2010), culturing (Madigan *et al.*, 2011), filtration (Sweetman *et al.*, 2013), microscopic examination (Lindh *et al.*, 2010), and fluorescence (Rattray *et al.*, 2012). Of course, more than one of these techniques, or indeed others, could be used simultaneously. These methods are briefly described.

1.1.1 Imprint

Imprint or pressing techniques are simple and relatively reliable methods used to investigate spatial distributions of bacteria and determine absolute counts on different surfaces from biological samples such as skin or wounds to inanimate surfaces such as worktops, cutting blades and processing equipment. This method is also used to evaluate contamination on medical equipment, and recently the pressing method has even been used to print patterns of bacteria onto agar plates using lithographic techniques (Cohen *et al.*, 2010). The imprint technique does not require significant preparation time, processes or complex equipment. The only items required are agar plates which are pressed onto the sample surface. Often these are filled above their top, so that the agar and sample surface can easily touch when placed together. Following sampling, the plates would be incubated for the appropriate time-temperature period depending on the likely requirements of the suspected contaminants. Further selectivity can be achieved with specific choice of the agar medium. Although some imprint techniques require complex or long procedures all these techniques work on the same principle - to print or remove the microorganisms from the surface in a definite distribution, onto a plate, replicating the same spatial distribution as would be seen on the sample, but reversed as in a mirrored view. Imprint techniques enable visualizing the distribution of microorganisms such as their location and population. This allows opportunities to study the cause and effect of the spatial distribution over an area. Understanding the spatial patterns of microorganisms may help to understand associated risks and thereby reduce contamination. For example, if the distribution of

microorganisms is assessed on say a decontamination system, within some food production process or operating theatre, then critical control points can be highlighted that can receive additional engineering solutions to reduce or eliminate the problem if the bacterial numbers are excessively high or above a certain threshold value.

Few reports are available regarding the spatial distribution of bacteria using imprint techniques. Imprint techniques using velvet pads to quantify bacterial contamination in surgical wounds has been studied by some investigators (Raahave 1975; Craythorn *et al.*, 1980). Stanghellini & Rasmussen (1989) visualized the spatial distribution of bacteria on rhizoplane of beetroot by imprinting, which was a simple technique to identify *in situ* the location of different bacteria in the same rhizoplane. A few investigators have studied microarray printing (lithography) of microorganisms on agar; Weibel *et al.* (2005) used agarose stamps to imprint patterns of bacteria on agar surface. Koibuchi *et al.* (2009) used imprinting methods to evaluate the bacterial contamination of ultrasound probes; the work showed that the imprinting method was more suitable to detect the bacteria than swabbing methods. Some researchers used cell imprinting technology with polymeric materials to identify and detect microorganisms (Alexander *et al.*, 2006).

1.1.2 Filtration

Filtration is a technique to isolate or remove contaminants from a fluid, such as water or air. Microscopic particles, microorganisms or any other materials within the fluid medium above a certain threshold size are removed by using a micro-porous material (filter). Particulate matter, smaller than the pore size, may pass through the filter. Enumeration and removal of microorganisms by filter techniques have been studied extensively, with this technology used in most air filtration applications, for example in hospitals or water cleaning facilities. Various methods have been developed. Jannasch (1958) studied the spatial distribution of planktonic bacteria by using membrane filtration techniques. The historical development and review of membranes has been reviewed by Goetz & Tsuneishi (1951) and Wolochow (1958). The use of membrane filters in aerosol analysis has been investigated by researchers. Webber *et al.* (2007) used membrane filters in the recovery of asbestos for transmission electron microscopy (TEM) analysis. Membrane filters were used in analysis of aerosols for microscopy and in the aerosol size spectra determination (Melo & Phillips 1974). The use of membrane filter techniques to test the potability of drinking water has been reported by many researchers (Bancroft *et al.*, 1989; Habash &

Johns 2009). The high efficiency particulate air (HEPA) filters are used to filter the airborne particles. The HEPA filter is widely used in biological applications and air purification systems with high collection efficiency (Osaki & Kanagawa 1990). Sakuraoka & Madsen (2001) reported that membrane filters of pore size 0.45 μm were effective in removing heat resistance spores from soft drinks. Membrane filter techniques are widely used in dairy products (Peterkin & Sharpe 1980). The size of bacteria and other common particulates between around 0.0001-1000 μm can be seen in Figure 1.4 (TBH Company, Straubenhardt, Germany 2013), with the smaller size corresponding to gaseous molecules where activated carbon is one method of filtration, up to large dust particles where specific filters can be selected.

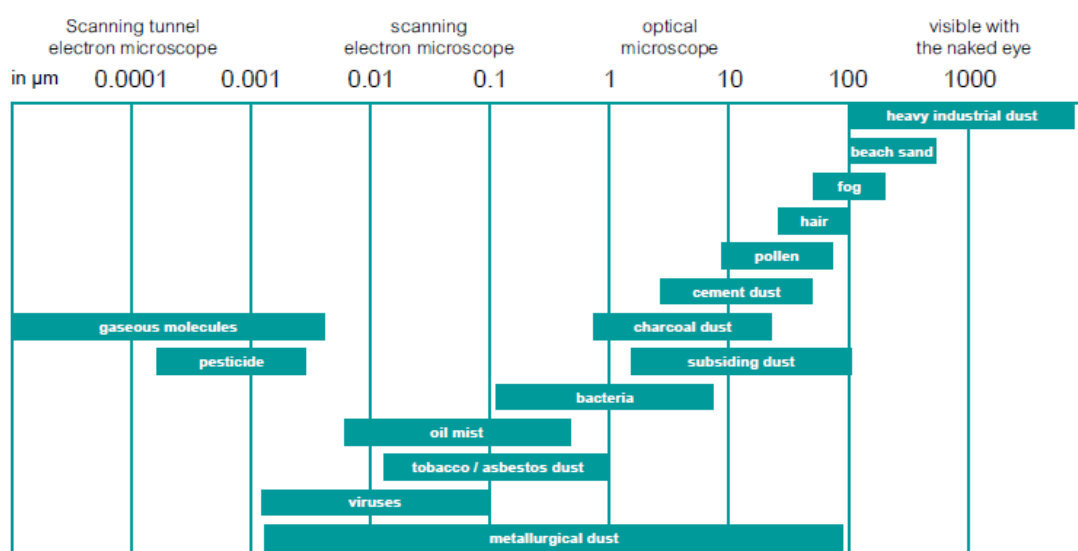


Figure 1.4 Size of bacteria and other particulates (TBH Company, Straubenhardt, Germany 2013)

Different filtration methods are available depending on the application that they are designed for, these types are (Purchas 1996; Sutherland 2008):

- Gas – solid filtration for aerosol sampling and airborne analysis, such as activated carbon, gelatine and PTFE.
- Solid separation from liquids requires strainers, deep bed, cartridge and membranes filters are used.
- Liquid filtration separates liquid droplets such as coalescing filter.
- Dissolved material filtration (diffusion membranes) is widely used in reverse osmosis, nanofiltration and ultrafiltration processes.
- Gas separation such as dense membrane.

Since membrane filter techniques are widely used in separation of microorganisms for environmental analysis or in tests requiring accurate quantification, economy and simplicity, it is an area of interest relevant to this work, so the membrane filters are discussed in more detail in the next section.

1.1.2.1 Membrane filtration

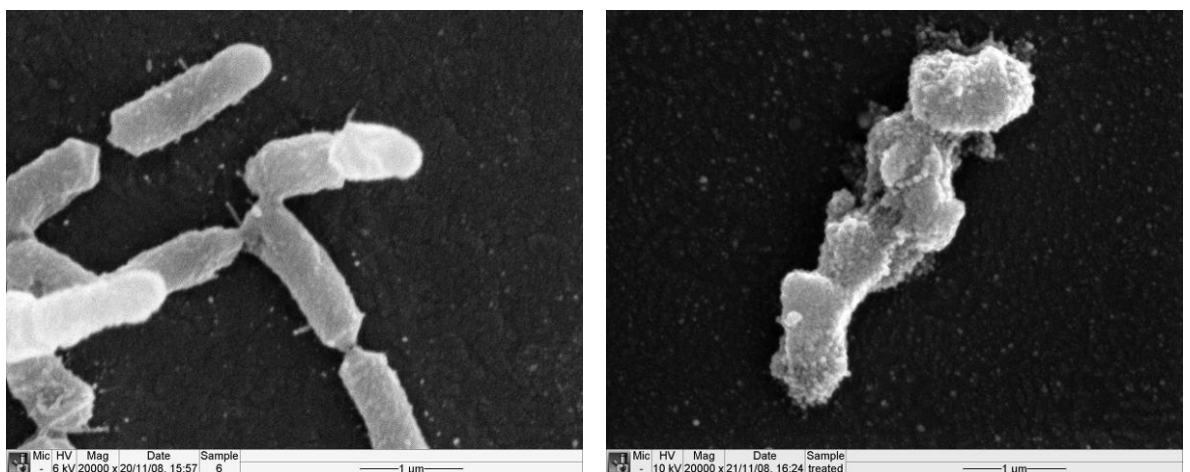
Membrane filters are used for relatively accurate determination of the numbers of microorganisms in a liquid or air medium. This method increases the sensitivity of detection compared to swabbing techniques because the fluid containing the spores is passed through the filter and the spores are retained on the filter surface. In the membrane filter, the speed of the fluid being drawn through the pores can be increased by using a driving force (pressure or vacuum driven separation process) in addition to gravity and the microorganisms are trapped on the filter's surface. The particles can easily be re-cultured and analysed by placing the filter on a nutrient plate and then incubating the plate. Some filters are placed on absorbent pads soaked in nutrient medium and dried to avoid wasting agar and plate preparation time. Membrane filters with different pore sizes are available, and the chosen pore size depends on the intended application, but generally they are between 0.015-12 μm (Whatman Manual 2010); microorganisms larger than the filter pore size are trapped on the membrane surface. The membranes are not soluble in water or alcohol and they are thermally stable and inflammable. Membrane filters are manufactured in different geometry and materials. The most common materials are: cellulose ester, cellulose nitrate, polymer, PTFE (Teflon), quartz, glass fibre and nylon (Sutherland 2008; Whatman Manual 2010).

1.1.3 Microscopic examination and counting

Microscopes are an important research technique widely used in biomedical fields, the microelectronics industry and other fields of science. Microscopes are used to view and magnify organisms and other objects. In microscopic examination, the microorganisms are pipetted or spread onto a glass slide, flow cell or any other plate suitable for microscopic viewing. The basic types of microscopes are optical microscopes, electron microscopes, scanning probe microscopes and scanning acoustic microscope. Optical microscopes such as compound, stereo, ultraviolet, fluorescence and confocal microscopes use different methods of lighting to illuminate the sample (Olympus 2010). An excellent overview and development of optical microscopy is given by Davidson & Abramowitz (2011). There are

various techniques for improving the contrast in optical microscopy, such as brightfield, darkfield, Rheinberg illumination, phase contrast, differential interference contrast (DIC), Hoffman modulation contrast, polarized light and fluorescence techniques (Mertz 2010; Davidson & Abramowitz 2011). It is possible to combine two techniques together as for example with fluorescence microscopy and phase contrast techniques. Electron microscopes (EM) use electrons to “illuminate” and scan the specimen instead of light (Leamy 1982). The major types of electron microscope are: transmission (TEM), scanning (SEM) and the scanning transmission (STEM) microscopes (Rullgard *et al.*, 2011). The scanning probe microscope (SPM) is used to study the structure of surfaces by using a probe tip that scans across the specimen; the most important and well known one is the atomic force microscope (AFM) (Yongho & Wonho 2008). The scanning acoustic microscopes (SAM) uses sound waves to investigate an object, using methods similar to the sonar principle; they are often used in the semiconductor industry and medicine and biological research (Miura & Yamamoto 2013).

Figure 1.5 shows the SEM images of the *B. atrophaeus* spores treated with cold plasma and ozone at exposure time of 2 min. The plasma system was investigated by Watson (Foss-Smith & Watson 2008) and Mine (Mine 2010). Figure 1.5 (a) shows the healthy spores without treatment while Figure 1.5 (b) shows the killed spores.



(a) Control (no treatment)

(b) Cluster of the plasma treated spores

Figure 1.5 SEM of *B. atrophaeus* spores

1.1.4 Culturing techniques

In culturing, the microorganism specimen is inoculated by pipetting or looping them into a nutrient medium such as an agar plate or liquid broth. Then the microorganism samples are incubated in optimal conditions for growth and subsequent analysis. To avoid contamination, the culturing of microorganisms must be done in aseptic conditions (Madigan *et al.*, 2011).

1.1.5 Fluorescence spectroscopy

The fluorescence spectra of spores and other microorganisms can play an important role in their detection and discrimination. The sample (biological or non-biological) is illuminated with a light that excites the fluorescence within the sample. The fluorescence is emitted at a wavelength that is different from the excited one, then the fluorescence spectra is collected with a suitable detector such as spectrometer or photomultiplier tube (PMT). Most materials have intrinsic or endogenous fluorophores, which emit characteristic fluorescence spectra which can be used to distinguish different materials from each other. Autofluorescence in spores and biological cells is due to some materials (auto-fluorophores) such as aromatic amino acids (tyrosine, tryptophan and phenylalanine), enzymes and coenzymes (nicotinamide adenine dinucleotide (NADH), flavin adenine dinucleotide (FAD) and nicotinamide adenine dinucleotide phosphate (NADPH)), lipids and antibodies (Ramanujam 2006). Various biological and chemical materials are affected by electromagnetic radiation, such as UV radiation which efficiently excites natural fluorophores. As an example, a wavelength of 266 nm excites amino acids, and their emission wavelength is usually between 300–400 nm (Sivaprakasam *et al.*, 2004). Cyanine dyes such as Cy3 and Cy5 have been recently used in biological fluorescent labelling (Feng *et al.*, 2006). Table 1.1 shows the intrinsic fluorophores in spores and other microorganisms.

Table 1.1 Excitation and emission wavelengths of the intrinsic fluorophores (Powers & Lloyd 2004; Ramanujam 2006; Foss-Smith & Watson 2008)

Fluorophore	Excitation wavelength (nm)	Emission wavelength (nm)
Amino acids		
Tryptophan	280 , 295	300 , 353, 400
Tyrosine	275	305 – 400
Phenylalanine	260 – 280	288 – 400
Enzymes		
FAD	450	535, 550
NADH	290 , 350	440 , 460
NADPH	260 , 336	450 , 464
Proteins		
Collagen	270 – 370	300 - 450
Elastin	290 , 325	400
Lipids		
Phospholipids	436	584
Lipofuscin	395	540
Vitamins		
<i>A, B₆, K, D</i>	315 – 390	300 – 510

Chlorophyll (Chl) fluorescence measurements are used to understand the photosynthesis process of microalgae and also to evaluate growth and oil production (Torzillo *et al.*, 1996). The first discovery of the fluorescence of green algae was by Kautsky & Hirsh in 1931 (Khalida *et al.*, 2012). A good review of chlorophyll fluorescence discovery was reported by Papageorgiou & Govindjee (2004). Vonshak *et al.* (1994) used chlorophyll fluorescence to estimate the effect of temperature on photoinhibition in *Spirulina* cultures. Chl fluorescence can be used to control microalgal cultivation by monitoring the photochemical activities (Suggett *et al.*, 2010). Fluorescence imaging can be used to understand the photosynthesis processes and its associated metabolism such as herbicide and stomatal heterogeneity (Baker 2008).

1.2 Laser decontamination

Another important reason for determining the spatial location of microorganisms is to determine methods and efficacy of inactivation, sterilization or more generally decontamination processes. The presence of unwanted microorganisms can lead to serious illness and even death. For example, foodborne illnesses (CDC 2013) in the USA affects 48 million people pa (per annum) with 128,000 people ending up in hospital and 3000 people dying. *Salmonella* sp. kills an estimated 380 people and *Listeria monocytogenes* kills 250 pa (Scallan *et al.*, 2011). Diarrhoeal diseases which are often foodborne infections kill 2.2 million people pa (Kuchenmuller *et al.*, 2009). The World Health Organization (WHO) reported a 15% increasing in death rate of severe acute respiratory syndrome (SARS) since the epidemic was first discovered in 2002 (Kamps & Hoffmann 2013). Pathogenic bacteria cause approximately 40% of the 50 million deaths pa worldwide (Rattray *et al.*, 2012) attributable to any cause.

Consequently, identifying and detecting microorganisms and evaluating methods of decontamination are highly desirable. The substrate and its associated parameters such as thermal and electrical properties or roughness for example, can of course determine the efficacy of the treatment, whether it is food, medical devices, or the environment such as within surgical operating theatres or even clean rooms. Lasers are one method of inactivation that has been investigated. They are considered as a trusted technology in many decontamination fields such as medical and industrial. Watson *et al.* (1996) investigated seven different laser wavelengths (0.355-118 μm) for killing of *E. coli* bacteria, and the highest bactericidal capability was with a CO_2 laser operating at 10.6 μm . The excimer laser radiation has high antimicrobial effects, and the bacterial reduction depends on the exposure time and applied energy density of the radiation and the strain of microorganisms (Folwaczny *et al.*, 1998). Lee *et al.* (2006) reported that a 7 W diode laser can kill 97.7% of *Streptococcus mutans* in 500 μm thickness of human dentin. Laser-induced breakdown spectroscopy (LIBS) is used to detect the contamination location and to decontaminate the surface using a scanning UV laser (Rehse *et al.*, 2012). Charvalos & Karoutis (2001) investigated the antibacterial activity of argon fluoride (ArF) excimer laser at 193 nm on various strains of gram negative bacteria. The results showed that no bacteria survived above a critical exposure value (8-16 J/cm^2). The CO_2 laser at irradiance of 50 W/cm^2 can be used to kill 99.5% of bacterial cells (Talebzadeh *et al.*, 1994). $\text{Nd}:\text{YAG}$ lasers have a bactericidal effect of killing both pigmented and non-pigmented bacteria, and the killing also depends on other factors such as the population and type of microorganism,

tissue type and pigmentation (Meral *et al.*, 2003). Udart *et al.* (2011) concluded that the mechanism of high power laser (940 nm) on inactivation of *Escherichia coli* was a thermal effect. Ultrashort pulsed (USP) lasers inactivate the viruses by exciting the mechanical vibrations of the virus capsid causing damage to the protein coat. In the inactivation of bacteria, the USP laser relaxes the super-coiled double stranded DNA leading to damage and inactivation (Tsen *et al.*, 2012). Ward *et al.* (1996) reported that *Nd:YAG* laser bacterial inactivation did not depend on cell size and shape, pigmentation and Gram reaction.

1.2.1 Introduction to the excimer laser

Ultraviolet (UV) light is widely used for disinfection and treatment of waste and drinking water and to sterilize medical equipment and facilities. UV lasers and diodes with a wavelength in the range around 250 to 400 nm are currently used in antimicrobial applications (Vermeulen *et al.*, 2008). UV radiation is absorbed by the DNA and causes damage and mutation; this leads to cell killing and mutagenesis (Kochevar 1992).

Excimer (excited dimer) lasers typically emit radiation in the UV region. They are extensively used in ophthalmic surgery, dermatological treatment, sterilization and disinfection, microlithography, and marking and ablation processing. Of the three types of excimer laser, *XeCl* (308 nm), *KrF* (248 nm) and *ArF* (193 nm), the *KrF* has proved to be the most mutagenic (Charvalos & Karoutis 2001), with its wavelength coinciding with the peak absorption to maximise cell killing. The excimer laser wavelengths are absorbed by biological and organic compounds with minimal thermal damage. So considering all of these features of excimer lasers this led to the use of *KrF* lasers for decontamination of microorganisms in this work. Although UV radiation has many useful applications, UV light can be hazardous and dangerous and care should be taken to prevent accidental exposures in its use.

1.2.2 Laser marking system

A plasma system was developed in-house by Watson *et al.* patented by (Foss-Smith & Watson 2008). The plasma system comprised laser marked electrodes that were found to improve the discharge stability and allowed the discharge gap to be increased so that a greater volume of air could be passed through the system. Hence increasing the volumetric decontamination rate. Additionally, Foss-Smith and Watson (2008) described enhanced

killing with flow shaping directed towards the electrodes. The system's performance was determined by Mine (2010). However, the improved decontamination efficiency due to the electrodes or the influence of the electrodes with directed flow shaping on their own i.e. without a discharge was not evaluated. Consequently, laser marking was used to modify the surface roughness of the electrodes, and assess how spores would be spatially deposited along the electrode length and aid the decontamination process. Surface roughness is described in Section 1.3.

Laser marking is one of the major industrial applications for material processing. Depending on the laser and substrate, a thermal process is often used, utilising a high intensity laser beam to make contrasting marks on the surface of the sample (Ng & Yeo 2001). Since laser marking used in this case is a heat treatment technique, the surface roughness is modified, which potentially has a significant influence on the distribution and adhesion of the microorganisms landing on that surface. The marking quality such as colour, surface modification, depth and width depends on the laser parameters which are power intensity, scanning speed and pulse repetition frequency. Therefore, suitable laser parameters need to be selected to provide a good quality laser marking process. Laser marking systems consist of three basic parts which are: the laser source, beam delivery optics to direct the laser in a x-y scanning system and software to control the laser and scanning parameters. Different terminology is used to classify laser marking techniques with respect to the scanning method (i.e. how the laser is moved over the work piece). There are two main techniques: galvanometric scanning (dots and vectors scan) and mask projection (Chen *et al.*, 2009). In the first technique, the laser beam is directed via two computer controlled galvanometer mirrors and a lens system to the object to be marked, and the second technique uses a mask which contains the shape of the pattern to be marked. Moreover, marking can be classified, with respect to the interaction between the laser beam and material, into two approaches which are surface modification and material removal (ablation) marking (Dahorte & Harimkar 2008).

In recent years some laser marking experiments have been reported. Tam *et al.* (1993) studied *Nd:YAG* laser marking of integrated circuit (IC) packages. Qi *et al.* (2003) studied laser marking of stainless steel with Q-switched *Nd:YAG* laser. Valette *et al.* (2006) studied the influence of laser marking on the corrosion resistance for biomaterials. Dusser *et al.* (2007) investigated deep marking of metals and polymers for information coding. Laakso *et al.* (2008) investigated colour marking of stainless steel with a fibre laser. Chen *et al.* (2009) used CO_2 laser marking to encode eggshells. Yasa & Kruth (2009) studied the

process parameters (scan speed, laser power and pulse frequency) in laser marking. New marking techniques in the nano-scale have been investigated by Pena *et al.* (2010) by using a diode pumped *Nd:YVO4* laser on a *Si* wafer. The most common lasers that are used in the industry for marking include *Nd:YAG*, *Nd:YVO4*, *Nd:YLF* and *Ti:sapphire* solid state lasers (60%), *CO₂* (35%) and excimer gas lasers (5%), as well as diode semiconductor lasers (Gu 2006; Chen *et al.*, 2009). Choosing the appropriate laser type depends on the workpiece material and required application.

The main advantages of laser marking compared with conventional methods such as ink-marking, mechanical engraving and electro-chemical methods are that they are easy to automate, have high efficiency and quality, produce permanent marks and have low operational costs (Qi *et al.*, 2003). These reasons have elevated laser marking techniques to the most common method in a modern industrial technologies (Gu 2004), from surface modification, to copyrighting, to component identification, to marking of electronics components, sterilization, decoration and material processing.

1.3 Surface roughness

Surface roughness plays a significant role in many industrial, medical and engineering applications. Surface roughness has effects on functional attributes of material, such as frictional losses on surfaces and in pipes, wearing, light reflection, heat transmission, lubricant distributing, coating, fatigue resisting and the drag on ships and aircraft (Lou *et al.*, 1999; Connelly 2006) and how bacteria interact with that surface. So the appropriate processes should be selected to reach the optimum surface roughness thereby providing the desired surface quality and finish. Surface roughness is a measure of irregularities on the material surface caused by a machining processes during manufacturing or due to some surface modification that maybe either mechanical or chemical, generally surface roughness excludes waviness and form errors or flaws (Vorburger & Raja 1990). The roughness of a surface is a two dimensional parameter, and it is a material property that can be measured by profilometer instruments either by a contact (mechanical) or by non-contact methods (optical) (Thomas 1999). The distances (height and width) between peaks and valleys are measured and the reading represents the roughness value. Figure 1.6 (a) shows profiles of the roughness. The roughness average parameter (R_a) is widely used to represent the roughness, which is an amplitude parameter and also known as the arithmetic mean or centre line average (Whitehead & Verran 2006; Mathew Mate 2008).

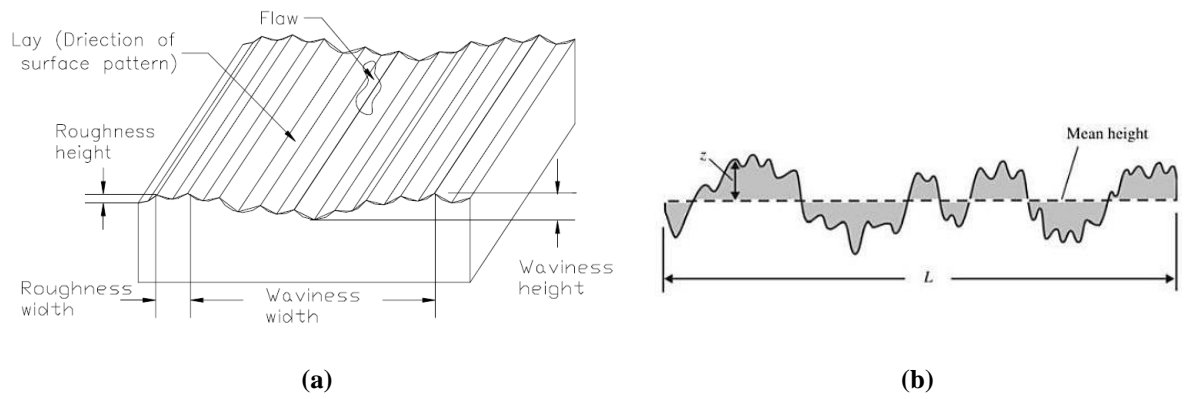


Figure 1.6 Schematic represents a) roughness profiles (Lou *et al.*, 1999) and b) surface roughness value (R_a) (Mathew Mate 2008)

R_a can be defined by (Mathew Mate 2008):

$$R_a = \frac{1}{L_l} \int_0^L |z| dx$$

Equation 1.1

Where z is the height of the profile starting from the mean height and L_l is the sampling length, as shown in Figure 1.6 (b).

A rough surface is often undesirable, especially if a maximum value is specified. Often surface roughness needs to be minimized as much as possible, because the rough surface usually wears and corrodes more than smooth surfaces (Hilbert *et al.*, 2003), which leads to scratch formation, and such defects may damage the workpiece. Rough surfaces also increase bacterial adherence and subsequently colonization which is a serious problem in some fields such as in the food industry and on medical equipment where contamination, infection and poisoning can result (Verran *et al.*, 2010). This may be difficult in manufacturing because it may be too expensive to reach a very smooth or flat surface. Occasionally high roughness may be desirable at some level, for example if high friction is important or beneficial as with say a smooth coating to stay on a pill (Rideout 2013), and localised surface roughness in the micro and nano-scale is useful in dental implants and for bone-cell interaction for implant surfaces (NovaesJr *et al.*, 2010).

Several studies investigated the effect of surface roughness on the distribution of microorganisms and the results are varied, some researchers said that there is a direct

relationship between surface roughness and adhesion of microorganisms. McAllister *et al.* (1993) demonstrated that ultra smooth polymeric surfaces do not allow bacterial adherence while irregularities promote adhesion. Flint *et al.* (2000) and Whitehead & Verran (2006) reported that microorganisms are retained in surface features of similar size to them. Tang *et al.* (2009) and Sousa *et al.* (2008) found that rougher surfaces encourage *Staphylococcus epidermidis* to adhere and colonize. While others have stated that there is no relationship. Tide *et al.* (1999) investigated the influence of grinding and polishing of welds to reach food industry roughness standards and found that this may have no significant influence on bacterial accumulation. Hilbert *et al.* (2003) reported those microorganisms attachment on stainless steel surfaces did not depend on surface roughness when varied between R_a values of 0.01 and 0.9 μm , which is smaller than bacterial samples.

Investigation of the effect of surface roughness and its influence on adhesion of microorganisms is important to determine the contamination level on the surfaces. The surface roughness of the electrodes promoted discharge stability of atmospheric plasma (Foss-Smith & Watson 2008). The electrode material and its roughness is a design choice, and selection is dependent on understanding of the potential spore distribution on the electrode surfaces. The laser marker Violino 2 was used to mark several metal samples, and a profilometer machine was used to measure the surface roughness against different laser marking parameters. The influence of laser marking on the surface roughness is described in detail in Chapter 2: Section 2.5.

1.4 *Bacillus atrophaeus* spores

Bacillus atrophaeus microorganisms (previously named *Bacillus globigii* (*B. globigii*) and *Bacillus subtilis*) (Buhr *et al.*, 2008) are gram positive and aerobes. Under harsh environmental conditions, the bacteria can produce spores which may stay dormant for long periods and with high resistance to radiation, heat and chemicals. *B. atrophaeus* spores are commonly used in biodefence and decontamination tests, because they are hard to kill and they are very similar to *B. anthrax*, but non-virulent and safe to handle. The dimensions of the spores are $1.21 \pm 0.18 \mu\text{m}$ a nominal length, $0.68 \pm 0.11 \mu\text{m}$ width and $0.97 \pm 0.07 \mu\text{m}$ spherical diameter (Buhr *et al.*, 2008). Figure 1.7 shows the structure of *Bacillus atrophaeus* spores.

B. atrophaeus spores were obtained from Dr. Bill Whyte, School of Engineering, University of Glasgow. The concentration of the original stock was approximately 10^{10}

spores/mL. Some photographs of the *B. atrophaeus* spores were taken under the Nikon microscope (Eclipse, ME600, Japan) that was used in this work (see Chapter 3: Section 3.1) which can be seen in Figure 1.8.

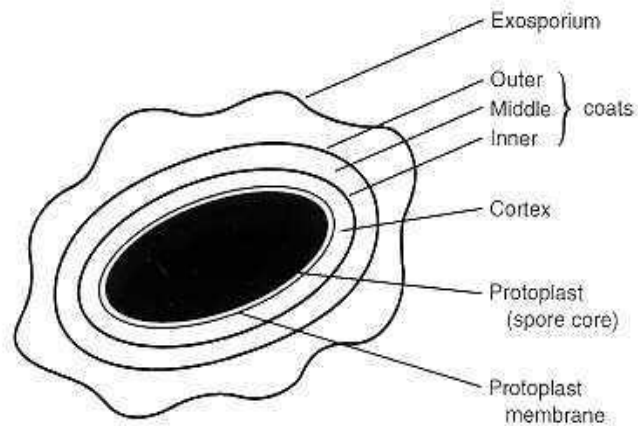


Figure 1.7 Structure of a *Bacillus* spore (cross-section), (Turnbull 1996)

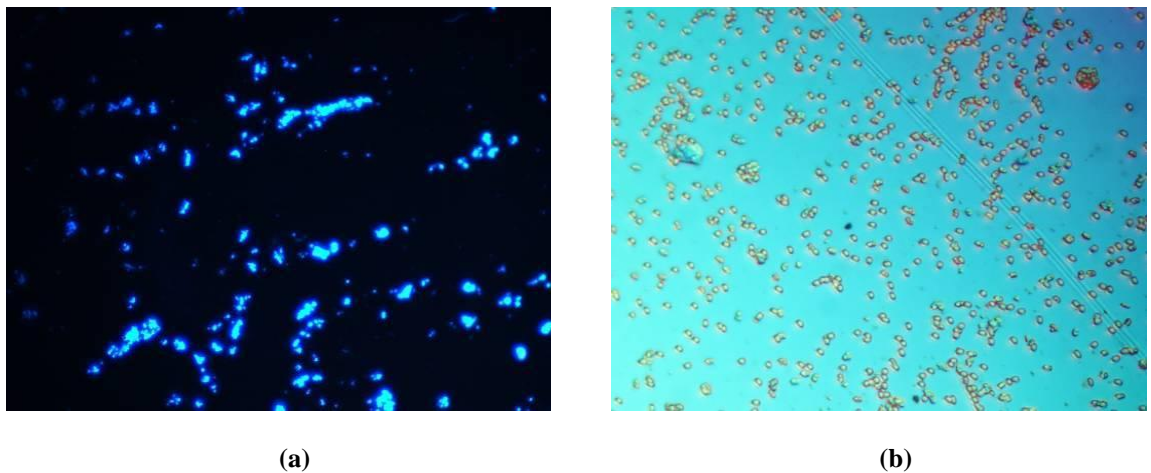


Figure 1.8 Microscopy of *Bacillus atrophaeus* spores under a) fluorescent Nikon microscope (345 nm) and b) bright field Nikon microscope

1.5 Introduction to NI Vision

Image processing is the art of automatically acquiring data from an image and enhancing that image to make the data or desired image artefact more evident. Image processing is often used in medicine, to assess product quality in industry, to capture motion in sports

video and photographic editing in TV and photography (Moeslund 2012). The typical image processing techniques include image enhancement for colour contrast, edge detection and noise cleaning, image restoration for geometry distortion and spatial filtering, and image detection and information extraction (Pratt 2007).

This section introduces how image processing software was used throughout this thesis to process biological images rapidly to obtain results that cannot easily be determined by human observation. NI Vision 8.5 (National Instruments, USA) was used in this work. This software is able to analyse images through a series of modules that are placed together under one script (see Figure 1.9, the main window of NI Vision). This script can be used for various applications with just slight modification by adding or removing modules to enhance the feature. Each module does a specific job, so the order or sequence of the modules is important. The analysis can be applied to one picture or many pictures sequentially.

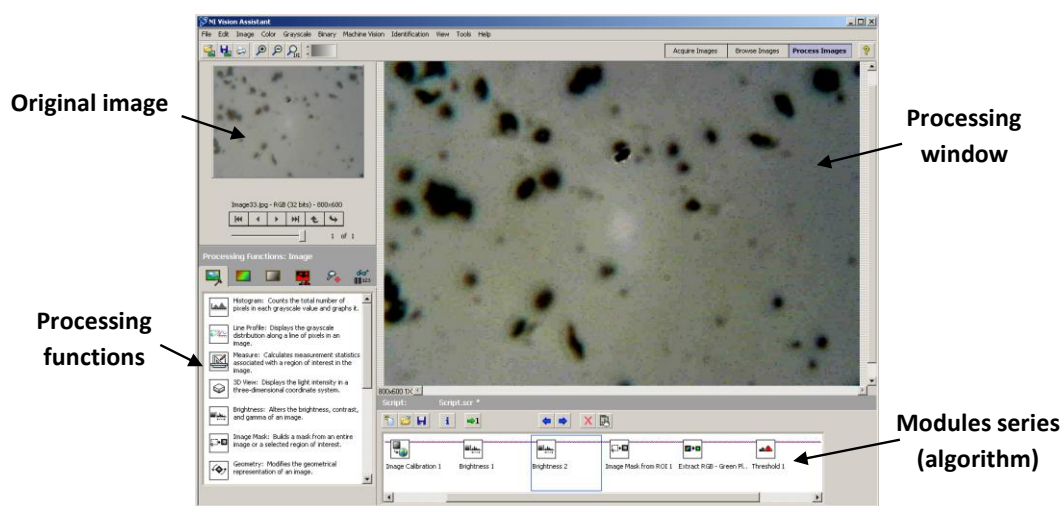


Figure 1.9 Main window of NI Vision

The images derived from the experiments were analysed using the NI software in order to detect the objects or particles in the image and create a database containing all of the relevant, desired information such as shape, size, location, texture and colour. As mentioned earlier, the script within NI Vision software contains modules which can be run to analyse and identify the particles or colonies depending on their morphology, for example by size or shape or colour, and all of the analysis can be saved as an image or exported to other programs such as Excel or Matlab for further analysis. As an example, the flowchart of NI steps that was applied on inoculated agar surfaces after laser treatment can be seen in Figure 1.10 (see Chapter 4: Section 4.1.4.1). Normally the module sequence

is calibration and processing, then colour correction and identification and measurement and counting.

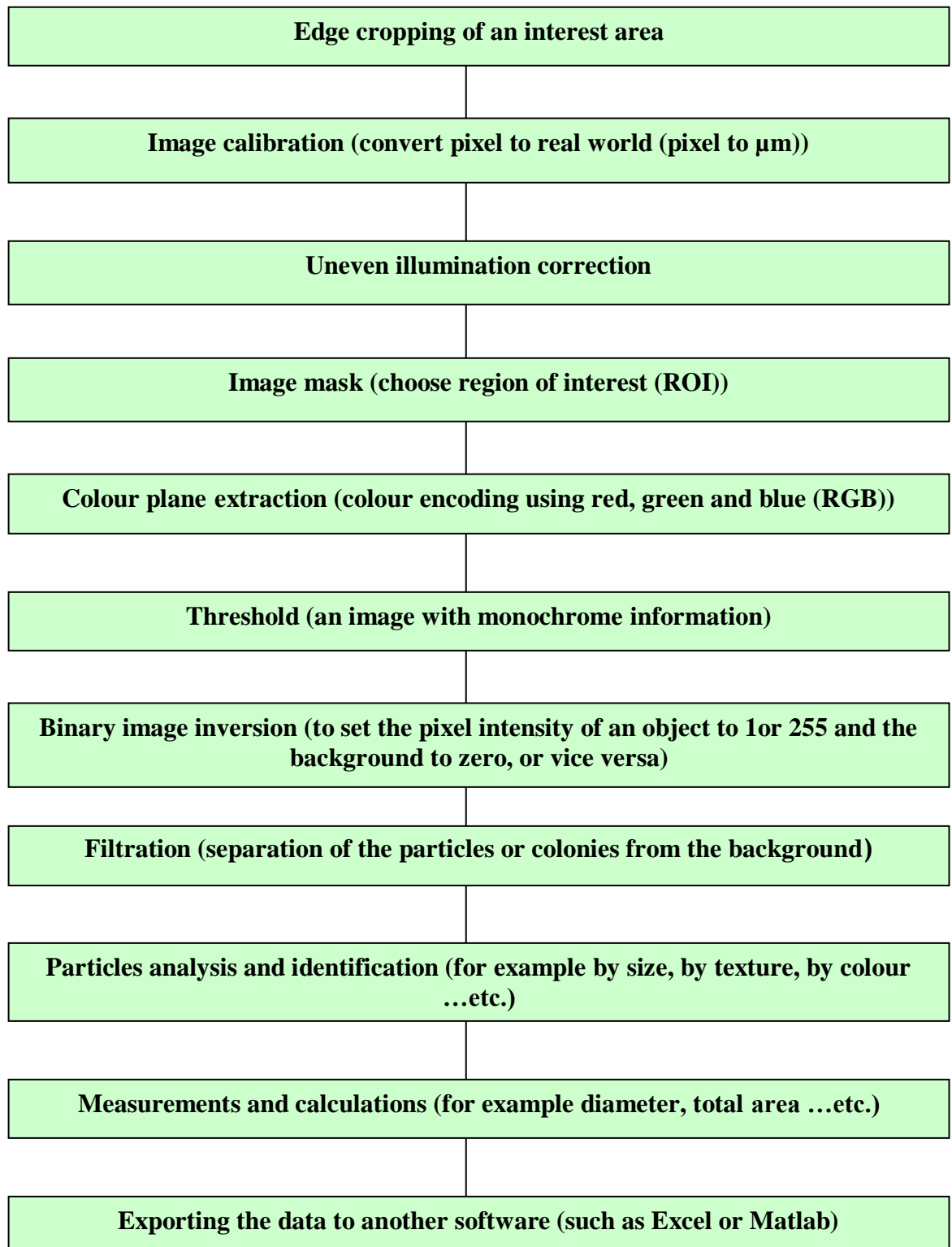
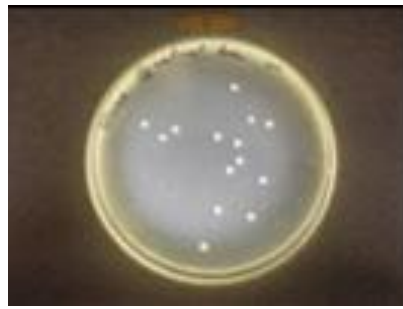
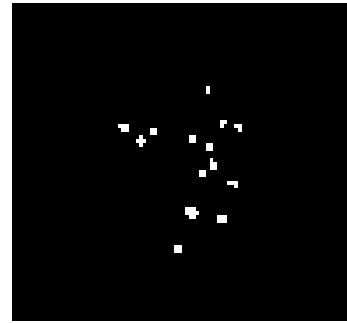


Figure 1.10 Diagram of the NI Vision analysis

Figure 1.11 shows an example of using image processing for colony counting. Each of the white dots in Figure 1.11 (b) shows a colony forming unit (CFU) after incubation.



(a) original image



(b) processed image (colony identification)

Figure 1.11 Image processing example using NI Vision analysis

1.6 Computational fluid dynamics (CFD) modelling

Fluent is a computational fluid dynamics (CFD) software package and is a simulation tool for many different fields of engineering and science, where modelling and design is required such as in fluid dynamics, electromagnetic design, thermal applications and combustion. A computational fluid dynamics (CFD) code was developed to model the flow-shape distribution and temperature profiles inside a glass system that acted as a decontamination chamber, known as the booster (Foss-Smith & Watson 2008). The particle flow trajectories were assessed between the two electrodes for the plasma system. This simulation describes how the flow velocity of the particles (*B. atrophaeus* spores in this case) varies along the length of the booster or through the two aluminium electrodes i.e. the flow shape distribution. The simulation was applied by using a Fluent 6.3 (ANSYS Inc., UK).

Various models can be developed in Fluent, these are briefly described below (Dehbi 2008; Fluent_Guide 2009):

- Standard *k-epsilon* model

In this simulation, the flow is assumed to be a steady turbulent flow. The Reynolds number (R_e , dimensionless) was calculated by Equation 1.2.

$$R_e = \frac{\rho v D_h}{\mu} \quad \text{Equation 1.2}$$

Where ρ is the fluid density (Kg/m³), v is the average inlet velocity (m/s), D_h is the hydraulic diameter (m) and μ is the fluid viscosity (Kg/m.s).

The volumetric flow rate \dot{V} (m³/s) was calculated as the product of the cross-sectional area A (m²) for the flow and the average inlet velocity v (m/s) as in Equation 1.3.

$$\dot{V} = Av \quad \text{Equation 1.3}$$

Since the Reynolds number is large and the flow is turbulent, the physical model $k - \varepsilon$ namely (standard k - ε model) was chosen to model the flow. The k variable (m²/s²) represents the turbulent kinetic energy, and ε (m²/s³) is the turbulent dissipation, given by:

$$\varepsilon = \frac{C_\mu^{3/4} k^{3/2}}{l_t} \quad \text{Equation 1.4}$$

Where C_μ is a turbulence model constant which has a value of 0.09, and l_t is the turbulent length scale ($l_t = 0.07 D_h$).

The turbulent energy k can be defined as:

$$k = \frac{3}{2} (v I_t)^2 \quad \text{Equation 1.5}$$

Where v is the average flow velocity and I_t is the turbulent intensity which is computed as:

$$I_t = 0.16 R_e^{-1/8} \quad \text{Equation 1.6}$$

Where R_e is the Reynolds number (see Equation 1.2).

- Discrete phase model (DPM)

Trajectories of the air flow and particles can be computed using DPM. In this method namely Lagrangian, the particles are represented by a discrete phase comprising spherical particles. The forces such as Saffman's lift force and drag forces can be defined.

- Boundary conditions

In this model, the collision was assumed elastic in the DPM, so the normal and tangential reflection coefficients were set to 1, this means that the particle holds the momentum after the rebound.

- Particles injection

The flow of the particles was modelled by a stochastic tracking, which can compute more than one track for each particle.

1.7 Microalgae

Various detection methods and applications were developed in this thesis relevant to surface and air (aerosols). Consequently, as an example for detection and growth within liquid, the emerging and important area of microalgae was addressed. Microalgae are considered today as one of the important sources of fatty acids for human food and biofuel production. *Chlorella vulgaris*, *Dunaliella* and *Spirulina* dominate the human nutrient market (Pulz & Gross 2004). Microalgae are promising as an alternative biofuel source because of their high growth rate, doubling per day, high lipid content and their ability to grow in a photobioreactor or on any land or saline water which is not suitable for conventional agriculture and microalgae can reduce greenhouse gas emissions (Hu *et al.*, 2008) by absorbing CO_2 . Microalgae are essential for aquaculture species productivity (Muller-Feuga 2000) and they are considered as an alternative to fish oils as many species are a rich source of Polyunsaturated Fatty Acids (PUFA) and lipids (Mendoza Guzman *et al.*, 2011). Third generation biofuels from microalgae are a good alternative energy source from the first and second generation biofuels (Nigam & Singh 2011). The processes to convert microalgal biomass to energy can be classified as biochemical, chemical reaction, direct combustion, and thermochemical (Wang *et al.*, 2008). Biodiesel from microalgae is a good substitute for petroleum and an important process in biodiesel production is the

disruption of the microalgal cell wall to aid extraction of the lipids. Various methods are used for cell disruption such as: microwaves, autoclaving, bead beating, 10% *NaCl*, waterbath, blender, ultrasonic and laser treatment (Lee *et al.*, 2010; McMillan *et al.*, 2013). Other potential applications of microalgae outside of biofuels include: foods, carotenoids, phycobiliproteins, fatty acids, isotopic biochemicals and animal feed (Milledge 2011).

All of these applications, described above, require that the microalgae counts or biomass concentration is known over their growth cycle. Bowe (2007) reported that the microscopic counting method is the most favoured technique to measure the algal biomass. Cole & Tinker (1996) used laser speckle spectroscopy (LSS) to monitor the activity of *Chlamydomonas reinhardtii* algae and other organisms, as LSS is a powerful tool to investigate the number and motion of microorganisms. Using a TV-camera with a microscope is a useful real time method of detection and velocity measurement of microalgae and microorganisms (Perner *et al.*, 2007). Nile red staining for fluorescent spectroscopy is now a fast technique for detection and determination of lipids in microalgal cells (Duong *et al.*, 2012) although there is no specificity over the lipid type. Bougaran *et al.* (2012) enhanced the neutral lipid content of microalgae by applying UV mutagenesis with flow cytometry, and a method for increasing the lipid productivity was assessed by Nile red staining. Flow cytometry in conjunction with lipid fluorescent dye Nile Red (NR) has been used to estimate the lipid cell content (De la Jara *et al.*, 2003).

1.7.1 Cultivation and harvesting systems

Microalgae can be cultivated in open and/or closed system. The advantages of closed photobioreactors over open systems is that they allow more control of the algal growth parameters such as light, pH, nutrients, intensity, light cycle, and contamination concentrations. The photobioreactor is a controlled environment that provides a high biomass (Chisti 2007). There are different types of photobioreactor (PBR), but the common designs are: tubular, column and flat (Carvalho *et al.*, 2006). The light distribution within the PBR is an important issue, as the light intensity decreases exponentially from the surface to the centre of the PBR (Hankamer *et al.*, 2007), so some designs use a thin layer approach to their design (Doucha *et al.*, 2005), flat panel air lifts (Issarapayup *et al.*, 2009) and immobilized systems (Laurinavichene *et al.*, 2006). Katsuda *et al.* (2004) used light emitting diodes (LEDs) of different wavelengths for illumination of photobioreactors and reported that the red LED was suitable for the growth of

Haematococcus pluvialis. The light emission must coincide with the photosynthetically active region (PAR) of the microalgae (Janssen 2002).

The recovery of microalgal biomass is an important issue due to low biomass to liquid ratio, which is about 0.3-5 g/L (Coward *et al.*, 2013). The recovery of microalgae can be substantially more expensive than the cultivation (Molina Grima *et al.*, 2003). Suitable harvesting of microalgae is an essential stage to separate the biomass for different microalgae production. The selection of the harvesting method is dependent on the density and size of microalgae and on the required products (Chen *et al.*, 2010). The harvesting methods for microalgae include: gravity sedimentation (Uduman *et al.*, 2010), flocculation (Danquah *et al.*, 2009), centrifugation (Dassey & Theegala 2013), foam flotation system (Csordas & Wang 2004), filtration (Bhave *et al.*, 2012), ultrasonic technique, the electrolytic removal (Alfafara *et al.*, 2002) and magnetic harvesting (Prochazkova *et al.*, 2013). Four harvesting methods were investigated in this research: filtration, centrifugation, gravity sedimentation and flocculation. Filtration is a high efficiency recovery method, relatively economic and no chemicals are required but the efficiency depends on the concentration and size of the microalgae. The sedimentation recovery method can be used for large volumes, however it is time consuming and may need further processing. The centrifugal method is the most rapid method with good recovery but high energy consumption. The efficiency of flocculation harvesting methods depends on the flocculent type.

1.7.2 Photosynthesis

Light is an important factor in microalgal cultivation and should be considered when choosing a photobioreactor design. Photosynthesis is the unique process in which the photosynthetic organisms convert the light energy to chemical energy. Microalgae are photosynthetic microorganisms and can be grown in marine and freshwater. Their photosynthetic mechanism is similar to plants, but they are more efficient in converting solar energy into biomass because of their simpler cellular structure (Anders *et al.*, 2007). The microalgae capture the light energy as an energy source and use CO_2 as a carbon source through the Calvin cycle (Yang *et al.*, 2000), i.e. they use the light reaction products (ATP and $NADPH_2$) to fix CO_2 (Reyes-Prieto & Bhattacharya 2007). The process can be represented in the reaction formula (Brennan & Owende 2010):



Equation 1.7

Photosynthesis considers the first stage of biofuel production as an increase in photosynthetic efficiency which will enhance biomass production hence this will increase biofuel production (Schenk *et al.*, 2008). Microalgal photosynthesis is an efficient way to decrease the carbon dioxide concentration in the atmosphere (Karube *et al.*, 1992). Jeon *et al.* (2005) developed a photosynthetic measurement system to investigate microalgal photosynthesis in terms of light intensity and spectra and algal concentration.

1.7.3 Decontamination protocols for microalgae

Decontamination is an essential factor in microalgal culturing and growing, as aseptic processing eliminates the growth of unwanted species and bacteria. The growing of more than one species may lead to depletion of the nutrients and kill or reduce the growth of microalgae. The culturing techniques and decontamination is an important tool in ecophysiological studies (Zacharias 2012). Fernandes *et al.*, (2011) decontamination protocols consisted of physical treatment (brushing and cutting) and chemical treatments (sodium sulfonate detergent solution and germanium dioxide) to obtain unialgal cultures. Keller *et al.*, (1988) used microwaves for sterilizing the culture media of phytoplankton. The decontamination process can include more than one method of decontamination such as chemical, physical or mechanical and a combination of antibiotics and disinfectant treatment (Xuewu & Kloareg 1992). The sterilization methods comprise: thermal/heating (flame, autoclaving, pasteurization), electromagnetic waves (UV, microwave, pulsed light, laser), chemical (ethylene oxide, ethanol, bleach) and filtration (Andersen 2005). Appendix E gives the protocols used for aseptic processing of the microalgae in this work. These methods of decontamination are similar to those that would be used for bacteria. It should be realised, however, that microalgae are usually in water and are only a problem on surfaces if a biofilm is produced. Bacterial biofilms are often eradicated with physical washing and the use of disinfectants and washing protocols.

1.8 The scope of the thesis

Chapter one: This chapter has given an overview of the spatial mapping techniques: imprint, lithography, culturing, filtration, microscopic examination, and fluorescence. Spatial mapping is beneficial to determine the distribution and location of pathogens, and

to determine the efficiency of decontamination methods. Laser decontamination is an effective process which can be used to kill air borne microorganisms or on surfaces, at a high killing rate. The importance of microalgae for biofuel and food production was discussed in this chapter. NI vision image processing and Fluent modelling technique that were used in this research were described in this chapter.

Chapter two: The results of the investigation into using the laser marking system on aluminium and stainless steel electrodes to obtain different surface roughnesses are discussed. A particle aerosol generator was used to generate the spore aerosols which were deposited onto the surface of the electrodes. The spatial distribution of *B. atrophaeus* spores on metal electrodes was investigated using membrane filtration techniques. Another technique to investigate the spatial distribution of *B. atrophaeus* spores on surfaces was imprinting (pressing). A spore laden aerosol was passed between the electrodes at two incident angles (10° and 30°) and the effect of flowshaping on capture of the spores assessed.

Chapter three: The detection of microorganisms is important in health and for safety reasons. This chapter provides an overview of the methods that were used to identify and detect microorganisms. A microscopic examination was used to find the minimum detectable level of *B. atrophaeus* spores on surfaces and these results were compared to theoretical estimates. A flow chamber system was developed that was used for cell counting of microalgae in liquid. Fluorescence techniques that were used included: fluorescence microscopy, excimer laser and a chlorophyll analyser. These systems were used to investigate the spatial detection of spores on surfaces and microalgal biomass growth in culture.

Chapter four: The aim of this work was to investigate the effects of excimer laser radiation from a *Kr:F* laser (248 nm) on bacterial and spore inactivation. The experiments investigated the laser inactivation efficiency on *E. coli* bacteria and *B. atrophaeus* spores lawned on agar surfaces by varying the number of laser pulses, the pulse repetition frequency (PRF) and exposure time. Additionally, the booster system (a laser based air decontamination system) was designed, fabricated and tested, where the air is passed through a chamber and exposed to the laser radiation.

Chapter five: With the world becoming depleted of fossil fuels, solutions are being sought to provide a sustainable, global solution to fuel security. One source that is showing

potential to help solve this problem is extracting biofuel from microalgae. Whilst this is simple to demonstrate at laboratory scale, there is considerable difficulty with scaling this to large production capacity, and maintaining financial viability. Many of the techniques for detection and decontamination developed in the early stages of the thesis are relevant to microalgae. *Nannochloropsis oculata* and *Chlorella vulgaris* are being grown within the School of Engineering at the University of Glasgow to investigate their biofuel and food potential. Every aspect of the production chain is being investigated, from optimising microalgal growth within photobioreactors, harvesting or dewatering the microalgae and component extraction. The implications of using some of the protocols and detection methods of earlier chapters on the pertinent processes for microalgae growth and culture were investigated.

Chapter six: Summarises the results, draws conclusions of the thesis, and highlights paths for further research in these areas.

Chapter 2

Spatial mapping of microorganisms on surfaces

2.1 Introduction to deposition of microorganisms onto surfaces and their resulting spatial distribution

The spatial distribution of microorganisms is the pattern in which they are arranged over an area. The investigation of the microorganism's distribution on surfaces is of importance in evaluating the contamination level, and it provides information on the likely way in which they were deposited onto that surface, which may help in optimising decontamination. Detection of microorganisms is essential to quantify their spatial distribution, and ideally the detection should not destroy their arrangement or distribution. It is also informative to investigate the distribution models for statistical analysis, such as how the organisms are arranged, this can be classified as: uniform (regular), random or clumped (aggregated).

Previous work at the University of Glasgow (Foss-Smith & Watson 2008; Mine 2010) developed a plasma based system to kill microorganisms in air, in particular the target organism was *Bacillus atrophaeus* spores, supplied by Dr Bill Whyte, University of Glasgow. It was found that the angle of entry of the air into the electrodes had a significant effect on the system's performance. The system utilised laser marking to produce electrodes of various roughnesses; this had the effect of reducing the breakdown voltage between the electrodes, allowing the electrode gap to be increased and a greater volume of air passed through the system. It was hypothesised that the electrode roughness also allowed preferential trapping of the microorganisms, allowing increased removal from the air stream and enhanced killing, essentially the spores were inactivated on the surface,

whilst other spores that remained in the air stream were exposed to the plasma treatment. The entry of air into the system was varied to direct the spores onto the electrode and improvement in killing was observed.

The spatial distribution of *B. atrophaeus* spores on surfaces was therefore of interest to investigate the hypothesis of preferential trapping of the microorganisms and to determine how the spores were deposited onto the electrode surfaces and whether any additional trapping effects could be seen, understood and enhanced. Generally, investigation of the spatial mapping required developing protocols to prepare the substrate surfaces of the specimen, establish a sampling process and methodology, detect the spores and then quantify the data. The spatial distribution, adhesion and observation of *B. atrophaeus* spores on metal electrodes were made by using two methods imprinting (pressing) and membrane filtration techniques. In these two techniques, the spatial distribution of the spores in an aerosol and of those deposited onto the rough surface can be determined on the agar and filter surfaces.

Aluminium and stainless steel electrodes were produced with different surface roughnesses using a laser scanning system. A *Bacillus atrophaeus* spore laden aerosol, generated from a SPG 350 particle generator (SPG 350, DOP Solutions Ltd, UK), was directed at these electrodes and the distribution of spores on the substrate samples assessed. The effect of flowshaping on the spore distribution was investigated by varying the angle of incidence (10° and 30°) of the aerosol onto the sample, which were the same angles as used by Mine (2010). Computational Fluid Dynamics (CFD) techniques were applied to model the particulate flow through the electrode geometry, comprising two parallel plates a set distance apart. The metal samples (electrodes in this work) were prepared by a series of processes: grinding and polishing and laser marking. The experiments were set up to investigate the spore distribution on the surfaces.

2.2 Sample preparation

Preparation of the sample is a highly important step prior to modification of the surface finish. It is important to have the same starting conditions so that the effects of the modification process can be quantified. In this work, the grinding and polishing techniques were used for the sample preparation before surface modification in the subsequent steps. The preparation steps starting from the initial cutting to the final polishing and all the other steps are equally important. The grinding and polishing

technique helped to ensure the same surface roughnesses for all the samples. The work investigated two metal samples namely aluminium and stainless steel. The procedure for the specimen preparation is as follows.

2.2.1 Grinding

Grinding removed irregularities and scratches on the surface and marks from the lathe made during cutting. The metal electrodes were cleaned with ethanol (analytical grade, ethyl alcohol, Fisher Scientific, UK) and rinsed with tap water to remove any oil or debris that remained from the cutting machine. The grinding operation was done by using a Beuhler semi automatic specimen preparation unit (Motopol 2000, UK). This machine is fully programmable, an electro-hydraulic operation and compressed air is required (4.8 Bar), variable head speed (60-150 rpm) and base speed (30-300 rpm) and variable force (5-200 N). This machine can grind and polish multiple samples automatically and provides an excellent surface finish, this is of course less time consuming compared with hand preparation. Figure 2.1 shows the grinder-polisher machine. In order to clamp the metal samples in the rotating head of the grinder, the moulds (holders) were designed from brass using CAD software (SolidWorks 2010, SP 4.0, UK).

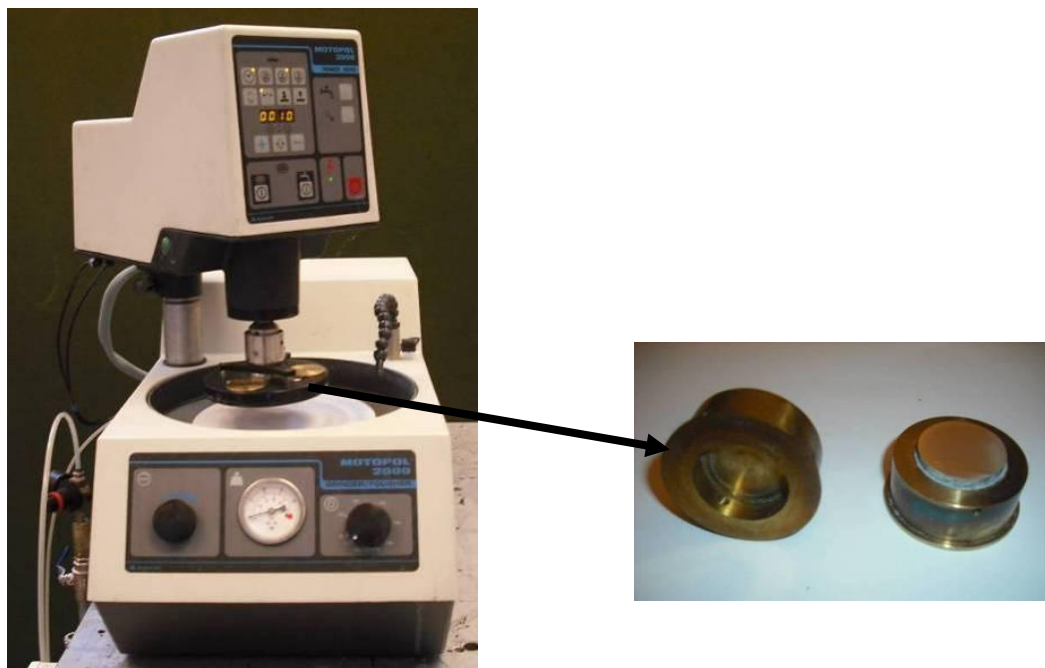


Figure 2.1 Beuhler semi automatic specimen preparation unit and the specimen holder

Modification of the metal surface was done with wet grinding; the wet method uses water to reduce the friction and grinding dust. The grinding method was done with emery paper

(silicon carbide abrasive paper, Struers, Denmark). The emery papers were placed on the grinding rotating wheel from a course to fine grit size (P220, P500 and P800 respectively). After the grinding processes, all the samples were rinsed thoroughly with running water to remove all residues. Then the metal samples were dried with filtered compressed air. After this operation, the samples were ready for laser marking.

2.2.2 Polishing

Polishing is a method to produce smooth, flat and mirror like surfaces. Polishing removes the very small debris remaining from the grinding operation. The polished samples were made for control and microscopic investigation. The polishing was done by using the grinder-polishing machine which was used in the grinding. The polishing abrasive 0.06 μm syton (colloidal silica, SILCO, UK) suspension in water was used on a polishing cloth (colloidal silica, Kemet, UK).

2.3 Laser marking system

Before investigating the effect of the laser beam on the surface modification, it is important to provide information and operation of the laser marking system. The laser marking system used in this work consisted of four main parts which are: the laser source, the galvanometer mirrors to direct the laser onto the sample, controlled x-y table and the control software.

An $Nd:YVO_4$ (1064 nm, Neodymium-doped Yttrium Orthovanadate) laser marking machine (Laservall, Violino 2, Italy) was used to mark the metal samples. The mean power output of laser was 10 W with a maximum pulse repetition frequency of 20 kHz, the maximum scanning speed was 200 mm/s. The focal length of the focusing lens was 175 mm and the spot diameter was 30 μm (see Appendix A: Laser marker (Violino2) detailed description for more specifications). Figure 2.2 shows the laser marker head and the rack which contains the electrical parts.



Figure 2.2 Laser marker head and the electrical rack

2.4 Surface roughness

Investigation of the effect of surface roughness and its influence on adhesion of microorganisms is important to determine the contamination level on the surfaces. This aids design and choice of electrode material, and allows understanding of the potential distribution of the spores on the electrode surfaces for different incident flow angles. The surface roughness (R_a) was measured using a surface profilometer Tallysurf (Surtronic 3P, Taylor Hobson, Denmark), this machine uses a diamond stylus tip, which moves across the central region of the metal surface. Figure 2.3 shows this Tallysurf machine.



Figure 2.3 Profilometer Tallysurf machine for surface roughness measurement

2.5 Influence of laser marking on the surface roughness

The laser marker Violino 2 was used to mark several metal samples, and a profilometer machine was used to measure the surface roughness against different laser marking parameters.

2.5.1 Electrode marking: varying scanning speed

An $Nd:YVO_4$ laser marker with various scanning speeds namely 10, 50, 100 and 200 mm/s was used to mark aluminium and stainless steel circular discs (25 mm diameter with 10 mm thickness) that were previously grind; this was done to modify the surface roughness. The beam profile from the laser is TEM_{00} , the minimum spot diameter of the laser was 30 μm and the focal length of the lens was 175 mm. The changeable parameters of the laser that can be controlled by control software Smartist 4 (Laservall, Italy) were set as shown in the Table 2.1:

Table 2.1 Laser marking parameters

Laser power 100%	10 W max
Shot frequency (PRF)	20 kHz
Scan speed	10, 50, 100 , 200 mm/s
Passes	1

Figure 2.4 shows the samples after laser processing, it is seen that they have different colours for both metal samples after laser marking with different scanning velocities. The top row shows the aluminium samples and the bottom row shows the stainless steel, with decreasing velocity from left to right of 200, 100 and 50 mm/s. It is seen that the lowest velocities created a larger roughness due to the greater energy density absorbed by the sample per unit area and hence resulted in a darker surface.

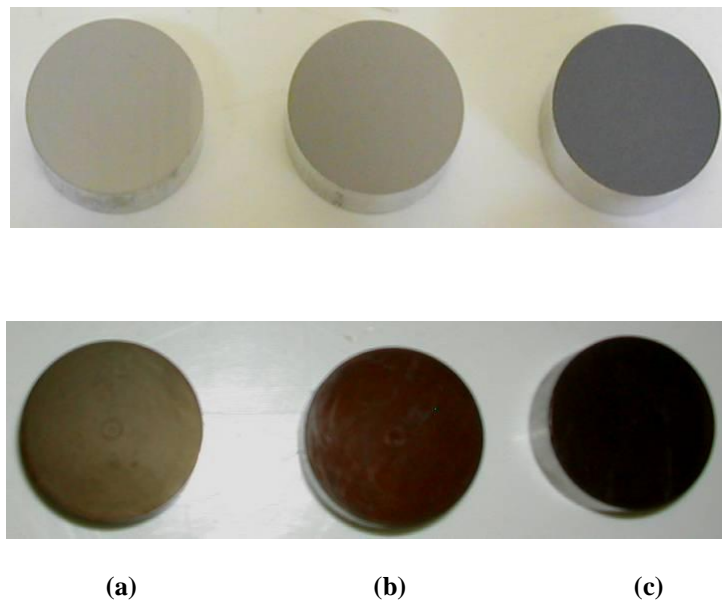


Figure 2.4 The top row shows the aluminium electrodes and the bottom row shows the stainless steel electrodes, with decreasing laser scanning velocity from left to right a) 200, b) 100 and c) 50 mm/s

The values of the surface roughness against different scanning speeds were measured by the tallysurf machine, as shown in Table 2.2. The measurements were taken along the surface of electrode, and the standard deviation (SD) was found from five measurements. With reduced scanning speed the roughness increased and was greater for the aluminium samples.

Table 2.2 Measured surface roughness R_a (mean \pm SD) of aluminium and stainless steel samples for different scan speeds (5 measurements)

Scanning speed (mm/s)	R_a (μm), Aluminium	R_a (μm), Stainless steel
200	0.71 ± 0.05	1.37 ± 0.57
100	1.12 ± 0.22	1.48 ± 0.14
50	1.32 ± 0.45	2.55 ± 0.16
10	3.03 ± 0.42	4.07 ± 0.91
Unmarked R_a (μm)	0.28 ± 0.02	0.33 ± 0.02

The increased roughness is due to the increased exposure time on the same area, thereby increasing the temperature gradient and input energy on the sample surface. The colour change can be appreciated by incident photons being more diffusely scattered and absorbed in the increasing crevice size with increasing roughness.

2.5.2 Microscopic examination of surface texture

To understanding the mechanism of the marking process, some photographs of the sample's surface were taken using an optical microscope (Nikon Eclipse, ME600, Japan), with an objective magnification of 20X (Nikon EPI, NA= 0.8, Japan). Figure 2.5 and Figure 2.6 show the surface of the aluminium and stainless steel samples unmarked as the control and marked with a scanning speed of 200 and 50 mm/s respectively. From the photographs, it is evident that the laser used in this experiment had a significant effect on the metal samples. For a scanning speed of 50 mm/s, deeper marks on the surface were seen because the laser beam was irradiated for a longer time on the same area thereby inducing a higher temperature on the material surface, this caused the solidified structures and the cavity formation to form a texture that looked like a cauliflower surface. With increased scanning speed to 200 mm/s, the texture of the surface seemed smoother and less

solidified material was observed, this means that the laser beam did not penetrate as deeply.

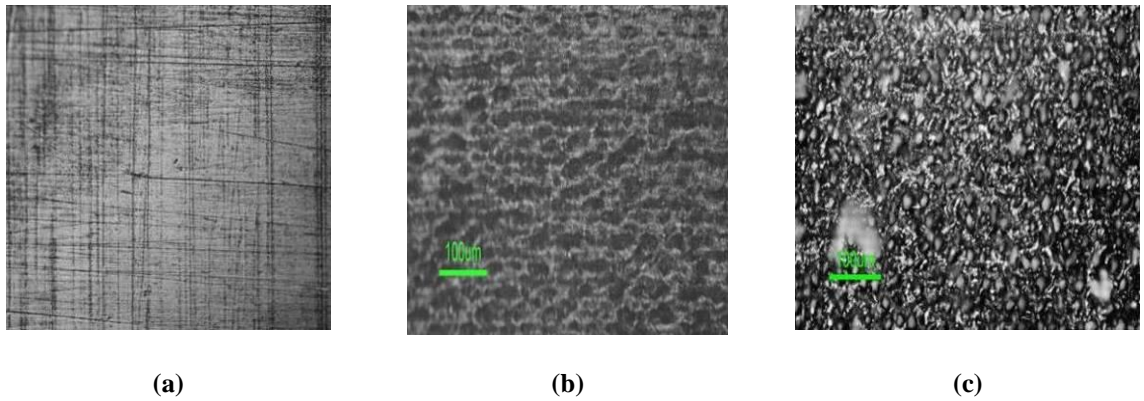


Figure 2.5 Stainless steel samples a) unmarked, b) marked with scanning speed of 200 mm/s and c) marked with scanning speed of 50 mm/s

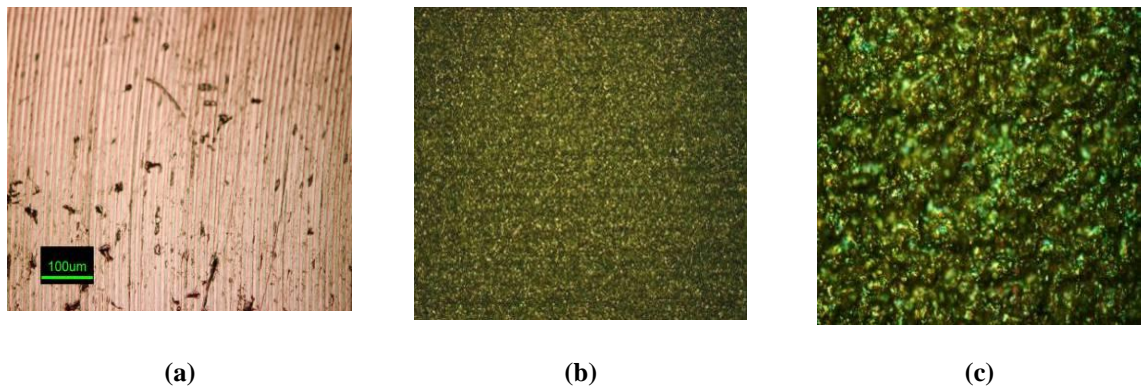


Figure 2.6 Aluminium samples a) unmarked, b) marked with scanning speed of 200 mm/s and c) marked with scanning speed of 50 mm/s, (b) and c) are photographs taken through a green filter)

2.5.3 *Overlap of laser pulses*

The laser marking technique is illustrated in Figure 2.7. The laser beam is moved over the electrode surface, and the traces overlapped between two successive pulses.

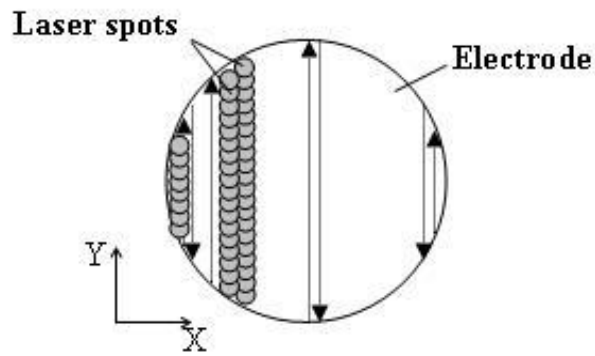


Figure 2.7 Schematic of the laser marking technique on the metal electrode shows the marking tracks

The marking patterns showed that there was an overlap between two subsequent pulses. Figure 2.8 represents a schematic of the laser marking overlapping and Figure 2.9 shows the overlap between the pulses in the direction of the laser beam on a stainless steel sample for scan velocities of 200 and 50 mm/s.

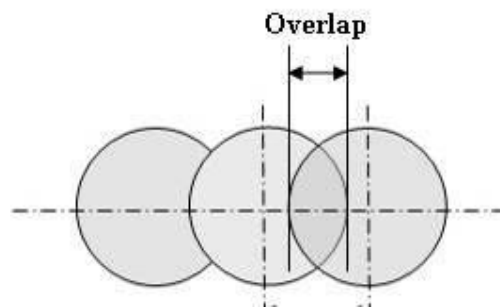


Figure 2.8 The overlap of laser spots

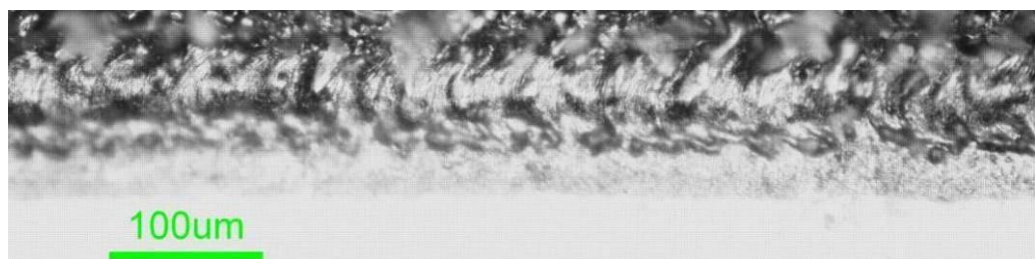
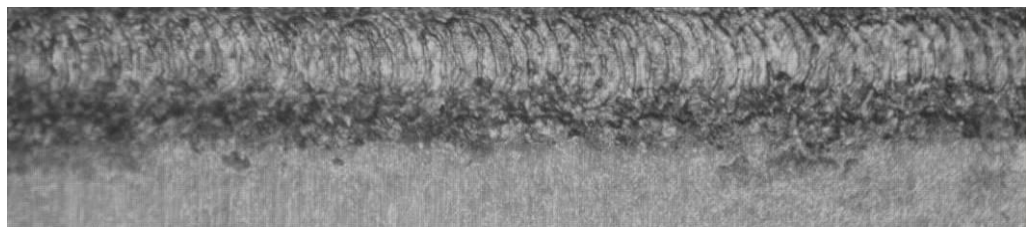


Figure 2.9 Overlap of laser spots on stainless steel surface marked with scanning speed of 200 mm/s (top) and 50 mm/s (bottom)

2.5.4 Electrode marking: varying scanning speed and laser power

In this work, a sheet of stainless steel (AISI 316) was cut into several specimens (8x40x1 mm³). The surface of the samples was marked with different laser scanning speeds (50, 100, 150 and 200 mm/s). The laser marker was fired at 100% output power (10 W) and 75% output power (7.5 W), while the pulse repetition frequency remained unaltered (20 kHz). The surface roughness was investigated using a Tallysurf machine, and it was measured ten times for each sample and the average of measurements was taken, the results can be seen in Table 2.3.

Table 2.3 Surface roughness of stainless steel samples against different scanning speeds, where the samples were marked with laser output power of 100% (10 W) and 75% (7.5 W)

Scanning speed (m/s)	R _a (average, μm) 10 W output power	R _a (average, μm) 7.5 W output power
200	0.64	0.56
150	0.68	0.61
100	0.76	0.74
50	1.6	1.42
Unmarked R_a (μm)	0.053	

The results showed that the surface roughness increased significantly when the scanning speed decreased, and a higher surface roughness was obtained when the laser marker was fired with 100% power (10 W). Figure 2.10 shows the roughness plotted as a function of scanning velocity. The same marking parameters and techniques were used to mark more stainless steel samples, but the scanning speeds were varied as 50, 75, 100, 125, 150, 175 and 200 mm/s to prove that the roughness decreased exponentially with the higher scanning speeds, as shown in Figure 2.11. The error bars show the standard deviation for the 10 measurements for each scanning speed.

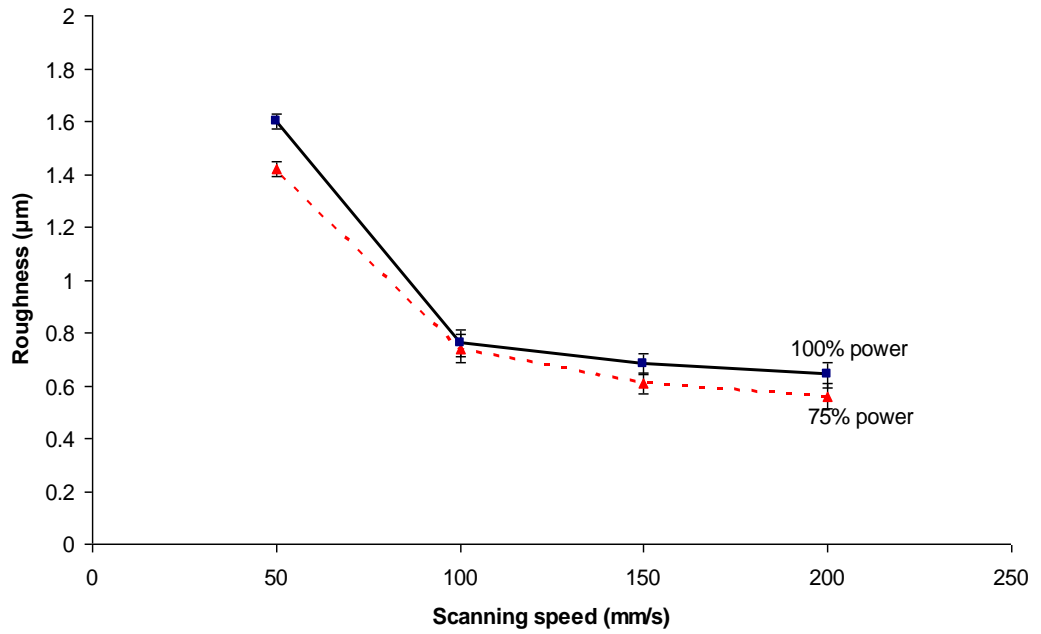


Figure 2.10 Surface roughnesses and laser scanning speeds for stainless steel samples marked with laser output power 100% (solid line) and 75% (dashed line), the error bars are the standard deviation taken from an average of ten data points

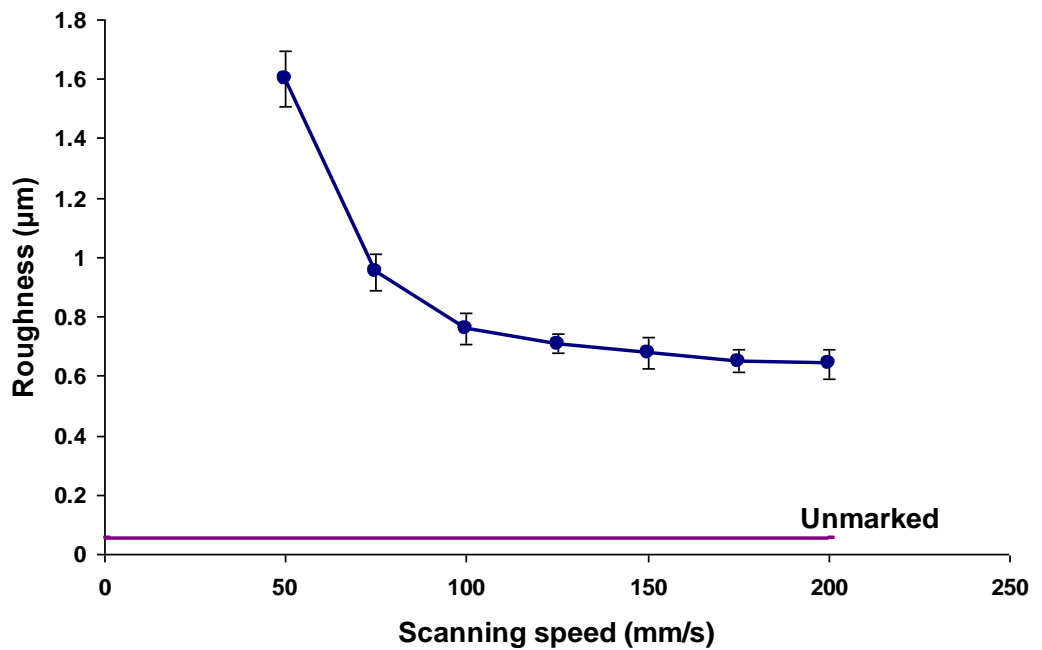


Figure 2.11 Surface roughness and laser scanning speeds for stainless steel samples marked with a laser output power of 10 W, the error bars show the standard deviation (n = 10)

2.5.5 Electrode marking: varying scanning speed pulse repetition frequency

The stainless steel samples were marked at different pulse repetition frequencies PRF (10, 15 and 20 kHz), for various scanning speeds (50, 100, 150 and 200 mm/s). After laser marking, the surface roughness of each sample was measured ten times and the average was taken. The results from the experiment showed that the surface roughness decreased with increasing PRF, as the energy per pulse is decreasing at high frequencies. The roughness measurements with different laser parameters were plotted in Figure 2.12.

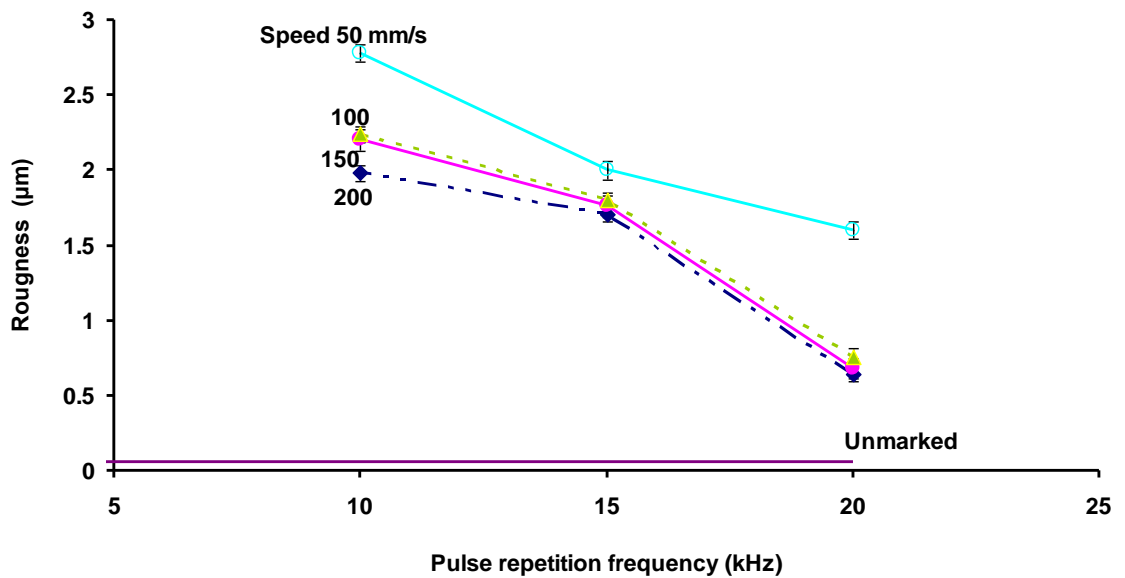


Figure 2.12 Surface roughness of stainless steel samples against pulse repetition frequencies for given laser scanning speeds, the error bars show the standard deviation (n =10)

2.5.6 Laser marking of wire mesh

An $Nd:YVO_4$ laser marker was used to mark a sheet of copper wire mesh with a measured mesh size of 180µm. The wire mesh was marked to see how the laser energy modified the surface, and for filtration applications (see Chapter 5: Section 5.10.3.4). The parameters for laser marking were: 10 W laser power, PRF of 20 kHz and a scanning speed of 100 mm/s. Figure 2.13 shows the laser system and the mesh, the laser treated regions are clearly identifiable. Figure 2.14 shows a close up of the laser marked (left) and untreated regions (right) of the mesh, the image was taken through a Nikon microscope. Impurities are evident on the untreated side but all of these were removed after laser treatment.

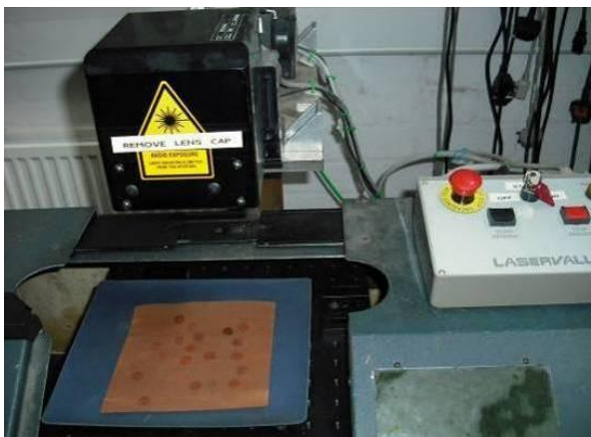


Figure 2.13 Wire mesh sheet processed under laser marking machine (left) and normal view of the mesh after marking, dark circles indicate laser treatment (right)

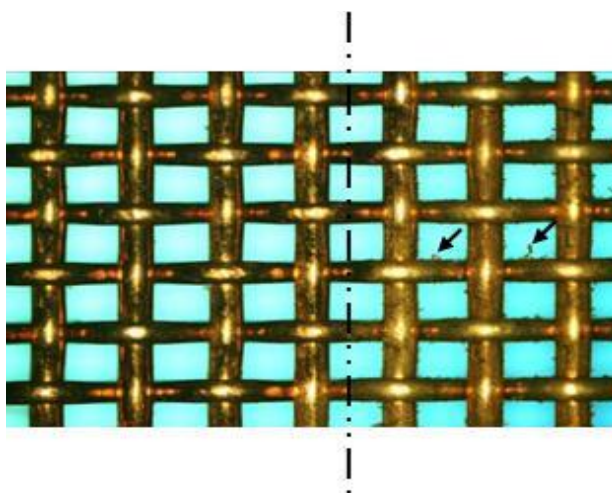


Figure 2.14 Wire mesh marked (left) and unmarked (right), the arrows indicate impurities, objective magnification of 20X

2.6 Spatial mapping techniques

The current work investigated spatial mapping of spore laden bioaerosols being passed through the electrodes that can be used to generate plasma and kill the spores. Two simple techniques were used to investigate the potential distribution of the spores. The samples produced from the laser processing were fitted into a plastic tube and exposed to an aerosol stream of the spore; spore recovery from the aluminium disks was then achieved using membrane filters and imprinting techniques.

2.6.1 Inherent antibacterial activity of the metal disc (electrode)

The metal discs/electrodes (unmarked) were tested to see if they had any inherent antibacterial activity, before using them in the main experiments, and to determine the natural reduction in viability over time. The electrodes were cleaned before the test by mixing 70% isopropanol solution (2-Propanol, Stratlab Ltd., UK) with 30% sterile distilled water in a beaker. The discs were soaked in the prepared solution for at least 20 min. After soaking, the discs were removed from the solution using a sterile forceps and rinsed with sterile distilled water to remove any chemical residue, and then the disks were allowed to air dry in a laminar air flow cabinet before use.

The lysogeny broth (LB) agar nutrient was poured into a Petri dish (see Appendix D: Preparing agar plate). A dilute suspension (100 μL at a concentration of 10^8 mL^{-1}) of the spores was spread on an agar plate and allowed to dry thoroughly, then the sterile discs were placed or pressed on the agar surface. The agar plate with discs still in position were incubated at 37°C overnight to see if a zone of inhibition was produced. After incubation, the surface showed growth close to the discs indicating no antibacterial activity from the material, see Figure 2.15. The yellow colonies are the *B. atrophaeus* spores after overnight incubation.

All of these procedures were done under sterile conditions to avoid contamination, and also the discs were sterilized after the experiment using 1:10 trigene dilution (Trigene, Medichem International Ltd, UK) for 10 min, as per the manufacturer instructions so that they could be used again.



Figure 2.15 Inherent antibacterial test of the metal disc

2.6.2 *Microorganism aerosol generator*

Biological aerosols (bioaerosols) are airborne particles which may consist of microorganisms such as bacteria, spores and viruses. In the atmosphere, harmful microorganisms can be inhaled and infect humans or animals and may land on plants causing disease. Biological warfare agents are usually delivered in aerosol form (Heimbuch *et al.*, 2009) as this is the most effective way to distribute the pathogens into the environment. A good review of biological aerosol was given by Ho (2002). There are several techniques available for generating and measuring bioaerosols, starting from simple test methods like the aerosol generator and settling chambers to special techniques such as flow cytometry (FCM), lidar technology (Brown *et al.*, 2011), fluorescence *in-situ* hybridization (FISH), and fluorescent aerodynamic particle sizer (FLAPS).

In this work, the generation and flow system used to generate the spore laden aerosols consisted of three main parts: particle aerosol generator (Laskin, SPG-300, UK), flow chamber and a high-efficiency particulate air (HEPA) filter. The flow chamber consists of the decontamination tube of inner diameter 34 mm and 300 mm length and the aerosol outlet pipe. HEPA carbon filters (Viva air purifier, VIA2/8, UK) were cut and fitted into this pipe. The view of the aerosol generator with flow chamber is shown in Figure 2.16.

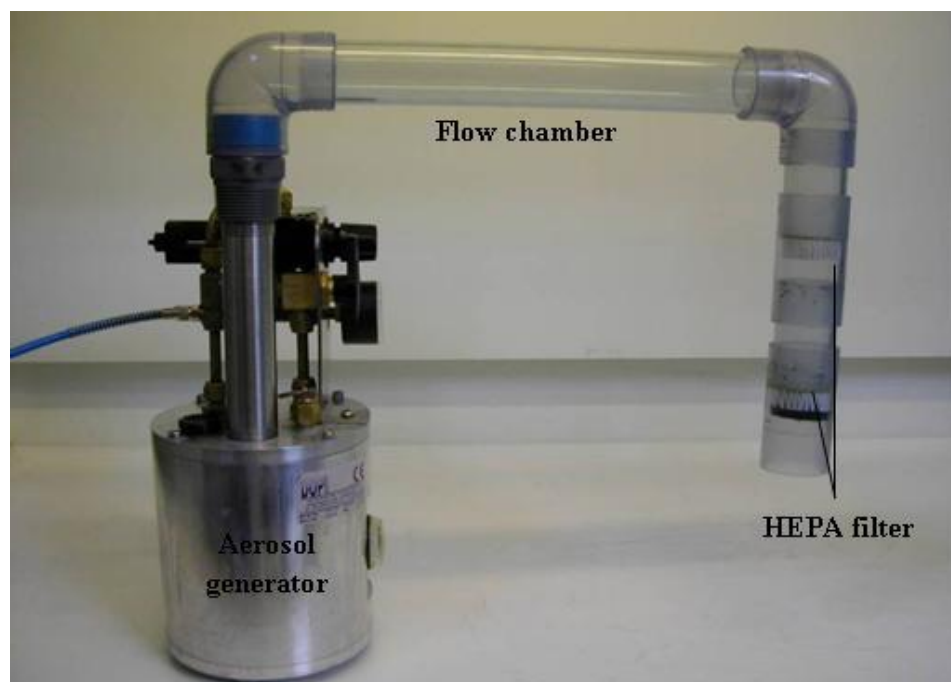


Figure 2.16 General view of the aerosol generator system

2.6.2.1 Calibration of the aerosol generator

The Laskin aerosol generator produces a well defined particle aerosol which can be seeded with microorganisms, the aerosol size is up to 2 μm . The aerosol generator is portable, highly stable, easy to work as it just requires compressed air, and is ideal for a wide range applications such as filter testing and aerosol investigations.

It is necessary to adjust the aerosol generator to know the ideal pressure and volume flow rate to satisfactorily flow the particles through the system and hence find the optimum concentration of the microorganisms for the specific applications. The volumetric flow rate of the aerosol can be controlled by varying the outlet pressure of the aerosol generator. Figure 2.17 shows the relationship between the outlet pressure and the volumetric flow rate. The optimum outlet pressure was 0.75 bar for a volumetric flow rate around 50 L/min. The outlet pressure was set to 0.75 bar, above this value the pressure built up inside the flow chamber and the air sampler stopped working.

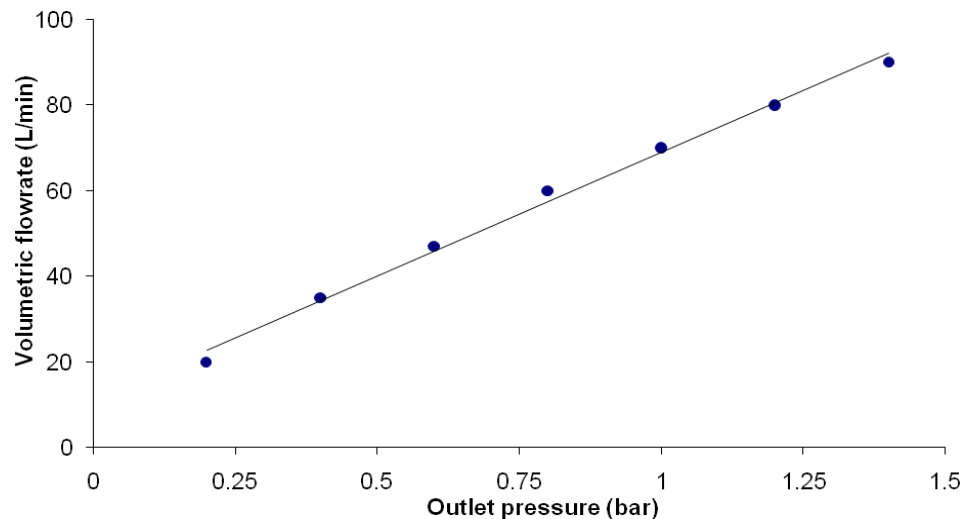


Figure 2.17 Outlet pressure versus the volumetric flow rate for aerosol generator calibration

2.6.2.2 Ideal concentration of the *B. atrophaeus* spores inside the aerosol generator

This experiment was planned to find the ideal concentration of microorganisms needed to put inside the tank at the optimum outlet pressure (0.75 bar). Serial dilutions of the original stock culture (10^{10} spore/mL) were made to obtain different concentrations, and then 5 mL of each culture was mixed with 495 mL of sterile distilled water in the aerosol generator,

so the final spore concentration was between 10^2 - 10^6 CFU/mL, as shown in Table 2.4, see Appendix F: serial dilution protocol of *Bacillus atrophaeus*, for more details about the dilution protocol.

Table 2.4 Ideal concentration test of *B. atrophaeus* suspension inside the aerosol generator tank

Serial dilution factor	Concentration in stock culture (CFU/mL)	Concentration inside the aerosol generator tank (CFU/mL)
$1:10^{-2}$	10^8	10^6
$1:10^{-3}$	10^7	10^5
$1:10^{-4}$	10^6	10^4
$1:10^{-5}$	10^5	10^3
$1:10^{-6}$	10^4	10^2
$1:10^{-7}$	10^3	10^1

The concentration tests were done by pumping the spore suspension from the aerosol generator to the flow chamber, and then the aerosolized spores were collected by the air sampler (Sartorius, MD8 airscan, Germany) at the output of the flow system, the air sampler maximum air inlet was 50 L/min. Although the spores are harmless, the experiment was set up in the fume cupboard for extra safety. A schematic diagram of the experiment can be seen in Figure 2.18.

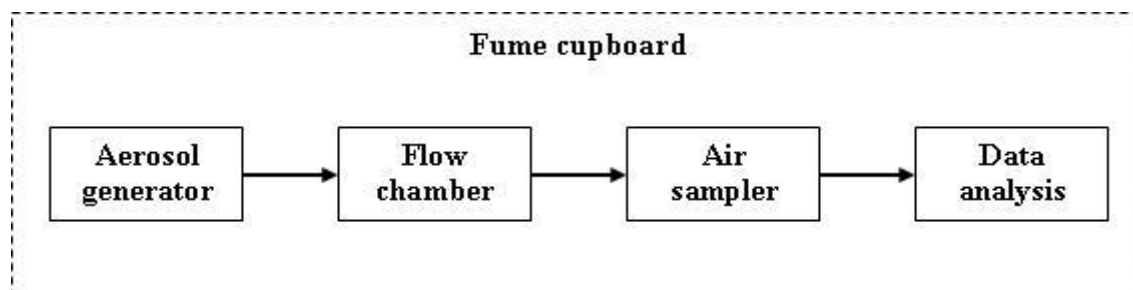


Figure 2.18 Schematic drawing of the ideal concentration experiment setup

The air sampler collected the air on the gelatine membrane filter (0.8 μ m pore size, 80 mm diameter, Sartorius, UK). The sampling time was 3 min for all of the prepared concentrations. Figure 2.19 shows the air sampler with the gelatine filter unit. The gelatine

filter retained the microorganisms which after the sampling time are ready for processing and counting. The air sampling procedure is described in detail in Figure 2.20. The flowchart shows steps of the air sampling process, generally the decontaminated air is collected with the air sampler and the contaminants are collected with a gelatine membrane filter and all the gelatine filters are transferred into the nutrient agar plates, and the plates are incubated for the growth assessment.

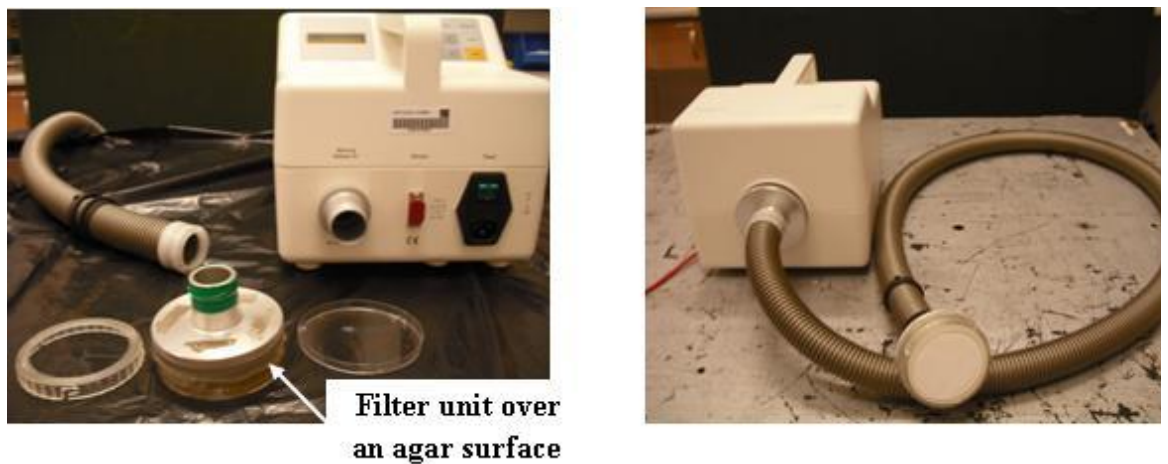


Figure 2.19 The air sampler and the gelatine filter unit

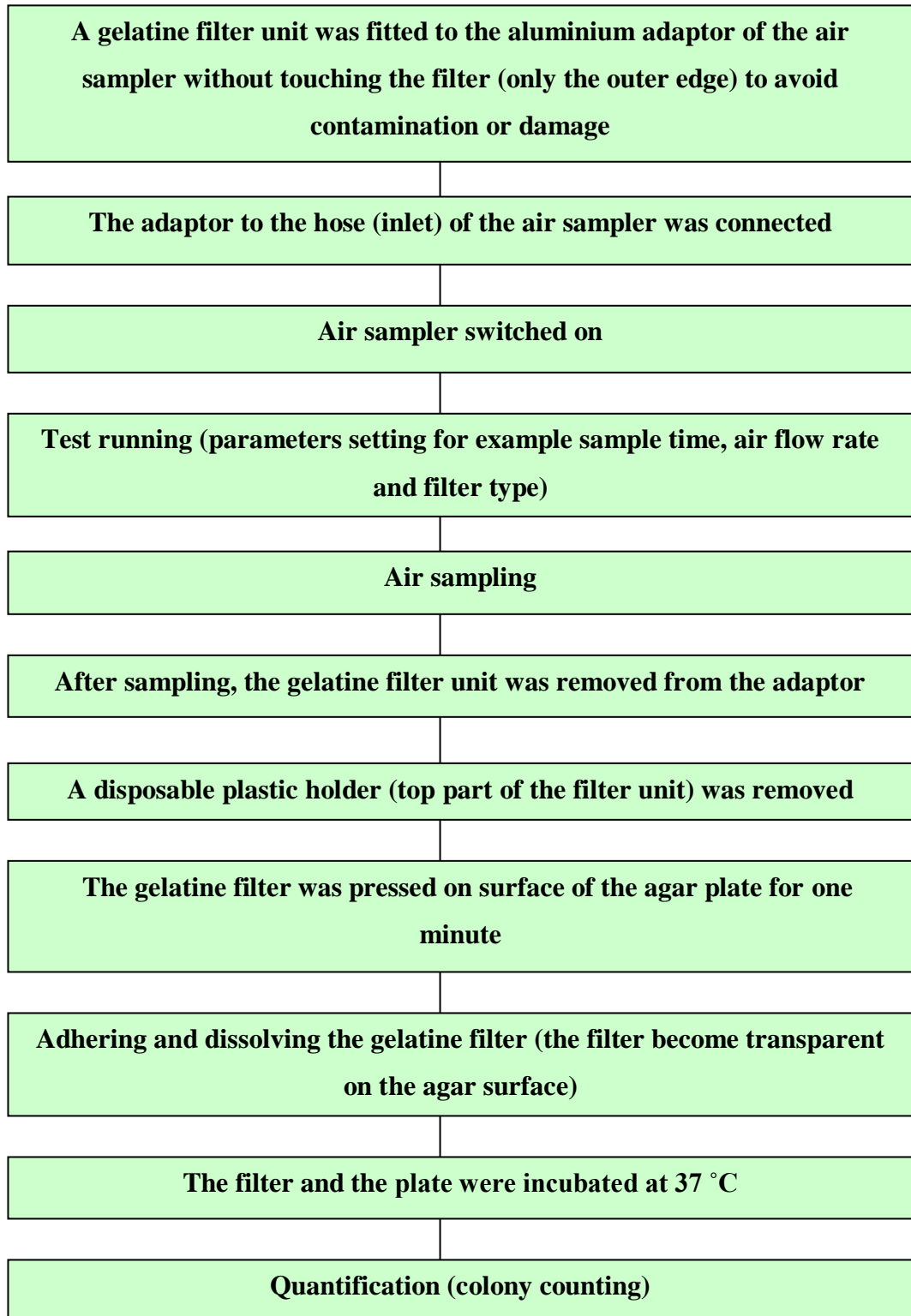


Figure 2.20 Air sampling procedure diagram

2.6.2.3 Results of ideal concentration of the *B. atrophaeus* suspension

The number of colonies counted on the agar plates for each concentration is shown in Table 2.5. The number of colonies (190) that was observed on the agar plate for the concentration of 10^4 CFU/mL was the order of the optimal number to get on the plate of *B. atrophaeus* (Sutton 2006), and also 10^3 CFU/mL was acceptable with 57 colonies detected. For plates with concentrations higher than 10^4 CFU/mL, the number of colonies was too numerous to count (TNTC). While, too few counts were observed for a concentration of 10^1 and 10^2 CFU/mL. Hence a concentration of 10^4 CFU/mL was chosen.

Table 2.5 Result of ideal concentration of *B. trophaeus* suspension inside the aerosol generator tank

Concentration (CFU/mL)	CFU
10^6	TNTC
10^5	510
10^4	190
10^3	57
10^2	20
10^1	11

2.6.3 Membrane filtration technique

The use of membrane filters offers a simple technique for sampling and counting the microorganisms in an air or a liquid solution. It is easy to use and does not need any expensive equipment or long preparation processes. The advantages of membrane filtration techniques compared with other traditional methods such as spread and pour plate techniques are: the microorganisms are easily and accurately quantified because the membrane permits a good separation of CFU, and this method is suitable for sampling a large volume of fluid. These advantages make membrane filters applicable to a wide range of uses for separation and enumeration of the particles, fluid sterilization and aerosol analysis. In this work, the effect of the laser induced surface roughness (R_a) of the metal samples on the spore adhesion was determined using the membrane filtration technique.

2.6.3.1 Experimental set up of the membrane filtration

The experimental set up consists of the particle generator, the flow chamber (as described in Section 2.6.2) and the metal discs and their holders. The holder was made from a Polytetrafluoroethylene (PTFE); it simply holds the disc in the flow chamber without any screws. A schematic of the experiment is shown in Figure 2.21, and the disc and its holder can be seen in Figure 2.22.

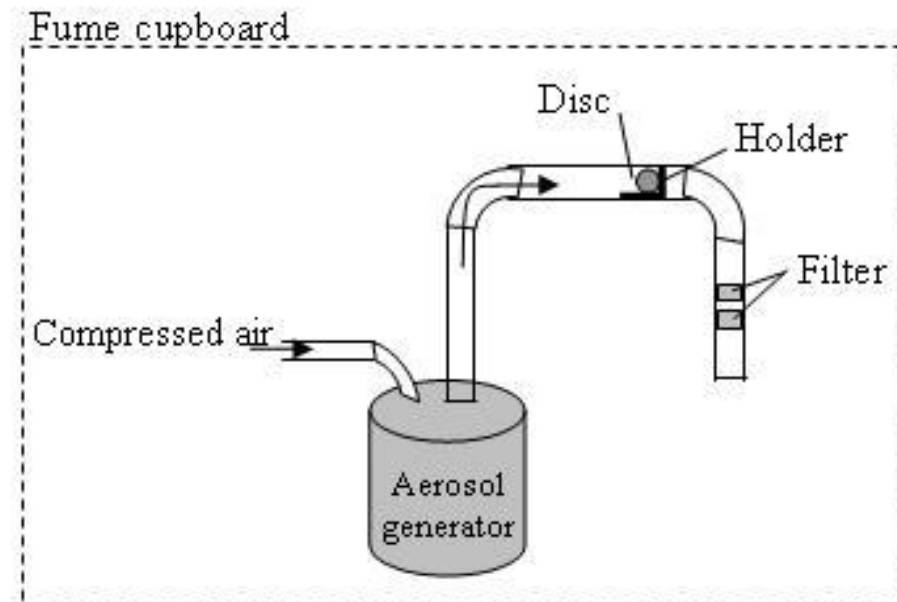


Figure 2.21 Schematic drawing of the membrane filtration experiment

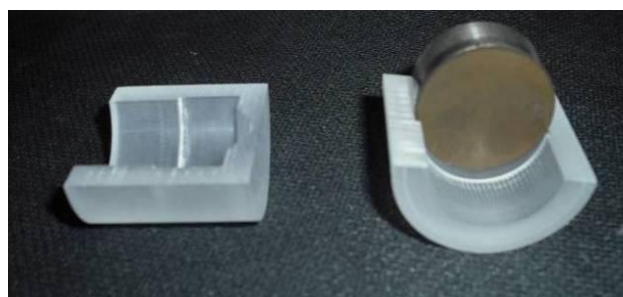


Figure 2.22 Disc with the holder

The aerosol generator and flow system were used to create a stream of spores that were directed into the flow cavity at an inlet velocity of 5 m/s, an air flow rate of 50 L/min and an air pressure of 0.75 bar on the aerosol generator. The contaminated air from the aerosol generator was passed to the metal disc. After exposure to the aerosol for 3 min, each disc

(where the material was chosen on the basis of its suitability to be used as electrode material - aluminium and stainless steel) was picked up aseptically and placed in a bottle (Duran) containing 20 mL of sterile distilled water. The effect of laser exposure time can be seen in Chapter 2: Section 2.5.1. The bottles were shaken at 100 rpm for three hr at 25 °C in a controlled environment incubator shaker (New Brunswick Scientific, G25, USA) to resuspend the spores in the liquid. Figure 2.23 shows the samples and the shaker.



Figure 2.23 The samples inside the shaker

After shaking, 10 mL of the 20 mL sample culture was taken and filtered through a membrane filter of 0.45 μm pore size, 47 mm diameter (Cellulose nitrate membrane, Whatman, UK) using compressed air or a vacuum source to provide faster filtration. The filter apparatus consists of two main parts: the filtration assembly and filtering flask. The filtration assembly consists of a filter funnel, filter support pad and O-rings, and filter base, see Figure 2.24. After the sample was completely drawn through the filter, sterile distilled water was used to rinse the funnel assembly to remove any spore residue. The filter was placed on the LB agar surface plate. Some electrode samples were used as controls for assaying and received no treatment. All the agar plates were incubated at 37 °C for 24 hr and analysed for growth.

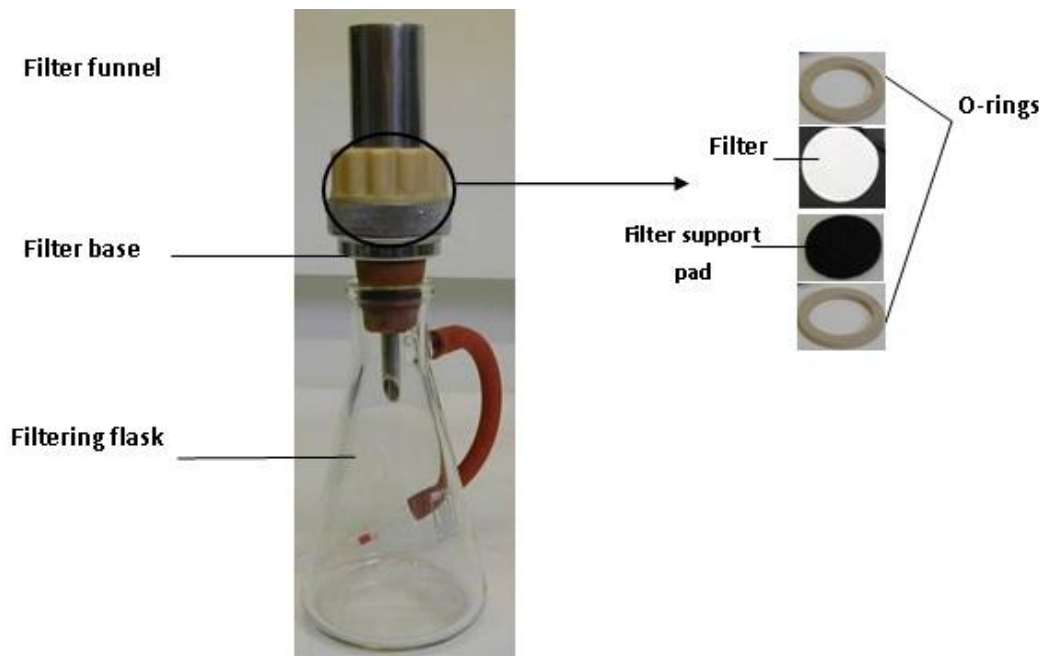


Figure 2.24 Membrane filter apparatus

2.6.3.2 Results and discussion of the membrane filtration

It is seen from Figure 2.25 and Figure 2.26 that the numbers of colony forming units (CFUs) increased with increasing surface roughness as can be seen from surface roughness values in Table 2.6. The highest adhesion was on the stainless steel samples (Figure 2.26(c)), although it is not the roughest surface it may be the surface features were of similar sizes to the spores. The spore size is 1 μm and the surface roughness of the disc with the highest recovery was 1.67 μm , this is in agreement with other results from other researchers showing that the bacterial cells are retained in a surface features of similar size to them (Whitehead & Verran 2006).

Table 2.6 Measured surface roughness R_a of aluminium and stainless steel samples for different scan speeds

Scanning speed (mm/s)	R_a (μm), Aluminium	R_a (μm), Stainless steel
200	0.67	1.35
100	1.09	1.67
50	1.33	2.45
Unmarked R_a (μm)	0.23	0.31

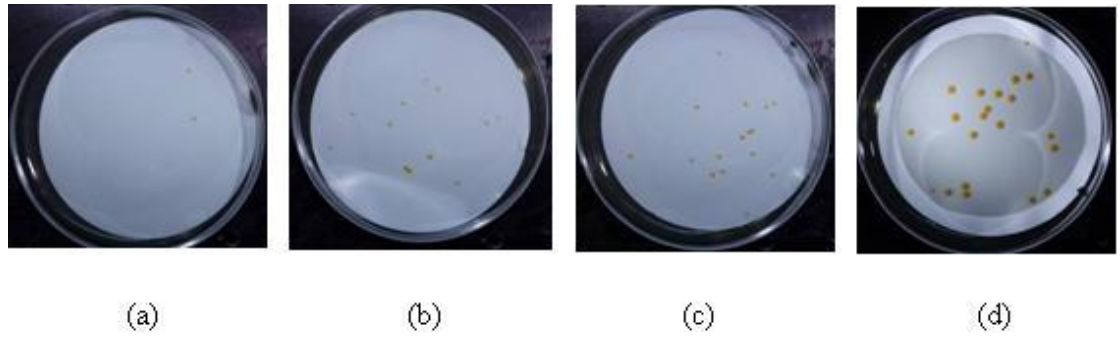


Figure 2.25 Agar plates with recovered *B. atrophaeus* for aluminium samples (a) unmarked (b) marked with scan speed 200 mm/s, (c) marked with scan speed 100 mm/s and (d) marked with scan speed 50 mm/s

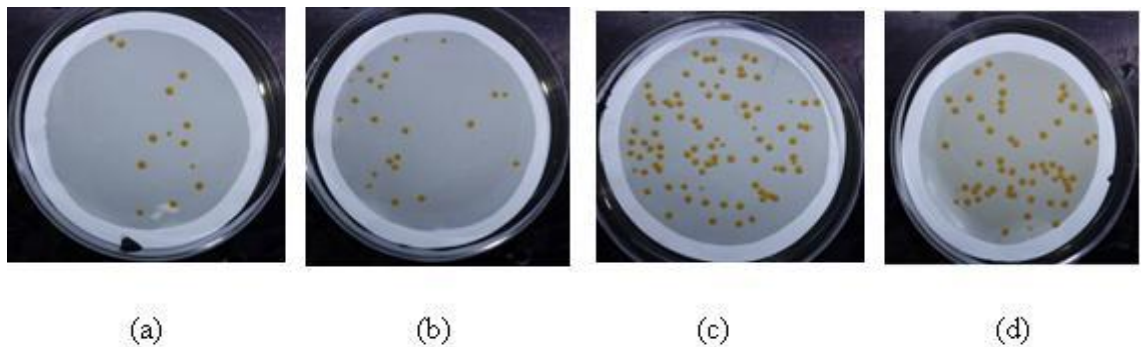


Figure 2.26 Agar plates with recovered *B. atrophaeus* for stainless steel samples (a) unmarked (b) marked with scan speed 200 mm/s, (c) marked with scan speed 100 mm/s and (d) marked with scan speed 50 mm/s

The difference in the level of microorganisms adhered to the discs between samples of high and low surface roughness (smooth surface) was significant. Figure 2.27 shows the numbers of CFUs against different laser marked scanning speeds, and Figure 2.28 shows the numbers of CFUs against roughness. The experiment was repeated and the error bars are the standard deviation for four readings.

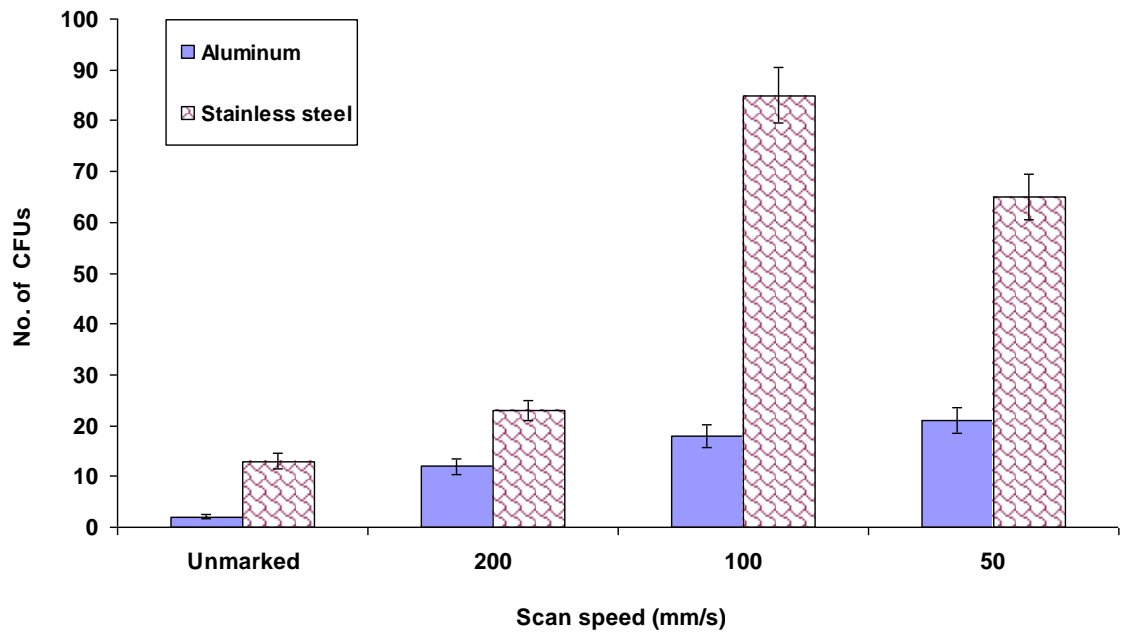


Figure 2.27 Number of colony forming units recovered from aluminium and stainless steel samples for different of laser marking speeds (n = 4)

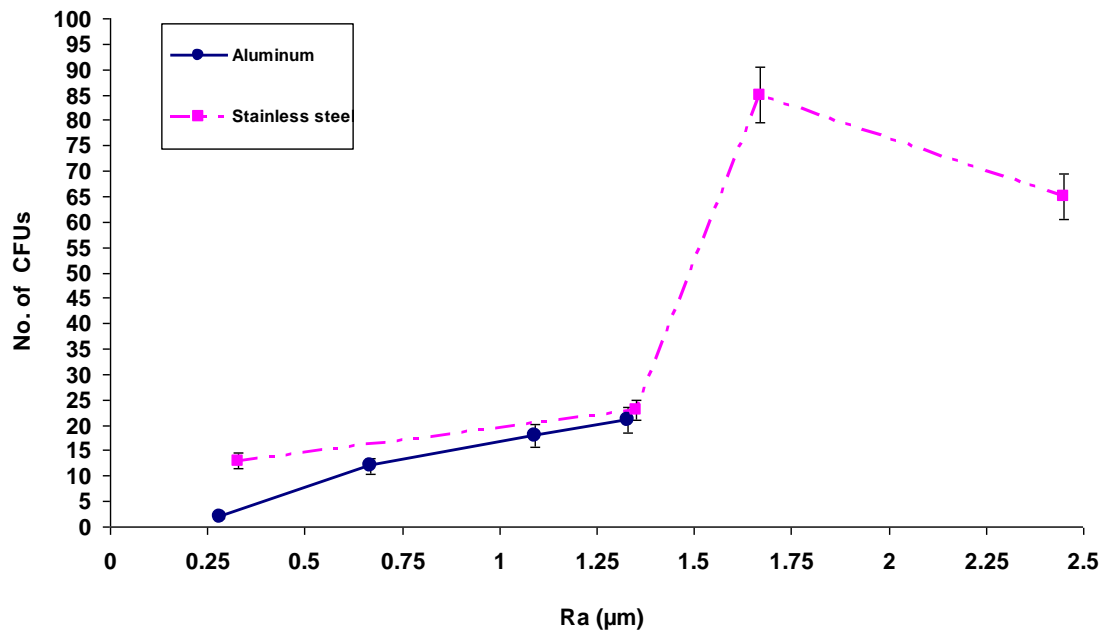


Figure 2.28 Number of colony forming units recovered from aluminium and stainless steel samples against roughness, the error bars show the standard deviation for four readings

A value of R_a nearly equal to $0.2 \mu\text{m}$ was reported as the threshold surface roughness value below which there is no significant difference in bacterial adhesion due to the large size of most bacteria (Carrera *et al.*, 2008). The German institute for standardization (DIN,

Deutsches Institut für Normung) subscribes to a value of $R_a \leq 0.8 \mu\text{m}$ for dairy machine (Flint *et al.*, 2000). These results agree with the results of this work, when the polished discs ($R_a < 0.2 \mu\text{m}$) were used as control no colonies attached on the disc surface. Figure 2.29 shows the polished aluminium and stainless steel discs and the incubated agar plate (control).



Figure 2.29 Polished aluminium and stainless steel discs and the incubated agar plate showing no cell recovery (control)

These results are in agreement with other workers, showing that there is a relationship between adhesion and increased surface roughness (Sousa *et al.*, 2008). This can be explained in that the spores colonizing the grooves or depressions probably get more protection from adverse environmental effects, in this case the airstream in which the spores were moving and they are stuck within these grooves. In this experiment, the laser processing caused raised profiles (grooves) on the metal surface, resulting in increase spore-surface contact area, thereby the spores are retained on the rough surface due to an increased binding energy (Whitehead & Verran 2006). It was observed in Figure 2.27, counts of spores on stainless steel surface marked with scan speed 50 mm/s decreased. It could be expected that higher roughness value, resulting in surface with the features influenced on the microorganism retention, and there may be an optimal roughness for microbial attachment (Verran & Boyd 2001). The level of spore adhesion on stainless steel samples was more than aluminium, this may be due to the stainless steel absorbing the incident laser more than aluminium resulting in deeper markings thereby increased spore adhesion; some researches reported that stainless steel is an attractive surface for adhesion compared with others metals (Flint *et al.*, 2000).

For statistical analysis, the experiments above were replicated and repeated ten times for the different surface roughnesses of the aluminium and stainless steel samples, and the effect of surface roughness on bacterial adhesion was evaluated by colony counting. Due to

some errors during filtration the results from this experiment were more variable. Observed errors included: the filter membrane breaking, microorganisms accumulating on the filtration assembly due to the system possibly not being rinsed efficiently, and during incubation it was possible that the filter lifted off from the plate and no nutrients diffused. So, consequently the numbers of colonies slightly varied for the 10 times of the experiment. This can be seen in Figure 2.30, some plates were uncountable or showed large deviation of CFU per membrane with respect to the others plates.

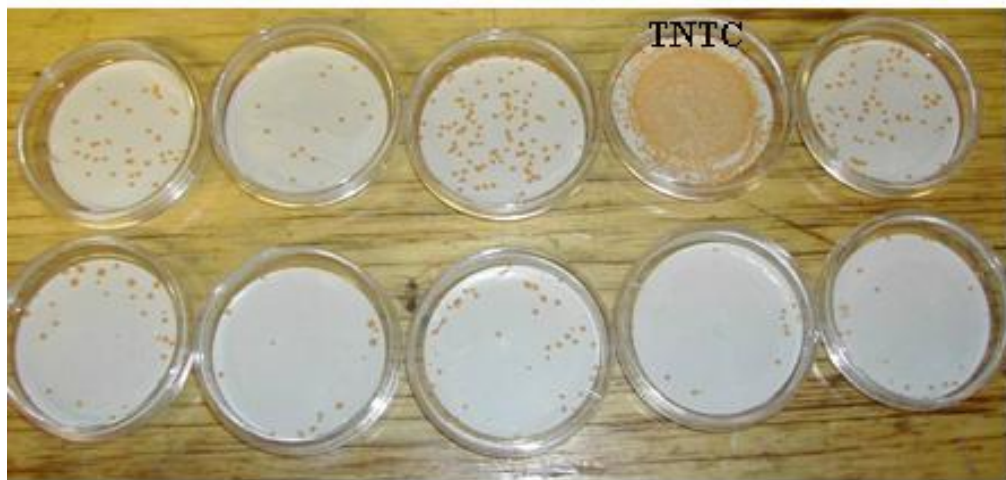
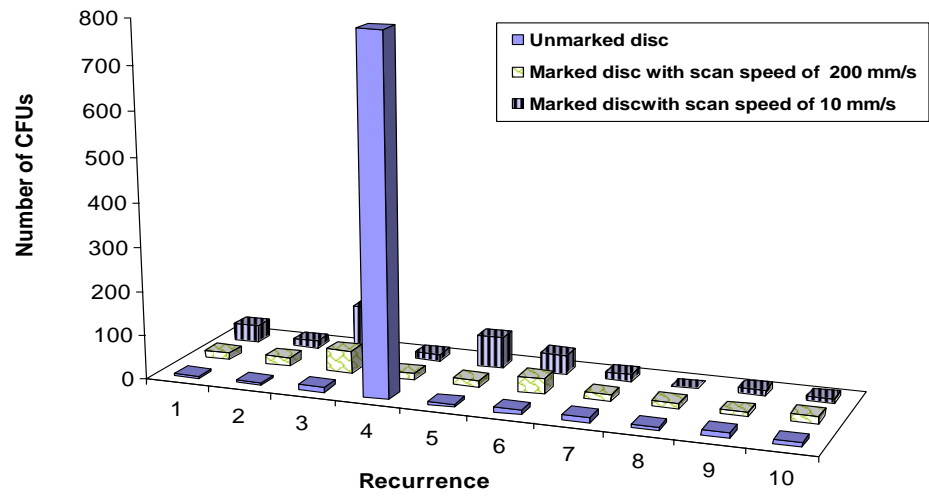
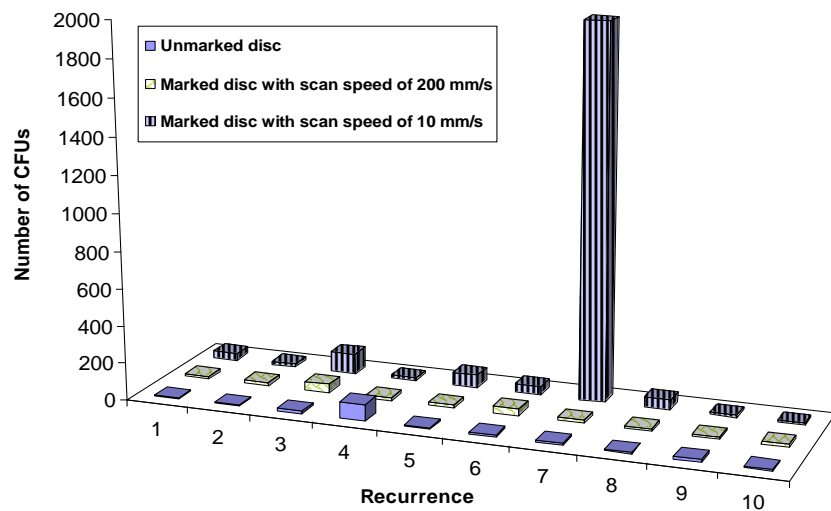


Figure 2.30 *B. atrophaeus* colonies on membrane filters after incubation on agar plates for aluminium discs marked with a laser scan speed of 10 mm/s. Results from one experiment indicating variation

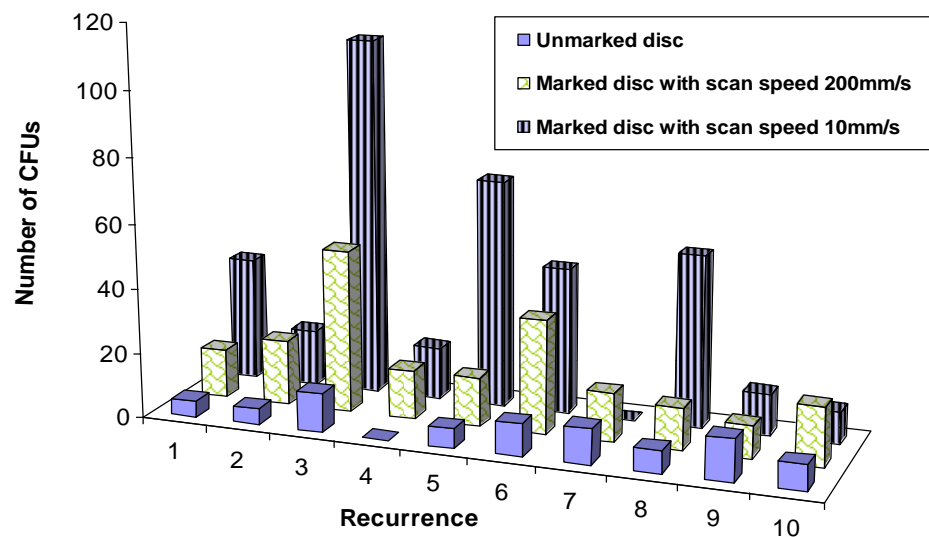
The uncountable plates were removed from the analysis, and the number of colonies greater than 80 per membrane filter were recorded as too numerous to count (TNTC) (Sutton 2006). Figure 2.31 shows the results before and after rejection of outliers.



(a)



(b)



(c)

Figure 2.31 Number of CFUs recovered from the aluminium sample, a) and b) showing some errors of filtration and c) final results after removing the outliers

2.6.4 *Imprinting (pressing) technique*

A spore laden aerosol was passed through an electrode assembly, designed to operate as a plasma for air cleaning and purification (Mine 2010), to determine the spatial distribution of spores on the electrode surface and over the disc used in Chapter 2: Section 2.6.3.1. In the present case, the spatial variation of microorganisms deposited onto the electrode surface with different inlet flow angles was investigated. After appropriate exposure time, the electrodes were pressed into nutrient agar plates and the plates were incubated overnight to determine the spatial distribution of the spores.

2.6.4.1 *Imprint technique with small discs*

5 mL aliquot of *B. atrophaeus* culture was added to 495 mL of sterile distilled water inside the aerosol generator tank, the final concentration of the spores was 10^4 spore/mL. The experimental setup is the same as previously described in the membrane filter protocols (see Figure 2.21, Section 2.6.3.1). The inoculated air from the aerosol generator was passed over the electrode discs for various exposure times (1, 2, 3, 4, 5, 6, 8 and 10 min). After each exposure to the aerosol, the circular discs were picked up using the sterile forceps and the inoculated surface of the disc was placed onto the agar surface at different places according to the exposure time labelled on the plate. The discs were pressed into place gently for approximately 5 s and then removed, as shown in Figure 2.32. After all the experiments were finished, the agar plates were incubated at 37 °C overnight and subsequently investigated for growth.

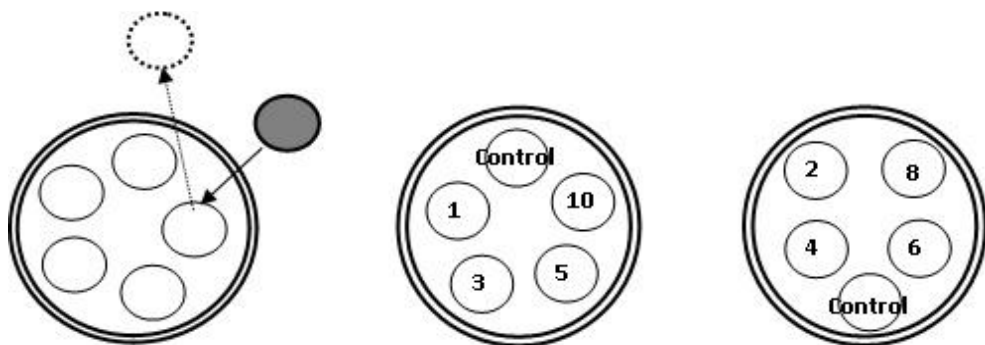


Figure 2.32 Schematic drawing of the circular discs pressed onto the agar surface

2.6.4.2 Results from imprint with small discs experiment

After the incubation, the results, as would be expected, showed that the spore numbers on the discs depended on the exposure time. The first place inoculated onto the agar surface i.e. circle marked 1 or 2 min showed few colonies, while the last circles 8 or 10 min showed the most growth, as shown Figure 2.33, there was no growth on the control discs that did not receive any spore deposition. A disadvantage of this technique is that the numbers are not readily quantifiable.



Figure 2.33 Circular discs pressed on the incubated agar plate for different exposure times

2.6.4.3 Experimental set up of the imprint technique using the long electrodes

The setup of the experiment can be seen in Figure 2.34, which consists of three main parts: the particle aerosol generator, the flow cavity and a HEPA filter, similar to the experimental system described in Section 2.6.3.1 for the membrane filtration.

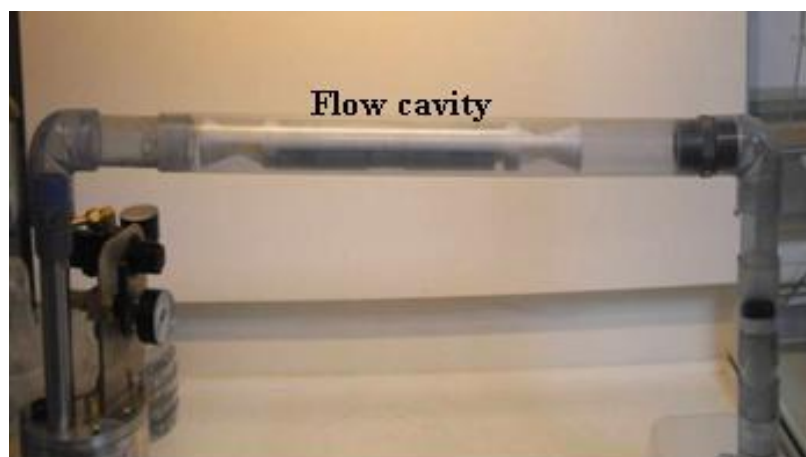
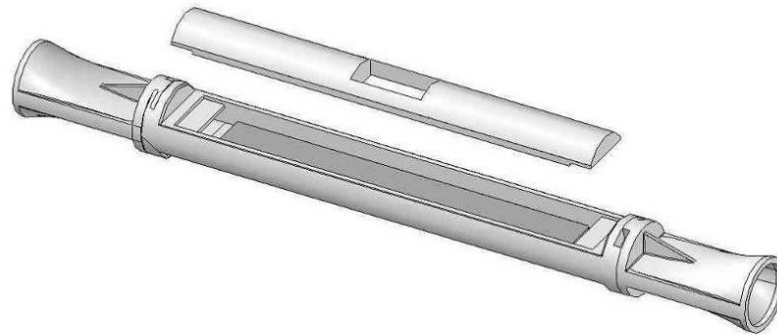


Figure 2.34 The flow system

The flow cavity was designed in-house (Mine 2010). A CAD design of the flow cavity is shown in Figure 2.35 and a detailed photograph of the actual flow cavity is shown in Figure 2.36, which comprises an inlet nozzle with a variable flow entry angle, two parallel aluminium electrodes 200x30x3 mm³ with an air flow gap of 3 mm between them, electrode holders and outlet nozzle.



(a) CAD design of the flow cavity



(b) CAD design of air flow inlet and outlet nozzles (different view)

Figure 2.35 CAD design of the flow cavity system



Figure 2.36 The flow cavity system

2.6.4.4 Generation of the spore aerosol and flow

The air flow stages and preparation of the microorganisms was done as previously described in Sections 2.6.2 and 2.6.2.2. The contaminated air from the aerosol generator was passed between the aluminium electrodes at different angles, 10° and 30° in this work. The air in the flow tubes was pumped out through HEPA filters into the atmosphere so the air was harmless. The experiment was conducted with two different speeds of air flow 2.5 and 5 m/s.

After exposure to the aerosol for about 15 min, the *Al* electrodes were picked up aseptically and the inoculated surface was placed onto the agar in the Petri dishes (240x240 mm²) and pressed gently into place with sterile forceps, the electrodes were left on the agar surface for about 10 min. Figure 2.37 shows the electrodes pressed onto the agar plate. After 10 min the electrodes were removed from the agar and the plates were incubated at 37 C° for 24 hr and analysed for growth.



Figure 2.37 Imprinting of aluminium electrodes

2.6.4.5 Results of the imprint experiment

The spatial distribution of spores at incident angles of flow shaping of 10° and 30° with air flow speed of 2.5 m/s is shown in Figure 2.38. The number of colonies was higher on the electrode end near to the input side (i.e. the flowshaping side) and decreased gradually

along the electrode length until the output end of the electrode. Interestingly, when the air flow speed was increased to 5 m/s (the results can be seen in Figure 2.39) with an inlet angle of 10° , the number of spore colonies on the two ends of the electrodes were higher than in the middle region. While with an inlet angle of 30° the colony numbers were higher on the electrode end nearer to the input side (i.e. the flowshaping side) and the middle region and gradually decreased along the electrode surface.

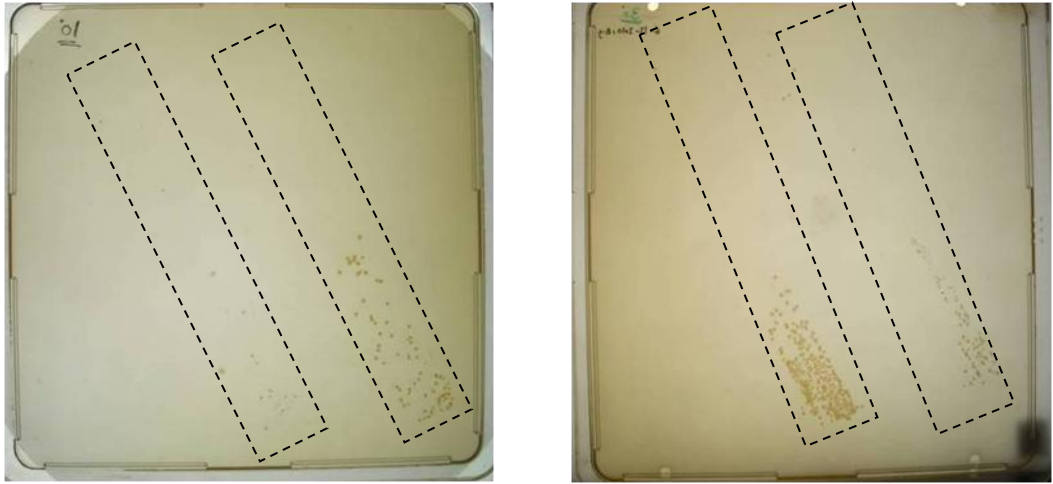


Figure 2.38 Incubated agar plate after exposing the *Al* electrodes to spore laden aerosol with 10° inlet flow angle (left) and 30° (right), aerosol flow speed of 2.5 m/s. The inlet is the bottom right hand corner of the photograph

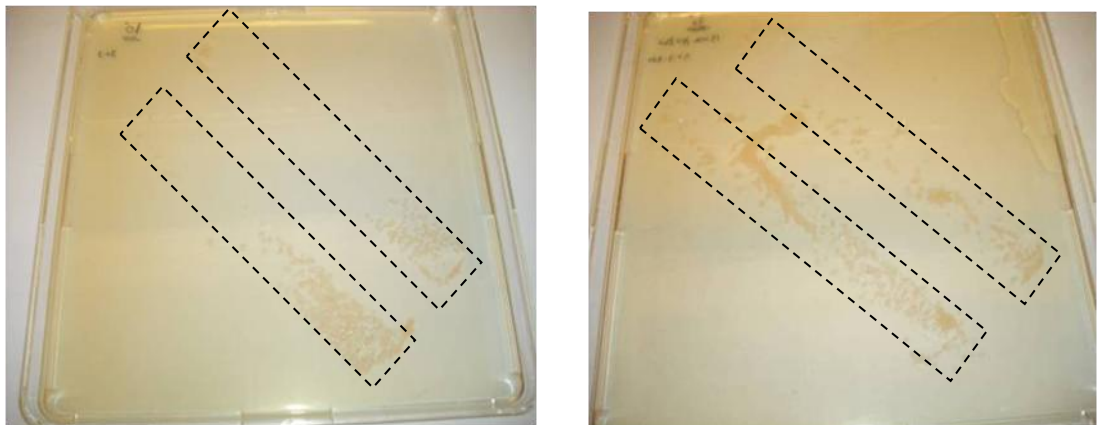
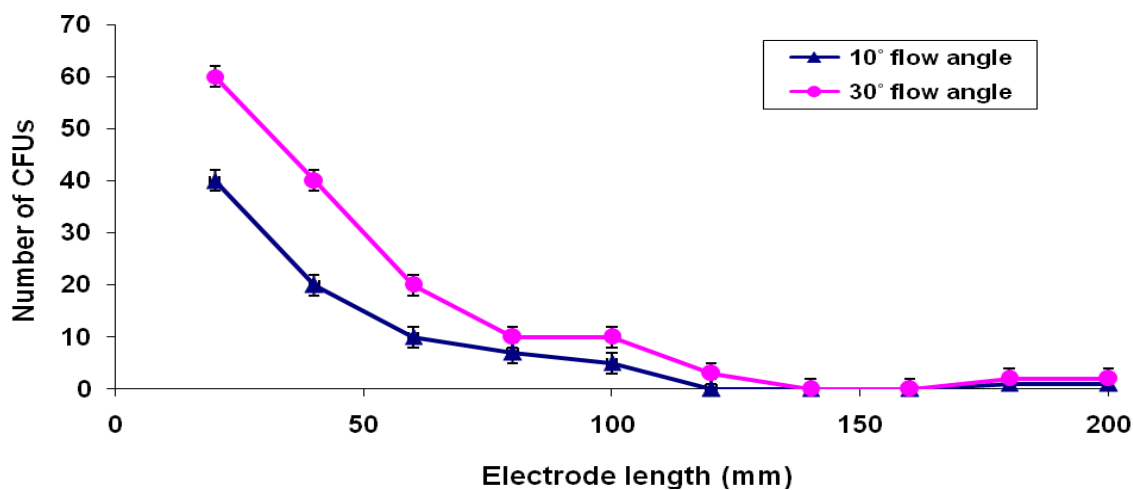
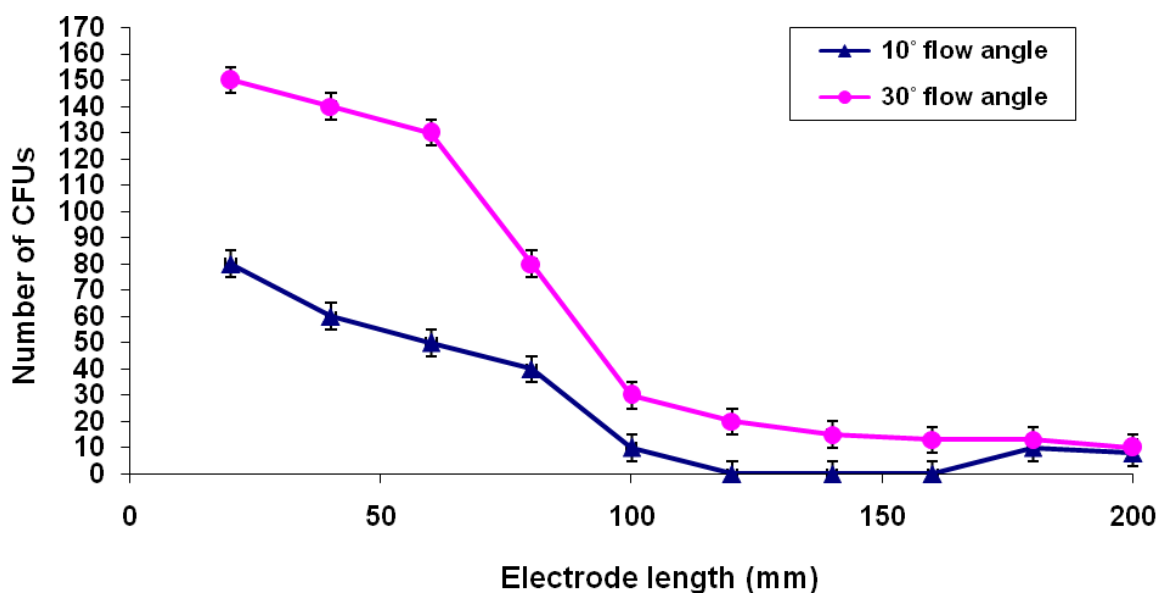


Figure 2.39 Incubated agar plate after exposing the *Al* electrodes to spore laden aerosol with 10° inlet flow angle (left) and 30° (right), aerosol flow speed of 5 m/s. The inlet is the bottom right hand corner of the photograph

The results from the imprinting experiments were analysed in NI vision. Figure 2.40 shows the effect of the inlet flow shaping nozzle angle on the number of colony forming units (CFUs) over different regions of the electrodes. For example, the measurements say at 60 mm is the number of CFU between 40 and 60 mm.



(a)



(b)

Figure 2.40 Number of colony forming units detected along the length of the aluminium sample for different inlet flow angles of 10° and 30° at an aerosol flow speed of a) 2.5 m/s and b) 5 m/s. The error bars show the standard deviation (n = 3)

2.6.5 CFD modelling

Computational Fluid Dynamics (CFD) models were developed to predict the particle (*Bacillus atrophaeus* spores) flow trajectories through two electrodes. The objective of the modelling was to track the particulate flow through the electrodes, and to determine the velocity profile and spatial concentration of particles. Figure 2.41 shows the schematic diagram of the model.



Figure 2.41 The electrode pair schematic

The electrodes were created and meshed with Gambit 2.4 (Fluent Inc., UK) and modelled with Fluent 6.3 (ANSYS Inc., UK). The 3D simulation with standard $k-\varepsilon$ model for turbulent simulation and discrete phase model were used to solve the particle flow on rough surfaces. See Chapter 1: Section 1.6 computational fluid dynamics (CFD) modelling for more details.

The particles/aerosol was released from the inlet surface of the electrodes with a velocity of 5 m/s and pressure 0.75 bar, to match the experimental conditions. The dispersion of particles due to the turbulent fluctuations in the flow was modelled by a stochastic tracking approach. The diameter of the particles (*Bacillus atrophaeus*) was 1 μm and the density was 1201 kg/m^3 (Carrera *et al.*, 2008). Figure 2.42 shows a view of the meshed electrodes.

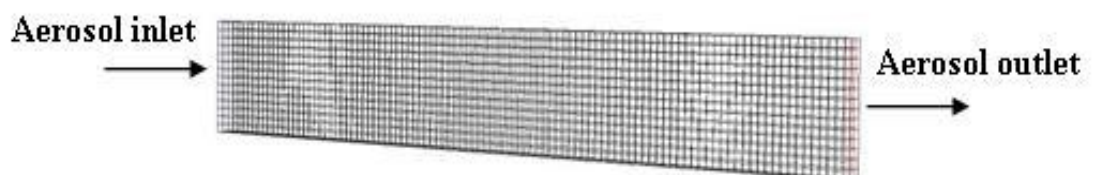


Figure 2.42 The meshed electrodes schematic

According to the CFD calculations, the particles were uniformly moved on the rough surface although the flow was turbulent; this is due to the small particle size ($1\ \mu\text{m}$ diameter) so the particles just follow the air stream. There was turbulence in the particle velocity near the inlet side and the edges due to the turbulent field in the boundary layer but the flow became smoother in the middle of the gap between the *Al* electrodes towards the outlet side. The variation in the aerosol velocity profile (on the inlet and outlet side) along the electrode length can be seen in Figure 2.43. The input velocity is 5 m/s compared to the output velocity (4.5 m/s).

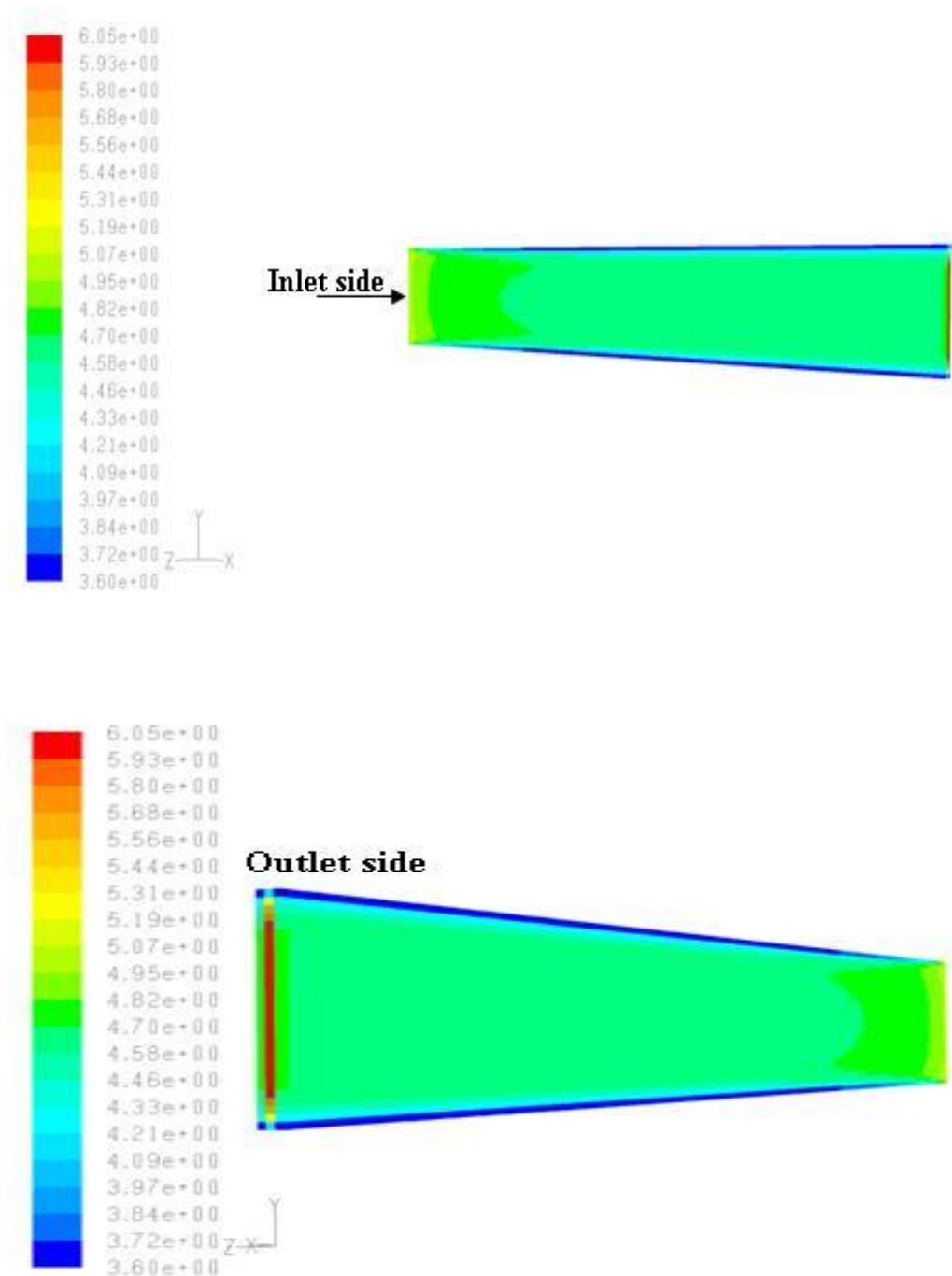
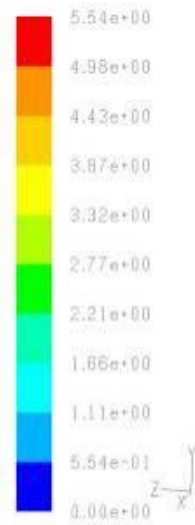


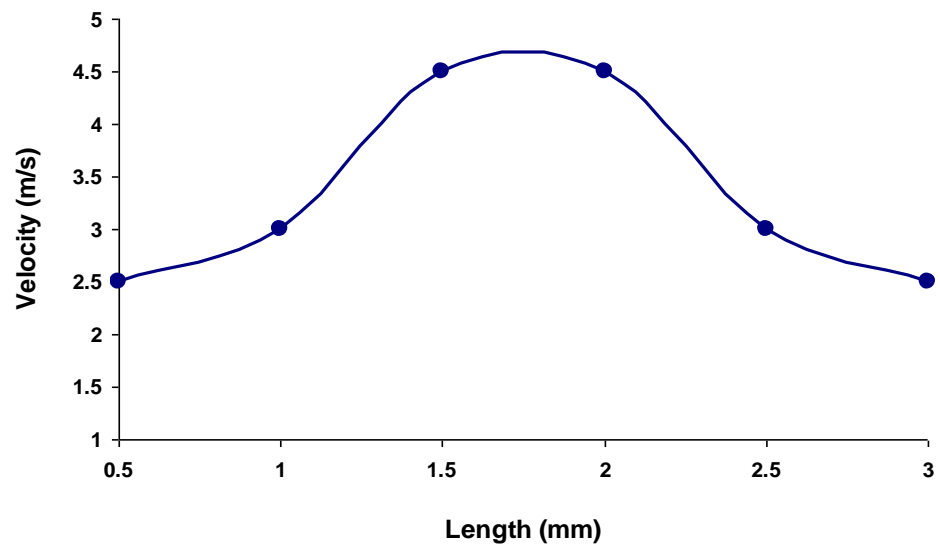
Figure 2.43 Velocity profile on the inlet and outlet side of the *Al* electrodes.

The flow velocity in units of m/s

The velocity profile at the vertical plane cutting through the outlet can be seen in Figure 2.44; the figure shows a zoom view on the outlet side (a), and the velocity profile with an air flow gap of 3 mm between the two electrodes (b).



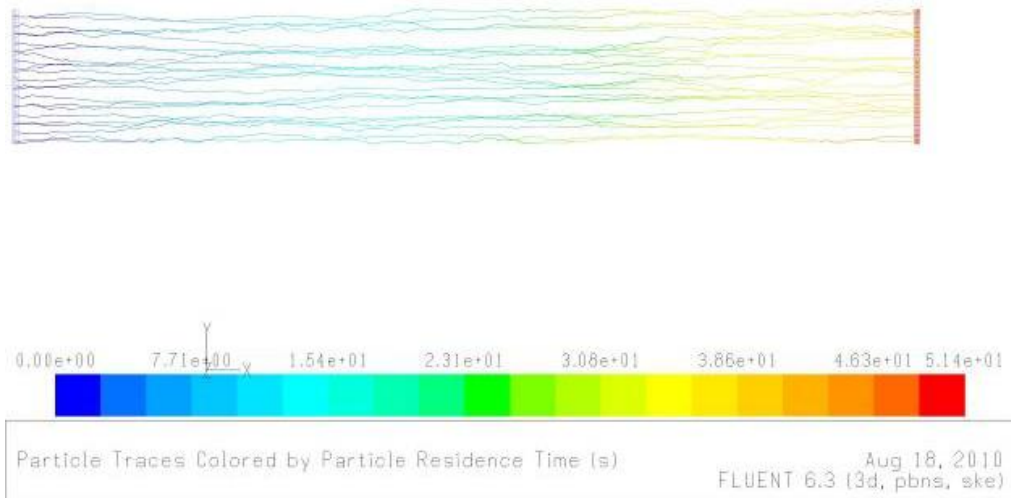
(a)



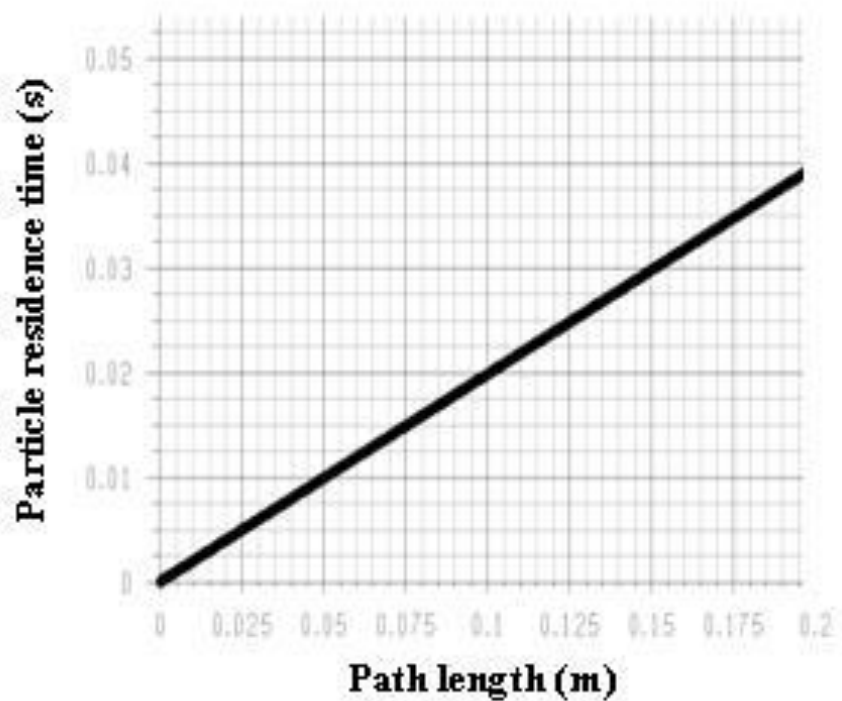
(b)

Figure 2.44 a) Velocity profile on the outlet side across the electrode, and b) particle velocity distribution on the outlet side between the electrodes, across the middle section of the gap

Figure 2.45 shows the stream lines of the spore flow and their residence time in a particular system that starts from the electrode inlet (time 0) and flows towards the outlet (exit time gives the residence time).



(a)



(b)

Figure 2.45 a) Spore stream lines and b) their residence time, path length is the electrode length (200 mm)

The concentration of the spores along the electrode length can be seen in Figure 2.46. It is seen from the concentration results that the particles are distributed all over the electrode surface but it seems to be considerably higher near the electrode edges, and the concentration on the inlet side and along the electrode length was higher than on the outlet side. This is in agreement with the experimental investigation into the bacterial deposition between the electrodes, Section 2.6.4.5. The concentration of the spores on the outlet side can be seen in Figure 2.47. The Fluent model revealed that the spore numbers were higher near the edges of the electrode outlet more than in the middle of the electrode.

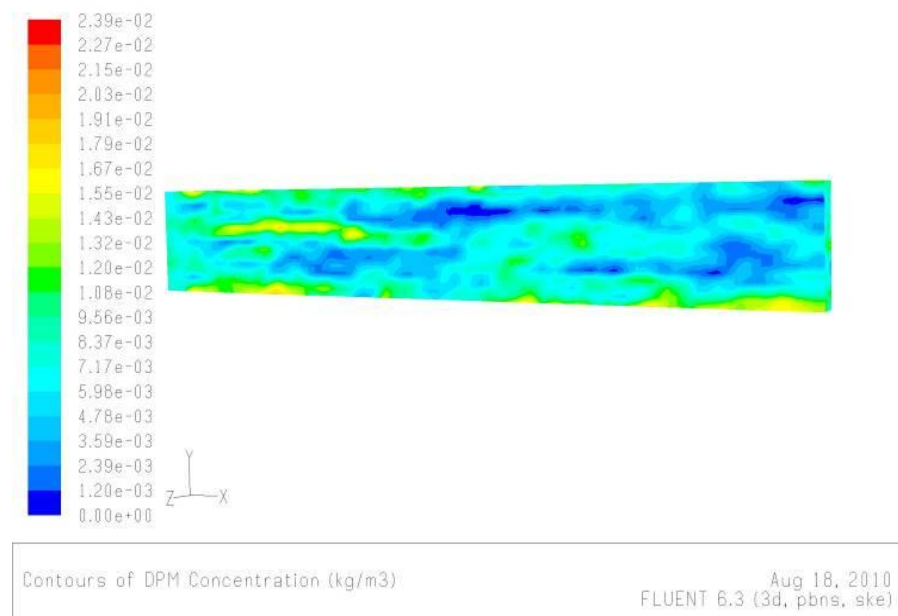


Figure 2.46 Concentration of the aerosol spores on the electrode surface (inlet side is on the left)

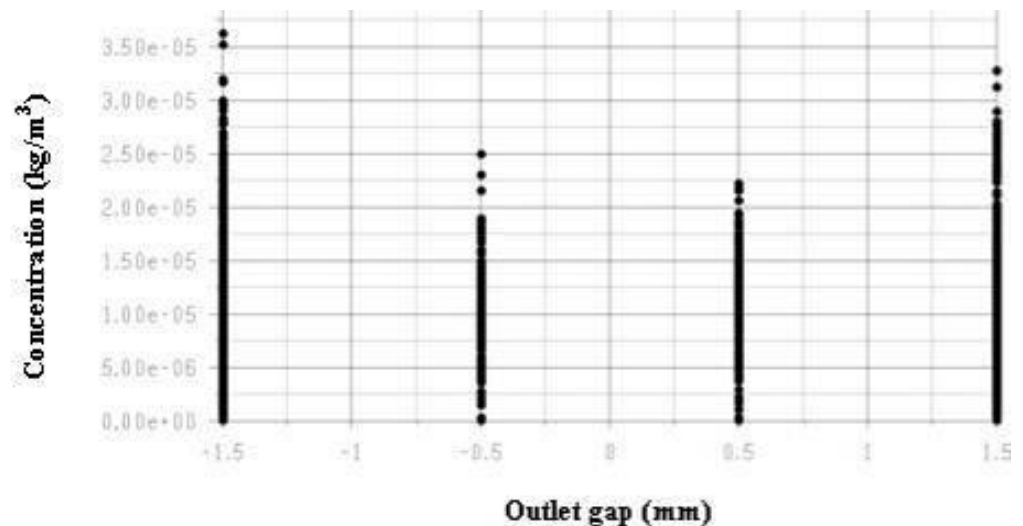


Figure 2.47 Concentration of the aerosol spores at the electrodes outlet, the gap length is 3 mm

Chapter 3

Spatial detection of microorganisms on surfaces and microalgae in liquid

Quantification and enumeration of microorganisms or microalgae is important in microbiological analysis, food and drink industries and environmental monitoring. The detection of microorganisms is important to avoid and identify health and safety problems (Liu 2008), and some pathogenic microorganisms which can be used as biological warfare agents (Ivnitski *et al.*, 1999). There are different techniques used to identify and detect microorganisms such as microscopic counting, culturing techniques, flow cytometric techniques (Wilks *et al.*, 2013), immunological detection methods (Schloter *et al.*, 1995), biosensors (Leonard *et al.*, 2003), chlorophyll fluorescence sensing (Obata *et al.*, 2009; Fernandez-Jaramillo *et al.*, 2012), chromatography (Noelia Isabel *et al.*, 2013), capillary electrophoresis CE (Desai & Armstrong 2003), DNA molecular techniques (Babalola 2003) and adenosine 5'-triphosphate (ATP) bioluminescence (Yue & Bai 2013). In many detection fields, two or more techniques need to be combined for accurate identification. However, easy, fast, inexpensive and reliable methods are required. In this chapter, various methods were used to cover some of these requirements and included: microscopic examination, use of a flow cell and fluorescence techniques. This chapter discusses the detectable level of *B. atrophaeus* (*B. globigii*) spores on rough, polished and glass surfaces by using microscopic detection. The fluorescence spectra measurements were investigated with an in house fluorescence microscope, excimer laser and a chlorophyll analyser was used to detect microalgae in water. A flow chamber system was developed for instantaneous cell counting of algal culture, and the captured microscopic images were analysed using NI vision software.

3.1 Probability of detection *B. atrophaeus* spores over an area on rough aluminium surface

The accuracy of counting microorganisms is an important part of any detection process, this is further complicated if there is a cocktail of particles and various microorganisms. For example, cell counting by epifluorescence microscopy and by direct microscopy were found to give more than one log (CFU/cm²) higher than the cultivation method (Fuster-Valls *et al.*, 2008). The accuracy of counting is dependent on many variables including the spatial distribution of the microorganisms, clustering, and their concentration. In the present case, this work was designed to find the minimum detectable level of spores. The efficiency of microscopy detection of *B. atrophaeus* spores deposited on an aluminium sample was investigated. Aliquots (50 µL) of the *B. atrophaeus* spore suspension of concentrations of 10³, 10⁴, 10⁵, 10⁶ and 10⁷ CFU/mL were pipetted onto the surface of rough aluminium discs (25 mm diameter) of average surface roughness $R_a = 2 \mu\text{m}$, measured with profilometer Tallysurf (Surtronic 3P, Taylor Hobson, Denmark). The culture drop ~ 8 mm diameter and ~ 1.4 mm high was dried for ~ 3-6 hr to allow evaporation without spreading, the spore distribution on the aluminium was then observed and the spores counted. The area around the culture drop was marked to ease locating the position of the drop during microscopic examination, as shown in Figure 3.1.



Figure 3.1 Drop of *B. atrophaeus* culture on different areas of aluminium disc (10³ and 10⁷ CFU/mL)

The samples were examined using a differential interference contrast (DIC) microscope (Nikon Eclipse, ME600, Japan) in the dark field mode. Figure 3.2 shows the microscopic setup. An introductory examination of the samples was done using low magnification

objectives of 5X or 10X (Nikon EPI, 0.4 NA, Japan) in order to locate the drops. Then a high magnification objective (100X) was used. The magnification power of the eyepiece is equal to 10X, and the overall optical magnification of the microscope is the product of objective magnification and eyepiece magnification. The microscopic inspection procedure was carried out using a manual scanning technique, starting at the edge of sample drop then continuing towards the centre then to the other edge, both in the horizontal and vertical direction, as shown in Figure 3.3. Each square represents the screen area at the magnification used with dimensions of 3072x3840 pixel. It was important to convert the screen dimensions from pixel to micrometer. The image calibration was done by using a stage graticule micrometer (Pysen-SGI, 100 μm in 10 μm divisions, UK), and the calibrated factor was found to be 0.0355 μm /pixel (see Appendix C: microscope calibration). At least 20 discs for each *B. atrophaeus* density were used and more than 40 measurements were taken both in the horizontal and vertical direction, these 80 images, taken with a CCD camera (Nikon, DXM1200, Japan) mounted on the microscope, were examined.

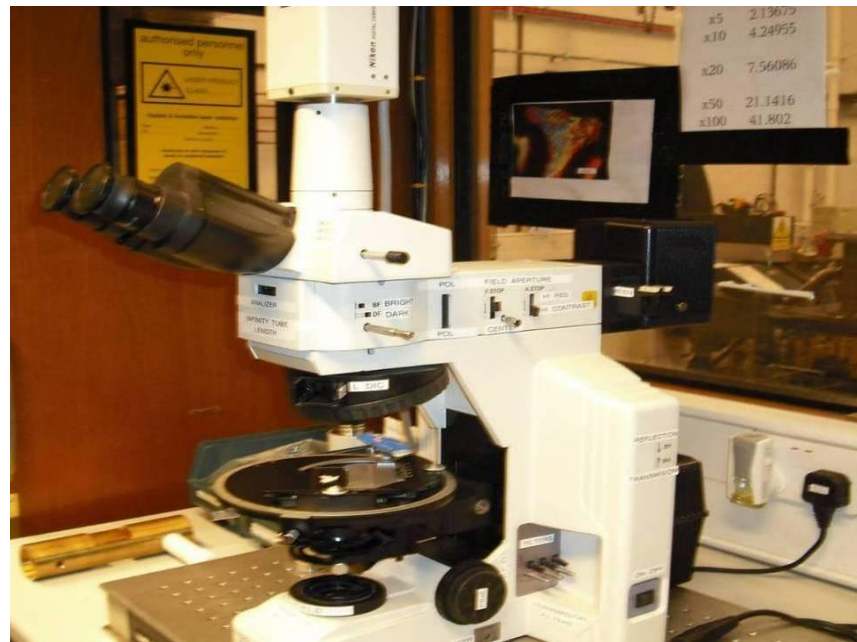


Figure 3.2 Nikon Eclipse ME600 microscope with Nikon camera DXM1200

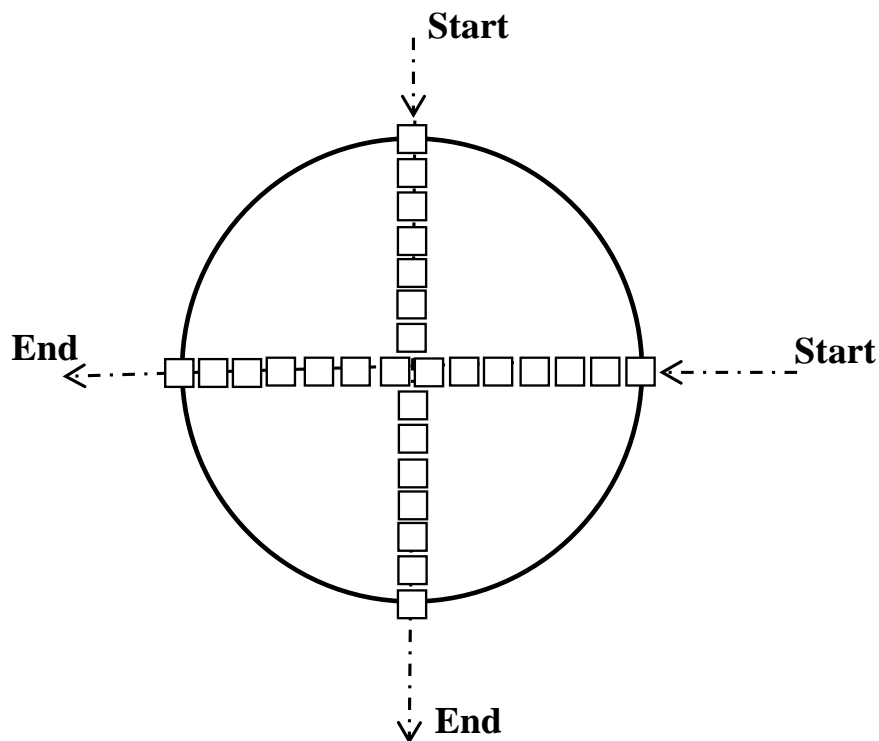
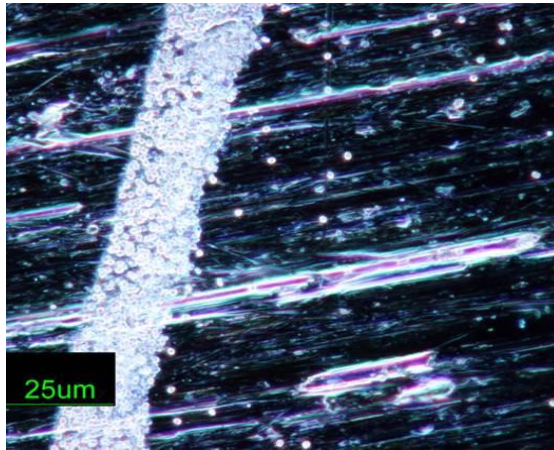


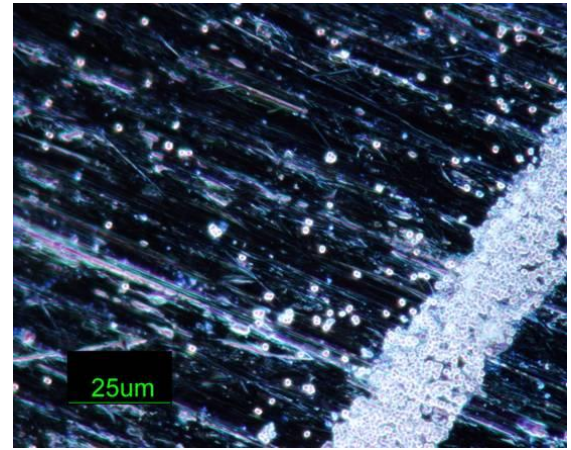
Figure 3.3 A systematic model used for microscopic analysis of aluminium samples inoculated with different concentrations of *B. atrophaeus* in a water droplet

3.1.1 Results of B. atrophaeus spores over an area on rough aluminium surface

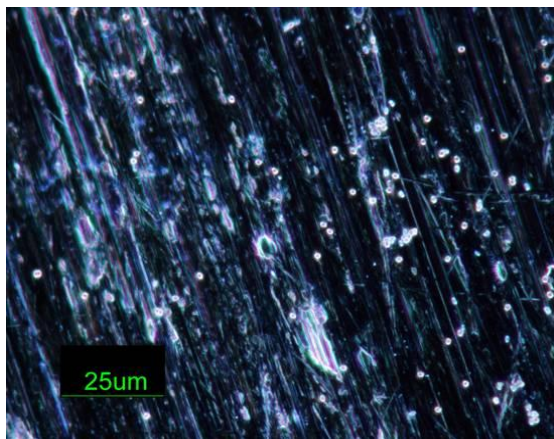
After microscopic examination, the results showed that at the edge of the drop a large number of spores had accumulated, as shown in Figure 3.4. This is agreement with Cardoso *et al.* (1998) who reported that *E. coli* accumulated at the edge of a drop of urine. The deposition of particles at the drop edge in the ring pattern is called the coffee-ring effect. This phenomena is due to the capillary flow during the drying processes, the particles suspended in liquid flow from the drop centre to the edge as evaporation proceeds (Yunker *et al.*, 2011). To accurately determine the spore counts in the high density regions, the data was analysed using image processing software (NI Vision 8.5, National Instruments, USA) and compared with manual counting procedures. The threshold value of detection was set to 1 μm to correspond to the size of the spores. The image intensity was optimised to try and distinguish between spore clusters; this was problematic but the occurrence of these clusters was relatively low, placing higher confidence on the detected counts. The steps for this process are detailed in Chapter 1: Section 1.5.



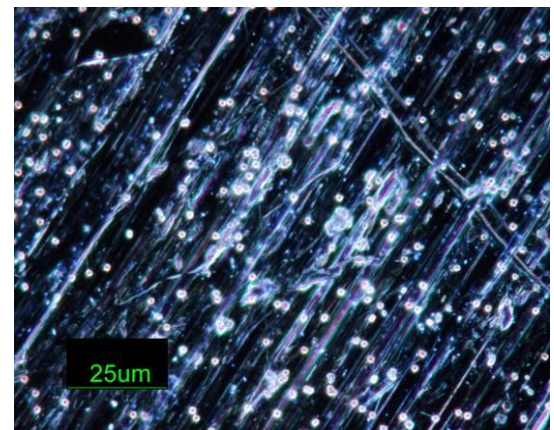
(a) at the edge



(b) at another edge



(c) between the edge and the centre



(d) at the centre

Figure 3.4 Microscopic distribution of *B. atrophaeus* spores from a culture drop (10^7 CFU/mL) on an aluminium surface. The thick white mark in (a) and (b) is the spores at the edges. Nikon Eclipse microscope ME600. Nikon camera DXM1200

The data in Figure 3.4 was analysed with NI Vision (see Chapter 1: Section 1.5) to estimate the number of spores over the drop area. The results can be seen in Figure 3.5. Analysis of the microscopic images showed that the number of spores decreased away from the edge of the drop and towards the middle, then increased again in the centre. And after that the spore number increased again towards the other edge, showing some symmetry as would be expected. It is seen that the counts were about 14 times greater at the edge than the first minimum, and about 4 times that at the centre.

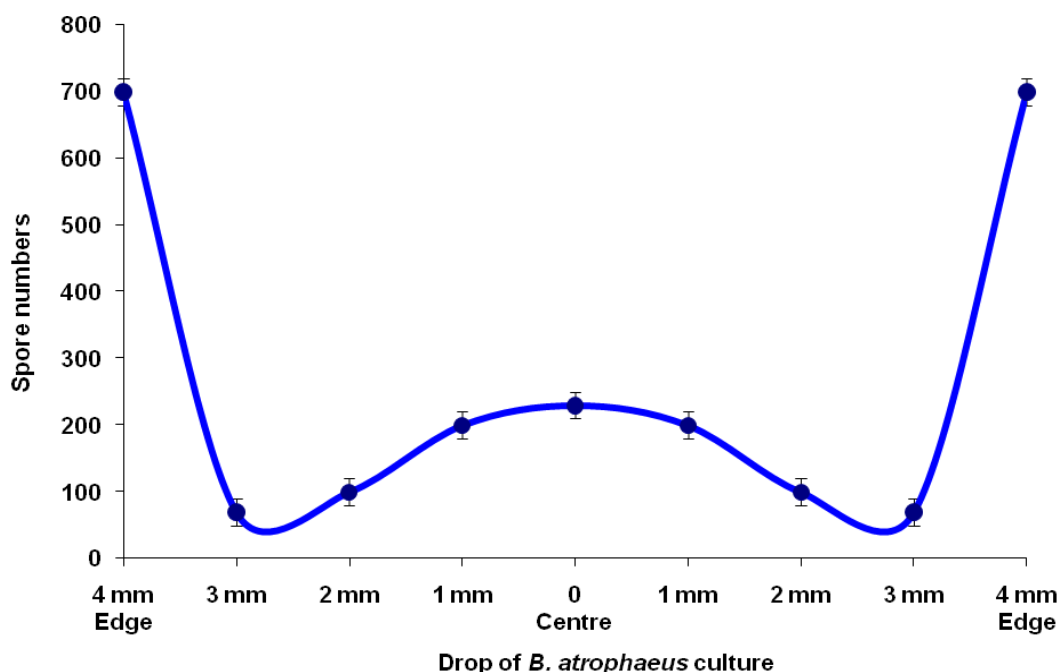


Figure 3.5 Distribution of *B. atrophaeus* spores from an evaporated drop on an aluminium surface (10^7 CFU/mL). The errors were calculated from the standard deviation of 20 reading ($\theta = \pi$)

3.1.2 *B. atrophaeus* suspension of different densities

Further tests were done to find the number of spores for different culture concentrations. Aliquots of *B. atrophaeus* suspension (50 μ L) were made for different densities namely 10^3 , 10^4 , 10^5 , 10^6 and 10^7 CFU/mL. The spores were counted using the same microscope system as described in Section 3.1 and NI vision, and the results can be seen in Table 3.1. The results showed that the minimum detectable level was $\geq 10^4$ CFU/mL, and below that concentration no spores were seen.

Table 3.1 Observed value of *B. atrophaeus* (CFU/area) on aluminium discs for different culture concentrations. The spores were taken per unit area (observation field of the microscope) of 0.0148 mm^2

Concentration (CFU/mL)	<i>B. atrophaeus</i> (CFU/area, average)
10^2	0
10^3	0
10^4	1
10^5	3
10^6	17
10^7	135

Theoretical calculations were done to compare the likely deposited number with the results from experimental detection. The average number of spores per surface area of deposition (CFU/area) was estimated by the following relation:

$$Spore\ number = \frac{V_c * C_c * A_s * C_f^2}{A_d} \quad \text{Equation 3.1}$$

Where V_c is the volume of culture (50×10^{-3} mL), C_c is the concentration of the culture (CFU/mL), A_s is the surface area of deposition (0.0148 mm^2) or observation field of the microscope (3072×3840 pixel), C_f is the calibration factor ($0.0355 \text{ }\mu\text{m/pixel}$) and A_d is the drop area (50 mm^2).

A comparison of the expected and observed spores/area can be seen in Table 3.2. The theoretical calculations showed that the applied spore numbers were slightly greater than the experimental counts, but there is no significant difference between them ($P < 0.93$) as confirmed by using student's t-test (Excel, 2007).

Table 3.2 Observed and expected values of *B. atrophaeus* spores per unit area (0.0148 mm^2) on Al disc

Concentration (CFU/mL)	<i>B. atrophaeus</i> (CFU/area)	
	Observed value	Expected value
10^2	0	0.0015
10^3	0	0.015
10^4	1	0.15
10^5	2	1.5
10^6	12	15
10^7	135	150

3.1.3 Detecting spores outside of the drop region

Spores were detected away from the drop's edge even though the spores are attracted to this region, as shown in Figure 3.6. This may be due to spore dispersal during pipetting or

due to contamination during microscopic examination, sample preparation or microfluidic motion during the evaporation process.

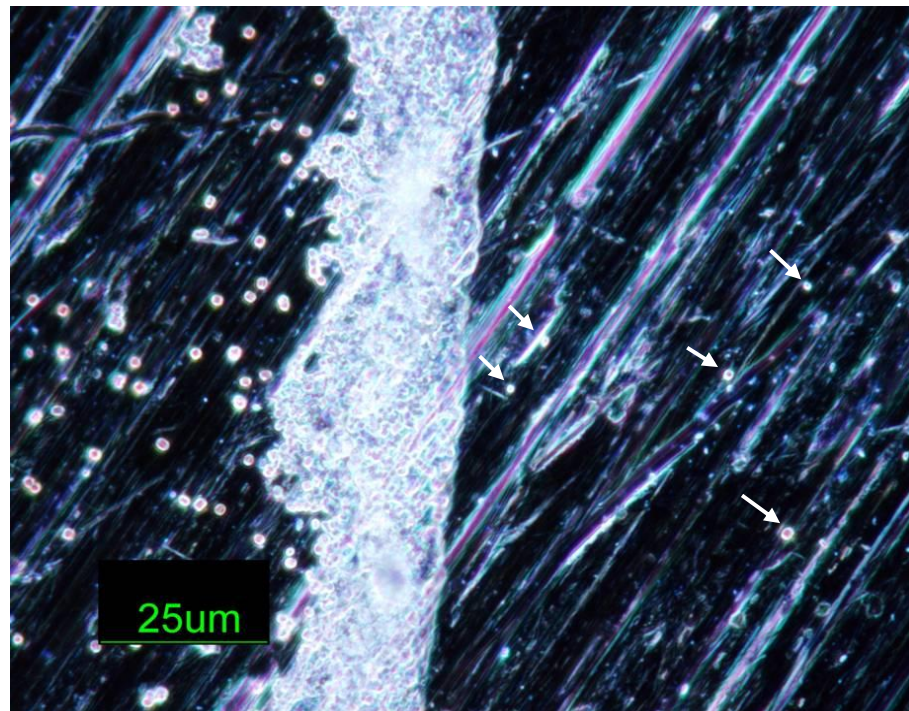


Figure 3.6 Arrows indicate the *B. atrophaeus* spores outside of the drop's edge, on the right hand side

3.1.4 Alignment of B. atrophaeus on aluminium surface

The effect of the surface roughness of the aluminium on alignment of the spores could be observed in some areas. The spores covered the scratches and irregularities in the same direction as the surface defects. The spatial arrangement of spores was observed using the Nikon microscope with a Wollaston prism and polarizer. Figure 3.7 shows the results of the spore alignment on the aluminium surface, coinciding with surface defects, these were approximately 2 µm roughness. The surface defects may increase the microorganism retention (Verran *et al.*, 2010), and the relative sizes of the defects to the size of the spore cells affect its attachment (Whitehead *et al.*, 2005). So as a consequence the aluminium discs were polished to remove these irregularities and determine the resulting spore distribution.

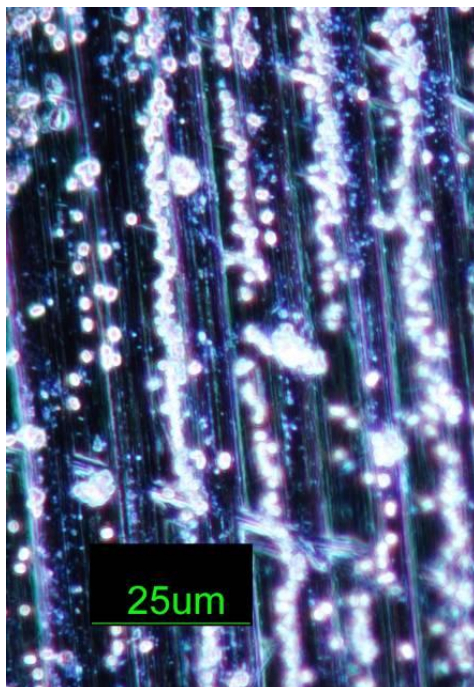
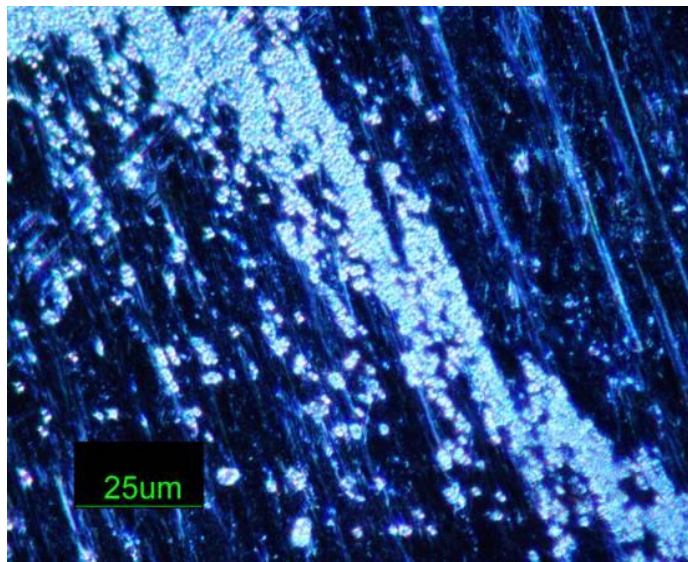
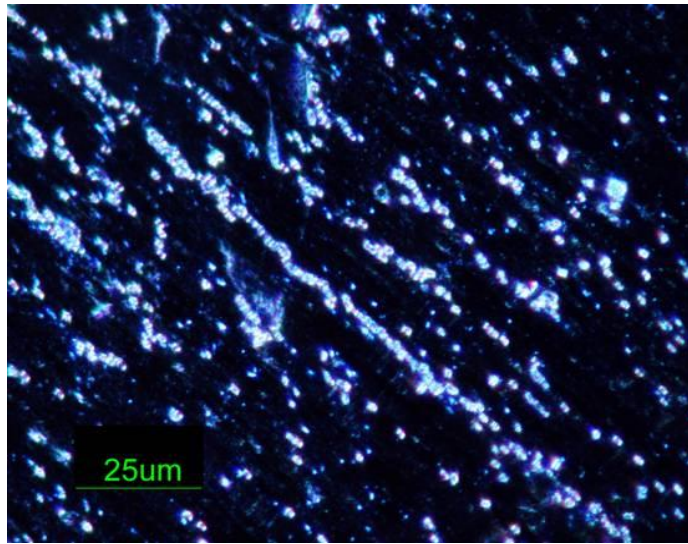
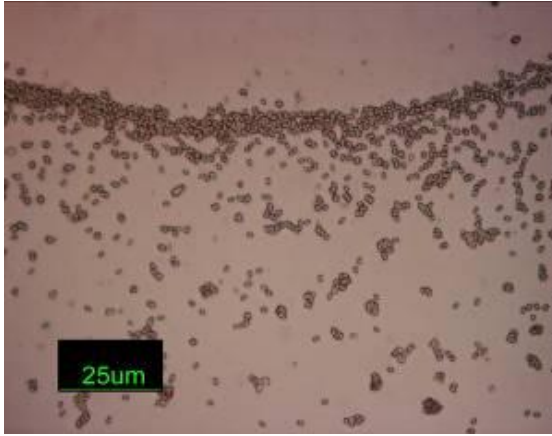


Figure 3.7 *B. atrophaeus* alignment on rough surface of aluminium sample, coinciding with surface defects

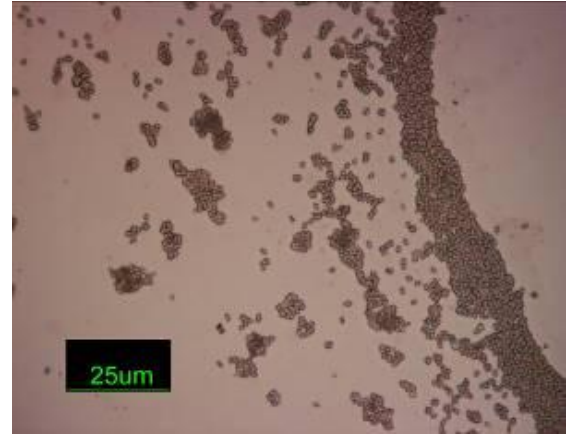
3.2 Microscopic detection of *B. atrophaeus* spores over an area on polished aluminium disc

Aliquots (50 μL) of *B. atrophaeus* spore suspension of 10^6 and 10^7 CFU/mL culture densities were pipetted on to the surface of polished aluminium disc ($R_a = 0.95 \mu\text{m}$) (see Chapter 2: Section 2.2.2: Polishing). The counts were done by taken 20 images on different locations of the aluminium sample, and following the same procedure for counting as described in Section 3.1. Figure 3.8 and Figure 3.9 show the results of the microscopic distribution of *B. atrophaeus* on the polished aluminium discs for the different deposition concentrations. Without surface defects there was no apparent spatial geometry of the spores, they were distributed randomly over the sample. There was no significant difference in the results for the different deposited spores either on the rough or smother surface (see Table 3.2).

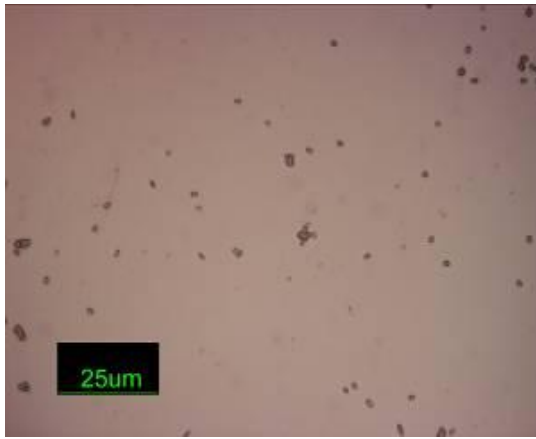
Surface defects on the aluminium had an effect on the drop shape. Large defects (unpolished disc, $R_a \sim 2 \mu\text{m}$) led to circularly shaped drops, but smaller surface defects (polished disc, $R_a < 2 \mu\text{m}$) provided irregular shaped drops because of the reduce contact angle.



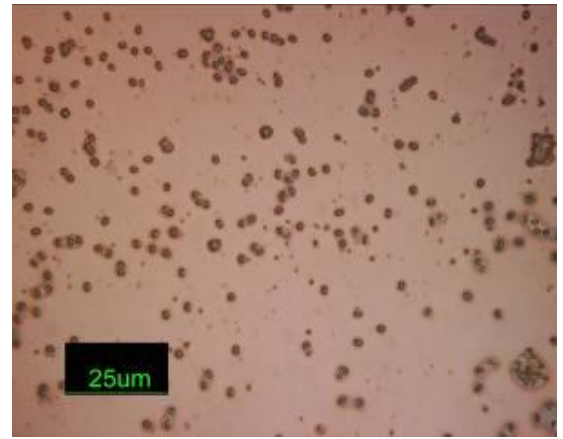
(a) at the edge



(b) at another edge



(c) between the edge and the centre

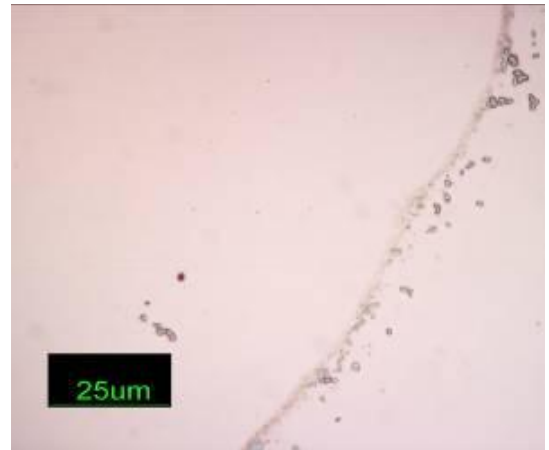


(d) at the centre

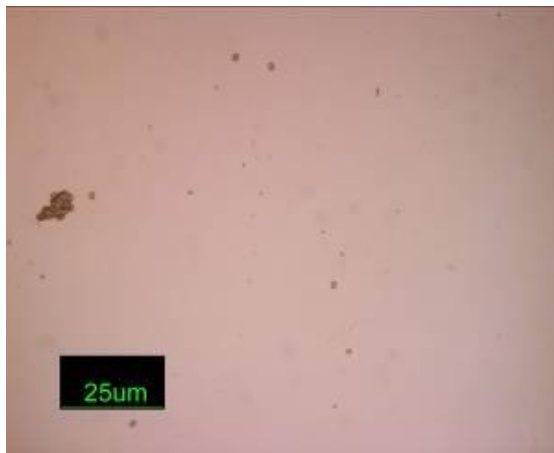
Figure 3.8 Microscopic distribution of *B. atrophaeus* spores (10^7 spore/mL) from a culture drop on a polished aluminium disc. Nikon Eclipse, Normasky ME600 (bright field mode). 100X objective EPI, NA= 0.8. Canon camera DXM 1200



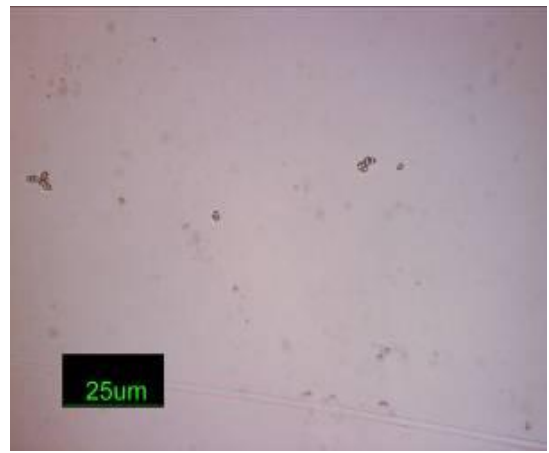
(a) at the edge



(b) at another edge



(c) between the edge and the centre



(d) at the centre

Figure 3.9 Microscopic distribution of *B. atrophaeus* spores (10^6 spore/mL) from a culture drop on a polished aluminium disc. Nikon Eclipse, Normasky ME600 (bright field mode). 100X objective EPI, NA= 0.8. Canon camera DXM 1200

3.3 Glass microscope slides

The experiments examining the spore distribution from a drop of culture, following evaporation, were repeated on glass using dried and fresh samples. A drop (50 μ L) of *B. atrophaeus* culture was laid on the glass microscope slides. Even though the same volume of culture was used the drop was \sim 10 mm in diameter which was larger than for aluminium (8 mm), and \sim 1 mm high. This was due to the contact angle with these different materials. The concentrations of the spores were 10^3 , 10^4 , 10^5 , 10^6 and 10^7 CFU/mL. The slides were kept in the fume-cupboard for about 4 hr to dry. The observation was conducted using a Leitz Wetzlar microscope (Orthoplan 2.2, Germany) at 60X objective (NA=0.85, Maopta, Czech), as the Leitz Wetzlar microscope is more suitable for examining spores on glass surface than Normasky. The observation field was 240x360 μ m.

The spores were detected more easily than on the metal surfaces. The results showed that again the spores were attracted to the edge, as shown in Figure 3.10, Figure 3.11 and Figure 3.12, which show the spore distribution for 10^7 , 10^6 and 10^5 CFU/mL respectively.

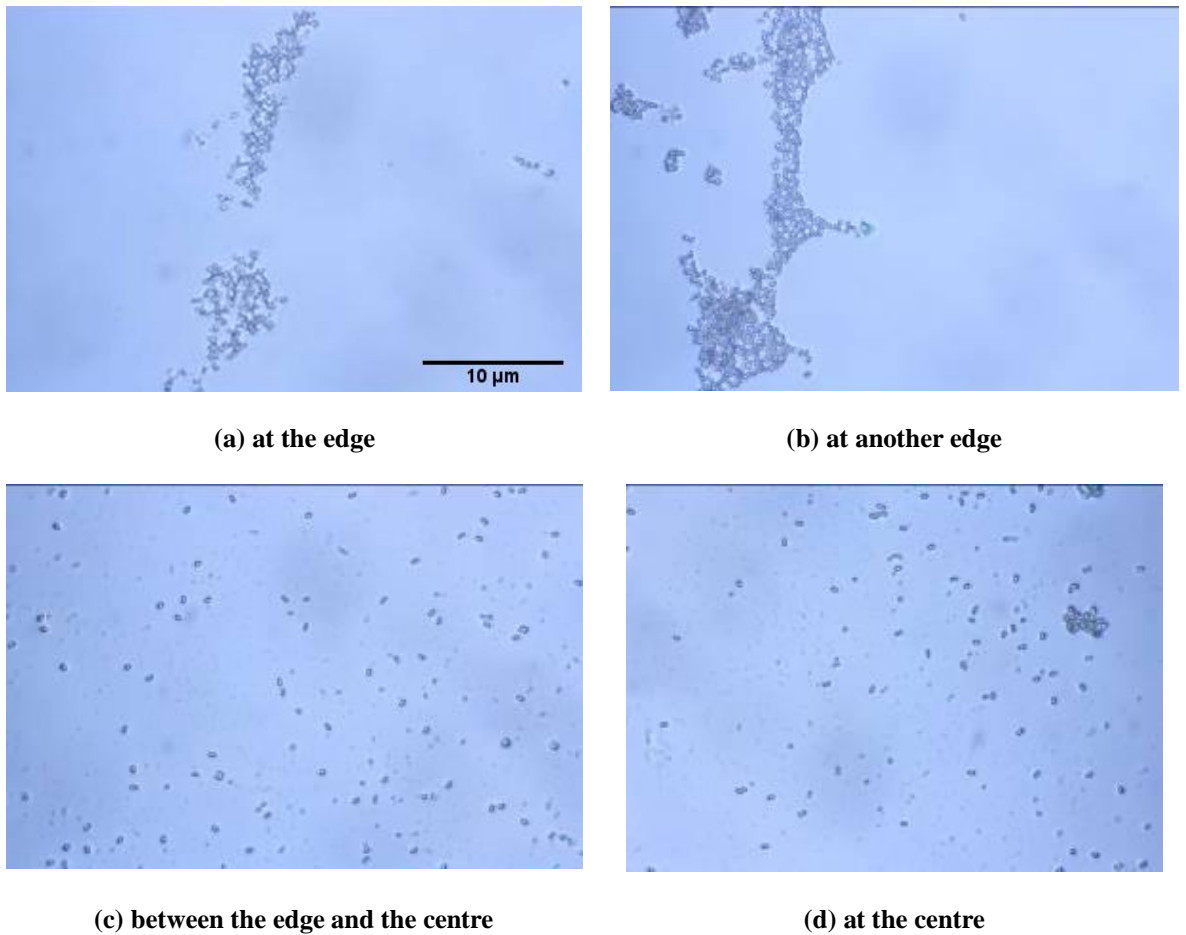
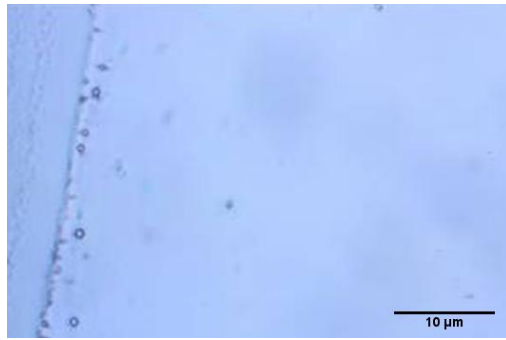


Figure 3.10 Microscopic distribution of *B. atrophaeus* spores (10^7 CFU/mL) from a culture drop on a glass surface. Leitz Wetzlar microscope, 60X objective, NA=0.85. Canon camera D1000



(a) at the edge



(b) at another edge



(c) between the edge and the centre



(d) at the centre

Figure 3.11 Microscopic distribution of *B. atrophaeus* spores (10^6 CFU/mL) from a culture drop on a glass surface. Leitz Wetzlar microscope, 60X objective, NA=0.85. Canon camera D1000



(a) at the edge



(b) at another edge



(c) between the edge and the centre



(d) at the centre

Figure 3.12 Microscopic distribution of *B. atrophaeus* spores (10^5 CFU/mL) from a culture drop on a glass surface. Leitz Wetzlar microscope, 60X objective, NA=0.85. Canon camera D1000

The spore numbers were quantified using the same protocol as described in Section 3.1 and Equation 3.1. Table 3.3 shows the counts of *B. atrophaeus* spores experimentally observed and the theoretically expected values. No significant difference was observed between the theoretical and experimental results by using the student t-test $P < 0.98$ ($P < 0.05$ is required for statistical significance), and the results showed that there is good agreement between the observed and the expected values.

Table 3.3 Counts of *B. atrophaeus* on the glass slide samples. Area is the observation field of the microscope which was 0.0864 mm^2

Concentration (CFU/mL)	<i>B. atrophaeus</i> (CFU/area)	
	Observed value	Expected value
10^2	0	0.0054
10^3	0	0.054
10^4	1	0.54
10^5	5	5.4
10^6	47	54
10^7	537	544

The number of spores in Figure 3.10, Figure 3.11 and Figure 3.12 was analysed using NI Vision 8.5 (National Instruments, USA) (see Chapter 1: Section 1.5 Introduction to NI vision). A spatial plot can be seen in Figure 3.13. The spore number over the drop area was similar to the counts in Section 3.1.1 (see Figure 3.5), but the spore number on glass was greater at the centre and smaller at the edge than on aluminium surface.

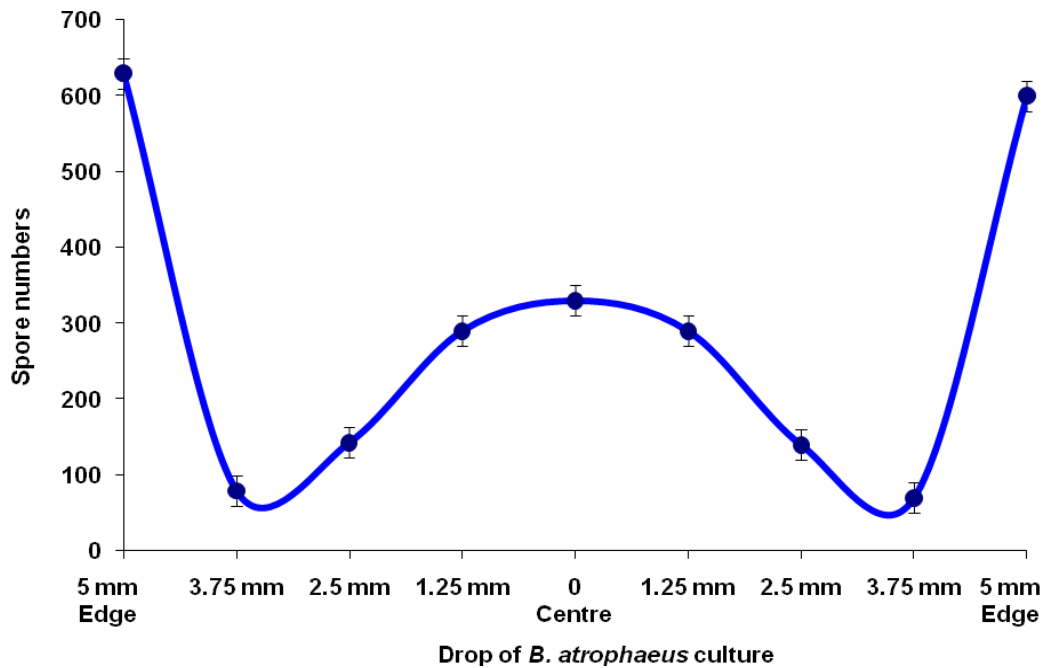


Figure 3.13 Distribution of *B. atrophaeus* spores from an evaporated drop on a glass surface (10^7 CFU/mL). The errors were calculated from the standard deviation of 20 reading ($\theta = \pi$)

Counts of *B. atrophaeus* were made on the glass microscopic slide using fresh samples without drying. The drops were placed over the slides and left for a few seconds for stability. There was no cover slip, so it was hard to control the depth of focus and determine the counts accurately. Microscopic examination showed that several circular rings surrounded the centre. Figure 3.14 shows the patterns of *B. atrophaeus* on the glass surface. The lines on the microscopic slide were generated as part of the drying process.



(a) at the edge



(b) at another edge



(c) between the edge and the centre



(d) at the centre

Figure 3.14 Microscopic examination of *B. atrophaeus* (not dry) of 10^7 spore/mL on the glass surface. Phase contrast microscope (Zernike, X5Z-H, China). 40X objective, NA=0.65. Digital camera (Canon, D450, Japan)

3.4 Microscope modification for fluorescence

Some simple techniques were used to enhance microscope performance for illumination and detection.

3.4.1 Detection of aerosolized *B. atrophaeus* deposited onto glass microscope slide

Recently, more attention has been paid to the use of light emitting diodes (LEDs) in bioaerosol sensing (Davitt 2006), and they are capable of exciting the chemical composition of *Bacillus atrophaeus* (Li *et al.*, 2004). It was decided to investigate the use of a LED in the microscopic as a rapid detection method of aerosolized *Bacillus atrophaeus* deposited onto glass. Glass slides were inoculated with the aerosolized *Bacillus atrophaeus* spores. An aerosol of 10^7 CFU/mL of *Bacillus atrophaeus* spores was passed through the flow chamber (see Chapter 2: Section 2.6.2: Microorganism aerosol generator)

for about 10 min. The slides were first observed using the Zhummell microscope (XSZ-H, China) and a conventional halogen light source. The images of the spores were blurry, and it was hard to recognise and detect the aerosolized spores at such low densities with a standard optical microscope and illumination. So it was decided to replace the halogen light source of the Zhummell microscope with a light emitting diode (LED). The LED (Luxeon, LXX2, USA) is low cost, with long operational lifetime and controllable output intensity. The input voltage was 3 V, input current was 1500 mA and the output power was 750 mW. The spectrometer (Photon Control, SPM002, Canada) was used to determine the peak spectral wavelength range from 400-460 nm, and the peak wavelength was at 450 nm. The LED was attached to a Peltier cooler (SuntekStore, TEC1-12709, UK) to dissipate the heat. The LED unit was attached to an aluminium holder and placed in the illumination chamber at the base of the microscope, as can be seen in Figure 3.15. The simplified diagram of the modified laboratory microscope can be seen in Figure 3.16. The filters were used to prevent the emission breaking into the output fluorescence i.e. the excitation filter was used to remove the unwanted out-of-band LED light and the emission filter was used to remove the unwanted fluorescence.

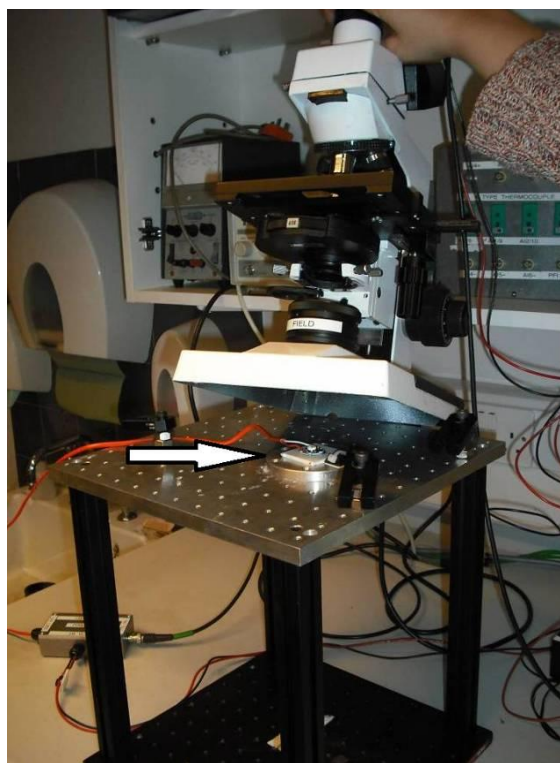


Figure 3.15 The LED set-up mounted at the illumination source of the Zhummell microscope, the arrow indicates the LED unit

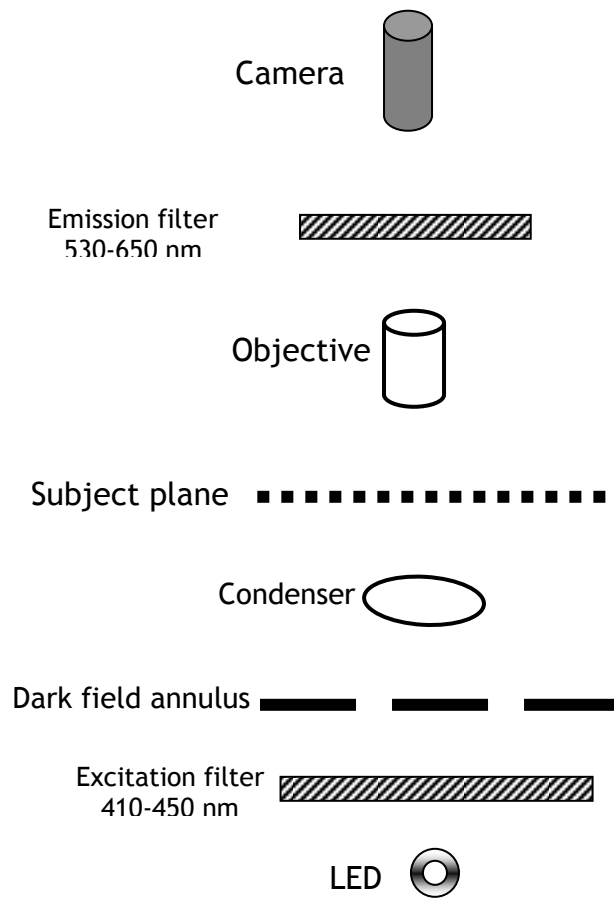


Figure 3.16 Dark field transmission and fluorescence microscope diagram

The LED was connected to the operating circuit (Solarox, KS1400, UK). Figure 3.17 shows the circuit diagram. The input voltage was 9 V DC supplied from the power supply (Altai EP-613, UK). The brightness of the LED was controlled via a 5 V TTL signal supplied from a function generator (Thurlby Thandar Instruments-TTi, TGP110, UK), and the TTL signal was connected to the pulse width modulation (PWM) input of the circuit. The circuit unit was placed inside an aluminium box, and some holes were drilled through the box for the TTL control signal and the other wire connections. Figure 3.18 shows the LED driver and the circuit unit.

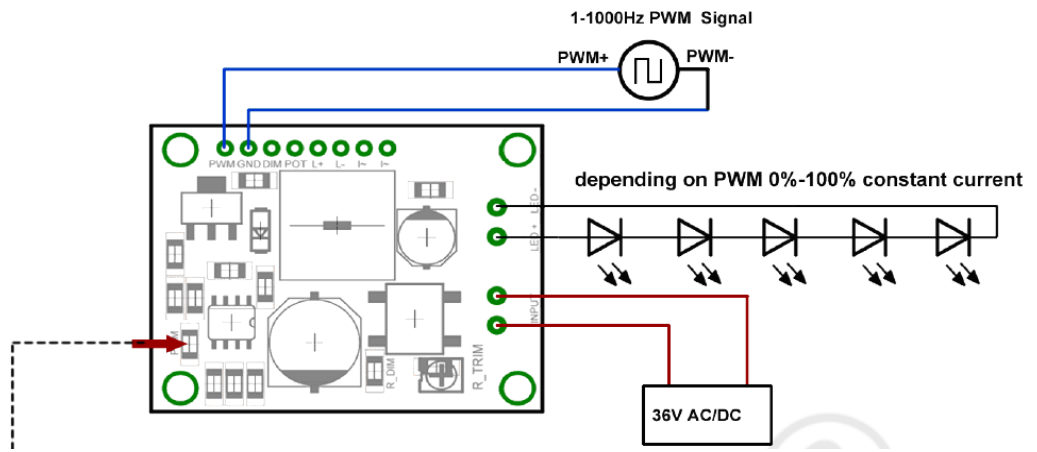


Figure 3.17 Diagram of the LED circuit connection (Solarox_Manual 2011)

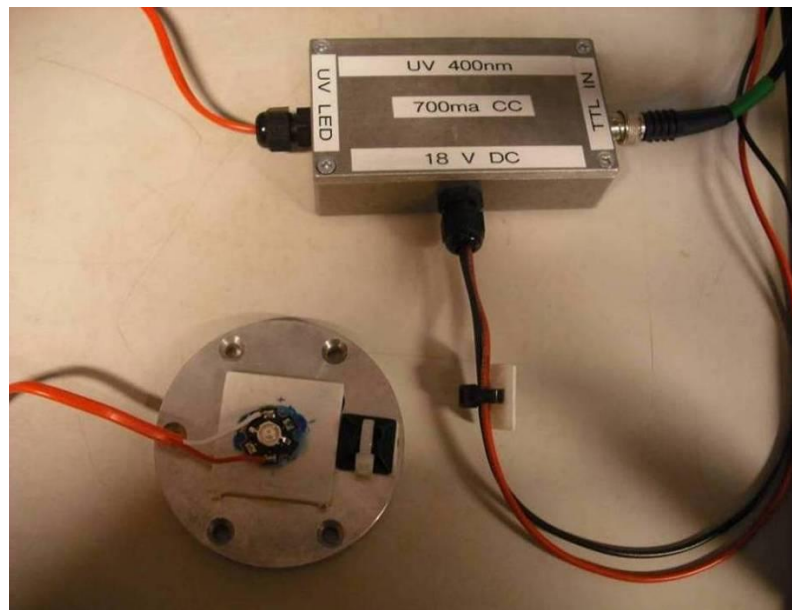
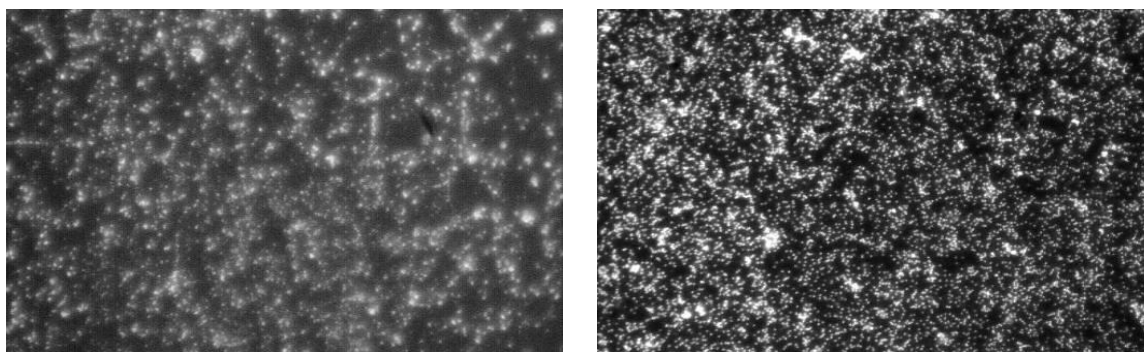


Figure 3.18 Front view of the LED unit and the operating circuit inside the box

Figure 3.19 shows micrographs of *Bacillus atrophaeus* spores taken with the conventional halogen bulb and using the modified microscope, for comparison. The LED illuminated samples produced higher quality images than the conventional illumination source, because the LED has a narrower spectral output than the conventional bulb, and the emission and transmission filter were appropriate for detection.



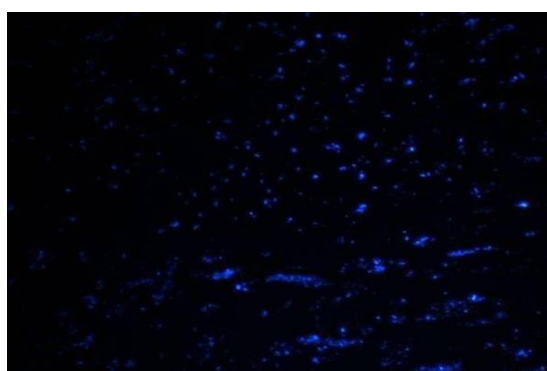
a) Halogen bulb

b) Luxeon power LED

Figure 3.19 *B. atrophaeus* spores imaged in the conventional light microscope and the modified microscope using a high power LED (40X objective)

3.4.2 Fluorescence microscope

The Nikon microscope (ME600, Japan) was developed with assistance from a Nikon representative. The mercury bulb unit was replaced with a UV mercury bulb. The UV mercury bulb has different emission wavelengths ranging from 380 to 420 nm, so filters are used to select a narrower wavelength range for illumination and fluorescence. A fluorescence filter cube unit was added to the head of the Nikon microscope. *Bacillus atrophaeus* spores are naturally fluorescent (autofluorophores) (Sarasanandarajah 2007), they fluoresced when excited by UV light. For example, the wavelength range 266-355 nm excites the NADH, tyrosine, phenylalanine and other natural fluorophores (Sivaprakasam *et al.*, 2004). The fluorescence of *B. atrophaeus* spores was high i.e. the detection was very good at a wavelength of 340 nm. Figure 3.20 shows the detection of *B. atrophaeus* spores with the Nikon microscope operated in the differential interference contrast mode and the fluorescence mode. The powerful UV bulb enabled the spores to be more easily detected than with a standard optical microscope.



a) with conventional mercury bulb illumination



b) with UV mercury bulb illumination

Figure 3.20 Microscopic images of *B. atrophaeus* on a glass surface using a Nikon microscope

3.5 Fluorescence spectra measurement

Fluorescence spectroscopic measurements are simple, sensitive (Donard *et al.*, 1989), reliable and cheap for detection and identification techniques of microorganisms (Shahzad *et al.*, 2009), proteins (Lakowicz 2009), heavy metal (Prestel *et al.*, 2000), DNA (Danielli *et al.*, 2008), dissolved organic matter (Murphy *et al.*, 2010), food product analysis (Sikorska *et al.*, 2008) and plant photosynthetic performance (Baker & Rosenqvist 2004). It is a fast method compared to culturing techniques which need many hours (~ 24-48 hr) to grow the spores or bacteria. A rapid technique is required in urgent contamination situations. Additionally, fluorescent techniques can often be used without reagents or dyes which is a disadvantage in many applications. In this experiment, the effect of excimer laser radiation on fluorescence of *B. atrophaeus* spores was investigated to see if auto-fluorescences could be detected with sufficient excitation energy and a simple detection system. The excimer laser used in this work was a Krypton Fluoride (*KrF*) device with a transition wavelength of 248 nm (GAM Laser Inc., EX5, USA), the maximum pulse energy is 38 mJ with a maximum pulse repetition rate of 200 Hz. For detailed specifications see Appendix B: Excimer laser (GAM laser, EX5).

Figure 3.21 shows a schematic of the system used, and the experimental setup can be seen in Figure 3.22. The agar plate was positioned inside a Perspex safety box at 45° to the excitation axis, in front of the laser beam. The fluorescence spectra from the spores was detected and recorded with the spectrometer (Photon Control, SPM002, Canada) through the optical fibre.

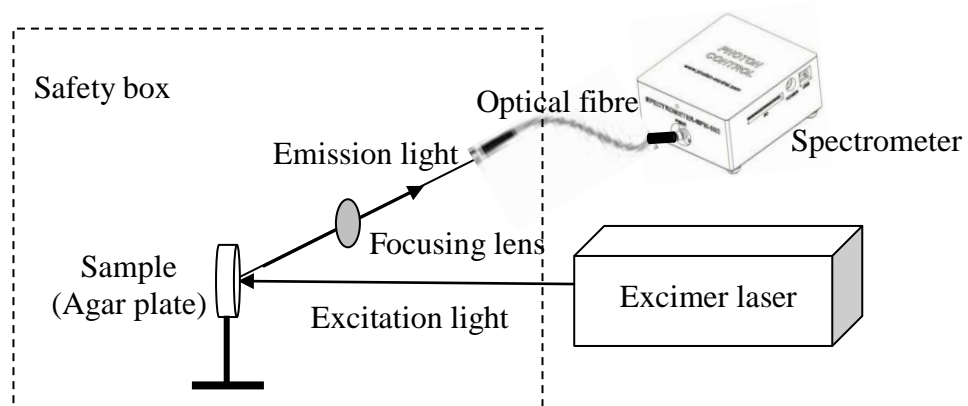


Figure 3.21 Schematic of the fluorescence spectra measurement system

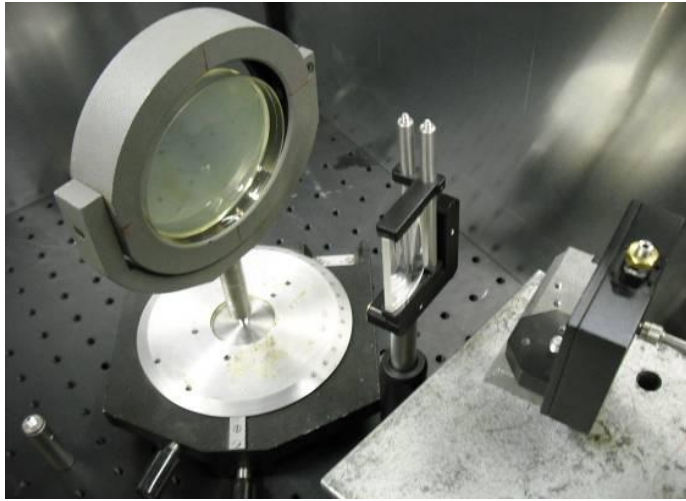
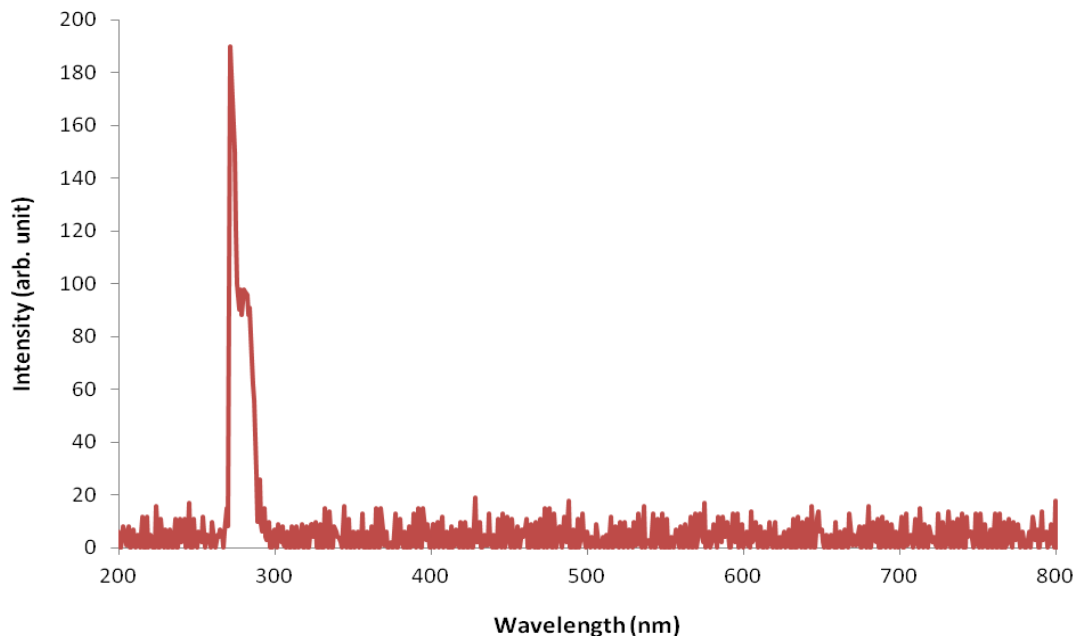


Figure 3.22 Experimental setup of fluorescence spectra measurement

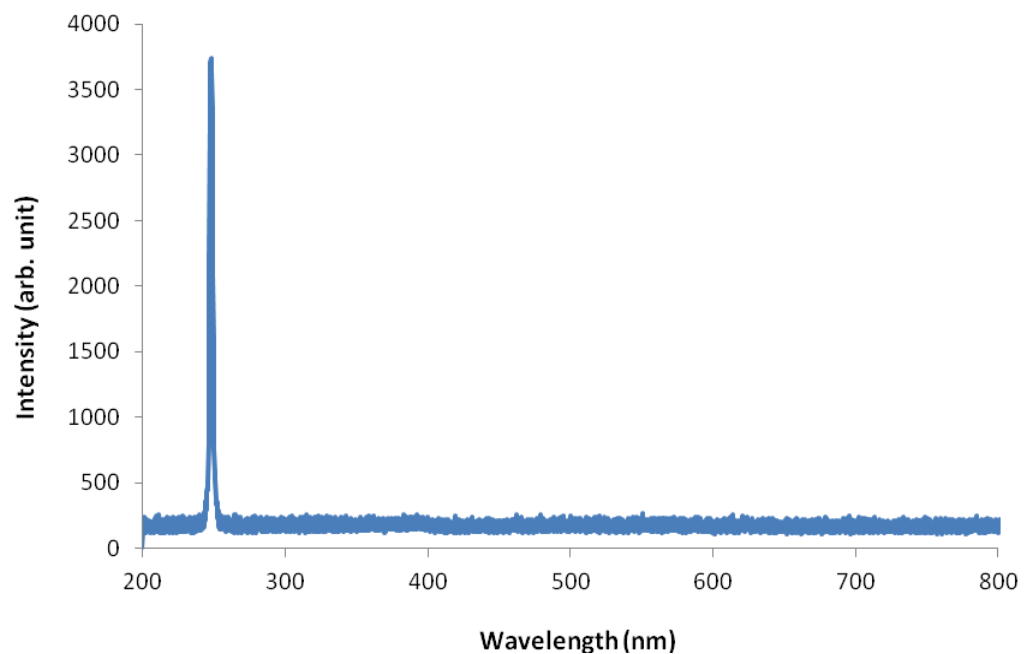
The background reference spectrum collected with the excimer laser irradiating just the agar in the Petri-dish is shown in Figure 3.23 (a). It is seen that there is significant noise within the spectrum. The spectrum of laser with the average background reference off is shown in Figure 3.23 (b). Then the agar plate was removed and replaced with an inoculated plate, 200 μL of *B. atrophaeus* spores. The plate was exposed to the excimer laser beam at a repetition rate of 20 Hz and 17 mJ laser energy over 5 min, and the spectrum was detected and recorded by the spectrometer with an exposure time of 3000 ms. The measurements were repeated five times each time with a fresh culture of *B. atrophaeus* samples, and the average spectra was taken. The fluorescence measurement can be expressed by the relationship (Photon_Control 2009):

$$F = \frac{(P - D)}{(P_0 - D)} \quad \text{Equation 3.2}$$

Where F is the fluorescence, P is the sample intensity (W/cm^2), P_0 is the reference intensity (W/cm^2) and D is the background intensity (W/cm^2).



(a)



(b)

Figure 3.23 Emission of excimer laser a) with background reference and b) without background reference (bottom)

3.6 Results of the fluorescence spectra measurement

Figure 3.24 shows the average fluorescent spectra of the laser irradiated agar plate compared to that measured with spores. It is seen that the excimer laser with an emission wavelength of 248 nm is excellent for *B. atrophaeus* spore excitation. The fluorescence

spectrum with spores was longer than the reference spectrum. It can be seen from the graph that the fluorescence spectra of *B. atrophaeus* spores are covered by a band which had two peaks at around 361 and 384 nm, with a completely different structure around this region. This is possibly due to either NADH fluorescence or it corresponds to the aromatic amino acids, because their excitation wavelength is in the range 250-450 nm and their emission wavelength is in the range 300-460 nm (Richards-Kortum & Sevick-Muraca 1996; Ramanujam 2006). There is also some additional spectral structure around 600 nm, although this is relatively small.

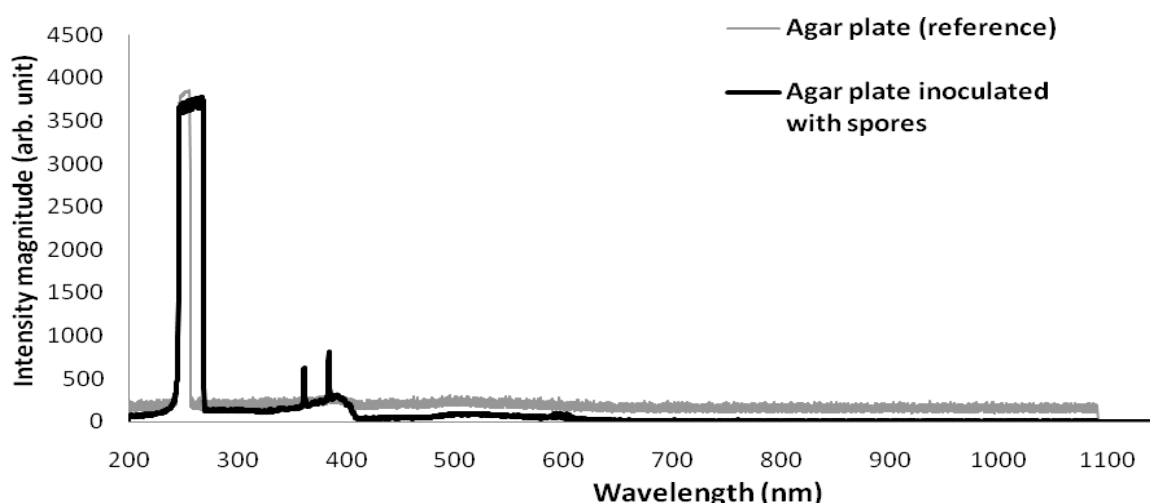


Figure 3.24 Fluorescence intensities (F) against excitation-emission wavelengths

3.7 Chlorophyll fluorescence measurements

Rapid detection of microalgae in water provides information on cell detection and cell numbers. Microscopy counting techniques are often used but they are somewhat laborious. Chlorophyll fluorescence is widely used in photosynthesis measurements (Vonshak *et al.*, 1994) and can be used to provide an estimate of biomass and cell numbers. Chlorophyll fluorescence is used as a proxy for microphytobenthic biomass (Jesus *et al.*, 2006). The variable to maximum fluorescence ratio (F_v/F_m) is used to investigate the fluctuation of nutrient supply on the photosynthetic efficiency (Lippemeier *et al.*, 2001). The F_v/F_m ratio is widely used to measure the maximum photochemical yield of Photosystem II (PSII) (Masojidek *et al.*, 2010), and decline of this ratio means that the microalgal cells may become stressed (Vonshak *et al.*, 1994). The PEA (plant efficiency analyser) fluorometers from Hansatech are widely used in *Chl a* fluorescence analysis, these instruments have

high temporal resolution and data acquisition capacity, they are very fast and have low power consumption (Strasser *et al.*, 2000).

This experiment was designed to find the relationship between the algal fluorescence and cell counts compared to microscopy techniques. Two identical photobioreactor tubes were used for culturing as shown in Figure 3.25. The culture volume was approximately 1000 mL (100 mL *N. oculata* culture medium, 900 mL tap water, 0.5 mL F/2 phyto nutrients (Reefphyto, UK)). Sea salt (20 g) was added to the culture, and the salinity was maintained at ~ 25 ppt. The illumination for the tubes was supplied by a fluorescent lamp (14 W), the lamp was placed between the two tubes for 12 hr on and 12 hr off. Two air pumps supplied continuous air agitation and the temperature was 26 ± 2 °C.



Figure 3.25 A photobioreactor setup for fluorescence measurements

The fluorescence was measured by a Hansatech system (Hansatech Instrument Ltd, Handy PEA, UK). The fluorescence analysis was based on the measurement of the variable fluorescence (F_v) to the maximum fluorescence (F_m), where $F_v = F_m - F_o$ and F_o is the minimum fluorescence level (fluorescence origin). The ratio F_v/F_m is found. Figure 3.26 shows the fluorescence parameters. The samples were collected using the sampling vessels as can be seen in Figure 3.27. To obtain the maximum fluorescence, the microalgal culture samples were dark adapted for around 10-15 min before the experiments. Three readings were measured every two days over a period of 14 days, and averaged for each sample of fresh algal suspension. The fluorescence signal was recorded over 30 s exposure times. The wavelength range was from 550-700 nm, and centred at 650 nm.

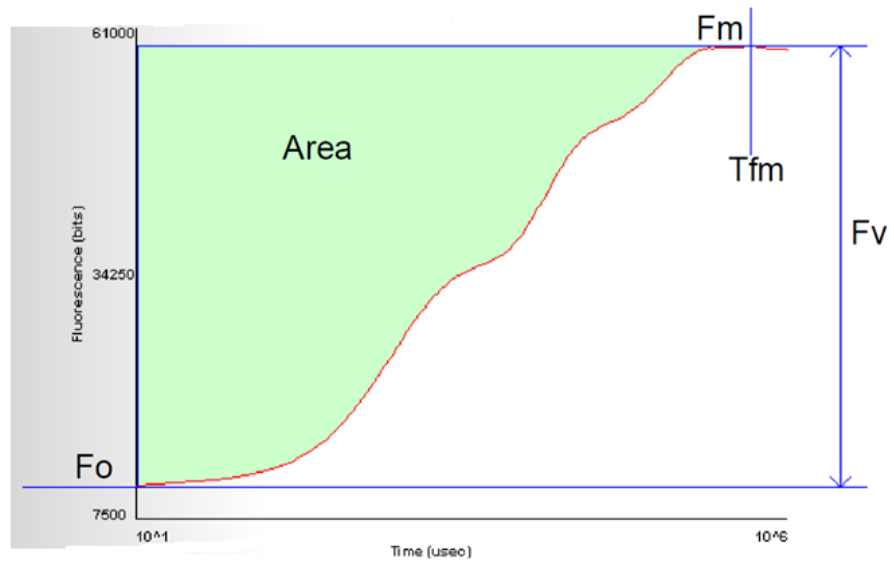


Figure 3.26 The fluorescence parameters of the PEA fluorimeter (Hansatech 2007)



Figure 3.27 A photosynthesis efficiency analyser (PEA) Hansatech instrument

3.8 Results of chlorophyll fluorescence measurements

Figure 3.28 shows a screen capture of the PEA plus software for one sample. The software recorded the data of three measurements for the same sample; the three graphs represent the fluorescence measurements over time. The relationship between the fluorescence F_v/F_m and the growth period of algae can be seen in Figure 3.29 and Figure 3.30 shows (F_v/F_m) as a function of the cell counts obtained from microscopy experiments. The results showed

that the fluorescence increased with growth time i.e. with increasing algal biomass. Consequently F_v/F_m can be used to investigate the cell growth of the fresh samples easily, reliably and quickly. From the investigation, F_v/F_m slightly decreased after ~ 8 hr of the test, which may be due to the effect of nutrient depletion or for other reasons such as decreased illumination or aeration in the small test vessels of 4 mL or due to reduced microalgal vitality. The range of F_v/F_m was around 0.5 to 0.7, and for healthy microalgae Masojidek *et al.* (2010) suggests F_v/F_m is 0.6 – 0.8. The correlation of the F_v/F_m with microscopy measurement of the cell concentration was excellent with $R^2 = 0.991$. Consequently, this system could be used instead of laborious, microscopy counting methods.

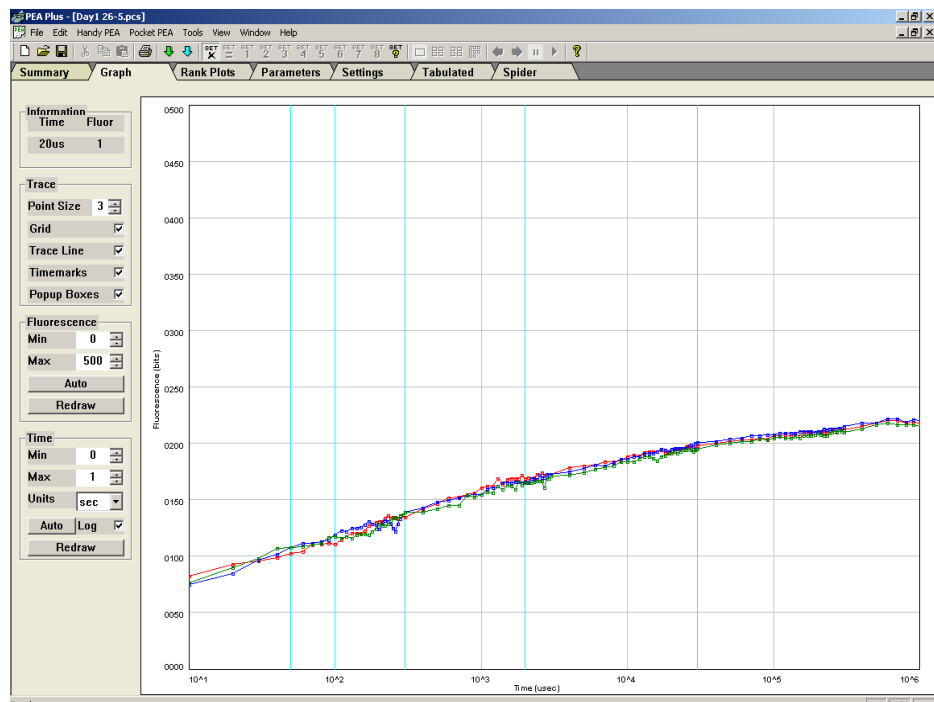


Figure 3.28 The screen of PEA plus software

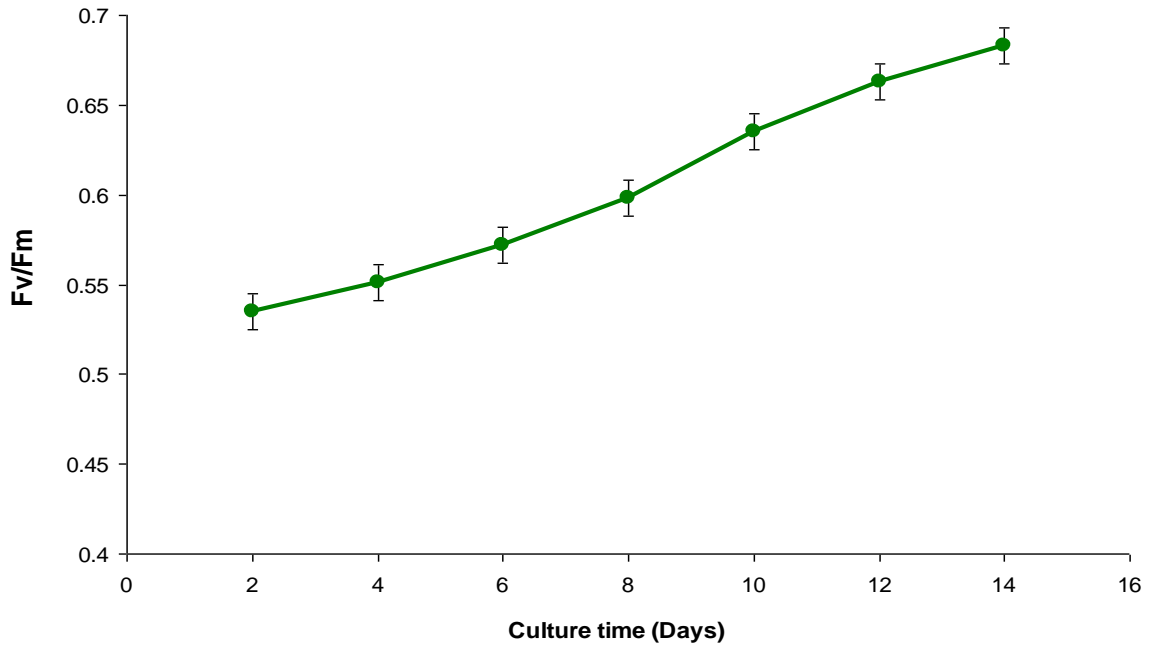


Figure 3.29 Variable fluorescence (F_v) and maximum fluorescence (F_m) ratio at various days of growth measured by a Hansatech instrument

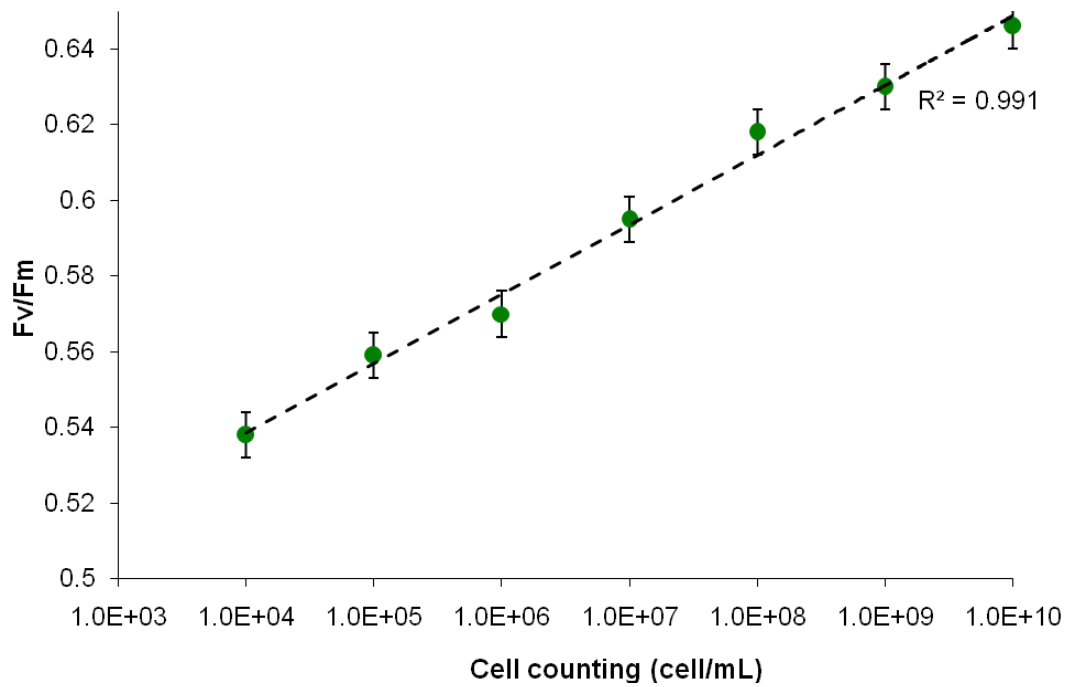


Figure 3.30 Variable fluorescence (F_v) and maximum fluorescence (F_m) ratio for different dilution factor

3.9 The flow chamber for cell microscopy

A flow chamber is a microscopic plastic slide which consists of a flow channel, as shown in the schematic given in Figure 3.31. The flow chamber is a low cost and simple method to allow rapid cell counting. The cells are counted and analysed under the microscope without any special preparations, as the fluid is pumped through the chamber. The flow chamber reduces the time to prepare the microscopic slide as with conventional methods by using pipettes. There is no need to use cover slips or use a small amount of culture to avoid cells floating.

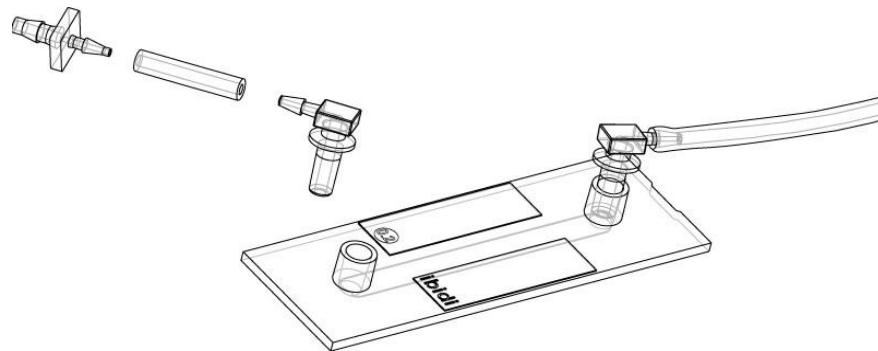


Figure 3.31 Schematic of the flow cell (Ibidi 2010)

The flow system consisted of a flow cell (μ -Slide I 0.1 Luer, Ibidi, Germany), air pressure pump (TCS Micropumps Ltd., UK), valves, soft plastic tubing and adapters. The flow cell was placed on the microscope stage as shown in Figure 3.32. The culture of cells was pumped from the cell culture beaker to the inlet channel of the flow cell, and the output from the flow cell was fed back into the beaker. The examination was done using a light microscope (Zhumell XSZ-H, 10X, 0.25 NA, China). The resulting photographs were viewed using NI image processing software. The setup of the experiment can be seen in Figure 3.33.

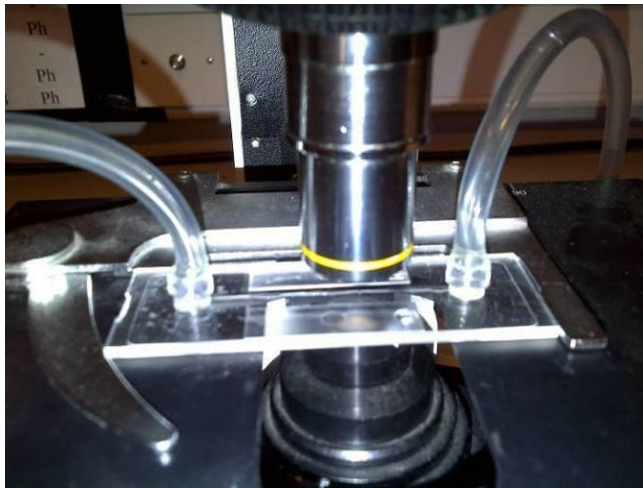


Figure 3.32 The slide under the microscope

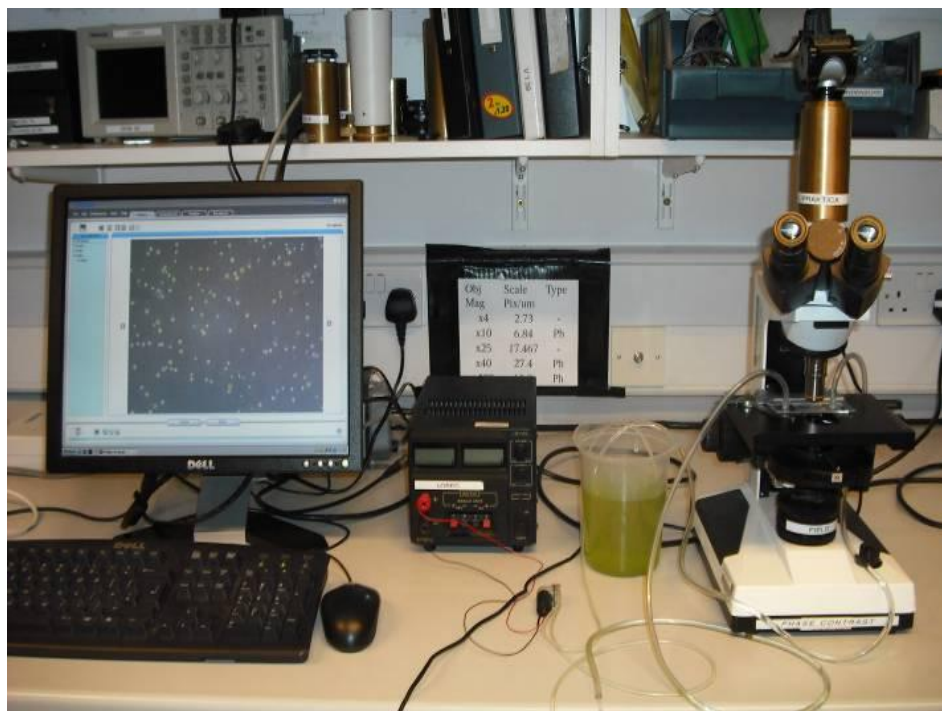
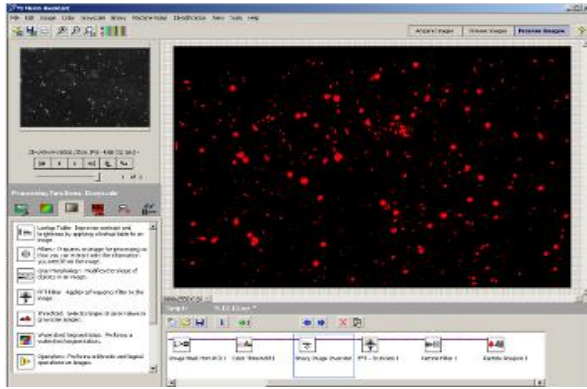
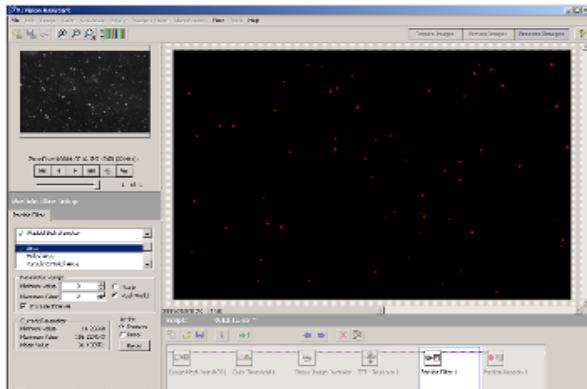


Figure 3.33 A flow cell system setup

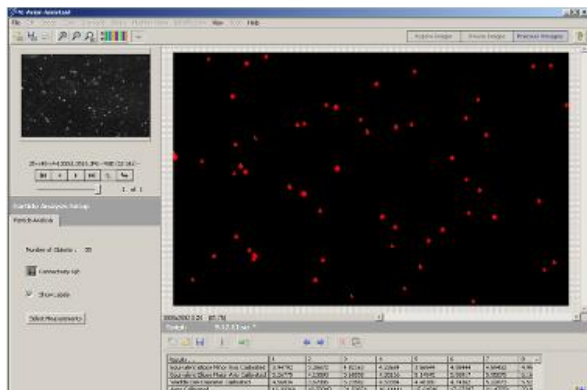
An initial test was done with the flow cell by starting the flow then switching off the pump to observe the cells under the microscope in a fixed position without motion. The images were viewed in the processing window of the NI vision software. There was some noise from the background in the resultant images, so the images were filtered and to separate the algae cells from the background. The particle filters function in NI vision was used to remove the unwanted particles by subtracting the original images and the background noise to extract the image of the cells. Figure 3.34 shows the results before and after filtering.



a) Original image



b) Background noise



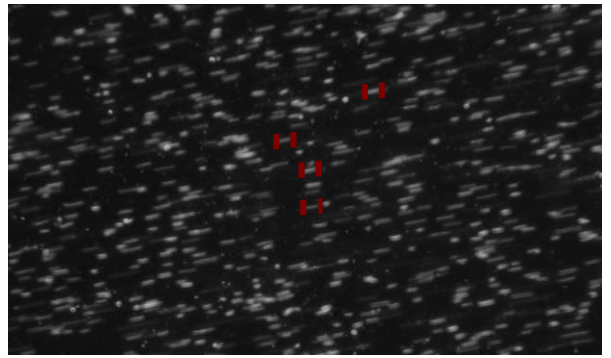
c) Image after analysis

Figure 3.34 Counting of algal cells using a flow slide

The algae cells were moved through the channel of the flow slide and the movement was recorded as a video and photographs. Figure 3.35 shows the results. The particle filter analysis was used to remove the noise and extract the content for the moving cells, as can be seen in Figure 3.36.

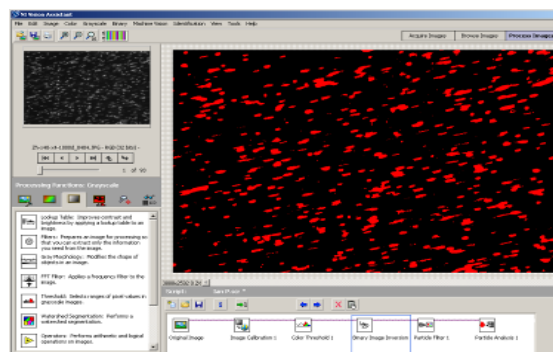


a) Video

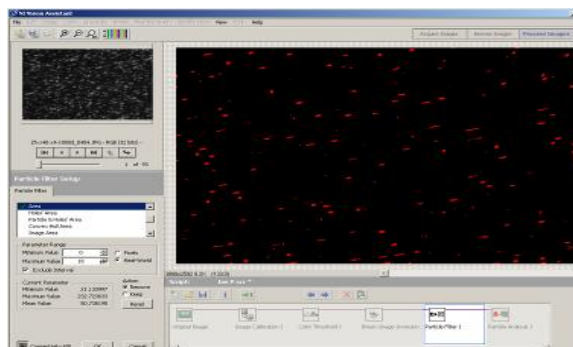


b) Image

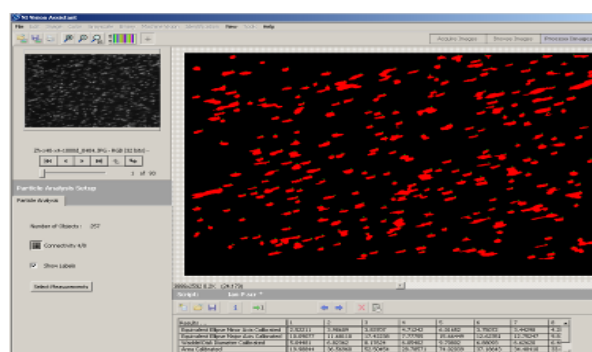
Figure 3.35 *N. oculata* algae in the flow slide



a) Original image



b) Background noise



c) Image after analysis

Figure 3.36 Counting of the moving algal cells in the flow slide using NI vision program

The particle analysis function in NI vision was applied to determine the track length of the particles. The velocity of particles V_p was calculated using Equation 3.3. The exposure time of the camera (t_f) was ¼ of second.

$$V_p = \frac{L_p}{t_f}$$

Equation 3.3

The density of particles D_p was calculated using Equation 3.4 and Equation 3.5.

$$D_p = \frac{N_c}{V_s}$$

Equation 3.4

$$V_s = X * Y * Z * C_f^2$$

Equation 3.5

Where N_c is the number of cells in the field of view and V_s is the volume of the flow channel of the slide ($X= 3888$ pixel, $Y= 2592$ pixel and the depth $Z= 3 \mu\text{m}$). The calibration or conversion factor C_f to convert from pixels to micrometer was $0.120688 \mu\text{m}/\text{pixel}$ (see Appendix C: microscope calibration).

The results showed that the track length of the particles (L_p) was about $5\text{-}6 \mu\text{m}$. The velocity of particles V_p was 0.02 mm/s . The density of particles D_p was 2×10^5 particles/ mm^3 . So this technique is perfect for cell growth observation and counting in real time and within defined speed and flow rate.

Chapter 4

Antimicrobial effects of excimer laser on *E. coli* and *B. atrophaeus*

The aim of this work was to investigate the effects of excimer laser radiation on bacterial and spore inactivation. The first experiments investigated the laser influence on *E. coli* bacteria and *B. atrophaeus* spores lawned on agar surface. While in the other experiments, the influence of excimer laser radiation on a spore laden aerosol both inside the resonator cavity (booster) and external to the cavity was investigated. The experimental results were assessed using NI Vision software and Fluent (CFD package). The microbiological tests showed that the antimicrobial activity of the *KrF* excimer laser was highly significant both on surfaces and in air.

4.1 Excimer irradiation treatment of *E. coli* on agar surfaces

The experiments were designed to investigate the killing efficiency of excimer laser radiation at 248 nm on *E. coli*. The optical density and growth of *E. coli* bacteria were measured as well.

4.1.1 Culturing *E. coli* and optical density (OD) measurements

The most common method to rapidly determine the growth of *E. coli* bacteria is the spectrophotometry method. In this method, the spectrometer is used to measure light scattered by a suspended culture (i.e. an optical density), and then using a calibrated, standard curve the cell number can be found.

4.1.1.1 LB broth preparation

LB nutrient broth (lysogeny broth) has been widely used as a nutritionally rich medium in molecular microbiology to grow cultures; it is popular with bacteriologists due to the rapid growth it allows. The composition of its ingredients are: tryptone (10 g/L), yeast extract (5 g/L) and sodium chloride (5 g/L) (Sezonov *et al.*, 2007). The difference between the nutrient broth and nutrient agar is that the broth has more nutrients than the agar so it is useful to grow a large number of cells for a range of experiments. The broth media, unlike agar, is not suitable to isolate different cells or colonies. The nutrient broth can be solid (agar) by adding a gel extracted from red seaweed (Bauman *et al.*, 2012).

LB broth was prepared by adding a 25 g of LB broth powder (Oxoid, UK) to a 1000 mL of distilled water, and mixed well using a shaker (Stuart, UK) until completely dissolved. Then the solution was autoclaved (Prestige Medical, Classic 2100, UK) for 30 min at 120 °C for sterilizing.

4.1.1.2 *E. coli* colony isolation and LB broth culture preparation

Escherichia (*E. coli* BL21) was supplied by Dr. Roger Parton, Division of Infection and Immunity, IBLS, University of Glasgow. In the beginning, a single colony of *E. coli* was isolated from a stocked agar plate (starter culture) by using a sterilized loop, and was re-plated by streaking it on a fresh LB agar plate and incubating overnight at 37 °C. It is not efficient to inoculate directly from the plate or glycerol stock that has been stored for a long time, as this may lead to detrimental effects on the plasmid. After incubation, a single colony of *E. coli* was picked using a sterilized loop and added to the LB broth (20 mL universal bottle), and then the LB broth bottle was incubated over night at 37 °C. Figure 4.1 shows the LB broth without *E. coli* (before the culturing) and with *E. coli* after incubation.

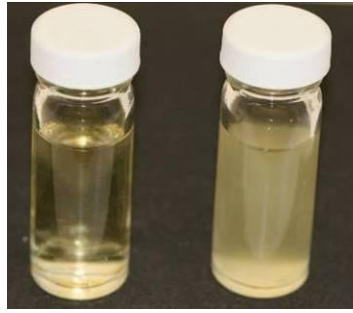


Figure 4.1 LB broth without *E. coli* (left) and with *E. coli* (right)

4.1.1.3 The optical density (OD) measurement

i. Introduction to optical density (OD) measurements

Spectrophotometry is a measurement of transmitted or reflected light by the sample as a function of the wavelength of the light source. Spectrophotometry includes the use of spectrophotometer instruments, namely a photometer to measure the light intensity and a spectrometer to produce different wavelengths. A spectrophotometer can be used to measure the density of the culture suspension or solids within a liquid. The instrument works by passing the light beam through the sample which absorbs an amount of light, then by measuring the light intensity with a detector at a given wavelength, the optical density (also called the turbidity and absorbance) can be found. In this research, OD represents a measure of the light that is absorbed by the bacterial cell suspension at 600 nm wavelength. When the OD is high, the transmittance is low, i.e there is a higher concentration of bacterial cells in the suspension.

The growth curve of *E. coli* against incubation time can be divided into several phases as shown in Figure 4.2. The first is the lag phase which occurs directly after culturing with a fresh medium, here the bacteria can still adapt or acclimatise to the new medium. Then the bacterial cell starts to divide rapidly during the exponential phase. Then the stationary phase starts, during which the cell density remains constant due to exhausted nutrients, at this point the growth rate equals the death rate. During the death phase (decline phase), the cell density decreases with time as the cells start to lyse as there are no nutrients available for them.

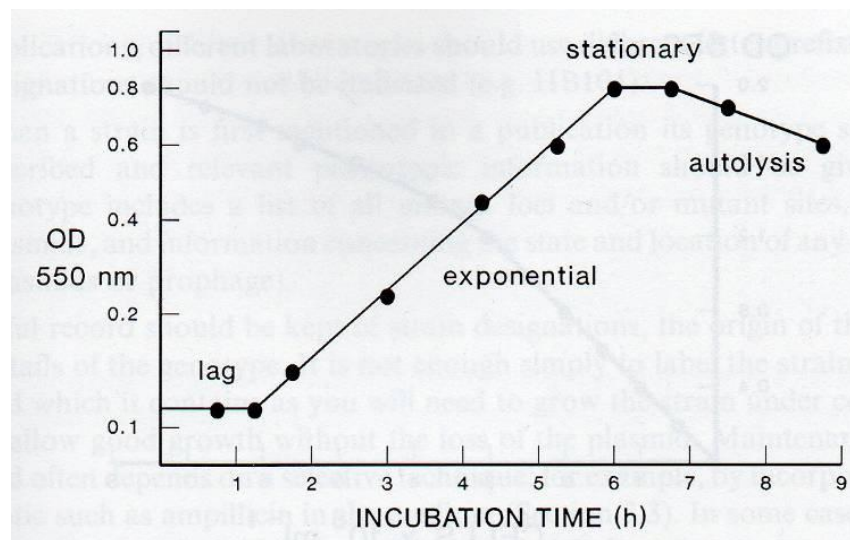


Figure 4.2 Typical growth curve for *E. coli* (Brown 2000)

ii. Experimental setup of the optical density (OD) measurement

A quartz cuvette (Fisher Scientific, UK) measuring 12.5x7.5x45 mm (as shown in Figure 4.3) was filled with 1 mL of LB broth as a reference. The optical density of the blank reference was measured by using a spectrophotometer (Biochrom WPA, Biowave CO8000, UK). A blank is the broth that is identical to the broth sample except without any *E. coli* that absorbs the light, i.e. the scale is read as zero absorbance. Then, a quartz cuvette was filled with 1 mL of *E. coli* culture and placed inside the spectrophotometer; the amount of light passing through the cuvette was measured. The optical density (OD) readings were measured over the time of the experiment with continuous sampling around every 20 min, and then the same experiment was repeated but the sampling or streaking was taken around every 60 min periodically with the optical density measurement. For each optical density, a serial dilution was made and an aliquot of *E. coli* culture (100 μ L) was streaked on a pre-pored LB agar plate and all the plates were incubated overnight. Then, the number of CFUs on each plate was counted and multiplied by the dilution factor to obtain the number of bacterial cells per millilitre in the original culture sample. These values were used to prepare a standard calibration curve of cell numbers of *E. coli* against optical density.



Figure 4.3 Quartz cuvette and the spectrophotometer

iii. Results from the optical density (OD₆₀₀) measurements for *E. coli*

Results of the OD measurements can be seen in Figure 4.4. The figure shows the standard curve for the relationship between the optical density and cell concentrations, the measurements have been taken periodically between OD and numbers of cells over a period of around 20-30 min. From this curve, the optical density reading can be converted to the number of *E. coli* cells per millilitre (cells/mL). Since OD values are the cell concentration or density, the OD increased over time due to the cell growth.

In this experiment, the measured optical density of *E. coli* culture was equal to 0.4, and by comparing this reading with the calibration curve, the concentration of *E. coli* was nearly 2×10^8 cells/mL, i.e. the density of *E. coli* that were spread onto the plates was 2×10^8 cells/mL, yielding an average cell coverage of $\sim 3.1 \times 10^5$ cells/cm².

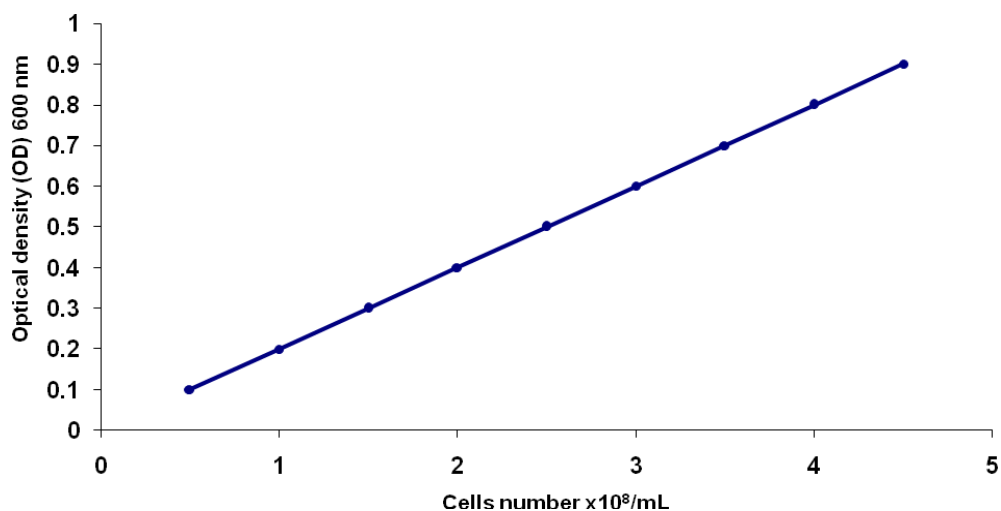


Figure 4.4 The optical density (OD₆₀₀) and cell concentration of *E. coli* were measured around every 20 min

4.1.2 E. coli experimental test protocol and setup

The pre-poured LB agar plate was inoculated with 200 μ L of *E. coli*, and the *E. coli* culture was distributed evenly all over the plate by using a sterilized spreader. Consequently, the approximate cell concentration on the agar plate was 6×10^5 cells/cm². The inoculated agar plate with the holder was placed in front of the laser beam output inside the Perspex safety box. A view of the experimental setup is shown in Figure 4.5 and a schematic drawing can be seen in Figure 4.6.

The excimer laser was turned on until it had warmed and stabilized (see Appendix B: GAM EX50_*KrF* Excimer laser operational procedure). Through the experiments the laser was set to work at a pulse repetition frequency (PRF) rate of 100 Hz with a laser output pulse energy of 37 mJ and the number of pulses was increased from 1 to 10 pulses. The agar plate was marked into four regions for four separate laser exposures.

Another experiment was done with the same setup. The excimer laser was set to fire at fixed power (37 mJ) for 10 second and 1 minute with PRF of 100 Hz. All the procedures were done under sterile conditions. After the experiments, the laser treated agar plates were incubated over night for growth and analysis at 37°C. The experiment was done in duplicate for more accurate results.

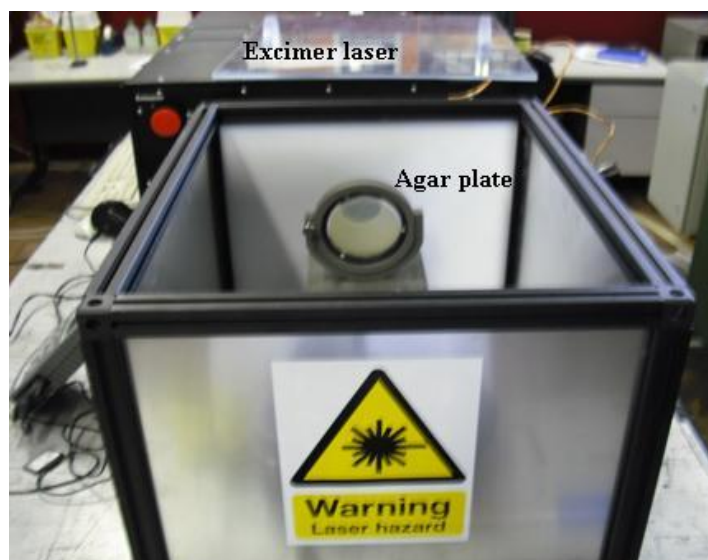


Figure 4.5 Experimental set-up of the excimer laser and agar plate inoculated with *E. coli*

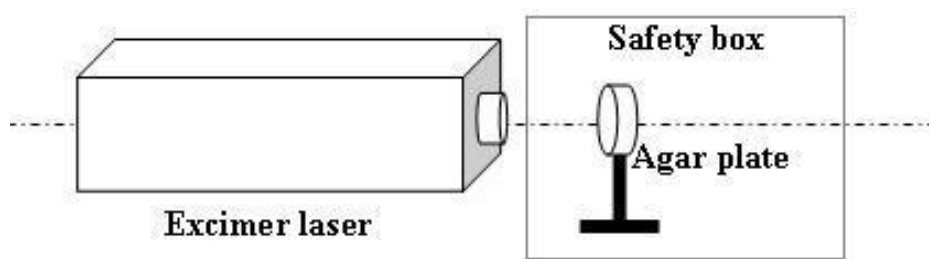


Figure 4.6 Schematic diagram of excimer laser set-up and agar plate inoculated with *E. coli*

4.1.3 Results from surface treatment using excimer laser of *E. coli* test

Figure 4.7 shows the areas of clearing on the agar plates after incubation and the killing effect of the excimer laser radiation on *E. coli* and the control plate that did not receive any irradiation. The treatment process showed a significant influence on killing and completely destroyed the *E. coli* in the beam hit area of the agar, as no growth was observed in the area exposed to the laser beam. It is seen that the area of clearing increased with the number of pulses. The inactivation achieved was 13% for one laser pulse and 60% for ten laser pulses (see section 4.1.4.3). Interestingly, the reduction in *E. coli* was apparent even in unexposed areas to laser light, indicating that scattering of the UV light was sufficient to affect other regions of the plate. This is clearly seen in plates (d) – (j). It should be noted that previous work by Ward *et al.* (1996) had shown that there was no recovery from the treated microorganisms after laser treatment, even after incubation of these regions for up to 2 weeks.

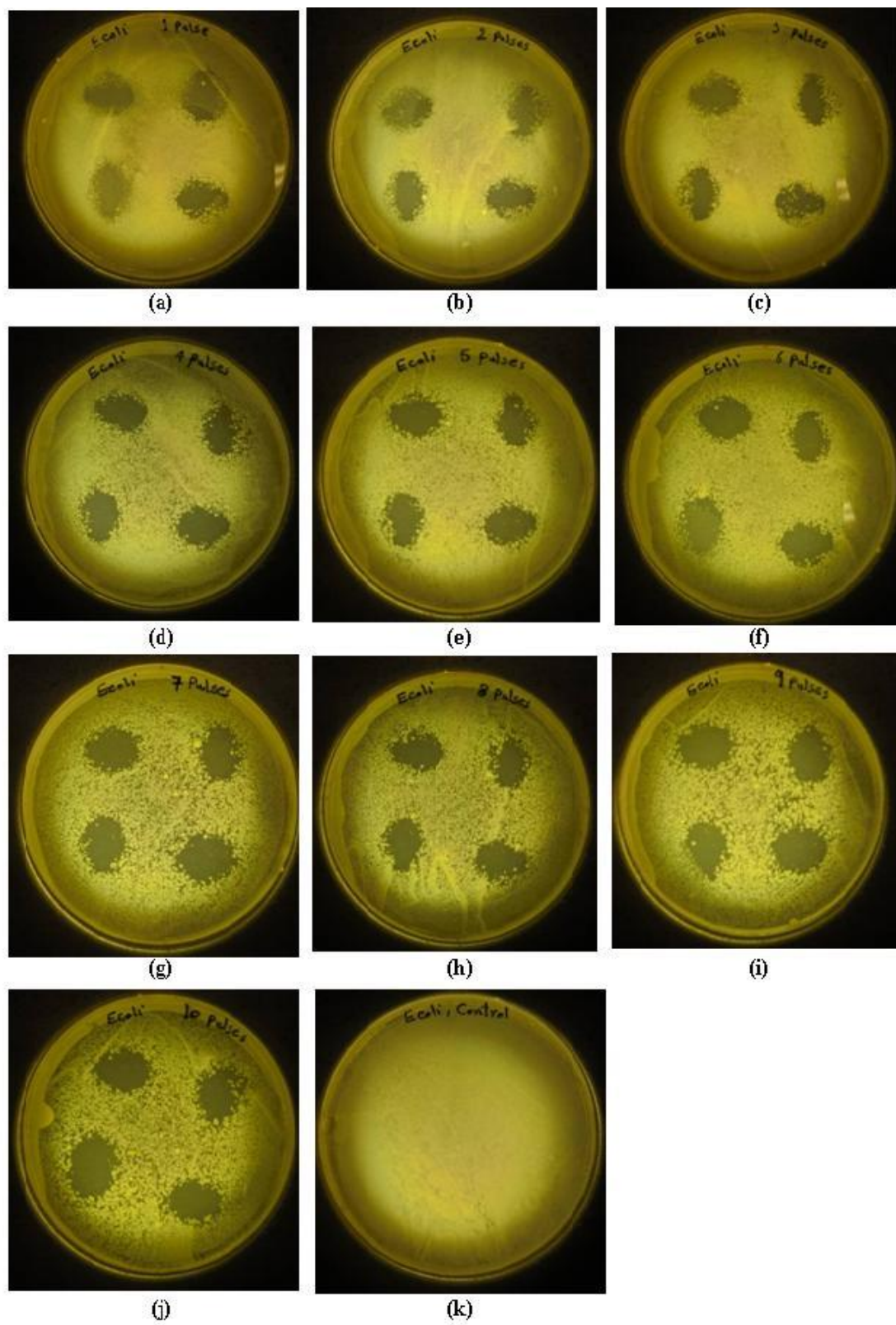


Figure 4.7 *E. coli* treated to excimer laser radiation of different pulse number a) 1, b) 2, c) 3, d) 4, e) 5, f) 6, g) 7, h) 8, i) 9, j) 10 pulses and k) control (no laser radiation)

Figure 4.8 shows the effect of a 10 s and 1 min laser exposure at a fixed power (1.8 W, 100 Hz) on the agar plate lawned with *E. coli*. The results show that the excimer laser had excellent kill efficiency on the micro-organisms, where there was no growth in the area which was directly exposed to the laser beam. The resultant picture also shows that there is considerable overlap between the regions that were treated the two different exposures, with these regions being considerably larger than the beam size itself. The area of laser beam was 12 mm² (2 mm by 6 mm), and the clearing area was approximately 1200 mm² (40 mm diameter) for 10 s and 2800 mm² (60 mm diameter) for 1 min. This means that the laser beam was less than about 5% of the total area of inactivation, and this is likely due to the laser scattering or thermal effects.



Figure 4.8 Fixed power for 10 seconds and 1 minute at 100 Hz PRF

4.1.4 Surface treatment analysis using the NI Vision software

Microscopy is an important method used in biological applications for example colony counting and classifying microorganisms, but in some analyses this requires processing large numbers of samples, the use of a microscope becomes time consuming and automation can benefit the speed of data acquisition with image analysis software. NI vision 8.5 (National Instruments, USA) was used to process the images in this work (see Chapter 1: Section 1.5 Introduction to NI vision).

4.1.4.1 Inactivation area analysis

Figure 4.9 shows the image analysis of the inactivation areas (white regions on the right plate) on one of the sample plates after laser treatment and incubation (left plate). This figure corresponds to data that was collected from the excimer laser surface treatment experiments (Section 4.1.3).



Figure 4.9 *E. coli* plate treated to excimer laser radiation (left) and Image processing of inactivation areas on the plate (right). The micro-colonies in Area 2 are either contaminant CFUs or harder *E.coli*

The inactivation areas were recorded in a script and then the NI Vision information was analysed using Microsoft Excel 2007, the results can be seen in Figure 4.10. From this graph, the results clearly show that UV light is a very effective decontamination tool. With increasing number of laser pulses, the areas of inactivation increased over the agar surface. Measurement of the area of inactivation is based on the image spatial calibration and these values are equal to a number of pixels, where every pixel represents one square unit in the real world. After calculation of this area, the average of areas was taken for each sample of the treated agar plate.

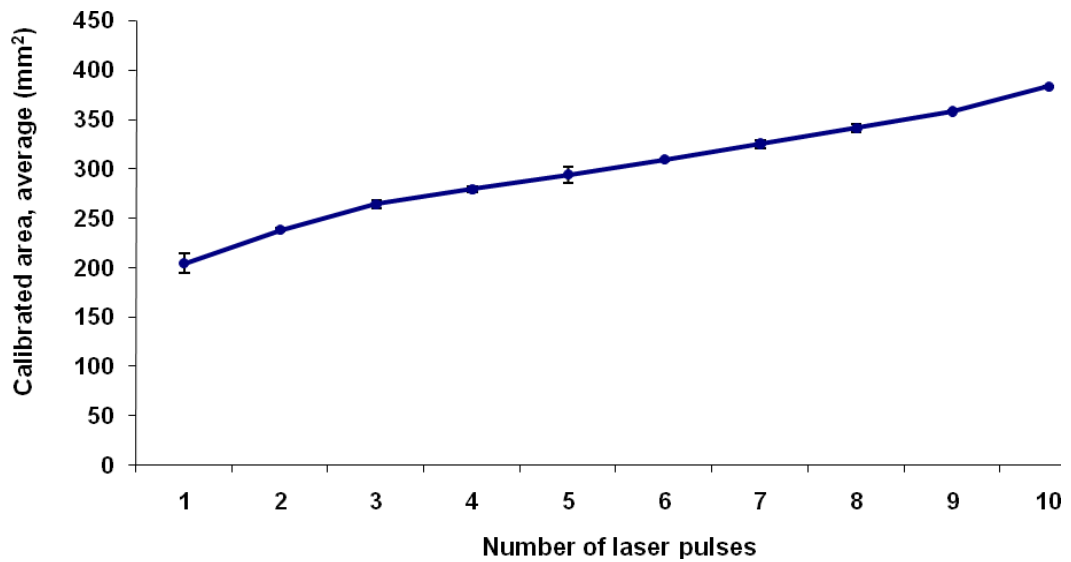


Figure 4.10 Treated areas against number of laser pulses, the experiment was done in duplicate and the error bars represent standard deviation of the average (n = 8)

4.1.4.2 Ellipse major and minor axes analysis

The length and width of the treated area, i.e. major and minor axis of the elliptical axes of the treated areas were measured. The area of inactivation was separated from the background (white regions in Figure 4.9, right plate), and the length or path of the outer perimeter of the area was determined (the dashed line in Figure 4.11). Then, the major and minor axes of this ellipse were measured and averaged as shown in Figure 4.12 for each area of clearing. The experiment was done twice and the error bars show the standard deviation of the average of eight values. The graph shows that as the number of laser pulses was increased, the length of the axes increased and thereby the lethal damage on *E. coli*.

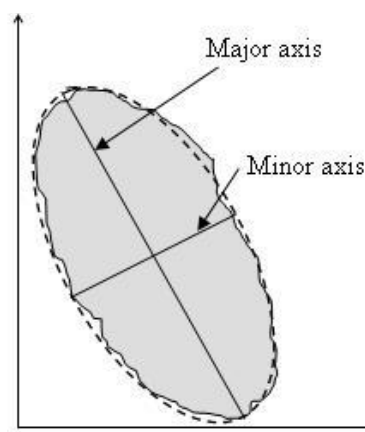


Figure 4.11 Schematic drawing of processed area with NI vision software

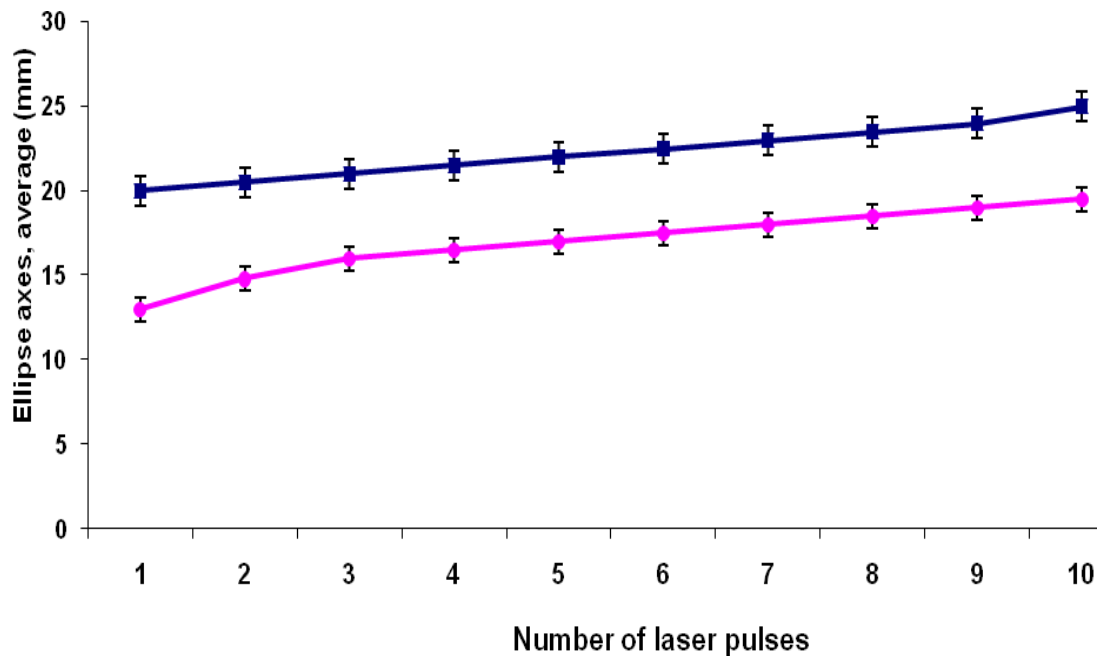


Figure 4.12 Major (■) and minor axes (●) of the inactivation areas against the number of laser pulses

4.1.4.3 Single colony to total colonies analysis on the agar surface

Although there were clear areas of inactivation of the GAM laser against *E. coli* on the agar surface, there seemed to be some effect on the background lawn of microorganisms that were not in the exposed region of the plate. To examine and quantify this effect in more detail, the agar plate was divided into many regions for ease of counting and to obtain an estimation of the results. The analysis was based on detection of “holes” i.e. no colonies (the white regions) inside each region, and then the ratio of the colony area to the entire scanned area (total area of the colonies) in each region was found through a series of processing operations. The average was taken for all the regions for each plate. Figure 4.13 shows a comparison of randomly selected areas inside the treated agar plate with either 1 (a), 10 (b) pulses or the control (c) i.e. no pulses. The results from the NI vision analysis can be seen in Figure 4.14.

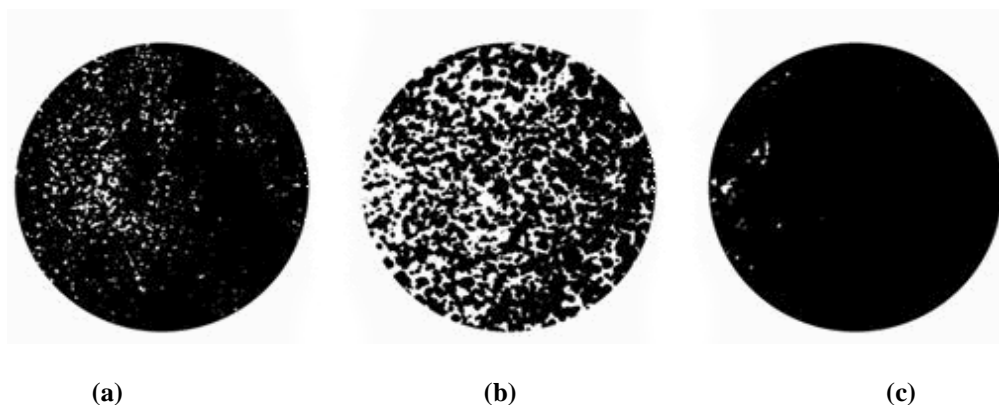


Figure 4.13 Processed, binary images comparing the treated area on agar surface with a) 1 pulse and b) 10 pulses compared to c) the control (the area of clearing is the white region)

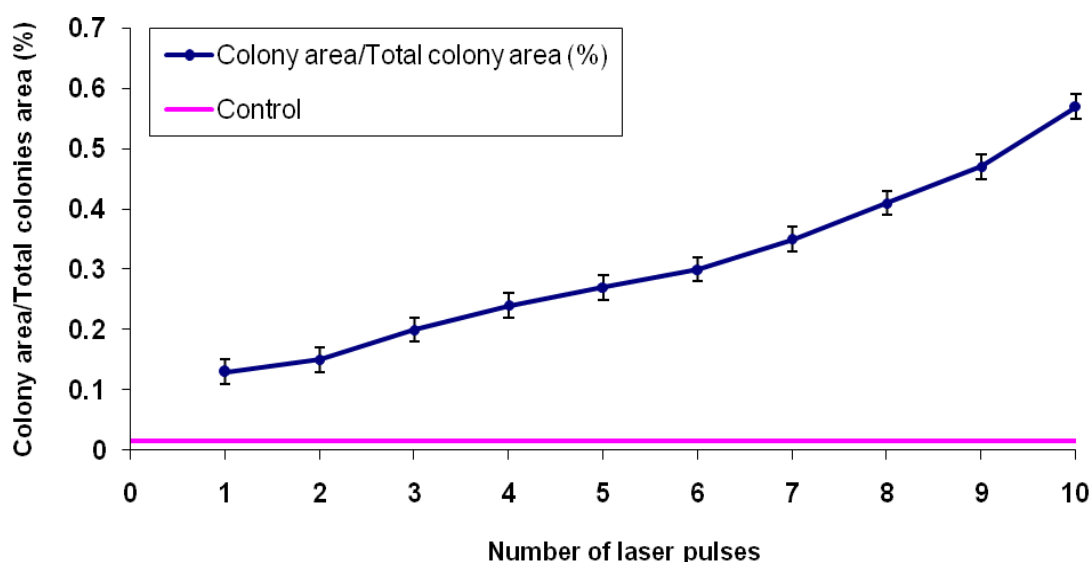


Figure 4.14 Ratio of the single colony area to the total area of colonies against number of laser pulses, control indicates (no laser radiation). The error calculated from the standard deviation over five readings

The results from Figure 4.14 indicate that the kill efficiency of the laser radiation away from the laser exposed area at 1 pulse was around 13% then the killing percentage increased to around 60% when the number of laser pulses increased to 10.

4.2 Killing of *B. atrophaeus* spores on LB agar surface with the excimer laser experiments

The killing efficiency of the excimer laser was investigated against *B. atrophaeus* spores on the agar surface. The experimental setup was similar to that used for the *E. coli*

experiments (see Section 4.1.2). The microbiological experiments were done under sterile conditions. LB nutrient agar plates were lawned with 200 μL of 1×10^8 CFU/mL *B. atrophaeus* spores and spread evenly, yielding a spore concentration of $\sim 3 \times 10^5$ spores/cm². The inoculated plate was placed in front of the laser beam at a distance of 150 mm, and exposed to various laser pulses (1, 2, 5 and 10 pulses, and 0 for the control). The laser was operated at a PRF of 100 Hz and the laser energy was 37 mJ. The agar plate was exposed clockwise from its designated top.

Another test was done on similarly lawned agar plates with *B. atrophaeus* spores. The plates were exposed to a fixed laser power for 10 s, 1 and 10 min and 0 (positive control) at 100 Hz. Then the PRF was decreased from 100 to 20 Hz to investigate the effect of repetition rate of the excimer laser on the inactivation of spores. And the inoculated plate was exposed for 10 s and 1 min.

4.2.1 Results from increasing number of pulses

The results in Figure 4.15 show that there was little clearing or inactivation of the spores on the plate that were treated with 1 pulse, however, the clearing increased with the number of pulses, as can be clearly observed in the agar plate treated with 2, 5 and 10 pulses. A comparison between the areas of clearing that were achieved from the *E. coli* experiments and these against *B. atrophaeus* indicate that *B. atrophaeus* spores are more resistant than *E. coli* bacteria to the laser irradiation at 248 nm.

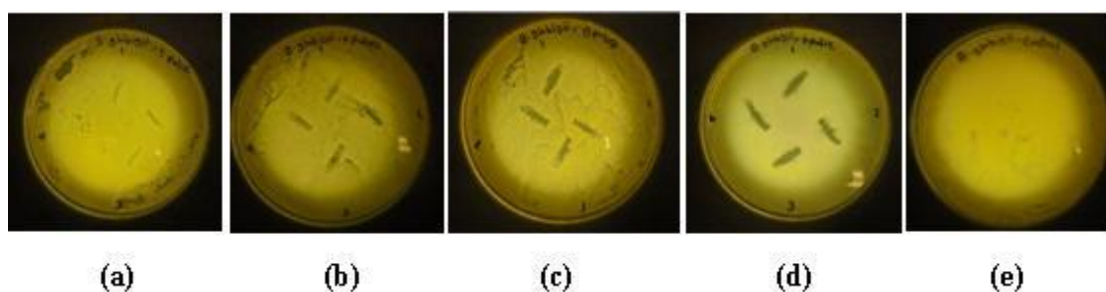


Figure 4.15 Agar plates lawned with *B. atrophaeus* spores and treated with a different number of pulses from the excimer laser a) 1 pulse, b) 2 pulses, c) 5 pulses, d) 10 pulses and e) control (no laser radiation)

Although the effect of the excimer laser was significant and obvious in the inactivation of spores, more analysis was done to quantify the area of clearing dependency with the number of laser pulses. The previous steps (see NI Vision diagram, Chapter 1: Section 1.5)

were applied for determining the areas of clearing and the results can be seen in Figure 4.16.

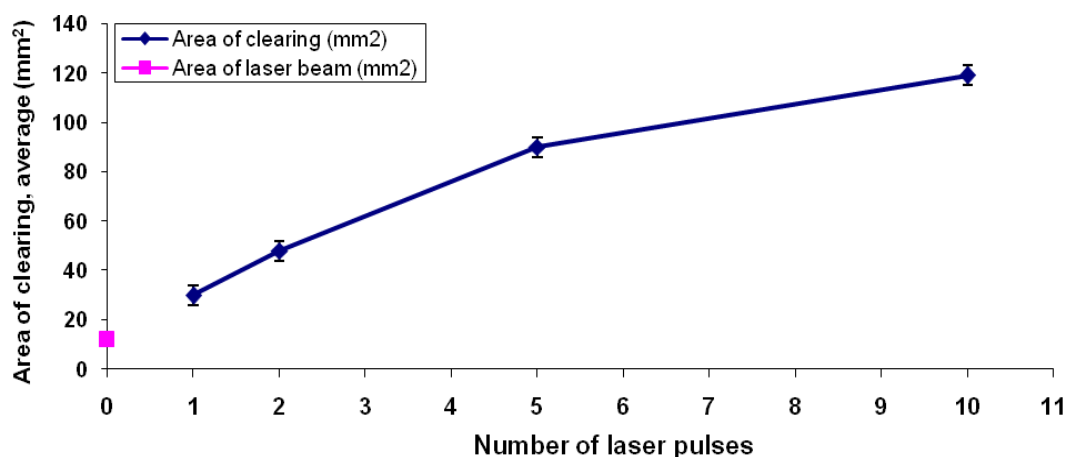


Figure 4.16 Area of inactivation against number of laser pulses, ■ indicates area of the laser beam (2 mm x 6 mm). The error bars for four readings

4.2.2 Results from fixed power exposure test

B. atrophaeus spores were successfully inactivated by the laser with a fixed power of 64 mW, at 100 Hz and with a varied exposure time of 10 s, 1 and 10 min, as shown in Figure 4.17. When the exposure time was increased to nearly 10 min, the laser irradiation was sufficiently high that the agar melted. The arrow on the Figure 4.17 (c) indicates the damage observed after 10 min, or see Figure 4.17 (d) for a close up view of this damage. So the treatment time should be not more than 7 min for this type of laser, or the PRF should be reduced to decrease the incident power.

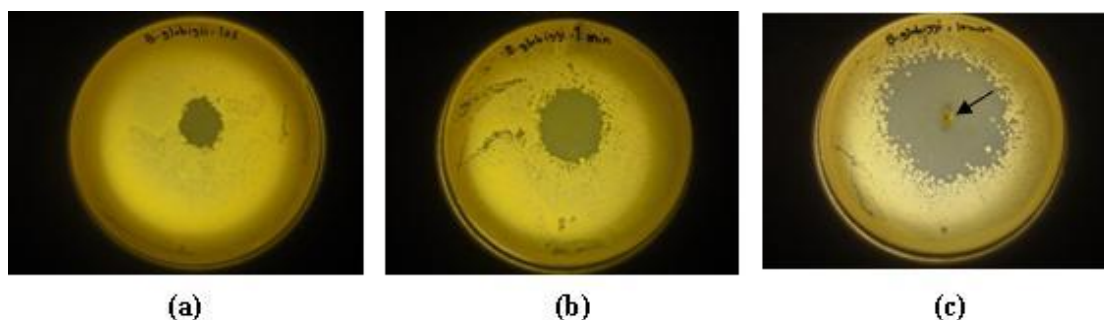


Figure 4.17 Agar plates lawned with *B. atrophaeus* spores and treated with excimer laser of fixed power for a) 10 seconds, b) 1 minute and c) 10 minutes at 100 Hz PRF



Figure 4.17 (d) A close up view of the laser damage on the agar plate

4.2.3 Results of varying the pulse repetition frequency

To see the effect of the PRF of the excimer laser on spore inactivation, the PRF was decreased from 100 to 20 Hz. Although, the exposure time (10 s and 1 min) was the same as in the previous experiment (Section 4.2.2) with fixed power. The area of clearing decreased significantly, as shown in Figure 4.18. In conclusion, the area of clearing increases with increasing PRF, as laser pulse energy increases.



Figure 4.18 Agar plate lawned with *B. atrophaeus* spores and exposed to 37 mJ laser pulses for 10 seconds (top) and 1 minute (bottom) at 20 Hz PRF

4.3 The Booster system for air decontamination

4.3.1 Introduction to the booster system

The booster system was designed to act as a laser based air decontamination system where the air is allowed to flow into a chamber that is exposed to laser radiation. Ideally the booster is positioned inside the laser cavity and exploits all aspects of the laser system for enhancing decontamination. Alternatively the chamber could be positioned outside of the laser cavity but will be less effective because the irradiance is lower. The idea of the booster system was originated by Watson (2007). The advantages of the booster system are its potentially high performance, safe operation, reliability and it can be easily located into an air flow. The three main components of the external decontamination system and testing stage are as sketched in Figure 4.19 (a) and include:

- **Inoculation stage:** a particle generator is used to produce an aerosol of microorganisms.
- **Decontamination stage:** the booster chamber and the laser system to treat the aerosol.
- **Collection stage:** the treated air samples are collected with an air sampler, incubated and analysed or a particle counter can be used.

Figure 4.19 (b) shows a schematic of the booster and its position relative to the mirrors of the laser cavity and where the decontamination occurs.

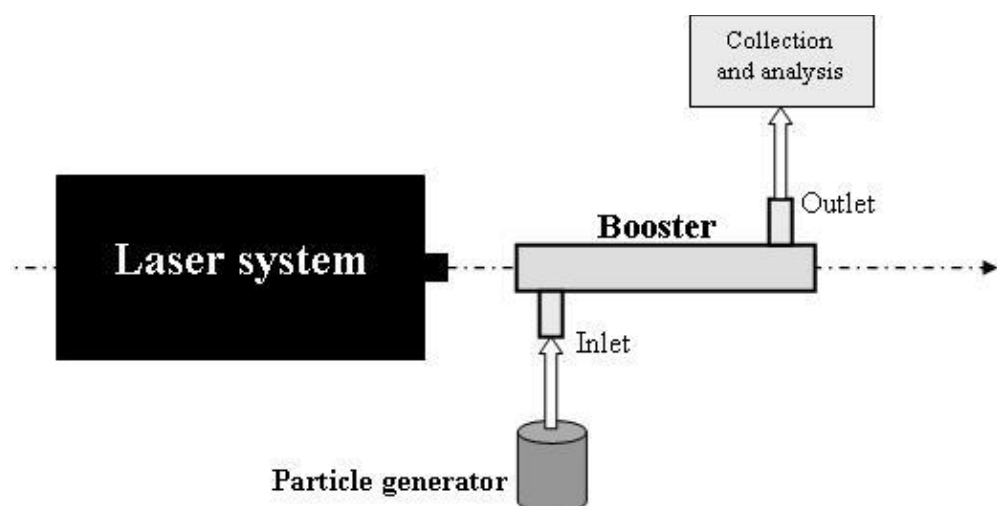


Figure 4.19 (a) External booster system stages

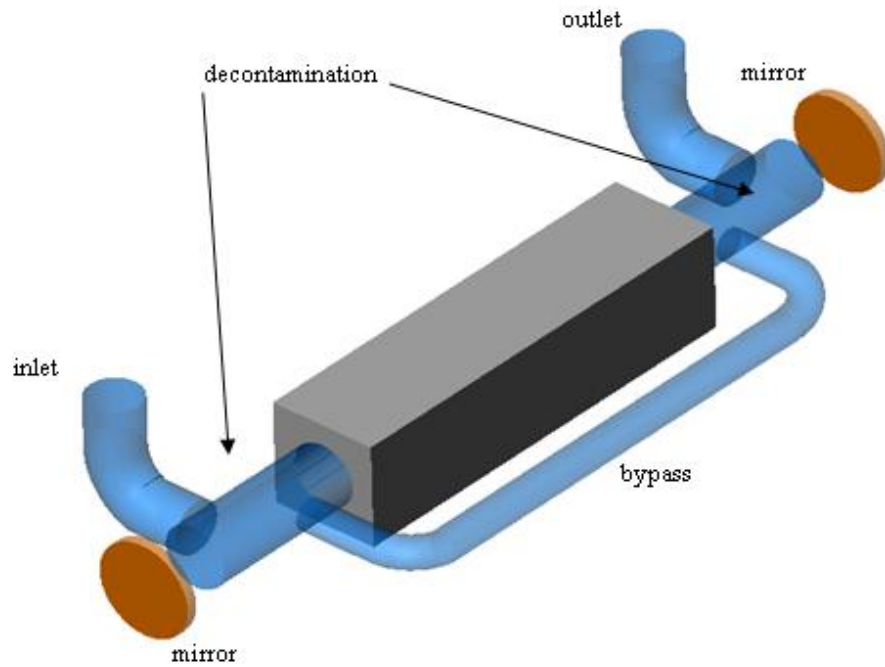


Figure 4.19 (b) Laser Booster for enhanced air decontamination

4.3.2 Glass booster system

The glass booster was fabricated from fused quartz material (SiO_2) by the glass blower Willy McCormack, University of Glasgow. Figure 4.20 shows a photograph and CAD drawing of the glass booster. The glass booster was 50 mm long and the internal diameter was 18 mm, more details can be seen in the CAD image in Figure 4.21.



Figure 4.20 Glass booster

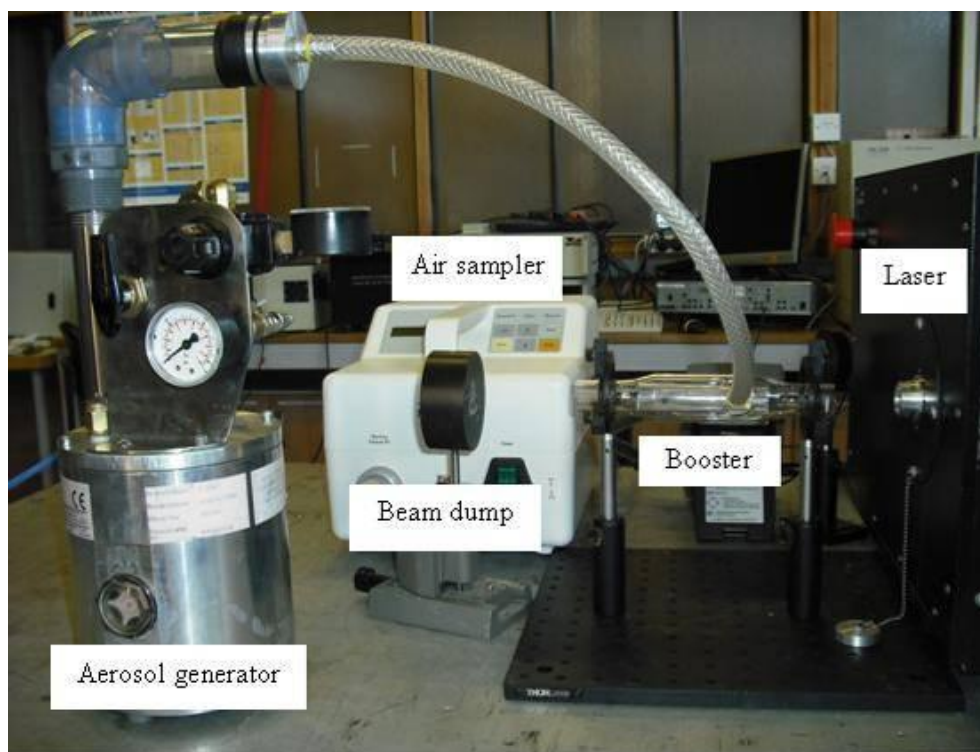


Figure 4.22 Glass booster experiment setup

ii. Experimental Procedure

The particle generator and the air sampler were switched on and the control samples (without laser treatment) were taken for 2 and 4 minutes. After the control sample, the excimer laser was switched on and the test samples were taken for the same sampling times. The laser was operated at 35 mJ and 100 Hz. The test samples were collected by the air sampler on the gelatine membrane filter (pore size of 0.8 μm , 80 mm diameter, Sartorius, UK). The air sampler draws the aerosol through the gelatine filter which collects and retains the micro-organisms for sampling periods (the gelatine viability was maintained of around 30 minutes). See chapter 2: Figure 2.20 the air sampling procedure summarize this process.

4.3.2.2 Results of the glass booster system with the excimer laser experiment

The results using the glass booster external to the laser cavity can be seen in Figure 4.23. The colonies were counted using NI Vision software. For 2 min collection time, the number of colonies collected was 110 CFUs compared to 226 CFUs in the control, giving an inactivation percentage of 51.33%. While for the 4 minutes treated sample, the number

of the colonies was 14 CFUs compared to 113 CFUs in the control (87.61% inactivation). These results were relatively good as only ~ 10% of the inoculated air was treated by the laser beam because the beam area of the excimer laser was 12 mm² (beam profile 2 x 6 mm) and the cross sectional area of the glass booster chamber was 113 mm² (12 mm in diameter).

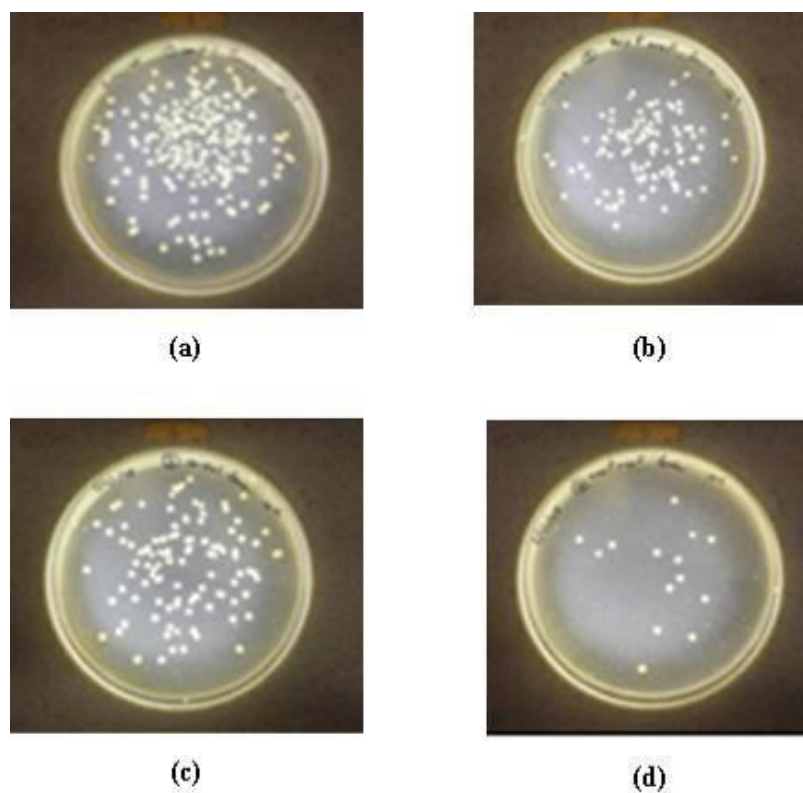


Figure 4.23 Glass booster experiment (top row) a) control and b) treated plate for 2 minutes, (bottom row) c) control and d) treated plate for 4 minutes

4.3.2.3 Flow shape distribution using Fluent

The Computational fluid dynamics (CFD) package Fluent 6.3 (ANSYS Inc., UK) was used to investigate the air flow and particle trajectories along the length of the glass booster. This is important as it is critical to know where the microorganisms are flowing and whether they will receive sufficient exposure during their residency time within the laser beam. For the simulation steps see Chapter 1: Section 1.6 Computational fluid dynamics (CFD) modelling. The glass booster was designed in a CAD package (SolidWorks 2010, SP 4.0, UK), and the booster model was exported into Gambit 2.4 (ANSYS Inc., UK). The solid volume of the booster was successfully meshed with tetrahedral and hexahedral mesh shapes; the final meshed geometry can be seen in Figure 4.24.

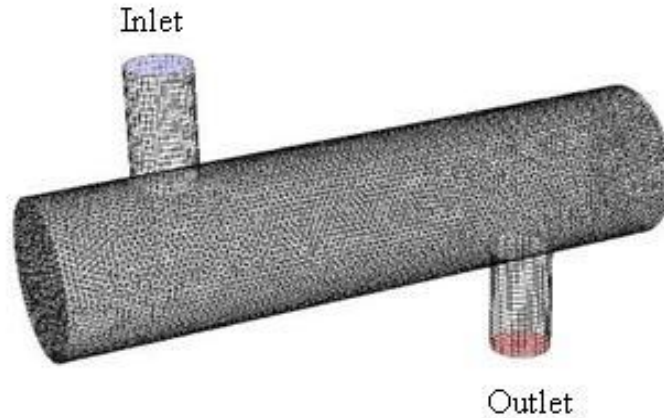
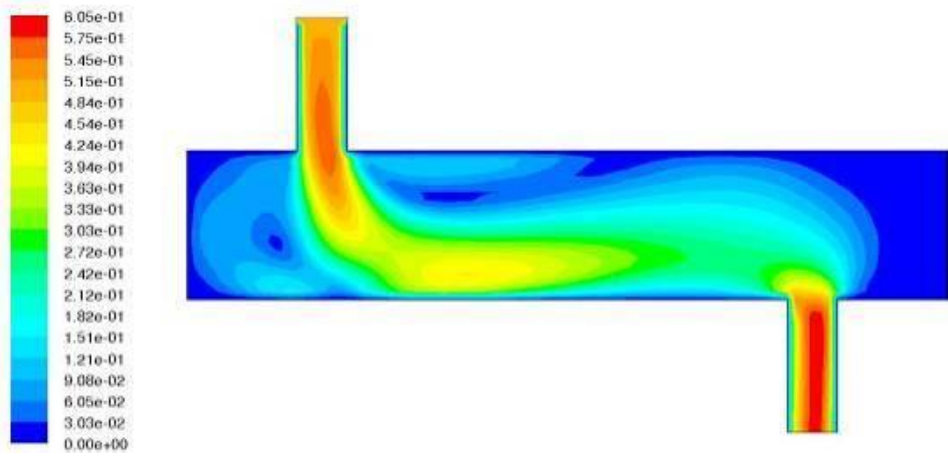


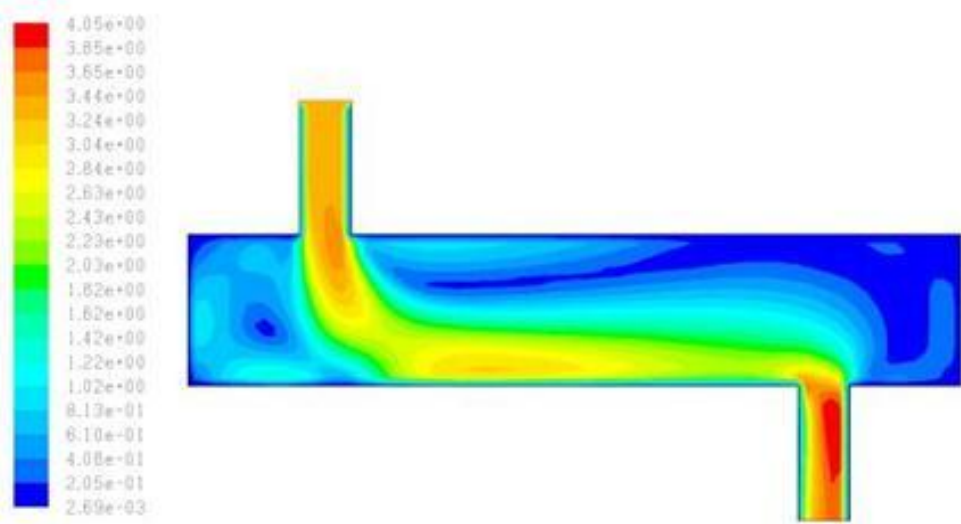
Figure 4.24 Mesh of the glass booster

After meshing, the model was imported into Fluent. The particle aerosol (*B. atrophaeus* spores of 1 μm diameter) was released from the inlet of the glass booster. The boundary conditions were specified as: three inlet velocities of 0.5, 3 and 5 m/s, operating pressure equal to 0.15, 0.5 and 0.75 bar respectively. The volumetric flow rates were 9, 50 and 90 L/min for inlet velocities of 0.5, 3 and 5 m/s respectively.

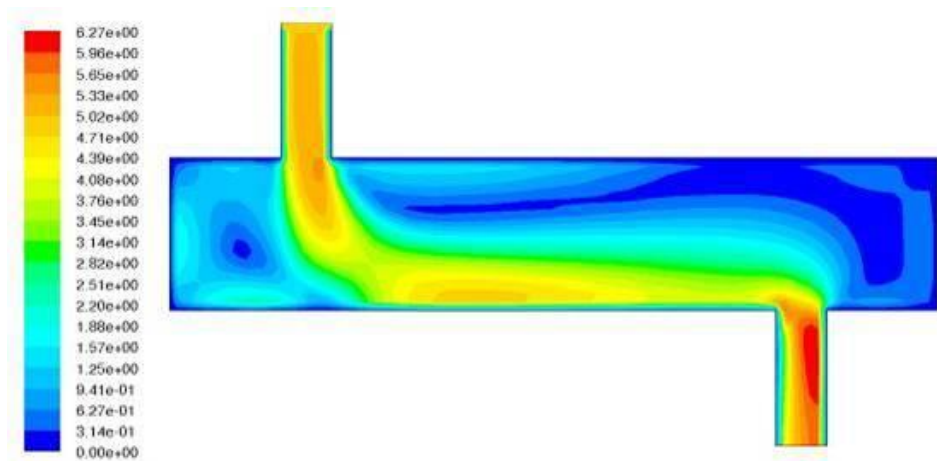
The flow field and the particle tracking were analysed in 2D (Figure 4.25) and 3D (Figure 4.26). For the lowest velocity of 0.5 m/s (Figure 4.25 (a) and Figure 4.26 (a)), the flow of the particles seemed steady and smooth with little aerosol deposition in the bottom region of the booster, such deposition is undesirable because the laser beam is located central to the longitudinal axis of the chamber, any microorganisms deposited in this region would be hard to kill as the laser exposure is low. At the two end regions of the booster, there were a quite few of spores landing or depositing on the beam inlet and outlet region of the booster. For the higher velocities 3 m/s and 5 m/s (Figure 4.25 (b and c) and Figure 4.26 (b and c)), the particle flow became more dispersive within the booster and this means that there is more chances of killing the microorganisms. However, the rate of aerosol spore deposition increased at the bottom of the chamber; this is undesirable in this region as it is away from the central axis and the position of the laser beam.



a) At inlet velocity of 0.5 m/s

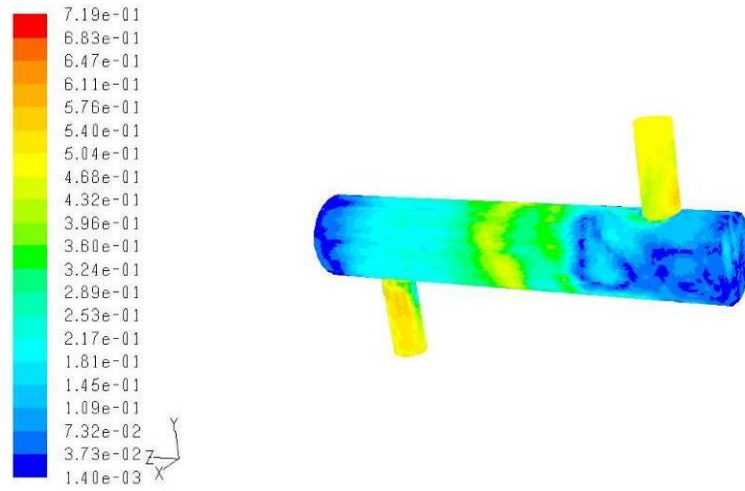


b) At inlet velocity of 3 m/s

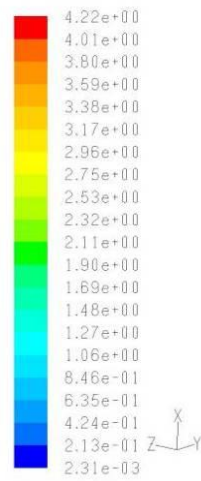


c) At inlet velocity of 5 m/s

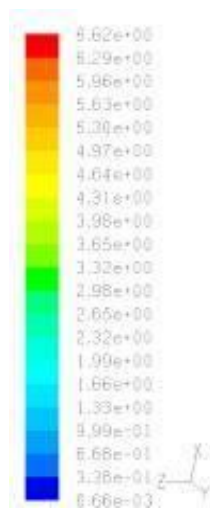
Figure 4.25 Flow distribution inside the glass booster with various inlet velocities (2D)



a) At inlet velocity of 0.5 m/s



b) At inlet velocity of 3 m/s



c) At inlet velocity of 5 m/s

Figure 4.26 Flow distribution inside the glass booster with various inlet velocities (3D)

4.3.3 Stainless steel booster system

While the glass booster (Section 4.3.2) successfully demonstrated the concept, the killing was relatively low because of the booster's short length and consequently the short residency time of the spores. Hence longer systems were designed and fabricated. Two stainless steel boosters were made from stainless steel tubes of length (inflow to outflow) 430 and 720 mm, and the internal diameter for both tubes was 12 mm (external diameter was 15 mm). The 25 mm windows were made from fused quartz (Lapmaster Quartz Optical Flats, UK). The two windows were placed at each end of the booster to pass the laser beam, and the distance between the windows was 600 mm and 870 mm for the short and long systems respectively. Windows at either end allowed the option for detecting the radiation transmitted, and hence absorbed, through the system. The optical holders were made from stainless steel, 15 mm rubber O-rings were placed between the holder and the window to prevent damage. The pipes were joined together by a brass 15 mm compression tee fittings (Conex, UK). This prevented warping of the tube as no welding was necessary. The stainless steel boosters are shown in Figure 4.27.



Figure 4.27 Stainless steel boosters

4.3.3.1 Microbiological experiments with the stainless steel booster system and excimer laser

The experiment was done to investigate the stainless steel booster performance with excimer laser treatment at 248 nm. The protocol and setup of the experiment were the same as that used in the glass booster experiment (see Section 4.3.2.1). The *B. atrophaeus*

spore laden aerosol was pumped into the inlet of the booster, and the air sampler was placed at the outlet. The excimer laser was passed into the booster through the input window and a beam dump was placed behind output window. Figure 4.28 shows the experimental setup, and Figure 4.29 shows a schematic diagram of the experiment. The experiment was done in triplicate to provide more accurate results. The system was run for 2 min.

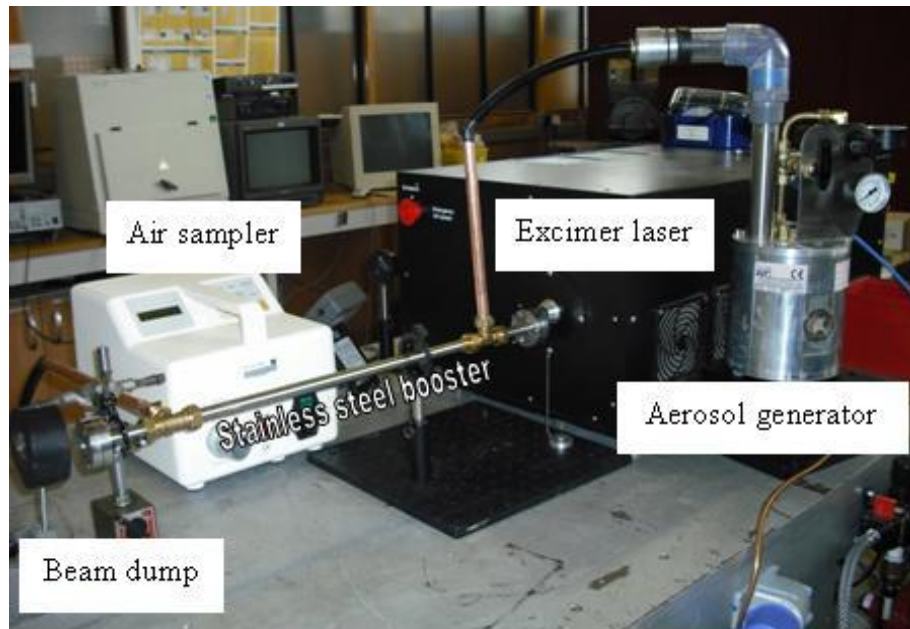


Figure 4.28 Excimer laser and the stainless steel booster experiment setup

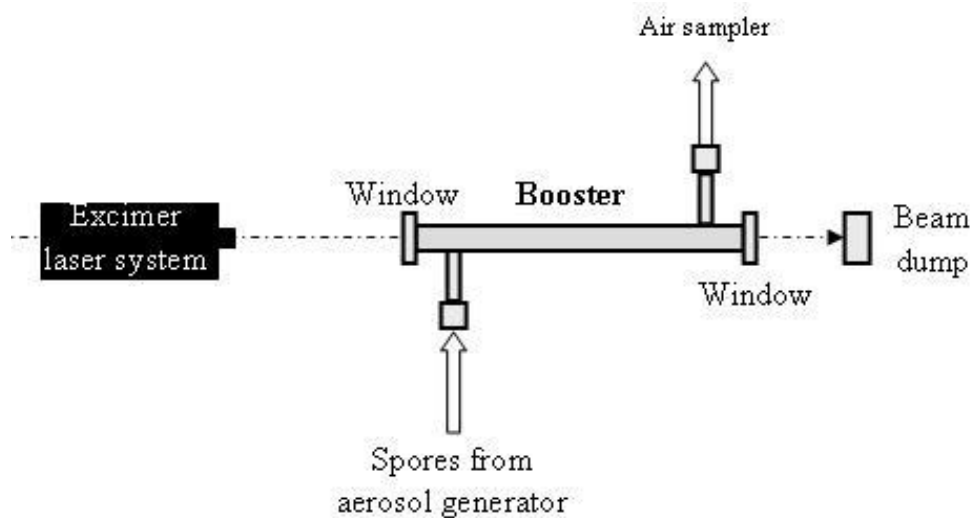


Figure 4.29 Excimer laser and the stainless steel booster schematic drawing

4.3.3.2 Results of the experiment with the stainless steel booster system and excimer laser treatment

In this experiment, the rate of killing using the excimer laser was very high and effective against *B. atrophaeus* spores. Clearance of the spores was more than in the glass booster experiment, because of the increased length of the booster and resulting increased residence time of the spores during the treatment, hence the inactivation level was significant. The residence (transit time) for the spores inside the stainless steel booster was 143 ms for the short one (430 mm length measured from inlet to outlet with an air velocity of 3 m/s) and 240 ms for the long one (720 mm length measured from inlet to outlet with an air velocity of 3 m/s), while for the glass booster it was only 17 ms (50 mm length measured from inlet to outlet with an air velocity of 3 m/s). As well this, the internal diameter of the stainless steel tube (12 mm) was narrower than the glass booster (18 mm), and this gave improved coupling with the laser beam profile. Although it should be mentioned that the beam profile for the laser was rectangular (2x6 mm) so the geometrical coupling was still not optimised.

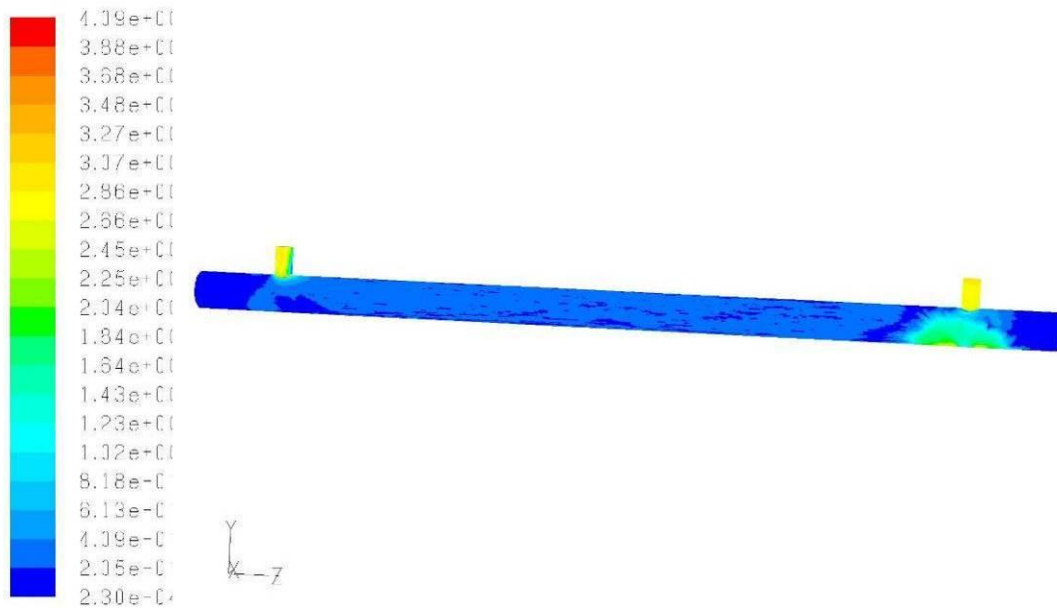
The treated plates were incubated over night. Then, the colony counts on the plates were quantified using NI vision software; the results of the experiment can be seen in Table 4.1. For the short stainless steel booster, the reduction of the *B. atrophaeus* spores exposed to the excimer laser was 97.54% and 99.80%, at 100 and 200 Hz respectively. While for the long stainless steel booster, the rate of reduction was over 99.80% for both 100 and 200 Hz treatments. For both lengths of stainless steel boosters, the killing percentage increased significantly with increasing pulse repetition frequency.

Table 4.1 Reduction of *B. atrophaeus* spores exposed to the excimer laser at 100 and 200 Hz (n = 3)

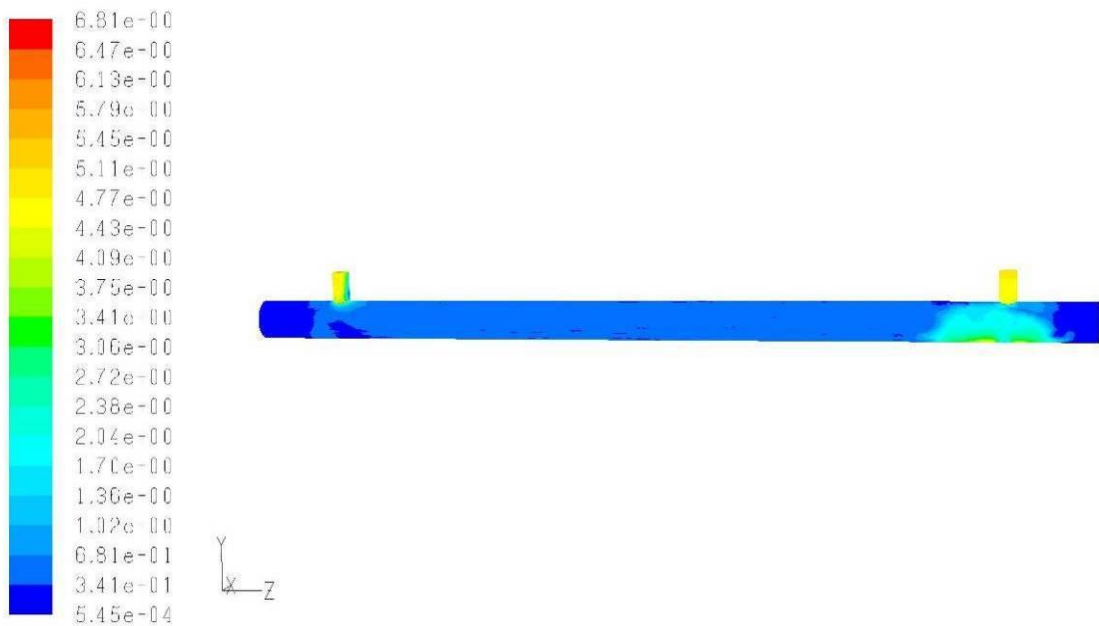
Short stainless steel booster (600 mm)						
Sample	CFUs Control	CFUs 100 Hz	Reduction %	CFUs Control	CFUs 200 Hz	Reduction %
1	1937	52	97.32	2017	4	99.80
2	1570	36	97.71	1430	3	99.79
3	1450	35	97.59	1493	3	99.80
Average			97.54±0.0019%			99.80±0.0001%
Long stainless steel booster (870 mm)						
Sample	CFUs Control	CFUs 100 Hz	Reduction %	CFUs Control	CFUs 200 Hz	Reduction %
1	1653	1	99.94	1543	1	99.94
2	1580	3	99.81	1651	0	100
3	1773	5	99.71	1755	1	99.94
Average			99.82±0.0012%			99.96±0.0014%

4.3.3.3 Results from the Fluent analysis

The flow was analysed inside the stainless steel booster using the Fluent package. The particles were released at the inlet of the booster with initial velocities of 3 and 5 m/s. The results of the particle trajectory profile showed that at a distance of around 100 mm from the input window (the right side of the graph) there were microorganisms landing on the bottom of the tube. At the booster ends (near the two windows), the air flow seemed low which would result in reduced circulation of the air in these regions. Figure 4.30 (a) and (b) show the flow shape distribution inside the stainless steel tube with inlet velocity of 3 m/s and 5 m/s, respectively.



a) An initial velocity of 3 m/s



b) An initial velocity of 5 m/s

**Figure 4.30 Flow distribution inside the stainless steel booster (short) with different initial velocities (3D).
Inlet side is on the right**

4.3.4 Internal cell booster system

The excimer laser was modified by the laser manufacturer (GAM Laser Inc., USA) so that an intracavity cell was placed towards the rear mirror. A CAD drawing of this modification can be seen in Figure 4.31. The aim of this modification was to pass the contaminated air between the resonator cavity where there is a greater laser irradiance and was the original embodiment of the idea by Watson (Foss-Smith & Watson 2008). The internal cell was

made from the stainless steel material. The internal booster was placed inside the laser cavity after the active medium, and separated by a Brewster window to prevent laser cavity contamination. Photographs of the position of the internal cell inside the laser systems are shown in Figure 4.32

This modification whilst safe and efficient was unfortunately not in line with that requested of the manufacturer. The inlet and outlet of the aerosol were located adjacent to each other rather than at opposite ends of the system as with the previous designs tested externally. Consequently, there was insufficient distance for the air flow between the inlet and outlet resulting in a very short residence time. The inoculated air intersects with the laser beam in a very small area equal to the beam width and not along the laser beam axis. However, experiments were done to determine the effect of using an intracavity booster system.

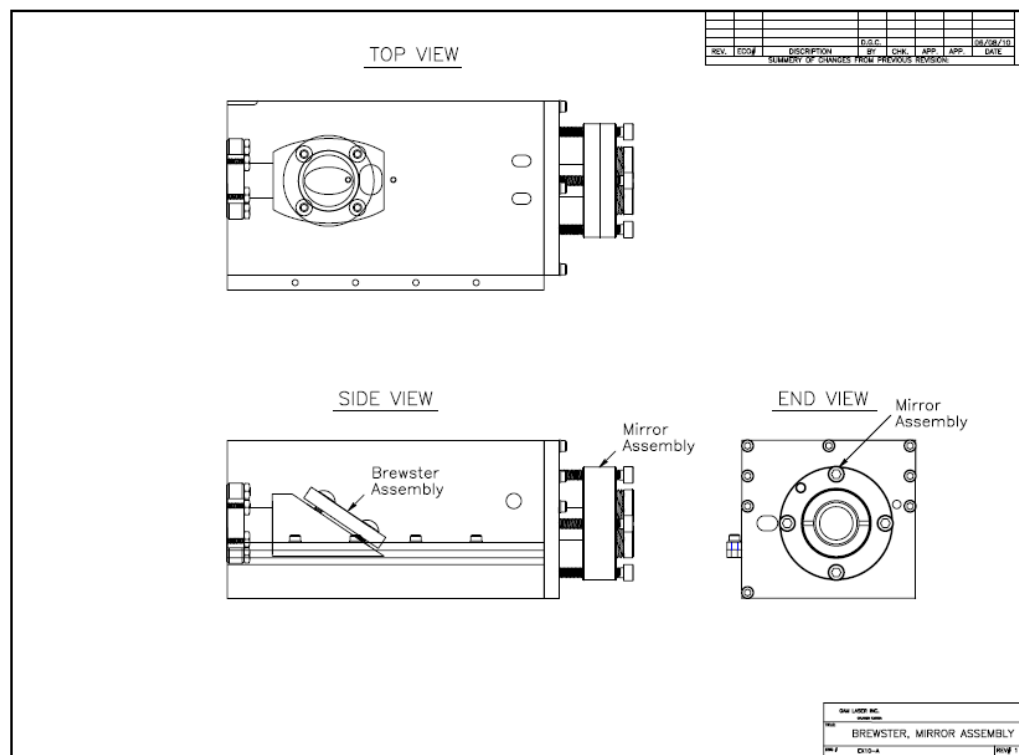


Figure 4.31 CAD drawing of the internal cell booster (supplied by GAM)

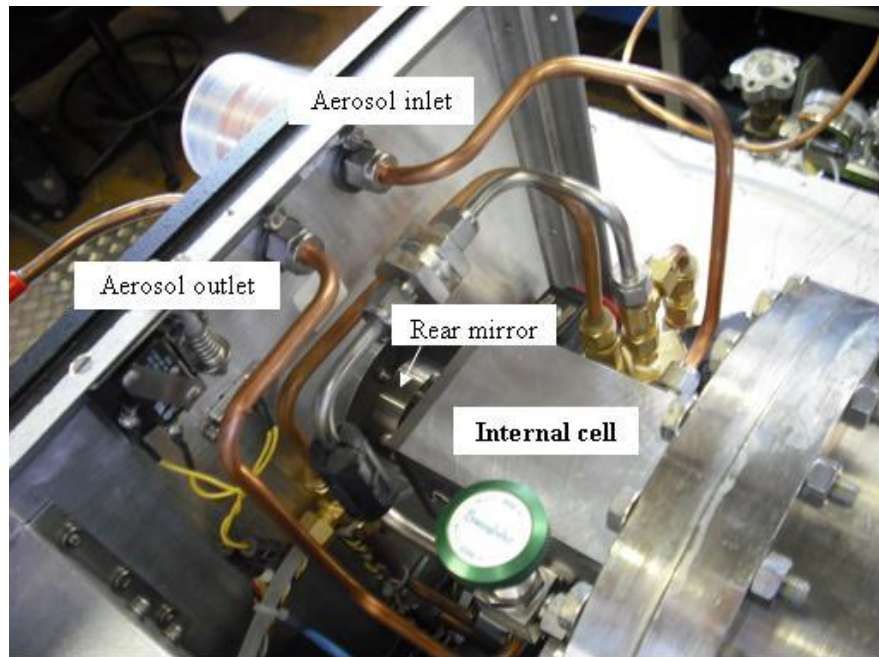
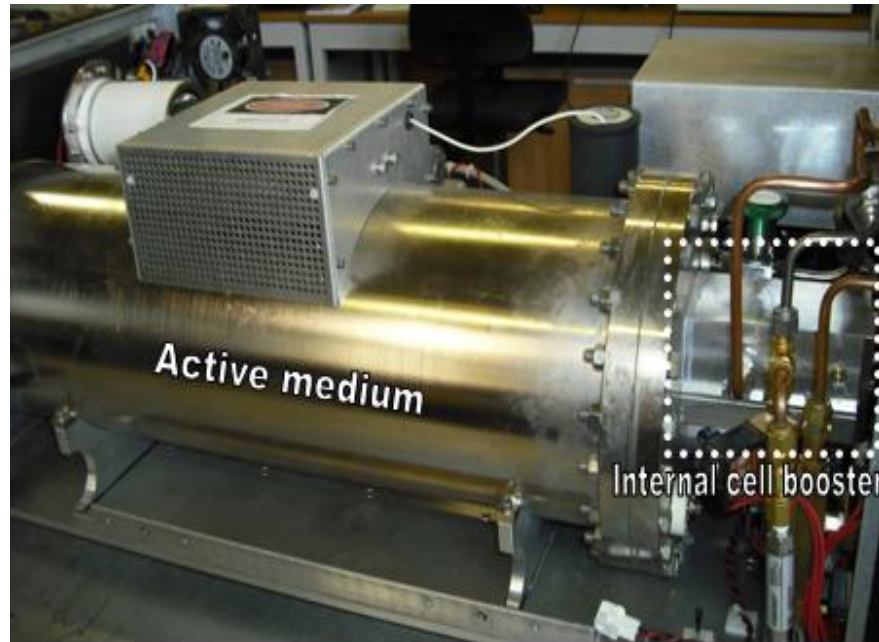


Figure 4.32 Views of the excimer laser with the internal cell booster

4.3.4.1 Microbiological experiments of the internal cell system with the excimer laser

The experiments were designed to study the excimer laser sporicidal effect inside the resonator cavity. 500 mL of 10^4 CFU/mL culture of *B. atrophaeus* was placed in the aerosol generator tank. The inoculated air was passed through the internal booster and treated with the excimer laser radiation. The sampling time was 2 min. Figure 4.33 shows

the schematic drawing of the experiment, and the experimental setup is shown in Figure 4.34.

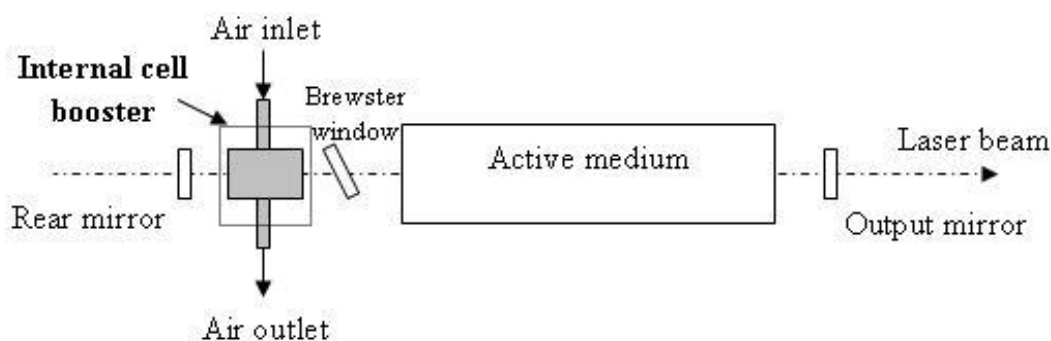


Figure 4.33 Schematic drawing of the internal cell booster

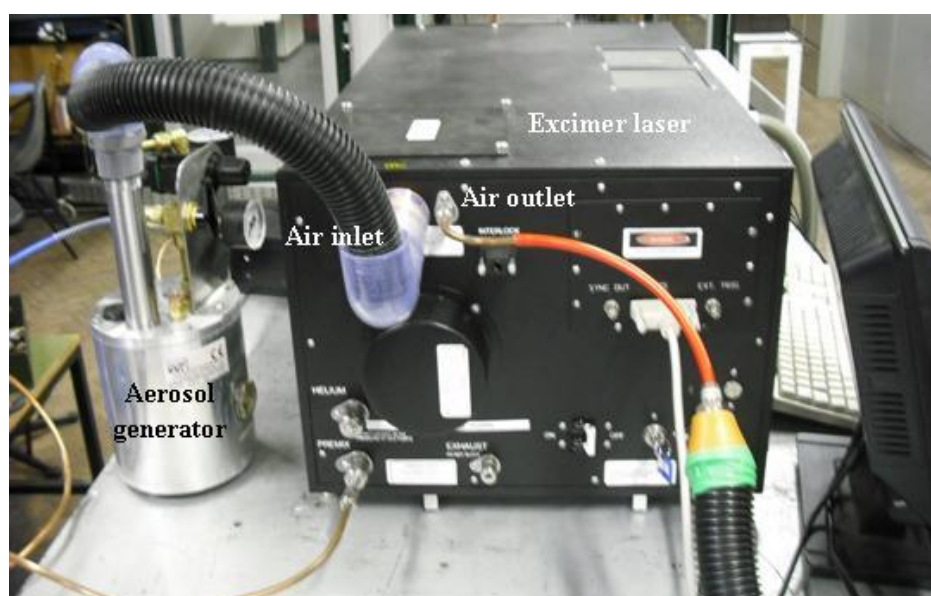


Figure 4.34 The experimental setup of the internal cell booster

Two different positions of the control measurement (see Figure 4.35) were taken (before and after the spore laden aerosol passed through the internal booster), this allowed estimating the potential losses of the spores through the cell and the pipes. In the first treatment, the control samples were taken before the spores passed through the internal booster, and the PRF was set to 20 and 200 Hz for subsequent treatment. In the second treatment, the control samples were taken at the aerosol output near the collector (air sampler), for different values of PRF (15, 20, 100 and 200 Hz). The experiments were done in triplicate to reduce the error and to obtain the average killing. After sampling, all the laser treated plates were incubated over night at 37 °C for growth and subsequent analysis.

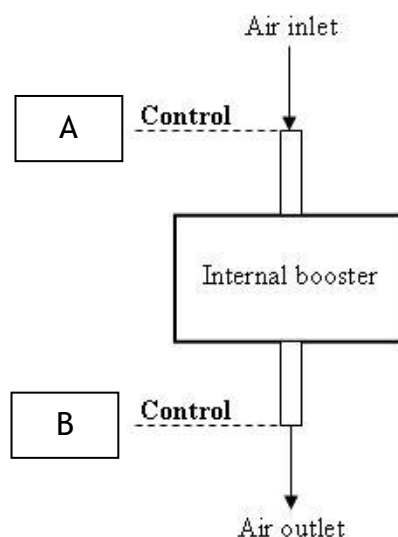


Figure 4.35 Schematic diagram showing the different positions where the controls were taken. The control samples were taken before and after the aerosol passed through the booster

4.3.4.2 Results of the internal cell booster system with the excimer laser experiment

The laser radiation provided a significant sporicidal action to *B. atrophaeus* even though the residence time was short. The results of the first part of the experiment (the control position at the air flow input (point A)) can be seen in Table 4.2.

Table 4.2 *B. atrophaeus* treated to the excimer radiation in the internal booster experiment (the control samples were taken at the aerosol input (point A)) at a pulse energy of 37 mJ and PRF of 20 and 200 Hz

Laser at PRF of 20 Hz			
Sample	Control - CFUs	CFUs	% of killing
1	4000	644	83.9
2	4000	284	92.9
3	6000	207	96.6
Average			91.13%
Laser at PRF of 200 Hz			
Sample	Control - CFUs	CFUs	% of killing
1	4000	224	94.4
2	6000	131	97.8
3	5400	300	94.5
Average			95.57%

The results from the second part of the experiment (where the control samples were taken at the aerosol output (point B)) are given in Table 4.3. Due to limitation of the internal booster and unsatisfactory design by the laser maker, the results showed that there was a small decrease in the spore numbers. So the results (first and second part) mean that the reduction in the microorganism's number is not only due to the laser interaction but were in fact due to the deposition within the system.

Table 4.3 *B. atrophaeus* spores treated to the excimer radiation in the internal booster experiment (the control samples were taken at the aerosol output (point B)) with flow rate of 35 L/min

PRF (Hz)	Control CFU	Sample 1 CFU	Control CFU	Sample 2 CFU	Average of killing (%)
15	190	190	243	241	0.82
20	210	208	190	187	1.27
100	190	188	280	272	1.96
200	200	187	175	153	9.54

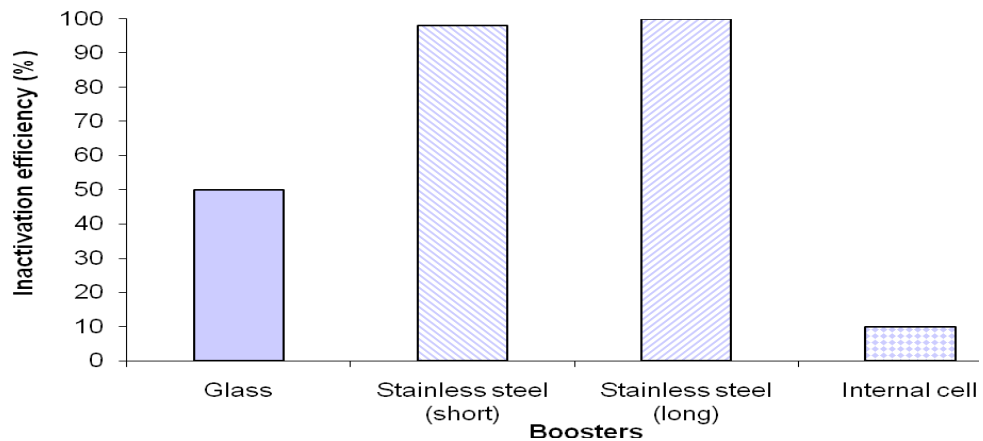
This showed minimal killing, but there was some dependency on PRF, indicating some effect albeit small. Consequently, the protocol of the previous experiments was modified by decreasing the compressed air pressure (0.5 bar to 0.25 bar), thereby decreasing the aerosol flow rate to increase the residency time of the spores in the internal cell, so the exposure time would be longer. The results showed there was a little increase in the efficiency of killing (from about 2 to 9.9% for 100 Hz treatment and from 9.5 to 30.6% for 200 Hz treatment). The results are shown in Table 4.4.

Table 4.4 *B. atrophaeus* spores treated to the excimer radiation in the internal booster experiment (the control samples were taken at the aerosol output (point B)) with flow rate of 20 L/min

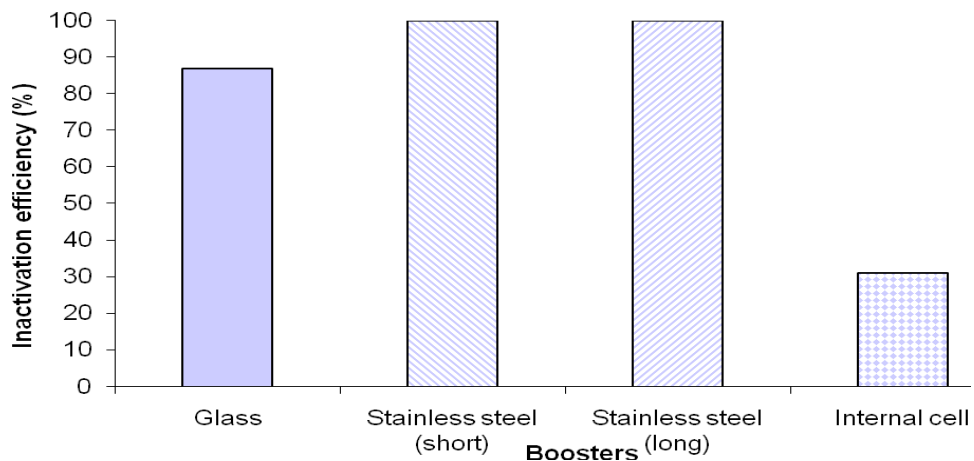
Laser at PRF of 100 Hz			
Sample	Control (CFUs)	CFUs count	% of killing
1	143	129	9.8
2	126	109	13.5
3	142	133	6.3
Average			9.9%
Laser at PRF of 200 Hz			
Sample	Control (CFUs)	CFUs count	% of killing
1	182	89	51.1
2	149	118	20.8
3	145	116	20.0
Average			30.6%

4.3.5 External and internal boosters comparison

The external boosters (glass and stainless steel) and the internal cell booster (stainless steel) were designed and made to investigate the efficiency of the excimer laser to kill the aerosolized microorganisms, *B. atrophaeus* in this case. This comparison allowed assessment of the different boosters' performances, and data were collected from the results in the previous sections. Figure 4.36 (a) and (b) shows the summary of the percentage of inactivation efficiency (reduction of the spore concentration due to exposure to laser radiation) of the excimer laser for various boosters operating at PRF of 100 and 200 Hz respectively. The results indicate that the excimer laser has a high inactivation capacity of *B. atrophaeus* spores in air using the booster system (over 97%). The comparison between the boosters showed that the percentage killing significantly increased using the external stainless steel booster system. A longer length of the booster allowed for a longer residency time and a good interaction between the laser beam and the microorganisms.



a) At PRF of 100 Hz



b) At PRF of 200 Hz

Figure 4.36 Percentage of killing of the excimer laser for various boosters at PRF of 100 and 200 Hz

Chapter 5

Detection and growth of microalgae

Biofuel is a potential replacement for a petroleum fuel, generally derived from sustainable resources (Griffiths & Harrison 2009). They are carbon neutral and produce fewer emissions than petrochemicals. The experiments were executed on the microalgal species *Nannochloropsis oculata* and *Chlorella vulgaris*. Techniques of microalgal detection were previously investigated (Chapter 3: Sections 3.7 and 3.9). This chapter lays the precursor for using some of these techniques for detection of microalgae in liquid and development of further techniques to quantify processes relating to biodiesel production from microalgae. The effects of different environmental conditions on the growth of these microalgae were investigated. Dewatering and extraction techniques were investigated. This chapter focuses on algal cultivation, harvesting and the oil extraction. Figure 5.1 shows the algal biomass and oil production stages. Decontamination processes previously investigated play a potentially important role in maintaining microalgae growth without contaminants, which can reduce growth and purity of harvested components.

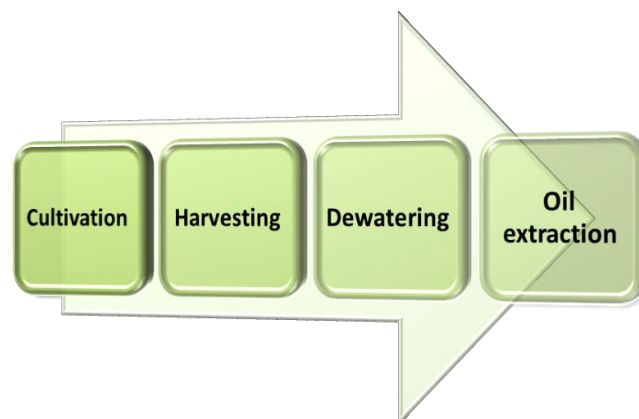


Figure 5.1 Schematic represents the algal biomass and oil production stages

5.1 Algal growth

The effect of various parameters on algal growth to obtain the optimal growth conditions was investigated. The important parameters that effect the growth include: light, temperature, nutrients, circulation, salinity, and CO_2 gas. The system of algal biomass production can be seen Figure 5.2.

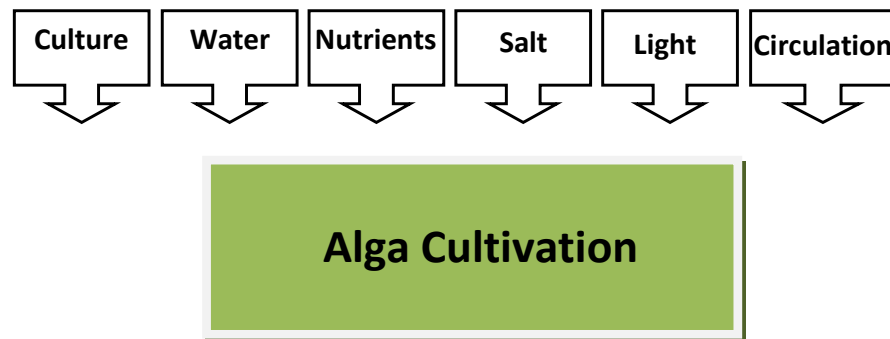


Figure 5.2 Schematic drawing of algal biomass production

5.1.1 Photobioreactors (PBR)

Photobioreactors (PBRs) allow algal growth by supplying light to a bioreactor. PBRs were built in-house in the Mechanical Engineering workshop to investigate and optimize the algal growth. There were three designs that were used: a vertical tubular PBR, a column vertical-tube PBR, and a large tank PBR. The tubular PBR was made from acrylic material. It consisted of six tubes arranged vertically (60 mm diameter, 500 mm length, 6 L total volume), and the tubes surrounded a fluorescent light of $9 \mu\text{mol}/\text{m}^2/\text{s}$ light intensity (14 W, 525 mm long, white (Ryness Lighting & Electrical Ltd, UK)). The culture inside the tubes is circulated by air bubbles using an air pump (Hailea, ACO-308, China) with a six way airline manifold (Hailea, China). The circulation is important to circulate the culture between the light and dark areas and to decrease the sedimentation, and provide a gaseous CO_2 input. Figure 5.3 shows the tubular PBR. Another tubular PBR was designed, consisting of one tube, see Figure 5.4. The length of the tube was 1090 mm, and the diameter was 177 mm with volume ~ 27 L. Other researchers use a diameter less than 200 mm to allow the light to reach the centre of the tube. The air is pumped in the long tube at the bottom by an air pump (Aqua, AP2 Interpet, UK).



Figure 5.3 The tubular vertical photobioreactor with six parallel tubes



Figure 5.4 The vertical column photobioreactor

The tank PBR is made from a glass material (200 L), see Figure 5.5. The culture media is circulating by using an air pump (Hailea, ACO-308, China) with four ring diffusers (KD, UK). Either a fluorescent light of $37 \mu\text{mol}/\text{m}^2/\text{s}$ light intensity (Crompton lighting (58 W), F58TB, Hungary) or a special growth light of $74 \mu\text{mol}/\text{m}^2/\text{s}$ light intensity (Sunmaster dual spectrum (250 W), SL.U46.DSP, USA) were placed over the tank.



Figure 5.5 A large glass tank PBR

5.1.2 Sample preparation for microscopy

The microalgal culture *Nannochloropsis oculata* (Reefphyto, UK) was grown, cultivated and harvested within the School of Engineering, at the University of Glasgow inside the photobioreactors (PBR) described in Section 5.1.1. The density and growth rate of the algae was examined and quantified using an optical microscope (Leitz Wetzlar, Orthoplan, Ploemopak 2.2, Germany) with a 25X objective (NA 0.4, Zhumell, China). A 30 μL sample of algae was transferred from a stock culture using a pipette, and dropped over a microscopic slide of 26x76 mm size (Deltalab, Spain). The coverslip of 0.17 mm thickness (Smethwick, UK) was placed over the sample drop. Figure 5.6 shows the preparation of the microscopic slide.



Figure 5.6 Microscopic sample preparation

5.2 Algal counting

The cell density and growth rate of algae under different environmental conditions was usually measured once per day. The Leitz Wetzlar microscope was used for the algal

counting. The same technique was used throughout the experiments, unless otherwise stated. The formula derived for algal counting (cell per mL) is:

$$N_t = \frac{\sum (\text{Cells per images})}{\text{No. of images} \times X \times Y \times C_f^2 \times Z} \quad \text{Equation 5.1}$$

Where N_t refers to the total number of cells per millilitre, X and Y represent the size of the microscopic image ($X = 1280$ pixel, $Y = 960$ pixel) over the experiments, and C_f refers to the calibration factor which was $0.085 \mu\text{m}/\text{pixel}$ for the objective lens of 25X (see Appendix C: microscope calibration). The variable Z represents the distance between the top of the slide and the coverslip i.e. the depth of sample.

The growth rate, r , was calculated using the following equation (Suchar & Chigbu 2006):

$$r = \frac{\ln\left(\frac{N_f}{N_0}\right)}{d} \quad \text{Equation 5.2}$$

Where N_f is the final cell number, N_0 is the initial cell number, and d is the days of growth.

5.3 The effect of salinity on cell density

Salinity is an important parameter that effects algae growth (Renaud & Parry 1994). The effect of ordinary salt and sea-salt on *Nannochloropsis oculata* (*N. oculata*) and their concentration on growth was investigated. Both salt samples were purchased from a local supermarket. The constituents of the salt contain 98% sodium chloride and 2% minerals. The salinity was measured with an electrical conductivity (EC) meter (Hanna Instruments, HI 8733, UK).

5.3.1 Salinity calibration curve

The salinity of the algal culture was measured using a conductivity meter, see Figure 5.7. A calibration curve was made to obtain standard EC (σ) measurements for a range of sea-

salt concentrations. The EC values against different concentrations of salt solution can be seen in Figure 5.8. The EC meter gives the readings in milliSiemens per cm (mS/cm), and with some calculations they can be converted into salt concentration in parts per thousand (ppt) which is a more common measured for salinity. To convert mS/cm to ppt the following calculations were done:

$$\text{mS/cm} \times 1000 = \mu\text{S/cm}$$

$$\mu\text{S/cm} \times \text{conversion factor (0.67)} = \text{mg/L or parts per million (ppm)}$$

$$\text{ppm}/1000 = \text{ppt}$$



Figure 5.7 Salinity measurements using the conductivity meter

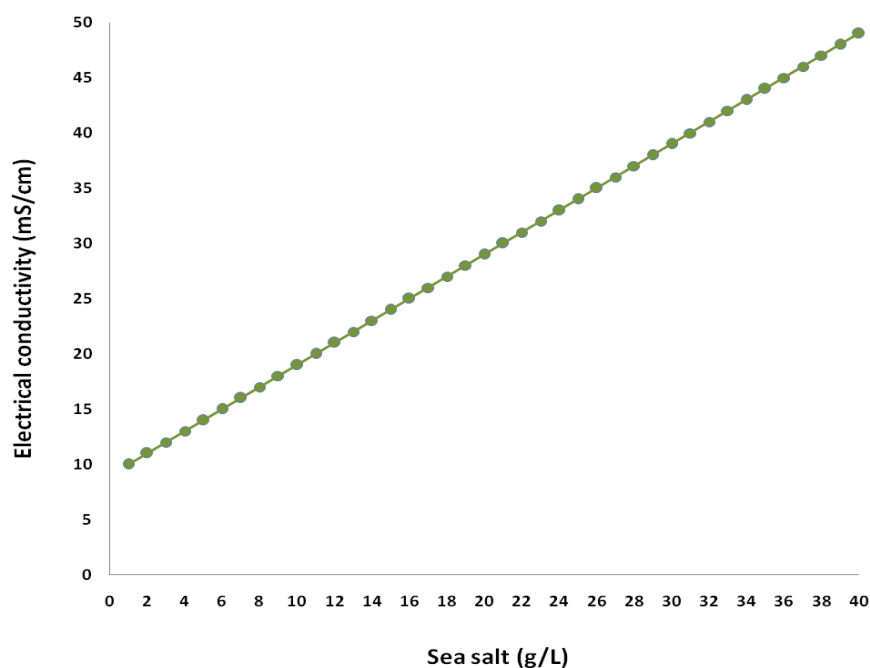


Figure 5.8 Calibration curve of electrical conductivity (EC)

The optimum range of salinity for *N. oculata* is approximately 25-35 ppt, (Renaud & Parry 1994), and *N. oculata* can be grown in high salinity up to 50 ppt (Das *et al.*, 2011). In the salinity calibration experiment, the salt concentrations to give ideal salinities were found to be within the range of 20 to 40 g per litre.

5.3.2 Ordinary salt and sea salt experiment

In this study, the effect of ordinary salt and sea-salt on *Nannochloropsis oculata* (*N. oculata*) growth was investigated. The algal suspension (100 mL) was cultured in the photobioreactor tubes containing 900 mL tap water at different salt concentrations, as given in Table 5.1:

Table 5.1 List of the salt concentrations used in the photobioreactor

Tube	Salt
1	No salt (control)
2	20 g/L ordinary salt
3	40 g/L ordinary salt
4	20 g/L sea salt
5	40 g/L sea salt
6	20 g/L sea salt + circulation

The photobioreactor was illuminated by a fluorescent lamp (16 hours on / 8 hours off), and the air flow was supplied to one of the tubes using an aquarium air pump (Aqua air, AP2 Interpet. UK). The experiment setup is shown in Figure 5.9. The growth was examined every day and the microalgae were counted using a Leitz Wetzlar microscope using the protocol described in Section 5.2.

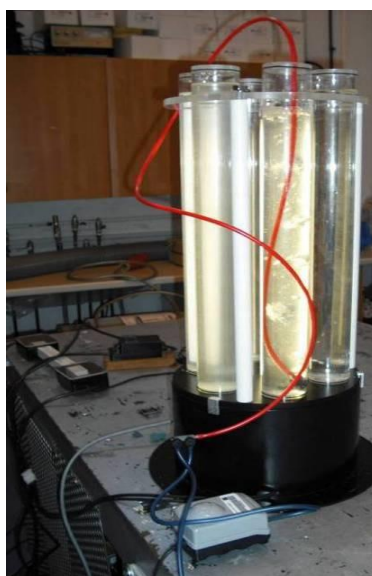
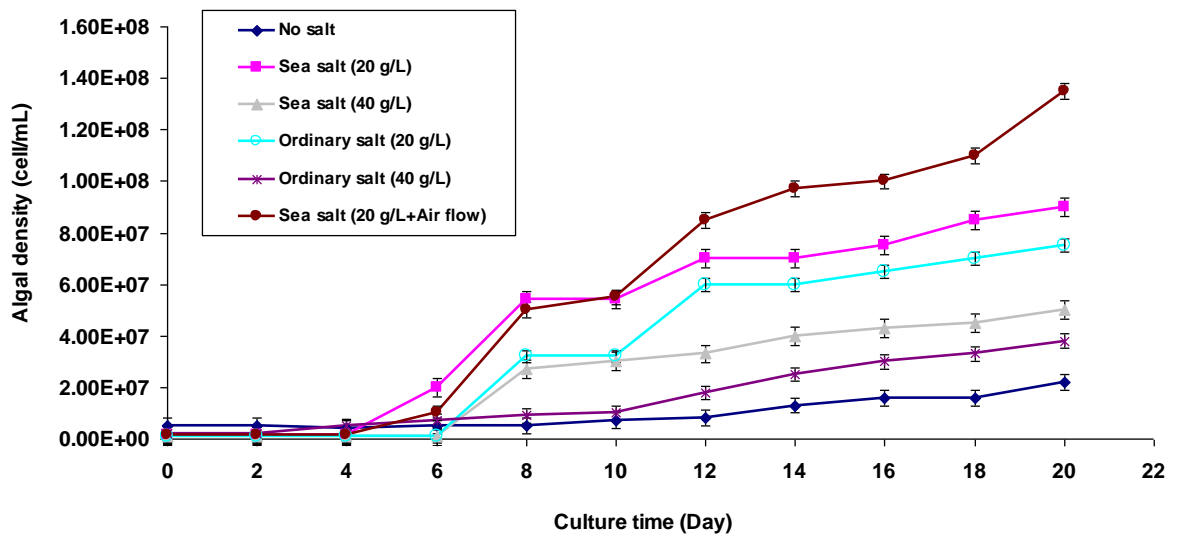


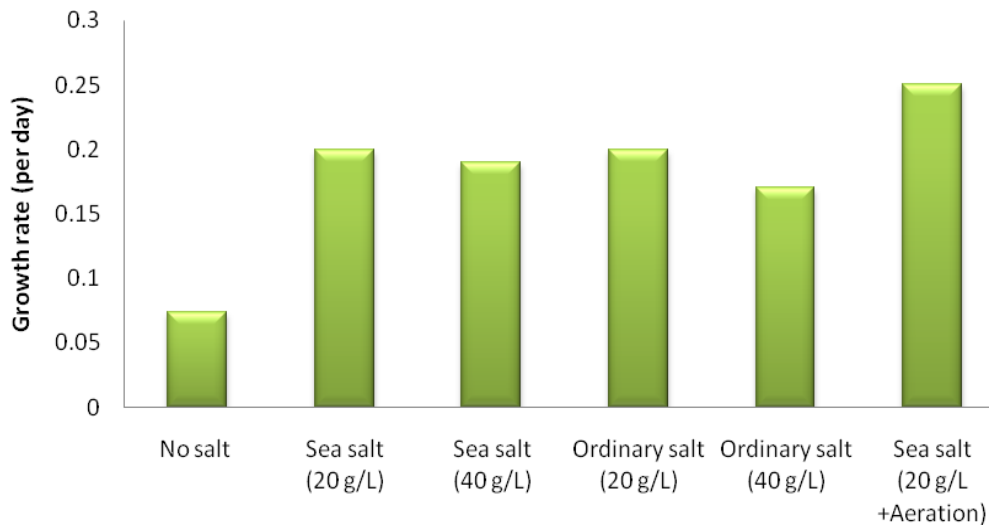
Figure 5.9 The tubular PBR for salinity experiment

5.3.3 Results of salinity experiment

The results of the salt concentration on the density and growth rate can be seen in Figure 5.10. It is obvious from the average growth rate taken over 20 days (Figure 5.10 (b)) that the algae were affected by 20 g sea and ordinary salt to the same degree. The optimal growth was observed with a sea salt concentration of 20 g with air circulation, while the lowest growth was observed with the control sample (no salt and no aeration). The data represents the average growth rate (Equation 5.2) \pm standard error, based on ten readings.



a) Density of *N. oculata* algae as a function of time



b) Average growth rate of *N. oculata* algae with different salt concentrations

Figure 5.10 Effect of salinities on *N. oculata*

5.3.4 Growth with different salt concentrations, with/without an evaporation correction factor

The 6 tube photobioreactor was used to cultivate the *N. oculata* with different salt concentrations namely 25, 30, 35, 40, 45, and 50 g/L for six tubes respectively. Each tube contained 100 mL culture, 900 mL water and 0.5 mL of F/2 phyto nutrients (Reefphyto, UK). It was observed that there were different evaporation rates in each tube during the cultivation time. This was probably due to the different velocities of the supplied air and possible due to preferential sunlight on one side of the PBR. Figure 5.11 shows the experimental setup.



Figure 5.11 PBR at the beginning of the experiment (left) and at the end of cultivation period (16 days) (right)

The consequences of evaporation were investigated. The *N. oculata* cells were counted every 2 days; the results can be seen Figure 5.12, which shows the cell density without taking account of the evaporation loss of water per day. The cell density was corrected by multiplying the cell number by the volume of the culture after evaporation and divided by the original culture volume. Figure 5.13 shows the corrected data for the evaporation. The results obtained from this test showed that the cell density decreased with increased salinity range. The cell densities of samples with high salt concentration, declined at the end of the cultivation period, indicating possible cell death.

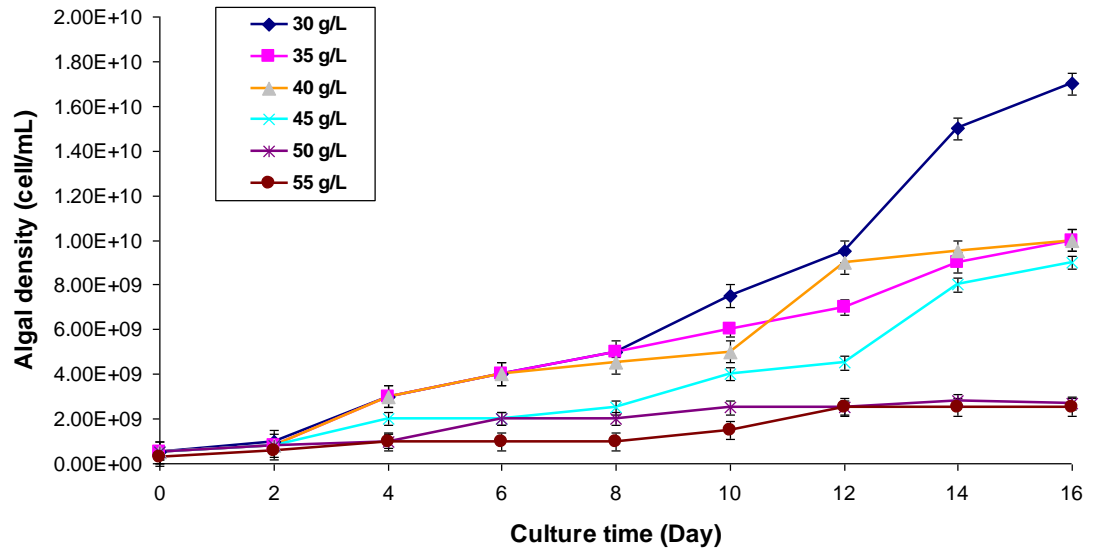


Figure 5.12 *N. oculata* densities for different salinities without evaporation correction factor

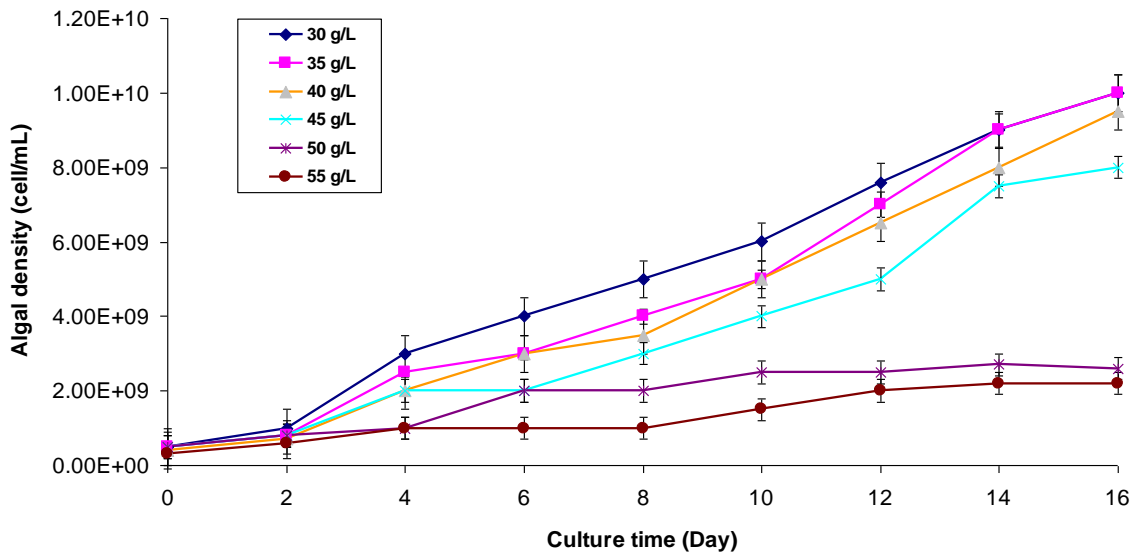


Figure 5.13 The corrected data for evaporation of *N. oculata*

5.4 Nutrient concentration experiment

In this experiment the effect of the nutrients supplied on cell growth was investigated. 50 mL algal stock culture was mixed with 950 mL tap water in each PBR tube, then F/2 phyto nutrient (Reefphyto, UK) was added to the culture as shown in Table 5.2.

Table 5.2 Nutrients in the six tubes of PBR

PBR tube	Nutrient
1	0 (control)
2	0.5 mL (standard)
3	1 mL
4	2 mL
5	4 mL
6	6 mL

The culture was illuminated with a 14 W fluorescent light, and air circulation was used. The temperature was kept at a range 15-20 °C, and the salinity was kept at 30 ppt. Figure 5.14 shows the PBR after assembly.



Figure 5.14 The tubular PBR for nutrient experiment

5.4.1 Results of nutrient experiment

The experiment was run for ten days, and the cells counted every two days. Figure 5.15 shows the cell density over the experimental period. The growth in tube 1 (no nutrient) was high over the six days but started to decline and the cells died due to nutrient depletion, and the culture was not as green as in the other tubes, see Figure 5.16. Tubes 2 and 3 had the highest growth among the others tubes. The amount 0.5 mL is recommended from the

supplier and double this amount (1 mL) showed similar growth, and when the amount was increased further the cell density did not increase.

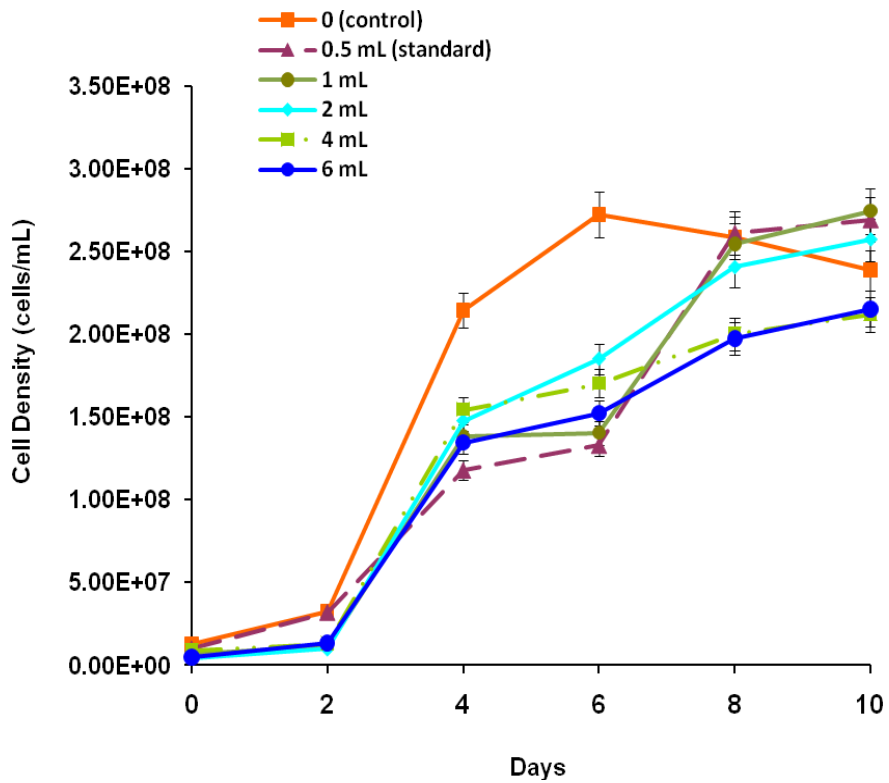


Figure 5.15 Cell density over time with various nutrient conditions

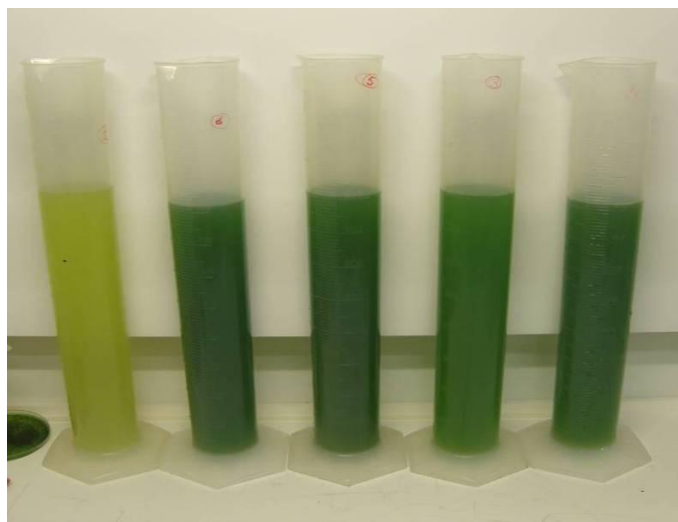


Figure 5.16 The control tube (no nutrient) is on the left side (tube 1-5 from left to right)

Another effect of the nutrient concentration was on the cell size. The cells of tube 1 were very small compared to the other cells that received nutrients, as can be seen in Figure 5.17.

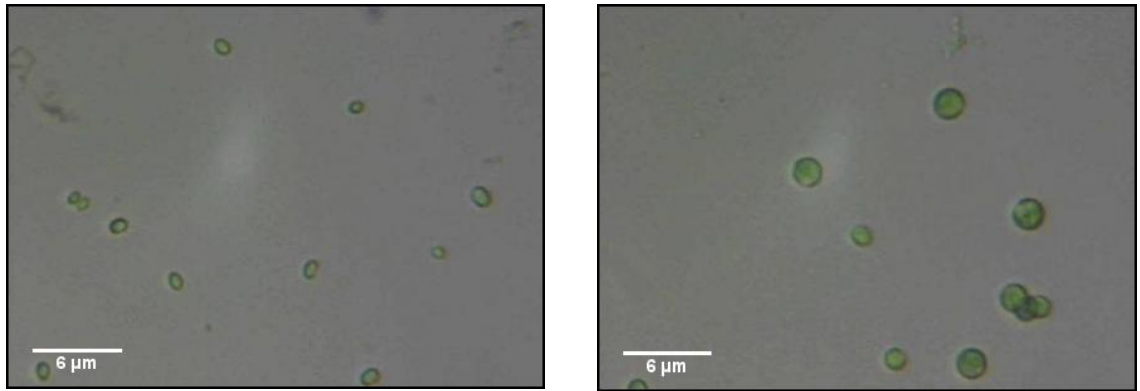


Figure 5.17 *N. oculata* cells without nutrients (left) and with 6 mL nutrients (right) (25X Zhumell objective)

For further investigation to the changes in cell size, the algal photographs were processed using the image processing software NI vision 8.5 (National Instruments, USA). The average cell diameter and the average cell area for each sample were calculated, as can be seen in Figure 5.18 and Figure 5.19 respectively. Doubling the nutrient concentration to 1 mL/L produced a higher cell density (see Figure 5.15), and the increase of nutrients above this did not seem to produce a higher cell density, but did produce larger cell. All of these data were corrected for evaporation rate.

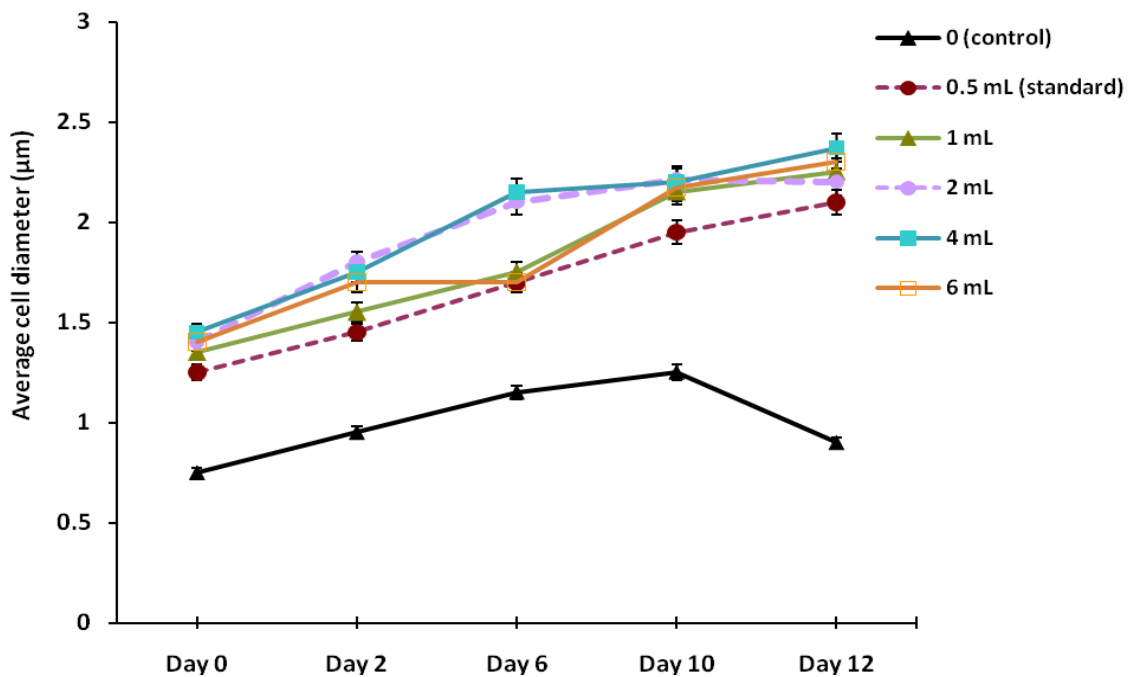


Figure 5.18 Cell diameter changing over the period of optimal nutrient experiment

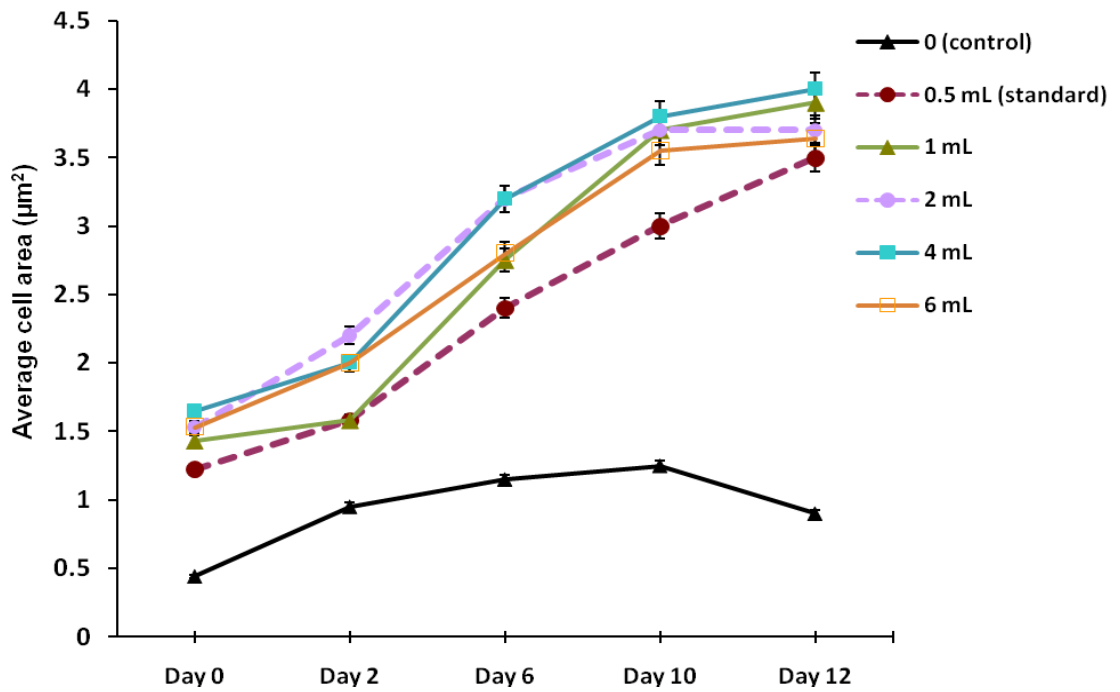


Figure 5.19 Cell area changing over the period of optimal nutrient experiment

5.5 Air velocity effect

During the previous experiment (Section 5.3.4), it was noted that the evaporation rate varied. The effect of the gas inlet velocity on evaporation and growth rate was subsequently examined. The 6-tube PBR was set-up as shown Figure 5.20. Each tube contained 950 mL tap water, 50 mL culture, 0.5 mL F/2 phyto nutrients, 20 g/L sea salt (30 ppt salinity) and the tubes were irradiated by the 14 W fluorescent light.



Figure 5.20 The 6-tubes PBR at the beginning of the test (left) and the end of the test (right) over 22 days for the air flow experiment

The PBR tubes were supplied with air flow using an air pump (Hailea, ACO-308, China) through the 6-manifold (3 mm inner diameter) with adjustable taps, see Figure 5.21. The air velocity was measured using an anemometer (Skywatch, Xplorer 2, USA), and the air velocities were set to either 1, 2 and 3 m/s for two tubes.



Figure 5.21 Six tube manifold and supply tubing

The microalgae concentration in the PBR tubes was counted every two days, the samples were examined under the microscope and ten pictures were taken for every tube. The evaporation volume was considered in correcting for the algal concentration in this experiment. The results can be seen in Figure 5.22. The tube that was provided with an air velocity of 3 m/s (volume flow rate of $2 \times 10^{-5} \text{ m}^3/\text{s}$) had the highest cell density.

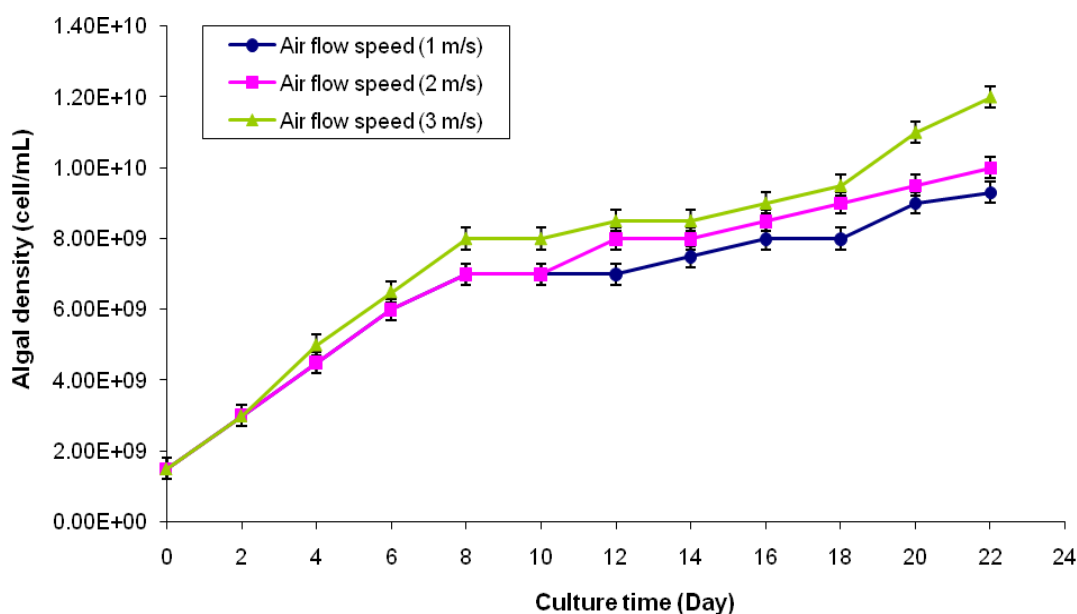


Figure 5.22 Counted cell density for various air velocities

Evaporation of the culture for the different air velocities can be seen in Table 5.3. The results showed that there was a small difference in the water volume for the same velocity, possibly due to direct sunlight from a window. The results in Table 5.3 were averaged and can be seen in Figure 5.23.

Table 5.3 Volume of the water for different velocities at the end of the growth period (~ 20 days). The original volume of the culture was 1000 mL

PBR tube	Air velocity (m/s)	Volume (mL)
1	1	800
2	1	850
3	2	700
4	2	720
5	3	600
6	3	600

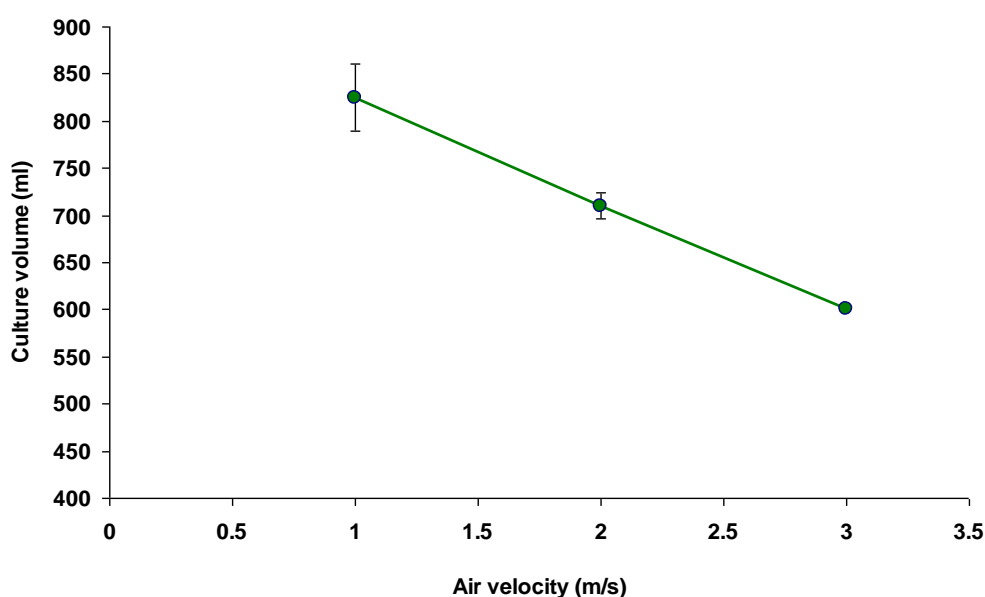


Figure 5.23 The average volume of the water for the different velocities, error bar shows an average of two readings

It is seen that culture volume reduced, i.e. evaporation increased, with increasing aeration. This appeared to be linear ($R^2 = 0.999$) from 1 to 3 m/s.

5.6 Glass tank experiments

Whilst the 6 tube PBR was designed to investigate parametric variation, little biomass was grown in the 1 L tubes. Consequently, a large PBR was produced to grow larger quantities of biomass for testing. A glass tank (1230x400x470) mm with a volume capacity up to 200 L was used to cultivate *N. oculata* algae.

5.6.1 *Fluorescent and grow light experiment*

In order to evaluate the algal growth under two different lighting conditions, the *N. oculata* algae were cultivated in the glass tank illuminated by a fluorescence lamp and the spectrum lamp. The algal culture of 17 L was cultivated in the large glass PBR containing 177 L tap water with 97 mL of F/2 phyto nutrient medium. The culture was grown in water with salinity of around 30 ppt and at the temperature of 20 ± 3 °C. The culture was circulated using an air pump (Hailea, ACO-308, China) with four ring diffusers (KD, UK). The culture was grown first with natural daylight and then additional photon input was provided with a fluorescent light of 58 W ($37 \mu\text{moles}/\text{m}^2/\text{s}$) (Crompton lighting, F58TB, Hungary), then the fluorescent lamp was replaced by a dual spectrum lamp of 250 W ($74 \mu\text{moles}/\text{m}^2/\text{s}$) (Sunmaster dual spectrum, SL.U46.DSP, USA). Figure 5.24 shows the experimental setup.

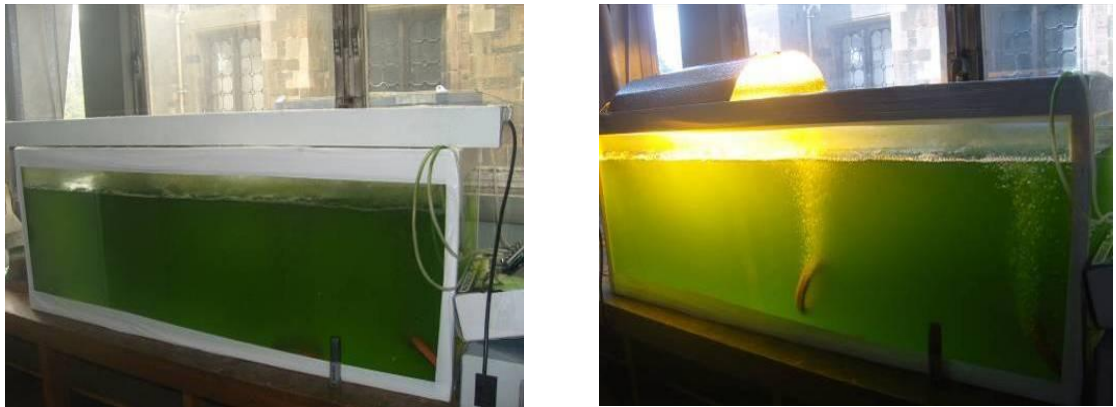


Figure 5.24 A glass tank with a fluorescent lamp (left) and a dual spectrum lamp (right)

5.6.2 *Results of fluorescent and grow light experiment*

The algal cell density was counted everyday using the microscopy technique (Section 5.2). It was observed that the growth was slow over the first two weeks of the experiment, so the fluorescent lamp was provided and more nutrient was added. A significant increase in cell density was noticed, as can be seen in Figure 5.25. Later the growth rate became almost steady (day 28), so the fluorescent lamp was replaced with a dual spectrum lamp. There was a significant influence on the growth rate and higher cell counts were seen compared with that achieved with the fluorescent lamp.

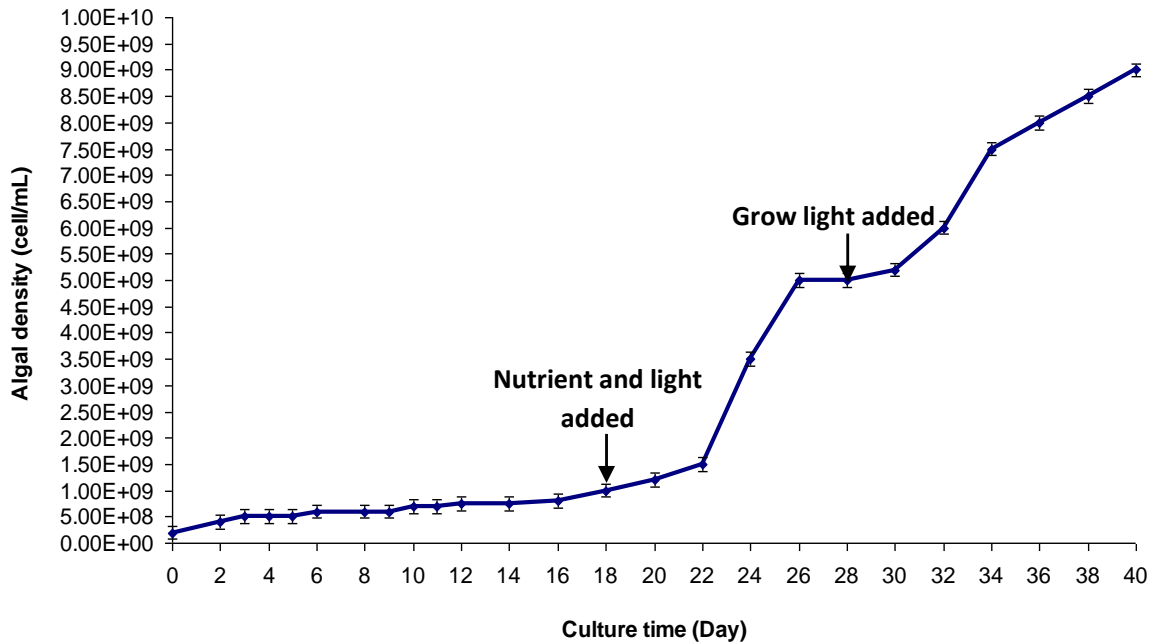


Figure 5.25 Cell count of *N. oculata* in a large glass PBR using two different lamp sources. Data were corrected for evaporation

5.6.3 Grow light experiment

The same experiment as in Section 5.6.1 was repeated with the dual spectrum lamp only, the experimental setup can be seen Figure 5.26. The algal cell density was measured daily, the culture grow significantly faster as can be seen from the results in Figure 5.27 compared to Figure 5.25. The growth reached a cell density of 3×10^9 cell/mL within 10 days (Figure 5.27), while the growth reached that on day 24 in the previous experiment (Figure 5.25).

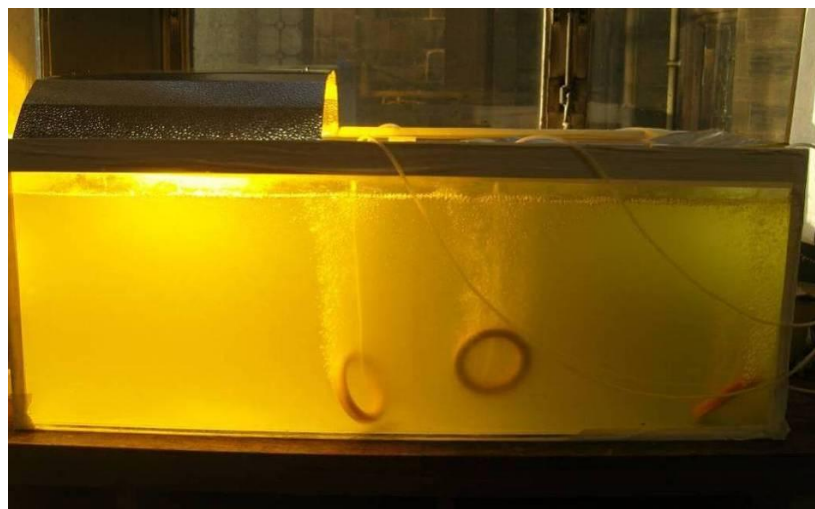


Figure 5.26 A large glass tank with the grow lamp

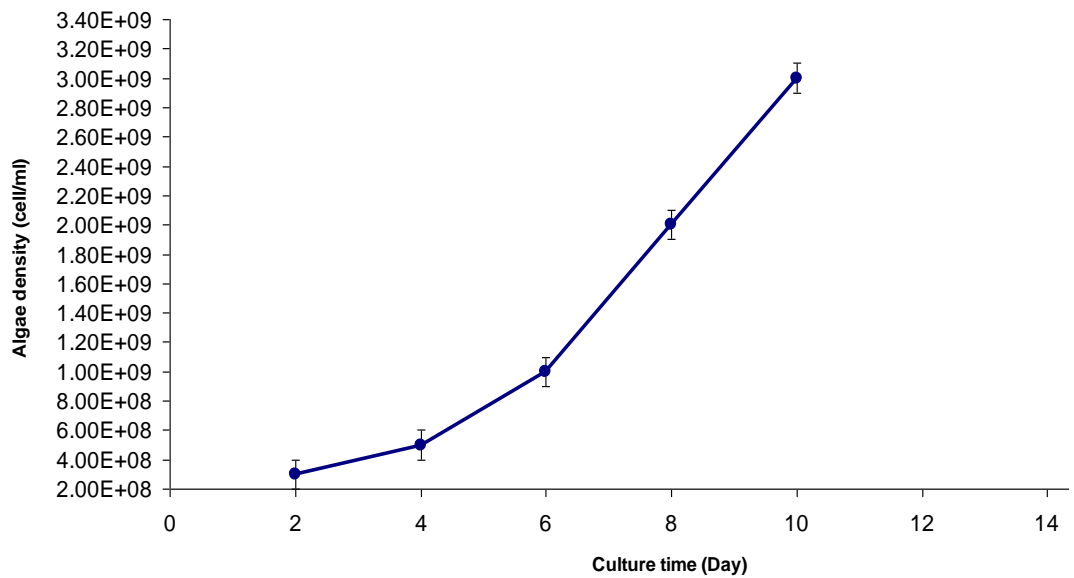


Figure 5.27 Cell count of *N. oculata* in a large glass tank illuminated with the grow lamp

5.7 *N. oculata* growth dependency on temperature

5.7.1 Practical experiment

Temperature is an important growth parameter for microalgae. In this experiment the *N. oculata* growth was investigated whilst monitoring the temperature. The algal culture was cultivated for 12 days in the PBR. K-type thermocouples (Reotemp, USA) were attached to each tube of the PBR, as can be seen in Figure 5.28. The thermocouples were connected to a data acquisition board and PC. The temperature values were collected every 300 s. The temperature measurements showed that some tubes were slightly higher in temperature. Figure 5.29 shows the temperature profiles; the tubes A and F were ~23-24 °C, and both had the highest cell density, as can be seen in Figure 5.30. The other tubes were ~21-22.5°C.



Figure 5.28 Experimental setup for the temperature effect experiment

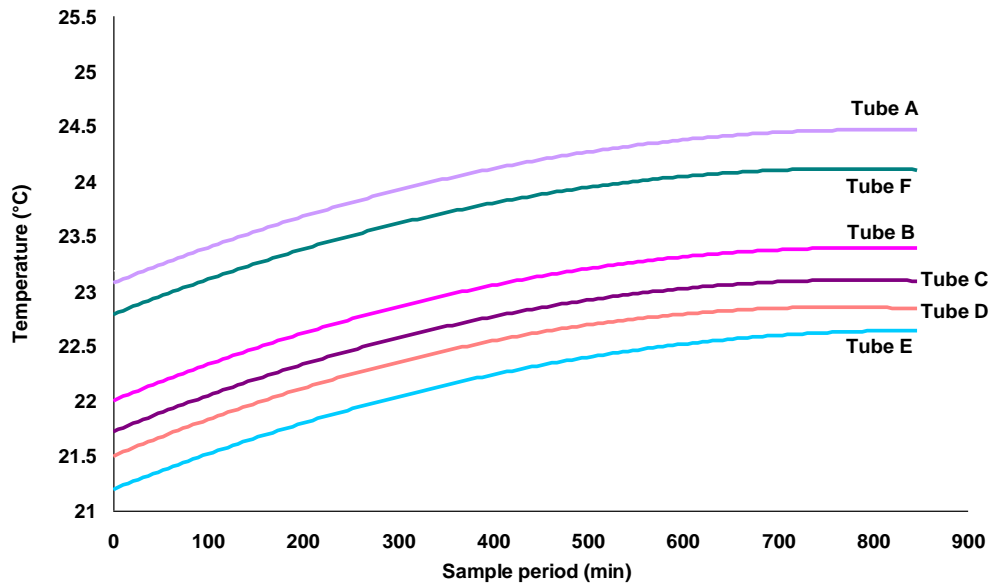


Figure 5.29 Temperature measurements for the six tubes of PBR

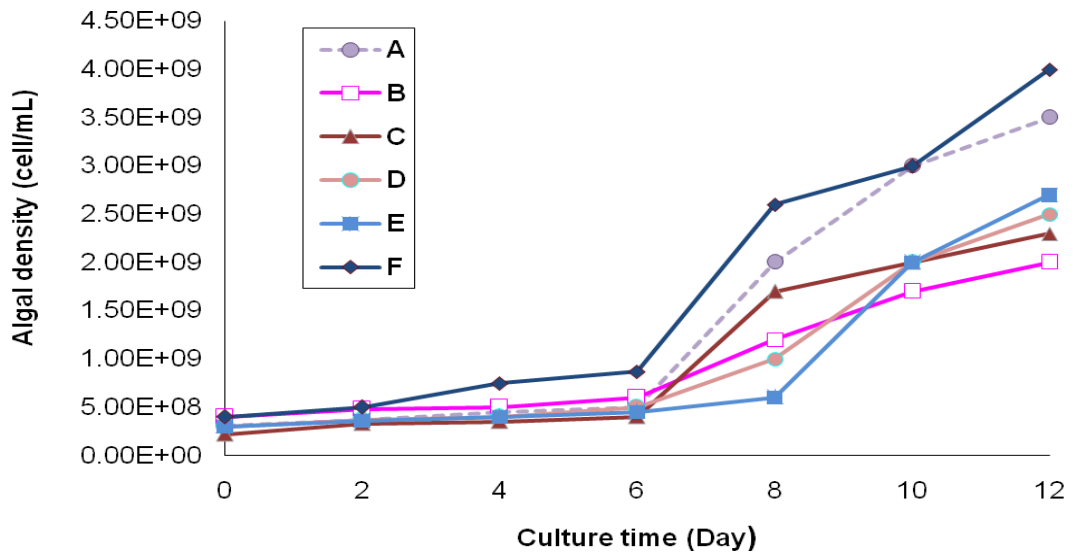


Figure 5.30 Microalgal density versus cultivation time

The results showed that *Nannochloropsis* growth rate increased with temperature, and the temperature levels over 22 °C are suitable to efficiently grow the microalgae.

5.7.2 A Fluent model of PBR temperature distribution

Fluent 6.3 (Ansys Inc., UK) was used to simulate the temperature of a PBR. A schematic view of the PBR system can be seen in Figure 5.31. The PBR was kept inside a chamber to simulate a closed environment.

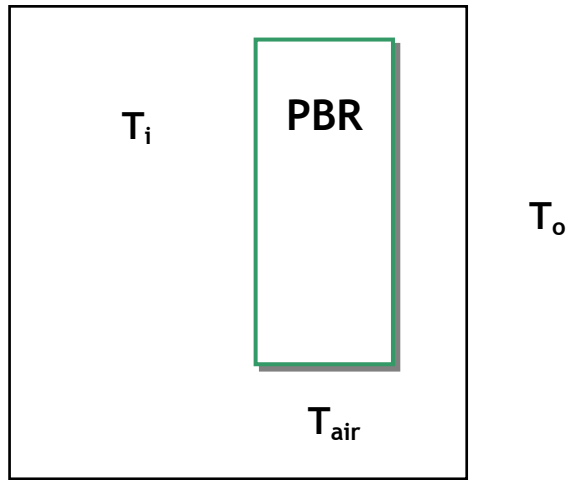


Figure 5.31 A schematic drawing of the PBR system

The simulation assumptions were: The optimum growth rate of the microalgae was ~ 15 - 25 $^{\circ}\text{C}$, so the initial temperature was assumed to be $T_i = 15$ $^{\circ}\text{C}$ (288 K) which is nearly equal to the ambient temperature inside the laboratory as measured during the experiments. The temperature of the chamber walls was assumed to be the same as the initial or ambient temperature T_i and the external temperature T_o was around 26 $^{\circ}\text{C}$ (300 K). The properties of the culture (algae and water) inside the PBR assumed to be the water properties. For simplification, the PBR model was one vertical tube, made from acrylic plastic material, with length of 500 mm, inner diameter of 6 mm and wall thickness of 3 mm. The air was assumed to be supplied from the bottom with an air velocity of 2 m/s and at temperature of $T_{air} \sim 17$ $^{\circ}\text{C}$ (290 K).

The one tube was meshed with gambit 2.4 (Fluent Inc., UK) before modelling with Fluent. The system was modelled in Fluent using a discrete ordinates (DO) model. After running the simulation, Figure 5.32 shows the results of the temperature profiles. The maximum temperature was around 300 K at the wall of chamber. The temperature of the PBR wall was 288-290 K, and the temperature at the centre of PBR was found to be 295 K.

The temperature of the air, T_{air} , was increased from 290 to 295 K. The results of this simulation showed that the wall temperature of the PBR increased from 290 to 297 K, and the temperature at the PBR centre was increased from 295 to 300 K. Figure 5.33 shows the temperature distributions after increasing the temperature.

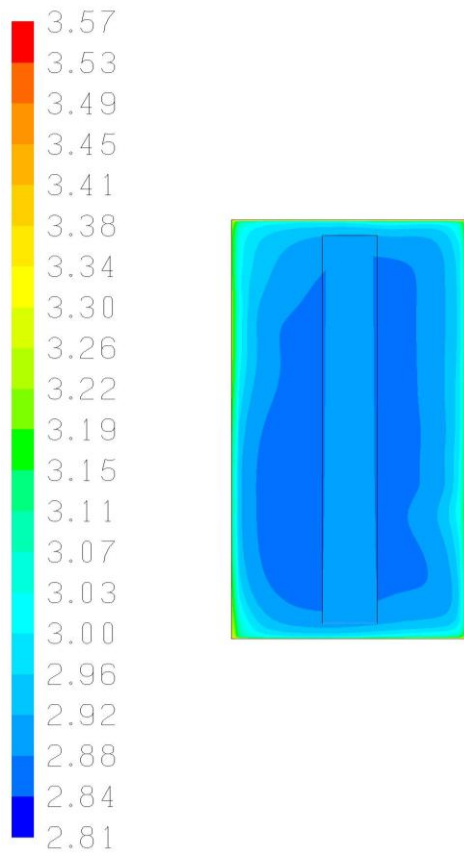


Figure 5.32 Results showing the temperature distribution around and inside of the PBR. Temperature (x100 K). The air temperature $T_{air} = 290$ K

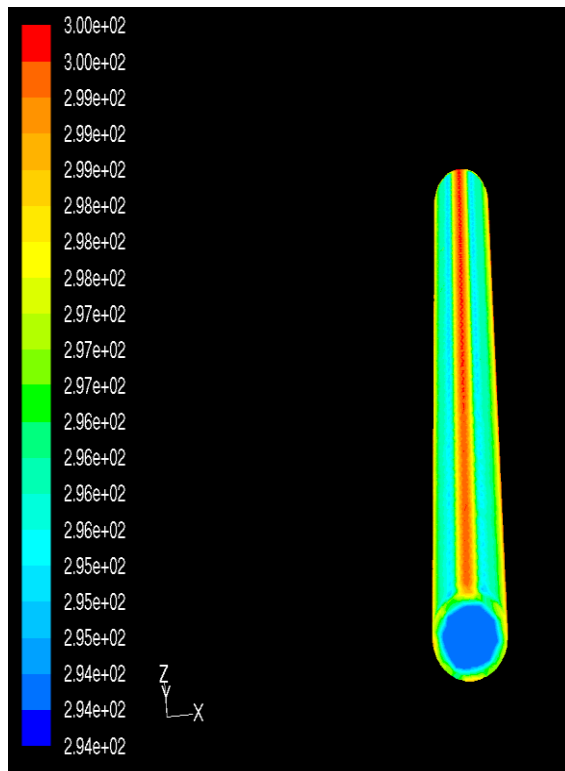


Figure 5.33 Results showing the temperature distribution of the PBR. The air temperature $T_{air} = 295$ K

This provides an initial model that can be expanded to incorporate temperature control of the PBR and assessment of local temperature gradients to ensure that the microalgae are kept at their optimal temperature to enable optimal growth.

5.8 *Chlorella vulgaris* experiments

Microalgae have recently been investigated for their potential for biofuel production, but algae and microalgae have been used for food for thousands of years. One species of microalgae suitable for food is *Chlorella vulgaris*. *Chlorella* contains healthy omega-3 and omega-6 fatty acids, and it is commonly found in nutritional supplements. Experiments were carried out on *Chlorella vulgaris* to determine its potential as a food source and to develop further methods for analysis and detection.

5.8.1 Cultivation

Chlorella vulgaris (SAG 211-11b) (from the University of Göttingen, Germany) was grown and cultivated within the School of Engineering, University of Glasgow. The *Chlorella vulgaris* (*C. vulgaris*) algae were received on an agar slope, as can be seen in Figure 5.34.



Figure 5.34 *Chlorella vulgaris* on agar slope

A loop of *C. vulgaris* was isolated from the agar, and the culture transferred into the nutrient media *3N-BBM+V* (culture collection, UK) for cultivation. Before inoculation, the nutrient culture was made up from the stock solutions of different ingredients, listed in Table 5.4 with their respective contributions per 1 litre.

Table 5.4 The nutrient media 3N-BBM+V (modified bold basal medium with 3-fold nitrogen plus vitamins)

Nutrient stock	Nutrient solution (mL/L)
$NaNO_3$	10
$CaCl_2 \cdot 2H_2O$	10
$MgSO_4 \cdot 7 H_2O$	10
$K_2HPO_4 \cdot 3 H_2O$	10
KH_2PO_4	10
$NaCl$	10
Trace element solution	6
Vitamin B_1	1
Vitamin B_{12}	1

The nutrient solutions were mixed with 1000 mL of sterilized distilled water in a sterilized glass beaker, and then the solution was divided into nine containers. 15 mL was made up in six universal tubes, 2 mL in one beaker and 1 mL in two beakers. Figure 5.35 shows nutrient samples inoculated with *Chlorella*.

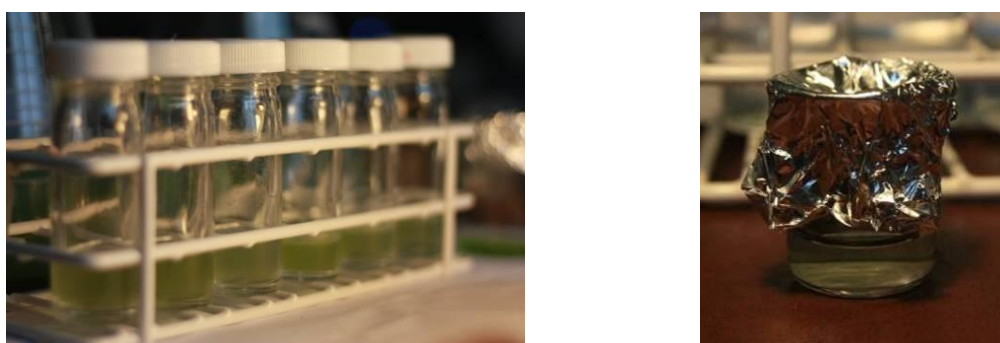


Figure 5.35 Universal tubes with 15 mL culture media (left) and a glass beaker with 2 mL culture media (right)

5.8.2 Nutrient concentration experiment for *C. vulgaris*

Because of previous experiments possibly linking microalgal size with nutrient concentration (Section 5.4), this experiment was repeated for *C. vulgaris*. The experiment was setup in the tubular PBR with four tubes; the air was supplied from an air pump through the four way manifold and a capsule air filter (Whatman, polycap, UK) was fitted at the air pump for ambient air filtration, as shown in Figure 5.36. The air was filtered to reduce the risk of contamination of the culture through any airborne microorganisms. This is particularly important if the microalgal crop is to be used for food applications.

The 14 W fluorescent light was cycled through 12 hours on and 12 hours off. The temperature range was 20-22 °C during the day time and 17-19 °C during the night-time.



Figure 5.36 Nutrient experiment for *C. vulgaris* and air filtration on the pump

75 mL of *Chlorella* culture was mixed with the sterilized distilled water and nutrients to a final volume of 1000 mL in each tube. The cultivation period was 7 days, and the evaporation of the culture was determined. The nutrient amounts are shown in Table 5.5.

Table 5.5 Nutrient amount (%) in the PBR tubes (1000 mL)

	Tube 1 (Control)	Tube 2 (Half amount)	Tube 3 (Normal amount)	Tube 4 (Double amount)
Algal culture	75 mL	75 mL	75 mL	75 mL
3N-BBM+V Nutrients	0 mL (0%)	34 mL (50%)	68 mL (100%)	136 mL (200%)

5.8.3 Results of nutrient concentration experiment for *C. vulgaris*

The *Chlorella* densities over the cultivation time can be seen in Figure 5.37. The standard concentration of nutrients gave the highest *Chlorella* cell density and the lowest value was with the control tube, with no added nutrients. The size of the algae was measured using NI

vision 8.5 (National Instruments, USA), and the results can be seen in Figure 5.38. The standard concentration had the largest cells among the other concentrations.

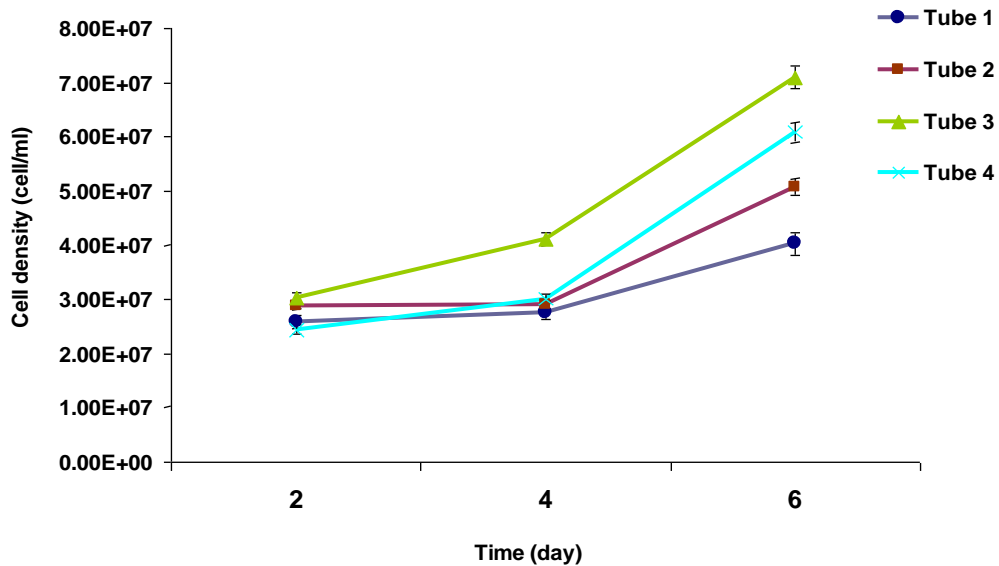


Figure 5.37 The effect of nutrient concentration on the *Chlorella* growth. The cell density represents an average of ten measurements. Tube 1 (0%), Tube 2 (50%), Tube 3 (100%) and Tube 4 (200%)

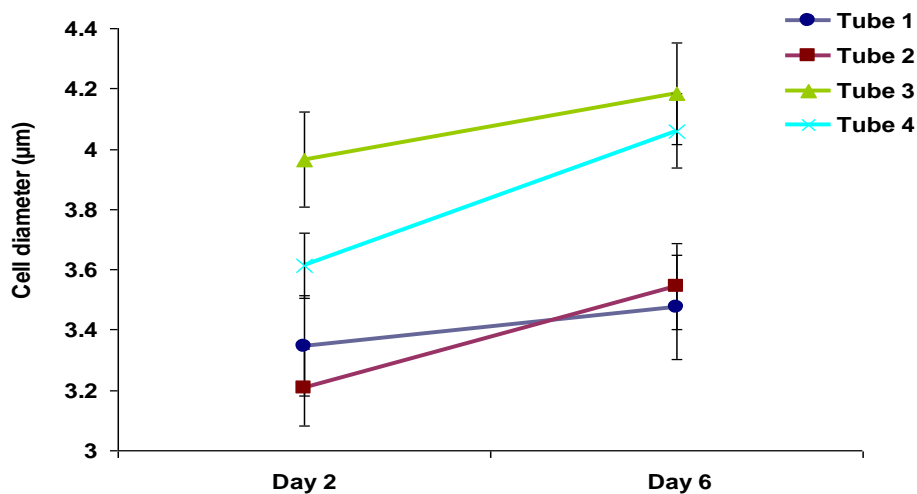


Figure 5.38 The effect of nutrient concentration on the *Chlorella* size. The cell diameter represents an average of ten measurements. Tube 1 (0%), Tube 2 (50%), Tube 3 (100%) and Tube 4 (200%)

5.9 Algal diameter distribution of *N. oculata*

In order to determine the cell diameter, *N. oculata* algae were cultivated in a photobioreactor in salty water (30 ppt) under the illumination of fluorescent light. The culture

was circulated by an air pump at a temperature between 20-22°C. F/2 phyto nutrients were added during culture growth. The cell density was counted every two days using a light microscope (Section 5.2); the cell density was 1×10^9 - 3×10^9 cell/mL at harvesting time. The photographs for algal counting were analysed using the NI vision software. The measurements for cell diameter can be seen in the histogram in Figure 5.39. From the results, the cell diameter was about 1 - 7 μm . 7 μm is a bit large for *N. oculata*, so it may be that the cells clustered and the software counted them as a large single cell or it may be contaminates. Figure 5.40 shows the *N. oculata* size distribution.

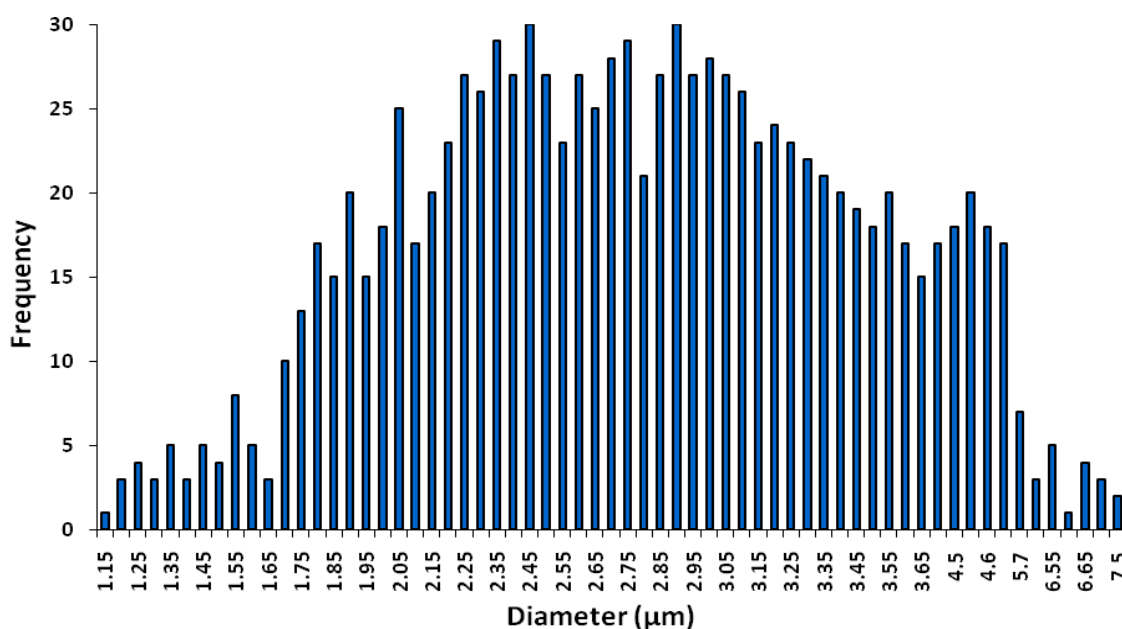


Figure 5.39 Diameter distribution of *N. oculata*



Figure 5.40 A microscopic view of different cell sizes of *N. oculata* algae (25X)

The data for cell counting for each day of the experiment was processed to evaluate the changes in cell diameter with days of growth. The cell diameter on days 2 and 10 can be

seen in Figure 5.41 and Figure 5.42 respectively. The results showed that the average cell diameter of *N. oculata* algae increased from ~1.5 to ~5 μm at end of the experiment, i.e. a greater change in cell sizes can be seen after 10 days of the cultivation period.

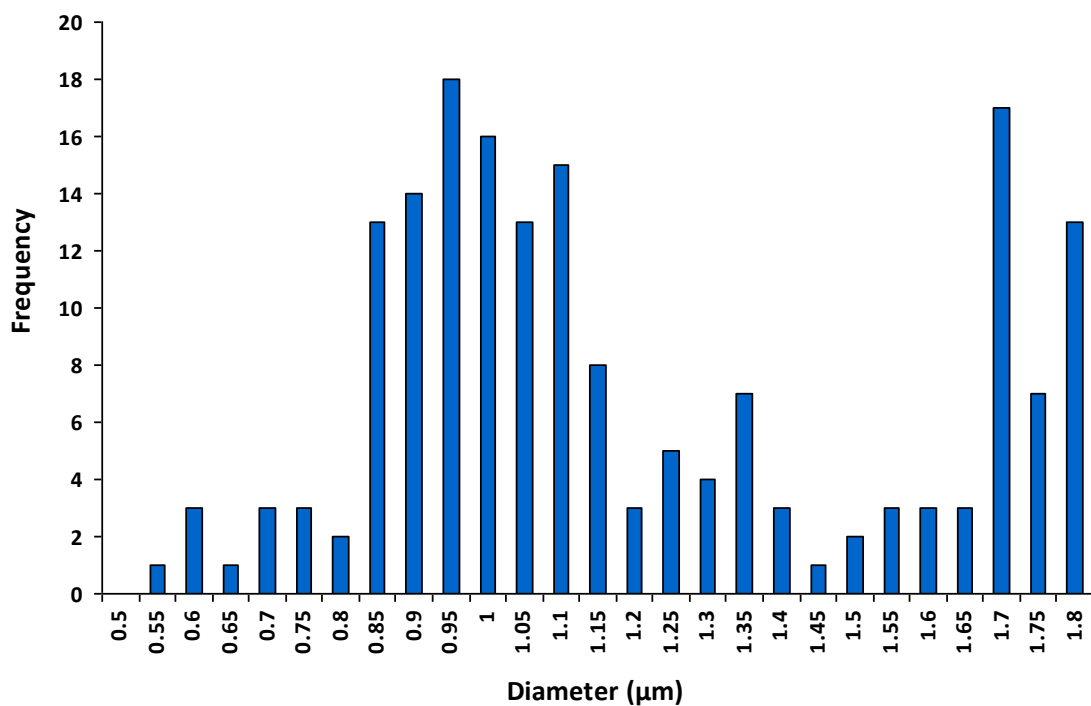


Figure 5.41 Diameter of *N. oculata* on day 2

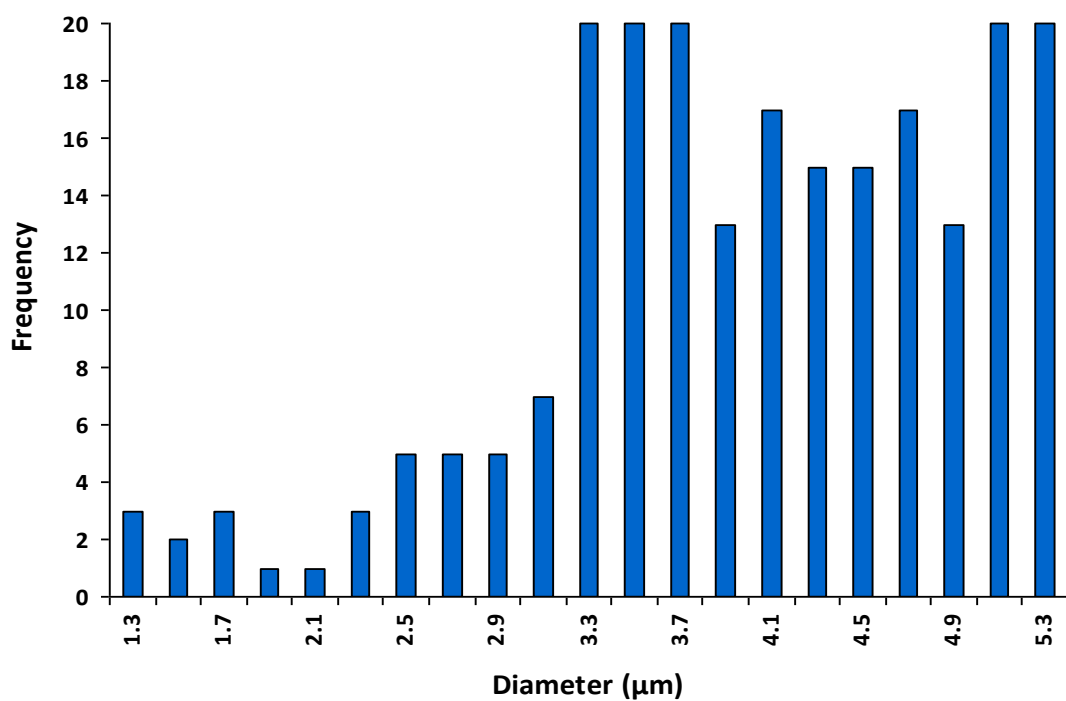


Figure 5.42 Diameter of *N. oculata* on day 10

5.10 Harvesting techniques

Biomass harvesting of microalgae is a solid-liquid separation process, and it represents the highest percentage of the total production cost (20-30%) (Gouveia 2011). Various methods of recovering the biomass were assessed, including: sedimentation, flocculation, centrifuging and filtration. It should be noted that more than one method may be required to separate the algal biomass from the suspension. The experiments were performed on *N. oculata* taken from the 6 tube PBR and glass tank (Sections 5.4 and 5.6). Microscopic examination was used to quantify the biomass yield. The algal harvesting process consists of two stages, as shown in Figure 5.43, solid separation and dewatering. All processes of harvesting will be explained in detail in the following sections.

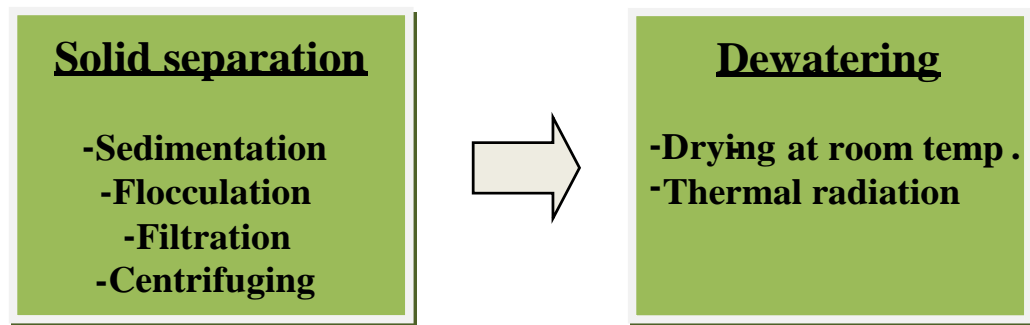


Figure 5.43 Schematic drawing of harvesting process

5.10.1 Sedimentation

Sedimentation, also called gravity sedimentation, is the simplest and cheapest method of separation in algal harvesting. However, natural sedimentation is a very slow process, the settling velocities range from 0.1-2.6 cm/h (Choi *et al.*, 2006). In the sedimentation process, the cells settle down to the bottom of PBR due to the gravitational and fluid drag forces (Harith *et al.*, 2009). The experiments were arranged using different methods to investigate the sedimentation rate and cell recovery.

5.10.1.1 Algal sedimentation using universal tubes

The *N. oculata* sample (4×10^8 cells/mL) was taken from the PBR using a peristaltic water pump (Cole Parmer Instrument, 7524-05, US), as shown in Figure 5.44. The culture was transferred into universal tubes (25 mL), the overall height of the sample tube was 95 mm

and 25 mm in diameter. Then the tubes were shaken for three minutes using a whirly mixer (Vortex-Genie 2, USA) to mix the contents, see Figure 5.45.



Figure 5.44 Extraction of *N. oculata* sample from a PBR

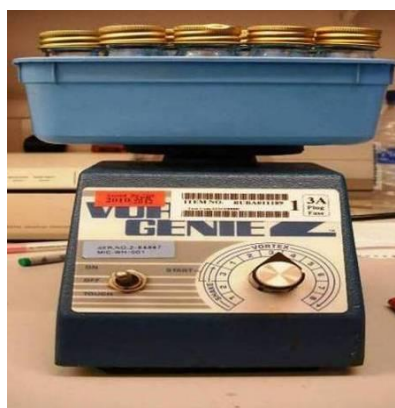


Figure 5.45 Whirly mixer with algal samples

The experimental set up can be seen in Figure 5.46. The algal samples were put on a stand in front of a camera (Canon EOS 1000D, Japan), and the samples were illuminated using a light box and glass diffuser.

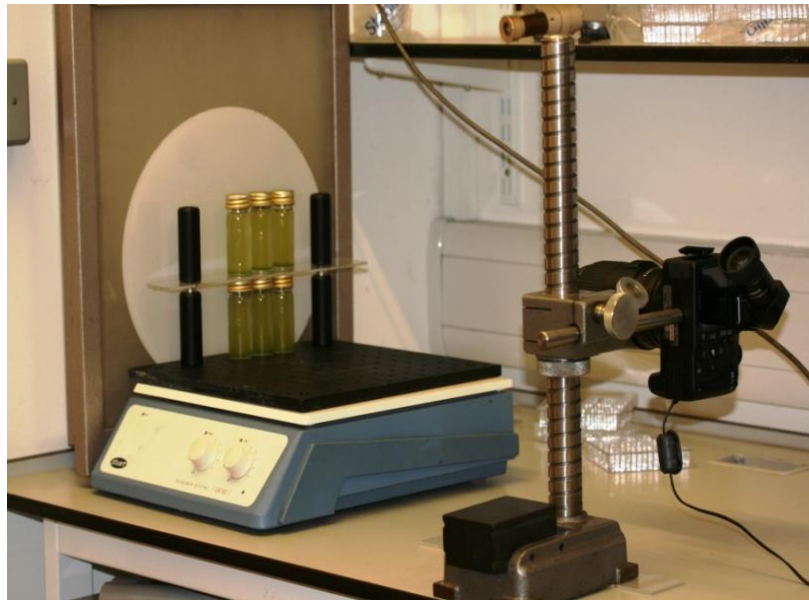


Figure 5.46 Experimental set up of universal tubes sedimentation

Images of the algal samples were captured over five days (120 hr) to determine the sedimentation process. The microscopic examination of samples was taken every 24 hr. The biomass yield (% cell recovery or cell settling) was calculated using Equation 5.3 (Harith *et al.*, 2009):

$$\text{Cell recovery (\%)} \text{ at time } t = \frac{C_1 - C_2}{C_1} \times 100 \quad \text{Equation 5.3}$$

Where C_1 is the initial concentration of the culture and C_2 is the final concentration at time t . The sample was taken from the cell suspension at a depth of ~20 mm. The total depth was ~90 mm.

The results of biomass yield can be seen in Table 5.6. High cell recovery was obtained in the fourth and fifth days of the experiment.

Table 5.6 Biomass yield from sedimentation experiment using a universal tubes

Time (hour)	Biomass sedimented yield (% Cell recovery)
24	41.2
48	56.8
72	76.8
96	91.1
120	94.3

Figure 5.47 shows the samples during the sedimentation process from 24 hr to 120 hr respectively. And Figure 5.48 shows the comparison between the control samples (0 hr) and the samples after 120 hr.

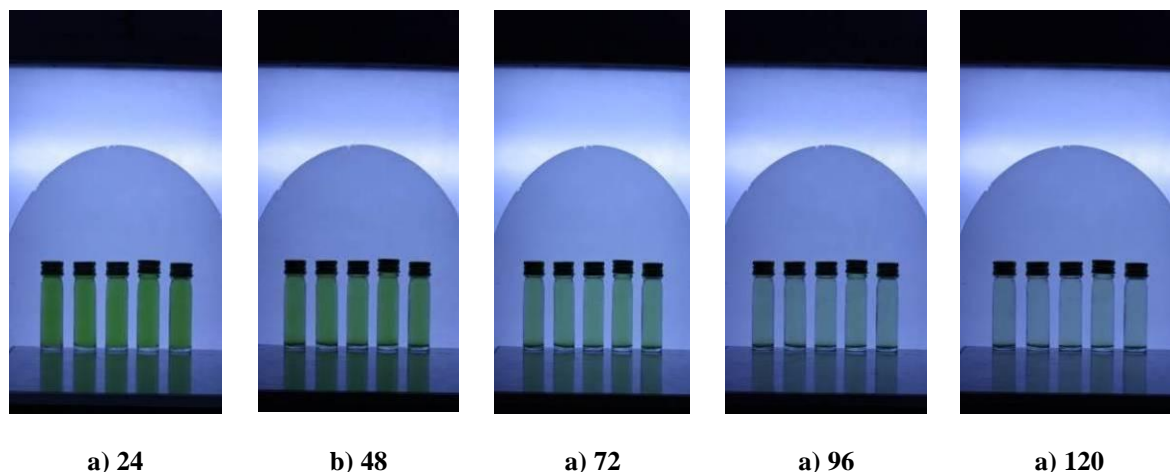


Figure 5.47 *N. oculata* samples during sedimentation process from 24 to 120 hr respectively



5.10.1.2 Algal sedimentation in conical flasks

In this experiment, *N. oculata* samples were settled in three 1000 mL beakers as shown in Figure 5.49 to increase the biomass collected. The overall height of the flask was 220 mm and 130 mm in diameter at the base. The beakers were investigated every day over a period of 120 hr, and liqueur samples taken from the top layer of the culture were examined microscopically.



Figure 5.49 *N. oculata* inside the conical flasks at 0 hr (left) and 120 hr (right) during sedimentation process

The cell recovery was determined using Equation 5.3. Obviously from the results in Table 5.7, the biomass yield increased with time. This indicates a high cell recovery i.e. a good harvesting of *N. oculata* after 120 hr of natural sedimentation with no additional energy input. The major disadvantage of this process is the time for separation.

Table 5.7 Sedimentation of *N. oculata* inside the conical flasks

Time (hour)	Biomass yield (% Cell recovery)
24	25.7
48	45.3
72	70.3
96	83.7
120	96.2

5.10.1.3 Glass tank sedimentation experiment

N. oculata was cultivated inside the glass tank PBR (see Section 5.6). The set up of the experiment can be seen in Figure 5.50. During sedimentation, photographs of the tank were captured using a digital camera (Canon, EON-D1000, Japan) and saved on the laptop. The cells were grown up until they reached a concentration of approximately 10^9 cells/mL, then the air circulation was stopped and the culture was settled for 120 hr. Photographs were taken every 30 min. The same procedure was followed as for cell recovery calculation detailed in Section 5.10.1.1.



Figure 5.50 Sedimentation setup for a large glass tank

Figure 5.51 shows the results of sedimentation of *N. oculata*, the clarity of the culture was obvious after 120 hr. The results of the microscopic examination of sedimentation can be seen in Table 5.8. When the length of time increased, a higher concentration of the algal layer was deposited on the bottom of the tank. The upper layer can be drawn off and the deposited layer can be collected, for harvesting and oil extraction processes.

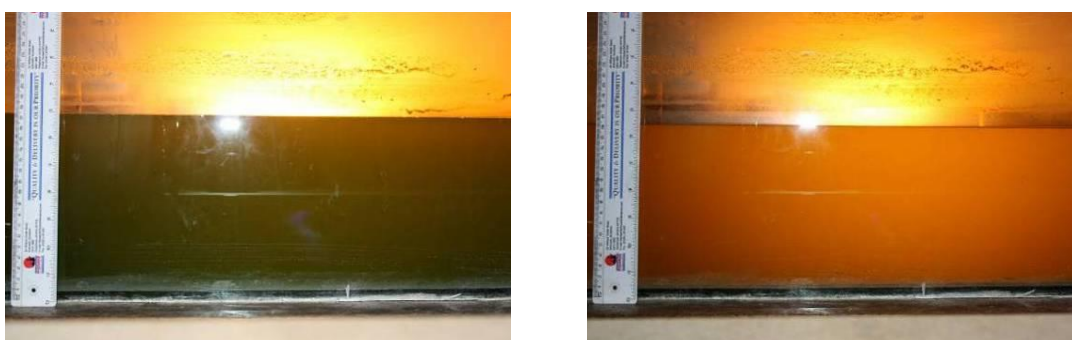


Figure 5.51 Sedimentation process for a large glass tank at 0 hr (left) and 120 hr (right)

Table 5.8 Microscopic examination of sedimentation for a large glass tank

Time (hour)	Biomass yield (% Cell recovery)
24	20.5
48	37.4
72	47.4
96	60.3
120	70.5

The biomass yield was lower than in previous experiments because the water was much deeper and even more time would be required for greater biomass yield.

5.10.2 Chemical flocculation

In order to increase the rate of sedimentation, flocculants were used in algae harvesting. The flocculants join many algal cells together and create particles of a larger size, which are then deposited at a faster rate. The flocculants used in this research include albumin, gelatine and bentonite. The experimental protocol was the same as that used in the natural sedimentation experiments, Section 5.10.1.1. Dosages of 100, 400, 700 and 1000 mg/L of each flocculent (albumin, gelatine, bentonite) were added to universal tubes containing 25 mL of alga culture. Figure 5.52 and Figure 5.53 show the samples after 24 hr of observation.



(a) at 0 hours



(b) at 24 hour

Figure 5.52 Bentonite at varying dosages (top row) and gelatine at varying dosages (bottom row)
(left to right, control, 100, 400, 700 and 1000 mg/L)



(a) at 0 hours



(b) at 24 hour

Figure 5.53 Control samples (top row) and albumin at varying dosages (bottom row)
(left to right, control, 100, 400, 700 and 1000 mg/L)

The cell recovery was calculated by microscopic examination using Equation 5.3, and the results can be seen in Table 5.9. From the results, all of the flocculants successfully accelerated the separation of the algae from the culture, but the percentage of cell recovery was not very high. Albumin and gelatine at lower concentrations accelerated the sedimentation rate as compared to the control without flocculent, and the optimum dose was about 100 - 400 mg/L. But increasing the dosage had no increased effect on the flocculation process. This means that there is an optimum dose for the flocculent and no effect after that level, this is in agreement with other work (Molina Grima *et al.*, 2003; Uduman *et al.*, 2010). Bentonite at a higher concentrations increased flocculation compared to the control.

Table 5.9 Chemical flocculation results over a period of 24 hr (n = 1)

Chemical flocculent (mg/L)	Biomass yield (% Cell recovery)
Albumin	
100	32.1
400	52.2
700	14.3
1000	13.3
Gelatine	
100	23.8
400	32.7
700	14.2
1000	19.2
Bentonite	
100	23.1
400	27.3
700	30.0
1000	35.0
Control (without flocculent)	21.3

5.10.3 Filtration

Filtration can be used to remove the algal cells from the liquid medium. The *N. oculata* culture was filtered using two methods: a cotton cloth and a membrane filter. The *N. oculata* culture was cultivated inside the glass tank of ~ 170 L of water. The phyto nutrient was added to the tank over the cultivation period. The growth lamp was attached over the culture to get a suitable illumination for growth, and the tank was aerated using an air pump, as previously described. The experiment was run for 14 days until a high concentration of algae was obtained. Figure 5.54 shows the growth results. The algal samples were prepared for dewatering using a filtration method.

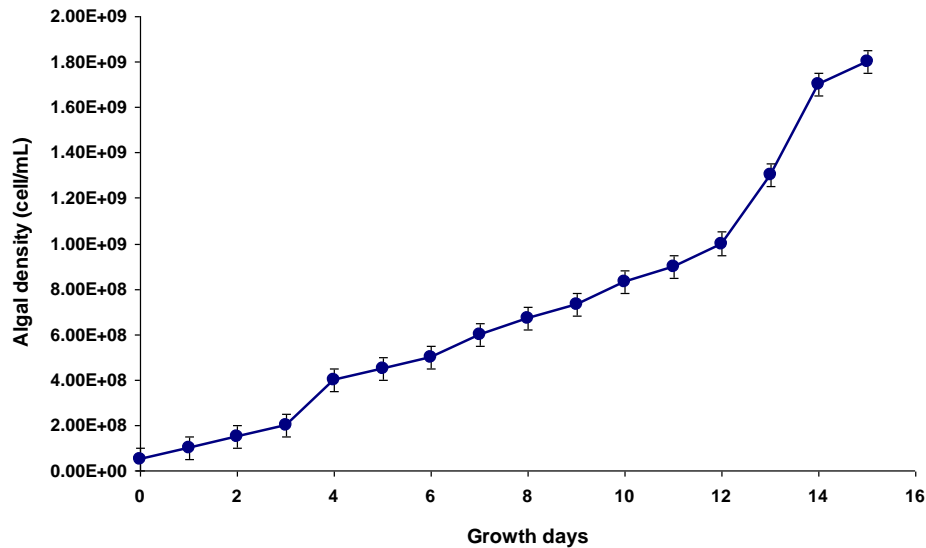


Figure 5.54 Algal growth for filtration experiment, the error bars are the standard deviation of ten samples

5.10.3.1 Vacuum filtration

Membrane filtration is the most suitable method for harvesting small algal cells ($< 30 \mu\text{m}$) compared to other conventional filtration methods (Petruševski *et al.*, 1995). The paper filtration process can be enhanced by applying a vacuum. The vacuum filtration was carried out using a vacuum flask (Buchner flask) connected to the pump (Watson Marlow, M-501, United States), as shown in Figure 5.55. The filter paper of $0.45 \mu\text{m}$ pore size (Whatman, UK) was chosen to recover the algae. For comparison, cotton cloth filters were used. The algal culture was added to the top of the funnel in different volumes (1, 5, 10 and 15 mL), and the pump was turned on for 2 min filtration time.



Figure 5.55 Filtration apparatus and the pump

5.10.3.2 Vacuum filtration results

The algal biomass recovery by the paper filter was efficient and rapid for the volumes of 1, 5 and 10 mL. The recovery of 15 mL algal culture was slow because of the relatively large volume of water and hence the greater number of algae, clogged the filter. Figure 5.56 shows the paper filter covered with a wet biomass cake. The cloth filters retained the algae rapidly without blocking the pores, but the cell recovery was less than the filter paper. The low recovery may be due to the algal cells penetrating through the cloth because of large pore size. The cloth is not suitable for this type of filtration; furthermore, the cloth did not fit probably inside the apparatus. Figure 5.57 shows the paper and cloth filters with filtered algal biomass after passing 1, 5 and 10 mL of culture (initial concentration of $\sim 1.85 \times 10^9$ cell/mL).



Figure 5.56 Filter paper inside a Buchner funnel and covered with a wet algal biomass

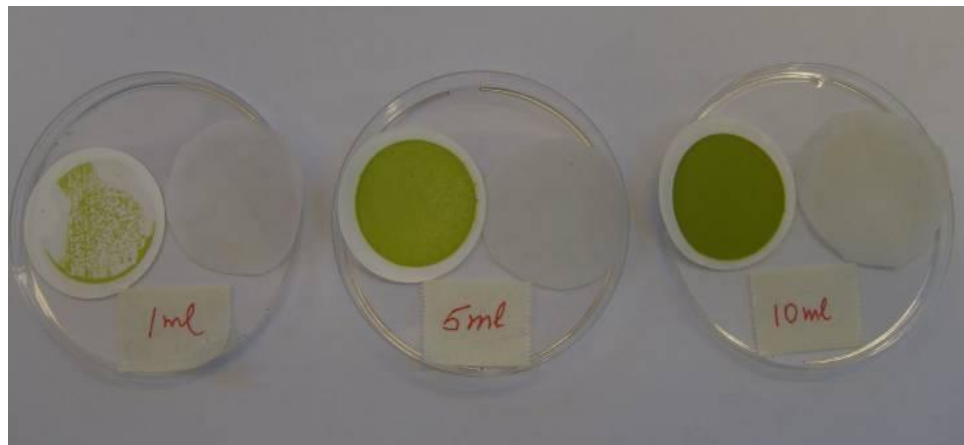


Figure 5.57 Algal biomass cake collected on paper (left) and cloth (right) filters for 1, 5 and 10 mL sample

After filtration, the filters were dried inside an incubator (Carbolite 20-701666, UK) at 80°C for 1 hr. To determine the biomass concentration, the filters were weighed on scales (Ohaus, AS120, USA) and compared with the original, unused filter weight. Table 5.10 shows the biomass recovery after drying the filters. From the results, it is evident that a higher biomass was recovered using the paper filters than the cloth filter.

Table 5.10 Vacuum filtration of *N. oculata* algae, filtration time of 2 min

	1 mL	5 mL	10 mL
Paper	7.2 mg	10.5 mg	15.3 mg
Cloth	2.5 mg	4.7 mg	7.4 mg

Further investigation using a vacuum filtration was done to determine the algal biomass productivity i.e the dried biomass per volume per day. Figure 5.58 shows that the dried biomass increases with the cultivation time, as would be expected. These are good results as the lipid productivity increases with dried biomass weight (Griffiths & Harrison 2009). Furthermore, this is an efficient and simple method to collect the biomass.

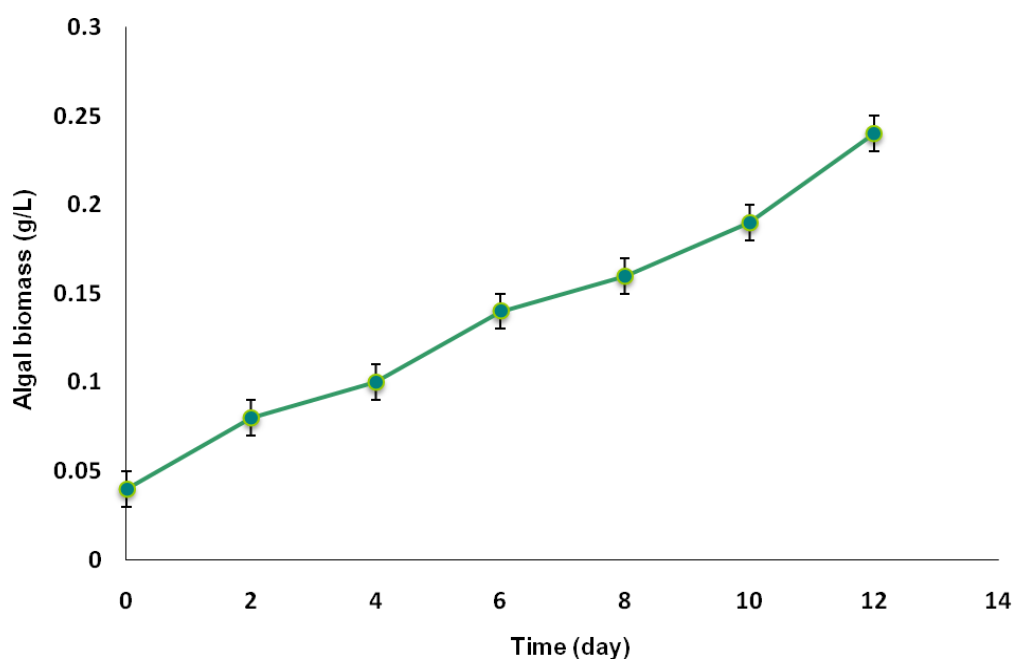


Figure 5.58 Algal biomass productivity per day (initial concentration of $\sim 1.85 \times 10^9$ cell/mL).

The error bars are the standard deviation of three samples

5.10.3.3 Cloth filtration

A liqueur of algal slurry was poured over a cloth filter, the samples were left near the window to aid evaporation. After 24 hr, the algal cakes were harvested manually by a scraper. The biomass cake was about 40 g/L dry wt. Figure 5.59 shows the dewatering of *N. oculata* using a cotton cloth filtration with drying at room temperature.

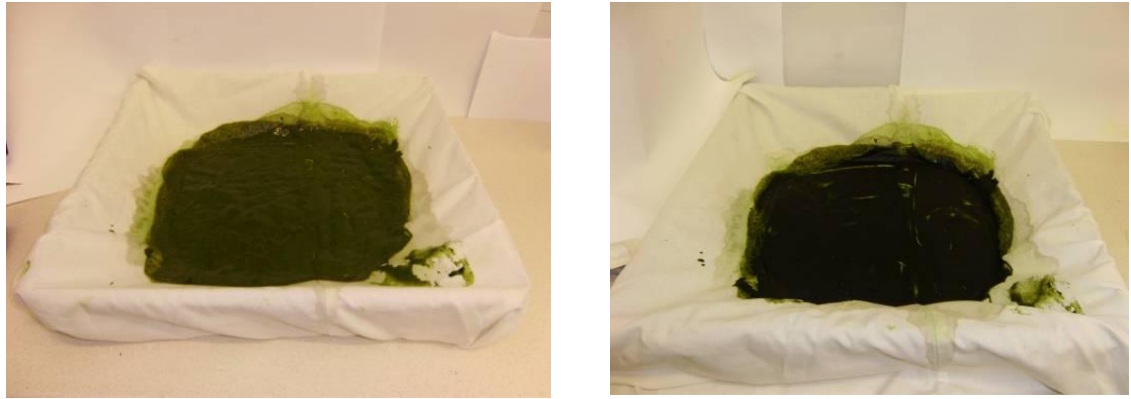


Figure 5.59 *N. oculata* biomass harvesting using a cotton cloth before dewatering (left) and drying at room temperature (right)

5.10.3.4 Mesh filtration

The algal slurry was passed through marked wire mesh (see Chapter 2: Section 2.5.6) and cloth with a wide pore size to avoid filter clogging. The pore size was 180 μm and 10 μm for the mesh and cloth filter respectively. The harvesting efficiency was not very high and the harvesting process was continuous without any blinding to the filters. After filtration, the algal particles built up over the filters and were easily removed using a manual scraper. The filtered liquid was too light a green colour and did not clear completely due to some biomass passing through the pores, so it was used again for the algae cultivation. Figure 5.60 shows the wire mesh and cloth filters.



Figure 5.60 Wire mesh (left) and cloth (right) filters

Figure 5.61 shows microscopic images of the filters. The algae formed clusters over the filter apertures without blocking the pores; there was no need for backwashing the filters, so it is possibly suitable for large scale harvesting in slurry form.

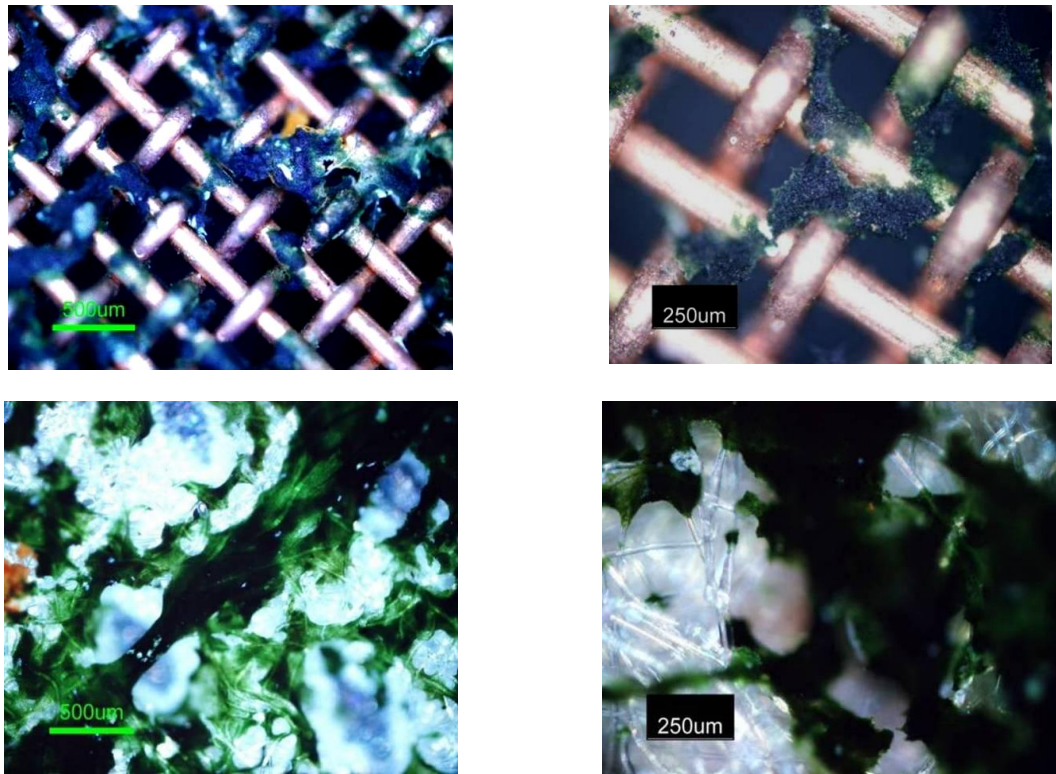


Figure 5.61 Microscopic images of the wire mesh (top) and cloth filters (bottom) covered with the microalgal biomass

5.10.4 Centrifuging

Centrifugal cell recovery is fast and often the preferred method in alga harvesting, but it is energy intensive (Molina Grima *et al.*, 2003). Three types of centrifuges were used: WIFUG Lab Centrifuge (500E, UK), an Eppendorf Centrifuge (5415D, UK) and an Extreme Raw Power Centrifuge (WVO Designs, USA). The first centrifuging process investigated using two types of centrifuging tubes: a 25 mL for the WIFUG Lab centrifuge (500E,UK) and a 0.5 mL for Eppendorf centrifuge (5415D, UK), as can be seen in Figure 5.62.



Figure 5.62 WIFUG Lab Centrifuge 500E (top row) and Eppendorf Centrifuge 5415D (bottom row)

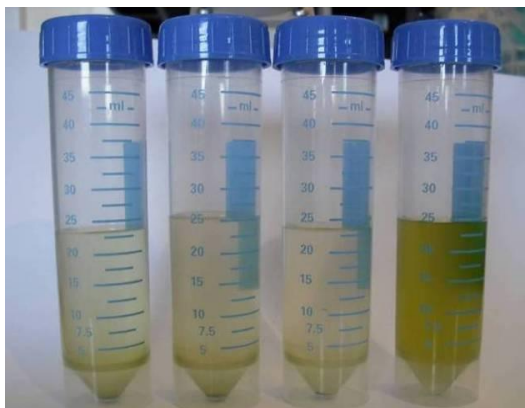
The test tubes of *N. oculata* were centrifuged at 1000G for various running times, and at 5000G and 10000G for 5 min. Table 5.11 shows the centrifugal parameters.

Table 5.11 Centrifugal parameters (25 mL tube WIFUG centrifuge, 0.5 mL tube Eppendorf centrifuge)

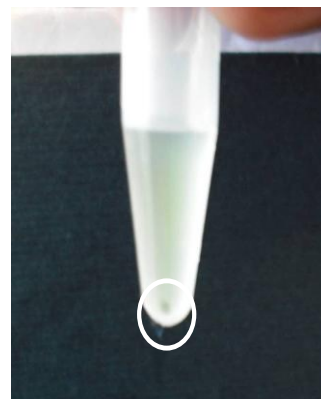
Sample volume (mL)	Centrifugal force (G-force)	Time (min)
25	1000G	5
25	1000G	10
25	1000G	15
25	1000G	20
0.5	5000G	5
0.5	10000G	5

5.10.4.1 Results of centrifugation test

Centrifugation of *N. oculata* separated the microalgal cells and they settled to the bottom of the test tubes, as can be seen in Figure 5.63 (a) and (b).



a) The algae separated gradually with increasing running time (15, 10, 5 min and control from left to right)



b) The microalgal cake settled to the bottom of the tube

Figure 5.63 *N. oculata* microalgal after centrifuging at 10000G

To evaluate the harvest efficiency, a 50 μL sample of the supernatant layer for each sample was examined under the microscope. Table 5.12 shows the biomass recovery (see Equation 5.3 for calculations). A centrifugal force at 5000G for 5 minutes were the best centrifugal parameters.

Table 5.12 Running parameters and results for centrifuging process

Centrifugal force	Harvest efficiency %	Time (min)
WIFUG centrifuge (25 mL tube)		
1000G	47.8	5
1000G	68.8	10
1000G	77.7	15
1000G	89.3	20
Eppendorf centrifuge (0.5 mL tube)		
5000G	100	5
10000G	100	5

5.10.4.2 Microscopic examination of centrifuging experiment

Liquate samples from the top (supernatant layer) and from the bottom of the centrifugal tubes were examined under the microscope. For 5 min centrifuging, the algal concentration from the upper layer was much less than the bottom layer as can be seen in Figure 5.64. For 20 min centrifuging, the total biomass in the sample was recovered as can be seen in

Figure 5.65. The bottom layer was highly concentrated, so it required to be resuspended in water for counting.

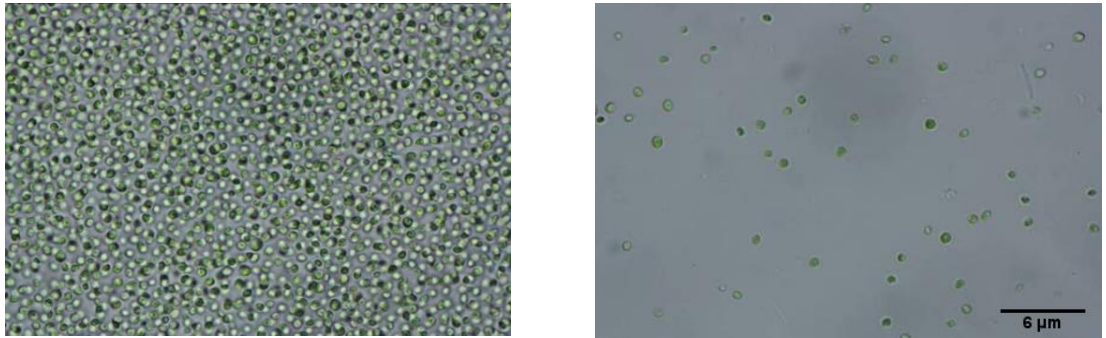


Figure 5.64 Microscopic images of *N. oculata* after 5 min of centrifuging WIFUG centrifuge.
The bottom layer (left) and top layer (right)

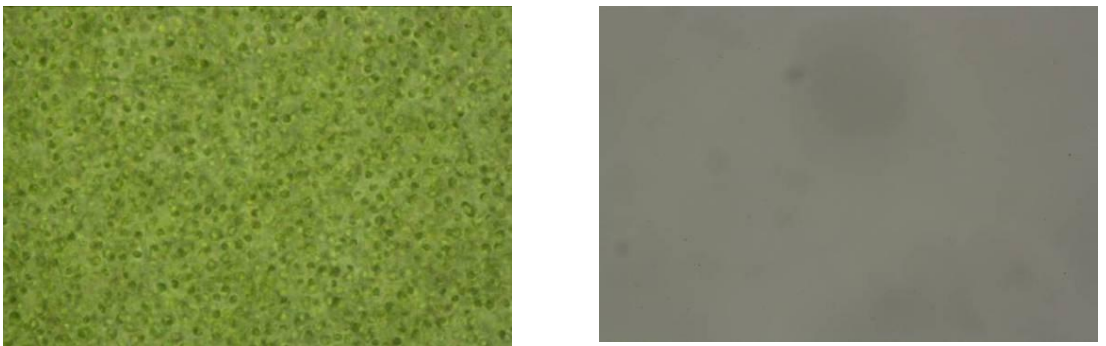


Figure 5.65 Microscopic images of *N. oculata* after 20 min of centrifuging WIFUG centrifuge.
The bottom layer (left) and top layer (right)

The second centrifuging process was investigated using an Extreme Raw Power centrifuge (WVO Designs, USA) working a G-force of 2150G (rpm of 4500). The algal culture was fed from the large glass tank (155 L) to the centrifuge. Figure 5.66 shows the experimental setup. In one and a half hours, the whole volume of cultured water was centrifuged. After centrifuging, the algal biomass was deposited on the inner surface of the centrifuge, as can be seen in Figure 5.67, and this harvesting method was very effective in obtaining a high concentration algal paste.

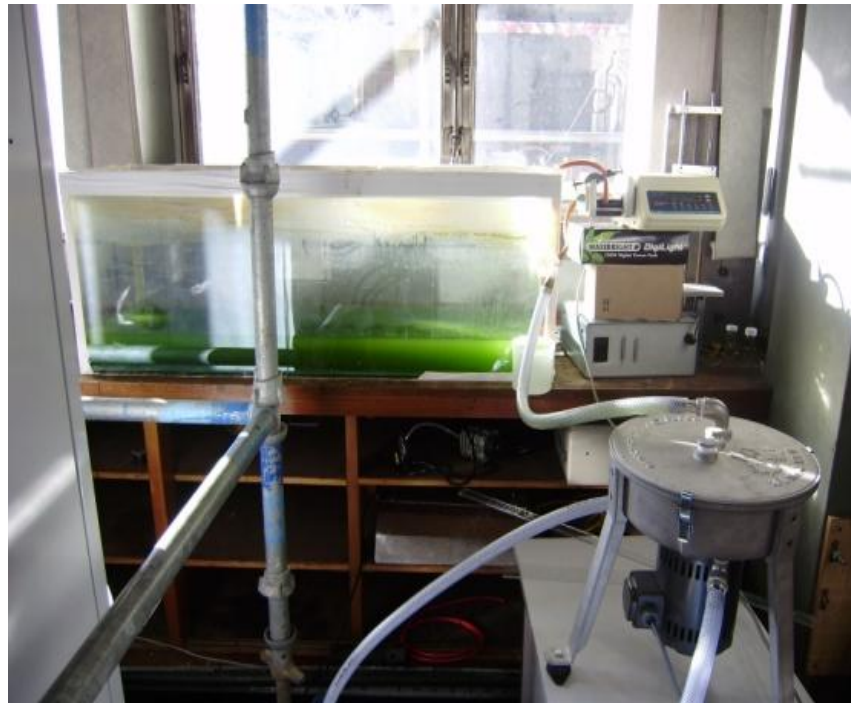


Figure 5.66 A large algal PBR and a centrifuge setup



Figure 5.67 *N. oculata* algal paste after centrifuging at 2150G

5.10.5 Dewatering of algae

A wet algal suspension was dried by placing it in a large flat tray (400x450x70 mm) (Figure 5.68). The suspension was left to dry at room temperature. It is possible to put the tray near the window to expose it to solar radiation for increased water evaporation. This process is easy, very cheap and consumes no extra energy, but it needs time for complete drying of the algae. The drying time for the tray was 2-4 days during summer time ($\sim 23^{\circ}\text{C}$) and 5-7 days at winter time ($\sim 10^{\circ}\text{C}$). The algal flakes were removed by scrubbing the tray with a scraper.

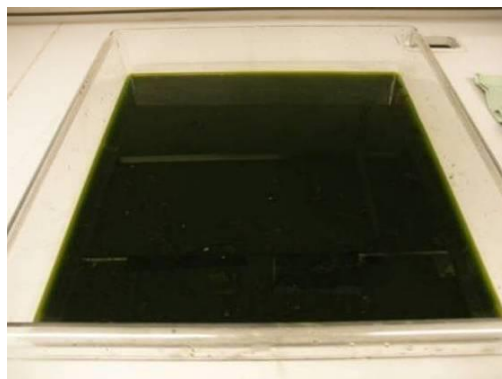
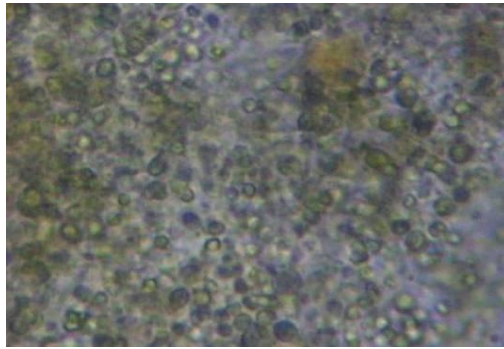


Figure 5.68 Drying of algae on the tray with low cell density (left) and high cell concentration (right)

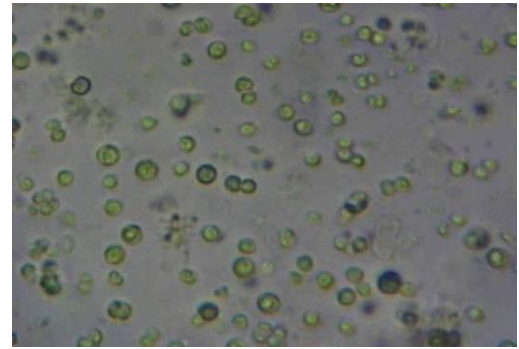
Another method of drying the algae was by using thermal radiation. It is a fast and very effective technique for dewatering the algae. The algal slurry was collected from the tank as can be seen in Figure 5.69. The very high density of algal cells in the slurry made the cell counting impractical, so the culture was diluted twice (by a factor of 10^2) for microscopic examination. After dilution, the average cell concentration in the original slurry was calculated to be 10^{12} cell/mL. Figure 5.70 shows the results of the microscopic examination of algal slurry. Interestingly, if the microalgae are $1\ \mu\text{m}$ in diameter and assumed to take up a volume of $1\ \mu\text{m}^3$, then the maximum number of cells per mL is 10^{12} . Packing spheres (e.g. cannonballs), however, is a well-known problem, and under the right conditions, it may be possible to have a cell number slightly greater than this.



Figure 5.69 The algal slurry



a) 10^{14} cell/mL



b) 10^{12} cell/mL

Figure 5.70 Microscopic photographs of algal slurry before and after dilution respectively

A 50 g sample of wet algal paste was taken from the slurry and spread into a container (200 mm diameter), which was then placed inside the incubator (Carbolite, PIN120, UK) at 80 °C for around 4 hr. A 39.7 g algal cake was obtained after heating, and the value of energy consumed for the drying was 346 kJ. Figure 5.71 shows the algal slurry after and before drying.

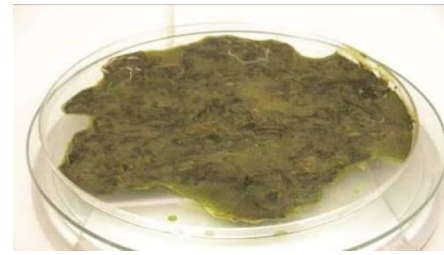


Figure 5.71 Algal slurry (left) and algal cake after drying by thermal radiation (right)

5.10.6 Laser marking

Various potential strategies for dewatering using roughened surfaces were considered. To assess the effect of surface roughness on microalgae adhesion, two samples of Perspex were laser processed. The material was cut into 400x30x5 mm sheets. An *Nd:YVO₄* laser marker (Laservall, Violino 2, UK) was used to mark the Perspex sheet at scanning speeds of 20, 40, 60, 80 and 100 m/s. The laser marking increased the surface roughness, and in general higher speeds produced higher roughnesses (see Chapter 2: Section 2.5). The sheets were put inside a tray containing the algal culture for 24 hr. Then the samples were removed from the culture by tilting the tray. The algal culture was attached on the Perspex

surface and there was greater attachment on the areas marked with laser as can be seen in Figure 5.72.



Figure 5.72 Algae attached to Perspex strip, higher adhesion when surface roughness increased, in the highlighted circular regions, from left to right

Two aluminium electrodes (200x30x3) mm (see Chapter 2: Section 2.6.4.3), one of which was marked with the laser to increase the surface roughness to $\sim 1.5 \mu\text{m}$, and the other left untreated, and used as the control, were soaked in the algal culture for 10 min, and the tray was tilted to remove the culture from the electrodes. The attachment of the microalgae over the marked surface was higher compared to the control sample i.e. the smooth surface. Marking the surface with the laser increased the surface roughness and hence improved the attachment, Figure 5.73 showing the results. This was not investigated further but may open up opportunities for new methods of separation.

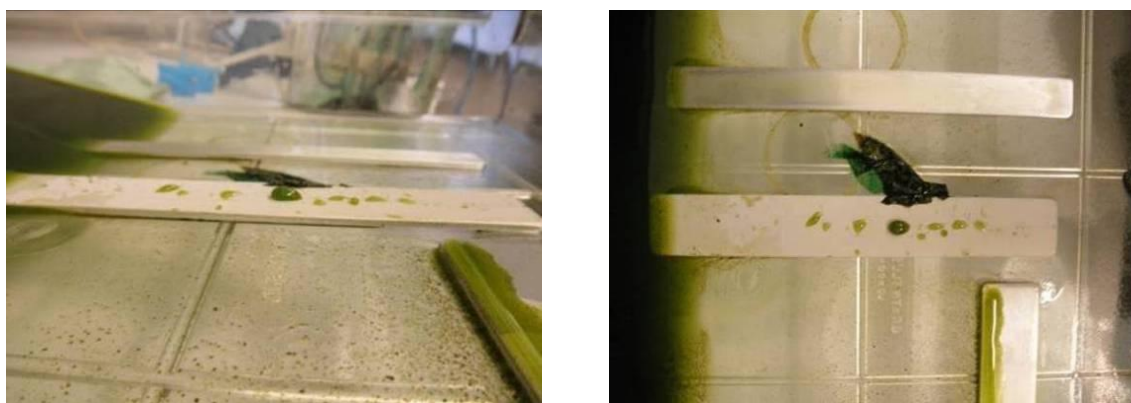


Figure 5.73 The control sample (top) and the laser marked sample (bottom)

5.11 Biofilm formation

The algal biofilm grew naturally on the wall and lid of the PBR during the cultivation period, as can be seen in Figure 5.74. These biofilms were easily harvested compared to suspended algae harvesting. The biofilms on the lid and the walls were harvested by a small scrapper.



Figure 5.74 Biofilm growing on the lid and wall of PBR

Small layers of biofilm were cut and assessed microscopically, as can in Figure 5.75. The results showed that the biofilms were a good source of high concentrated biomass. The layers attached to the walls of the tubes were more highly concentrated biomass than that returned from the lid. Figure 5.76 and Figure 5.77 show the results.



Figure 5.75 Biofilm on the microscopic slides

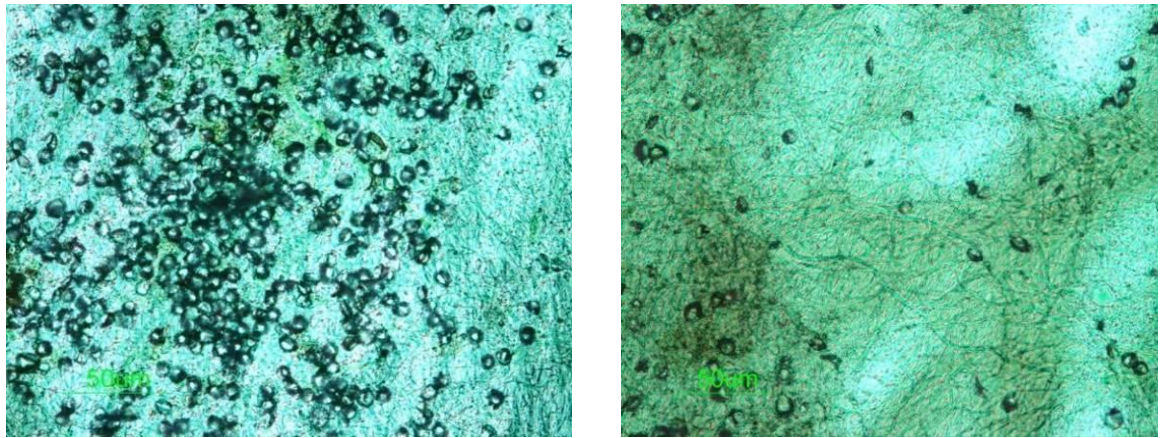


Figure 5.76 Microscopic examination of the biofilm attached to the wall (left) and lid of the PBR (right)

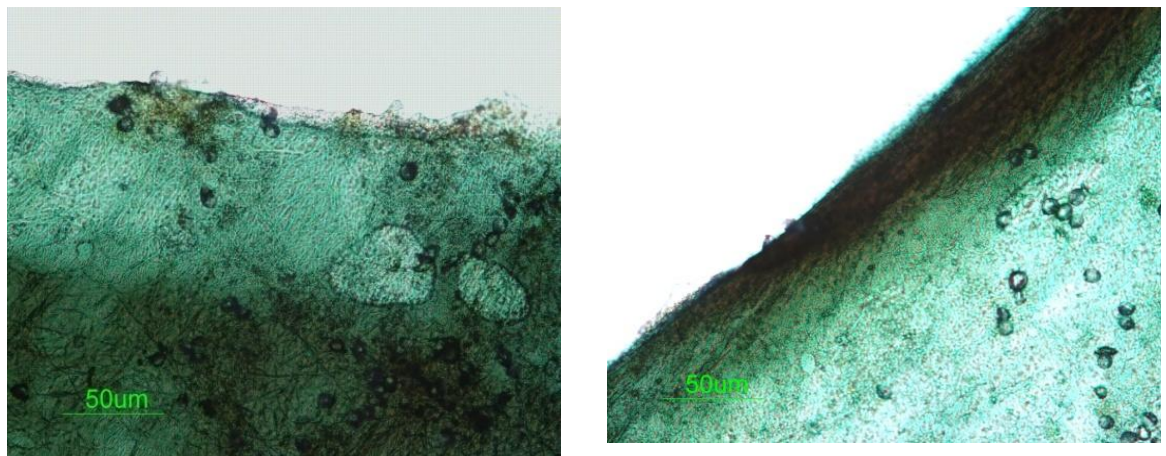


Figure 5.77 Biofilm edges under viewed microscopy from the wall (left) and lid (right) of the PBR

The atomic force microscope (AFM) is an important instrument for surface roughness measurements with high resolution and accuracy at the nanoscale (De Oliveira *et al.*, 2012). The AFM (VEECO Dimension 3100, USA) with tapping mode (non-contact mode) was used to scan the biofilm of microalgae; Figure 5.78 shows the AFM and the biofilm growth on the photobioreactor PBR wall. Figure 5.79 shows the analysis of the biofilm surface. The thickness of biofilm was 1.4 μm and the surface roughness R_a was 231 nm.

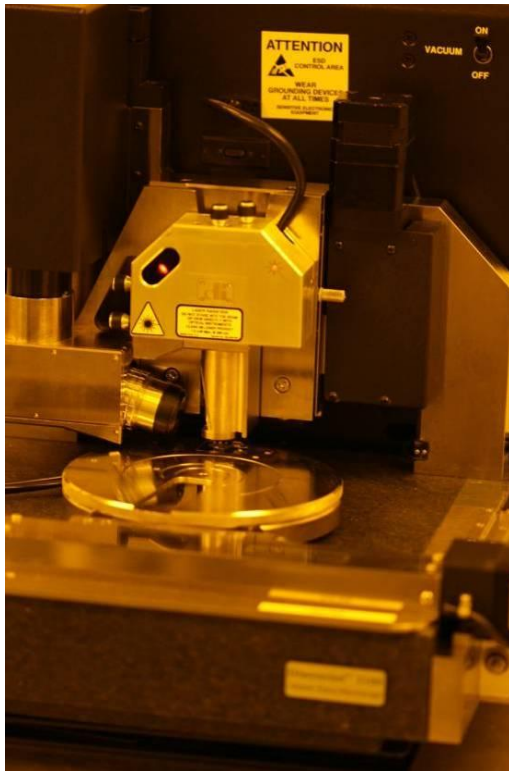


Figure 5.78 AFM view (left) and biofilm on PBR wall (right)

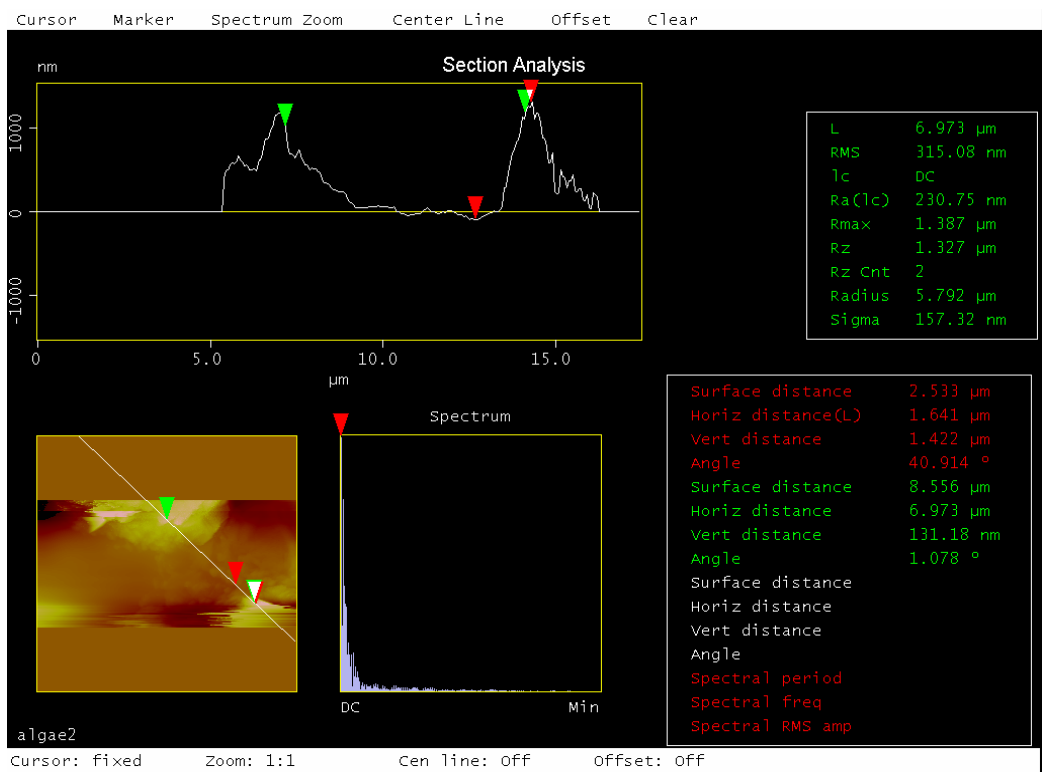


Figure 5.79 AFM scanning window shows the image and the surface roughness of *N. oculata* biofilm

5.12 Oil extraction

The oil extraction from the microalgae is the main feature in the production of biodiesel fuel. The microalgae contain a lipid-profile suitable for biodiesel (Nascimento *et al.*, 2013). Type and amount of fatty acids in microalgae such as oleic, palmitic, stearic, iso and linoleic are attractive components in fuel production (Demirbas & Demirbas 2010). Various techniques were investigated for oil extraction of *N. oculata* algae including: pressing, blending and solvent extraction.

5.12.1 Oil extraction with chemical solvents (methanol, isopropanol and ethanol)

The algal biomass was obtained from the previous work (see Section 5.10.5). The dried algae were ground into a powder and put inside the incubator (Carbolite, PIN 120, UK) at 80 °C for 5 hr to remove the moisture (an initial moisture content of 80% and a final moisture content of 19.6% after being dried). The moisture content determined by oven drying method i.e. the biomass loss after drying. Figure 5.80 shows the algal powder inside the incubator. Three algal samples of 5 g were mixed with 25 mL of three different solvents (a proportion of 1:5 g/mL). The organic solvents included methanol (Prolabo, France), iso-propane alcohol (Sigma Aldrich, France) and ethyl alcohol (Fisher Scientific, UK). The three samples were stored overnight in the fume cupboard at ~ 21 °C.



Figure 5.80 Dried algae on the scale (left) and the algal powder inside the incubator

After soaking for 24 hr, the algal mixtures were stirred for 5 hr using a magnetic stirrer (Stuart, CB-302, UK) as shown in Figure 5.81. Then the mixtures were heated on the hot plate magnetic stirrer for 2 hr at 50 °C and 166 rpm. The heating increases the oil extraction efficiency and evaporation process. The mixtures were subsequently allowed to

settle down for 2 hr. Figure 5.82 shows the samples after settling, there were two layers, the top layer is the oil-solvent and the bottom layer is the algal biomass residue.



Figure 5.81 The samples on the magnetic stirrer

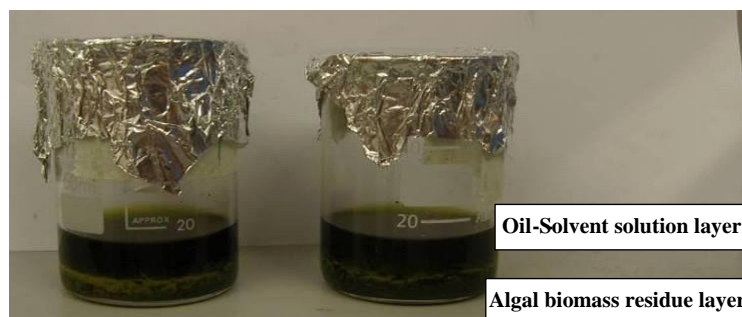


Figure 5.82 Oil-solvent layer (top) and biomass layer (bottom)

The algal biomass residue was separated from the oil-solvent solution by the cloth filtration as can be seen in Figure 5.83, and the algal biomass residue was washed with 10 mL of solvent to remove the residual oil. After filtration, each sample from using the three different solvents was put inside the hot water bath (Grant Instruments Ltd., SBB Aqua 12 Plus, England) at 50 °C to evaporate the solvents from the oil. Figure 5.84 shows the setup of the hot water bath.



Figure 5.83 Filtration process to separate the algal biomass from oil-solvent solution



Figure 5.84 Water bath to evaporate the organic solvents

5.12.2 Results of oil extraction using the chemical solvents

The extracted oil using iso-propane alcohol can be seen in Figure 5.85. The % oil yield for the three different solvents was evaluated and the results can be seen in Figure 5.86. The oil yield % was measured by weight, the extracted oil was highest using a methanol solvent (19.2%), followed by isopropanol (11.6%) then ethanol (11.4%).



Figure 5.85 Microalgal oil production by the chemical solvent - isopropanol

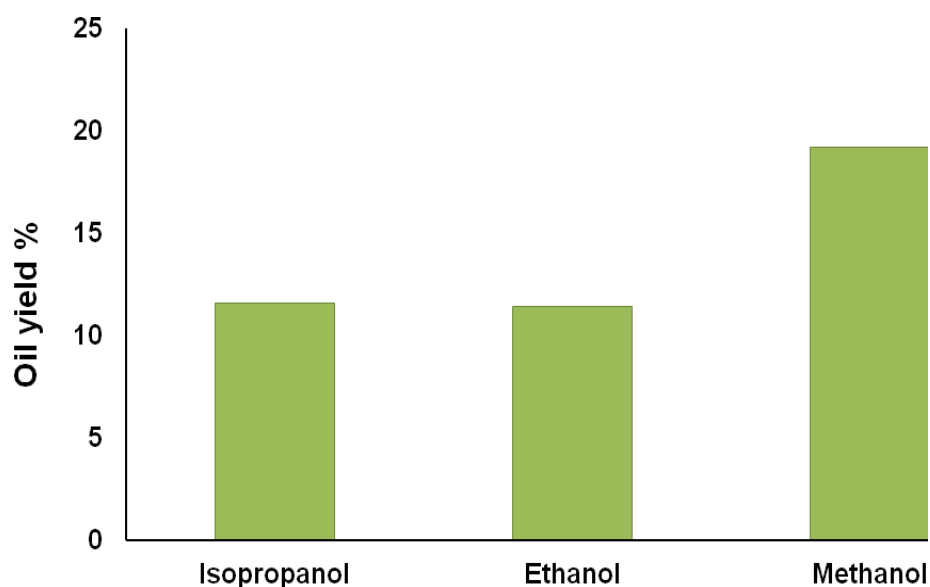


Figure 5.86 Oil yield by chemical solvents

5.12.3 Oil extraction by pressing

A homemade expresser was used for the oil extraction process of the fresh water algae and the dried algae. A schematic of the pre-press and press stages can be seen in Figure 5.87. The expresser was fabricated from aluminium, and was 50 mm high and 25 mm in diameter. The cylindrical column was placed inside the holders, where the microalgae were positioned. The algal culture was filtered out with a cotton cloth, then liqueate of 2 g of wet algal biomass was squeezed using the expresser. Figure 5.88 shows the expresser and the algal sample after pressing. At some stage in the expression, some liquid (lipid with water) was coming out from the expresser. Further processes should separate the lipid from the water.

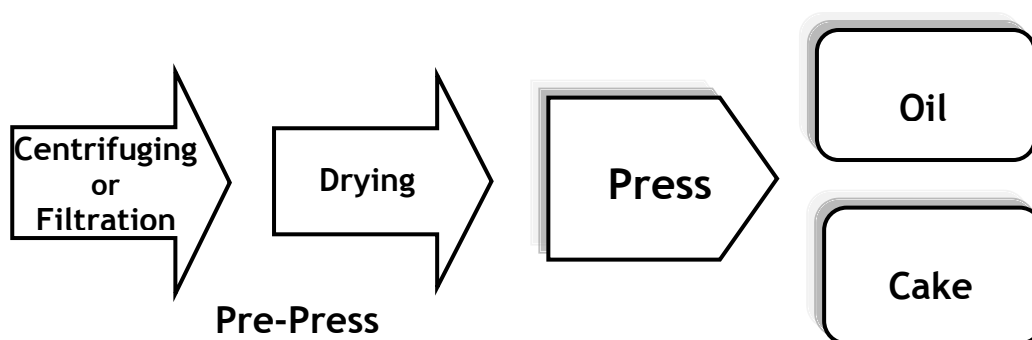


Figure 5.87 Schematic of press stages

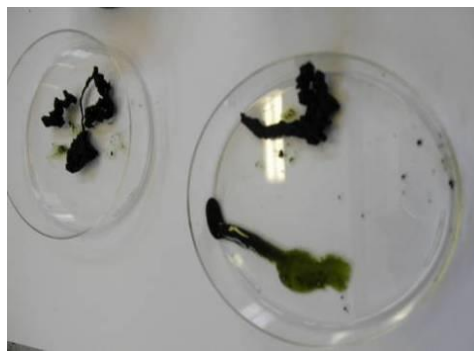


Figure 5.88 The expresser and the algal sample

The same pressing procedure was repeated but with dried algal biomass of 1.5 g. The amount of lipid was low, which may be due to over drying of algae, as lower lipid content with increasing drying time is observed up to 240 min (Vijayaraghavan & Hemanathan 2009). Figure 5.89 shows the expresser with the algal biomass cake.



Figure 5.89 Algal biomass cake sample after pressing

A microscopic examination using an optical microscope (Nikon Eclipse, ME600, Japan) was done on the algal biomass before and after pressing. A small needle was put over the sample which ruptured the cell walls and released lipids, as can be seen in Figure 5.90. Figure 5.91 and Figure 5.92 show the algae before and after pressing respectively. The pressing ruptured the cells and released their contents.

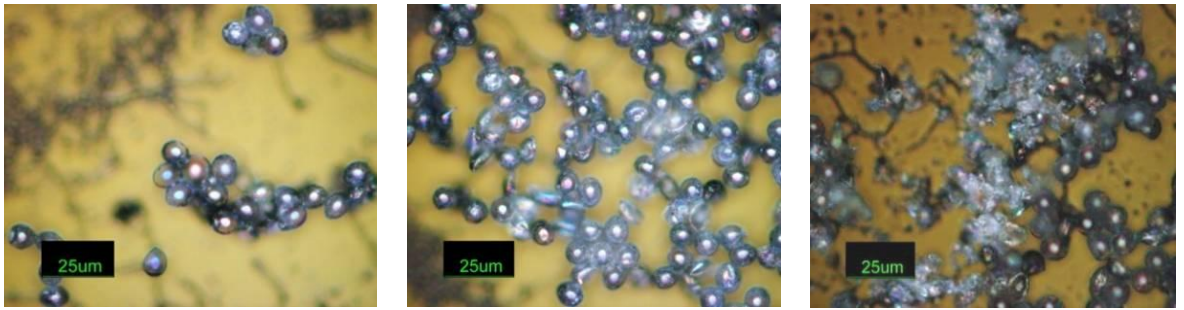


Figure 5.90 Cell rupturing using a needle

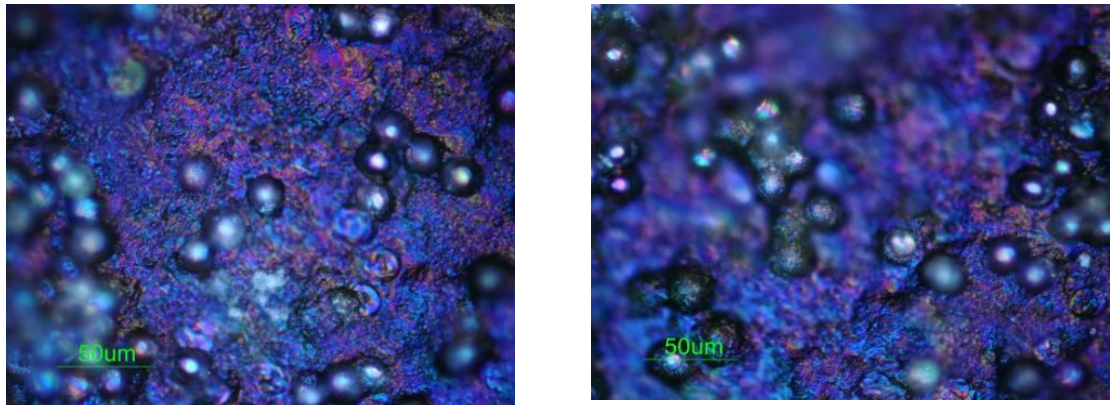


Figure 5.91 Algal biomass before pressing

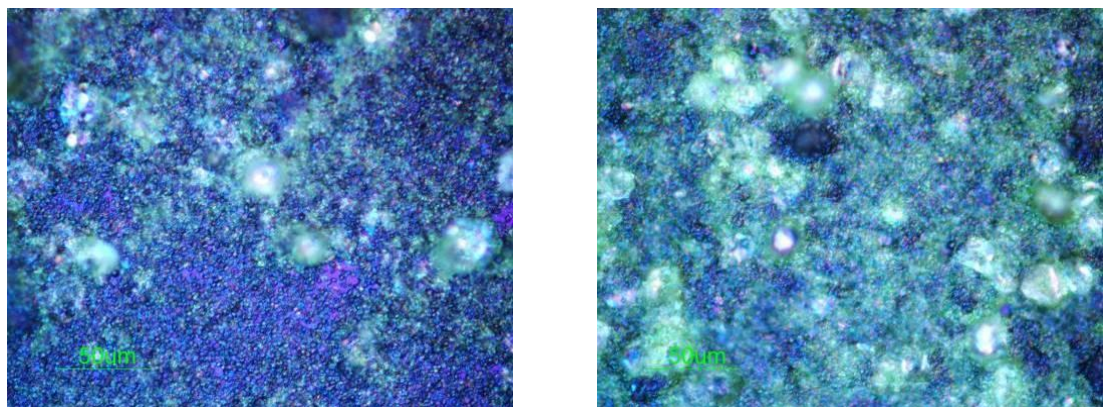


Figure 5.92 Algal biomass after pressing

5.12.4 Blending using a food mixer

Two 200 mL samples of algae were subjected to mechanical solid shear forces using a food mixer (120 W, Asda XB982, UK). The algal culture was blended for 4 min. Figure 5.93 shows the algal culture after blending.



Figure 5.93 The blended algal culture by using a hand blender, the bottle on the right side is the original stock

The same experiments were repeated to disrupt the cells. 80 mL of the algal culture was blended for 2, 4 and 6 min. Figure 5.94 shows the experimental setup.



Figure 5.94 The algal culture with the hand blender

5.12.5 Results of mechanical solid shear

A mechanical cell disruption process was effective in breaking down the cell walls and releasing the lipids. As can be seen in Figure 5.95, the oil layer rises to the top of culture. Further investigation on the top layer of the culture was done by taking some microscopic photographs as can be seen in Figure 5.96. From the microscopic results, the blended samples showed that the cell contents had been released, as compared to the control.



Figure 5.95 The algal culture cells after blending for 4 min

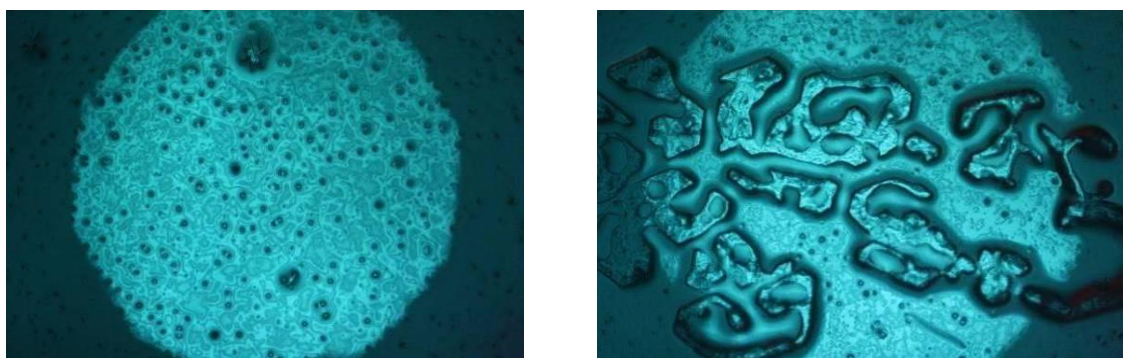


Figure 5.96 The microscopic images of the control without treatment (left) and the disrupted cells after blending for 4 min (10X LOMO objective)

The rotating blades of the blender were successful in the rupturing *N. oculata* cell wall. As shown in Figure 5.97, some cells were destroyed totally and there was some pitting on the walls of other cells. Figure 5.98 shows the average disruption of three samples with different treatment time. The average disruption was 92.44% of the initial intact cells for 6 min of treatment. The efficiency of disruption increased with treatment time.

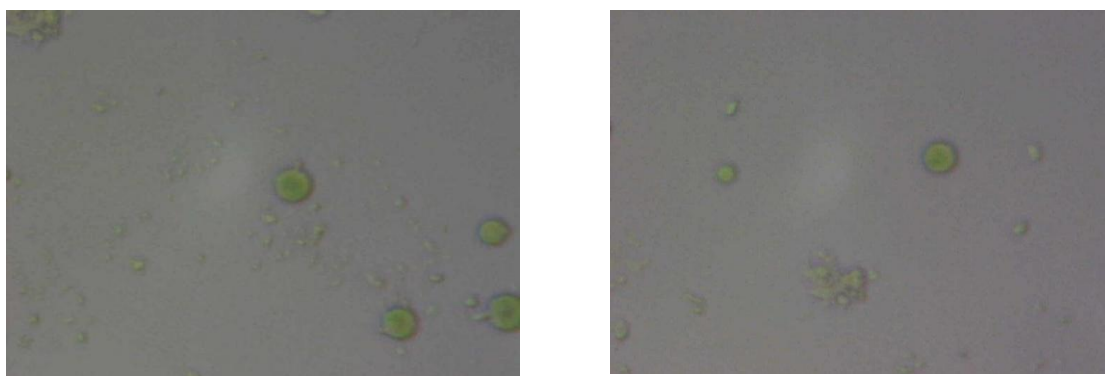


Figure 5.97 Microscopic images showing the damage of *N. oculata* cells with a blender (25X Zhumell objective)

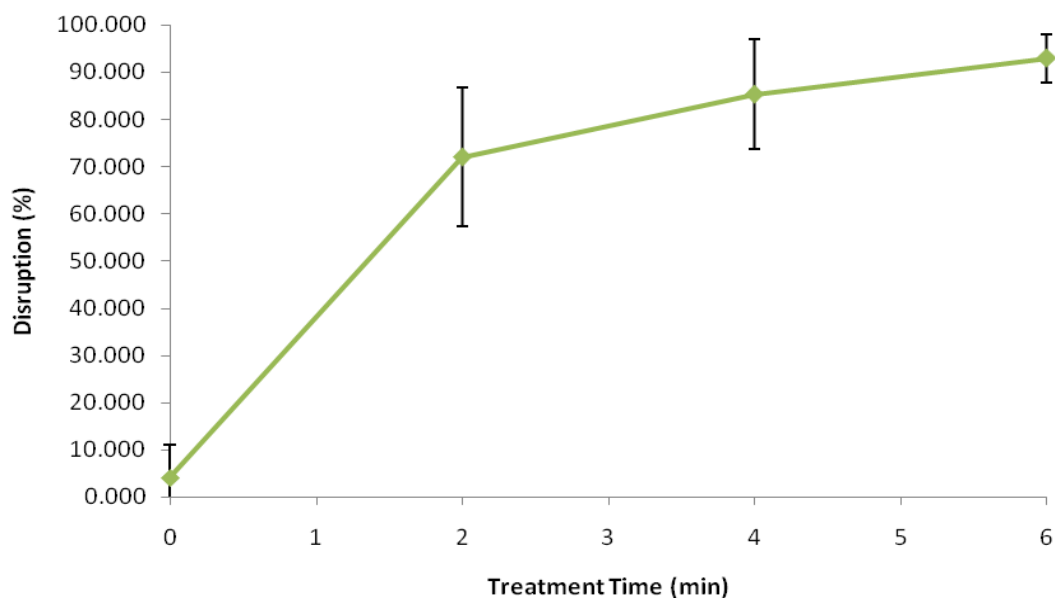


Figure 5.98 Mechanical cell disruption using the blender, the error bars are the average of standard deviation of the three samples

5.13 Oxygen bomb calorimeter

The calorific value of microalgal biomass collected from the glass tank (Section 5.10.5) was measured with an oxygen bomb calorimeter (Parr, 1431, USA). After assembling the calorimeter apparatus, 1 g of dried algae powder was put inside the combustion vessel and ignited. Figure 5.99 shows the oxygen bomb calorimeter system. The temperature readings were measured every 1 min for 5 min before the bomb firing, and on the 6th minute the bomb was ignited. Then the temperature measurements were continued at 1 min interval until the temperature became constant, as can be seen in Figure 5.100.



Figure 5.99 Oxygen bomb calorimeter (left) and the oxygen combustion vessel (right)

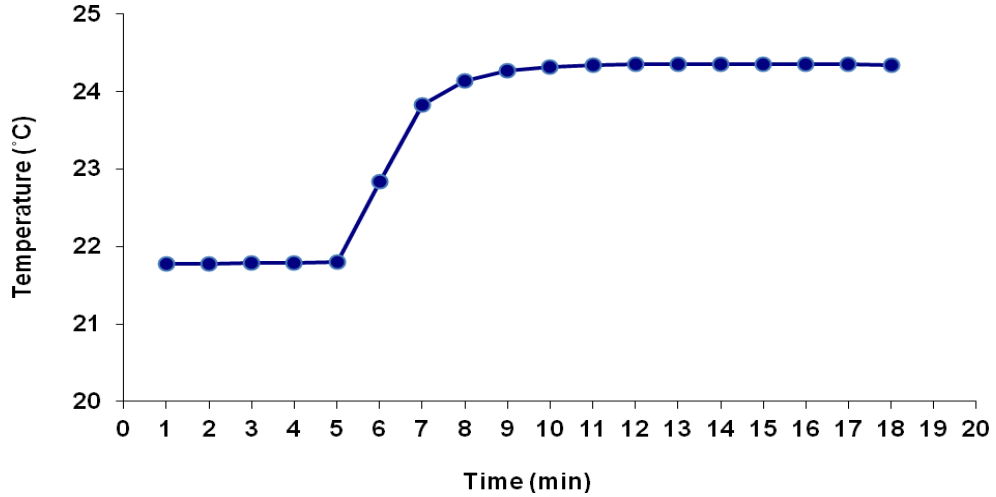


Figure 5.100 Temperature readings for the calorimeter

After the combustion was completed, the gross heat of combustion H_g (calories/gram) was calculated using the temperature readings in Figure 5.100 and the calorific equation H_g (Parr instruction manual 2013). After calculation, the calorific value of the *N. oculata* algal powder was found to be 33.968 MJ/kg. It can be seen that the algal powder has large energy density compared with flaxseed (30.297 MJ/kg) but it is lower than petroleum which is 43 MJ/kg.

$$H_g = T_r * W_c - \frac{e_3}{m_s} \quad \text{Equation 5.4}$$

$$T_r = T_c - T_a - r_1(t_b - t_a) - r_2(t_c - t_b) \quad \text{Equation 5.5}$$

$$e_3 = 2.3 * c_3 \quad \text{Equation 5.6}$$

Where:

t_a = Firing time (min)

t_b = Time when the temperature is 60% of the total increase (min)

t_c = Time at which the temperature become constant (min)

T_r = Temperature rise (°C)

T_a = Temperature at time of ignition (°C)

T_c = Maximum temperature, temperature at time t_c (°C)

r_1 = Rate at which the temperature rising before firing (°C/min)

r_2 = Rate at which the temperature rising after time t_c (°C/min)

e_3 = Correction for combustion heat of fuse wire (calories)

c_3 = Fuse wire length = 100 mm

W_c = Calorimeter energy equivalent = 2426 calories/°C

m_s = Sample mass = 1 g

Chapter 6

Conclusions and future work

Chapter 1 includes the background and the literature review of the research. Spatial mapping techniques were explained in a broader context and its relationship to bacterial contamination. The foundations of the image processing NI vision and computational fluid dynamics (CFD) software, which are important for analyses for the work in other chapters, was described.

Chapter 2 Spatial mapping of microorganisms in air and surfaces is important to allow detection of the particles and microorganisms in filtration and decontamination applications. From the results, laser marking with low scanning speeds caused higher surface roughness due to the increased exposure time and hence deep cavity formation. Higher laser power led to higher surface roughness; and increasing PRF decreased the surface roughness. The temperature effect on the surface with other laser parameters should be investigated for further studies.

This work was investigated to determine spore adhesion to electrode surfaces that formed part of a plasma decontamination system. In general, the rougher surfaces seemed to promote bacterial attachment compared to smooth surfaces. Membrane filtration and imprinting with different inlet flow angles were used to investigate the spatial variation of spores and microorganisms deposited via an aerosol to the electrode surfaces. Membrane filtering and imprinting techniques are simple methods of analysis that do not need complex equipment or control. Also developing complex protocols for accurate distribution and visualization of the microorganisms is time consuming. Further investigations should focus on developing imprinting techniques with microscopic

detection systems that offer the potential of real-time detection, or using different rapid detection techniques such as fluorescence methods to compare with the imprinting technique. The system utilising the excimer laser (Chapter 4: Section 4.3.2.1) and a spectral imaging system could be used to instantaneously map the spore distribution.

Chapter 3 investigates spatial detection methods of microorganisms. The first method utilised an optical microscope, which, of course is a highly effective technique for quantification and enumeration of microorganisms. Advantages of this method are its low cost, simple sample preparation and high detectable level. On rough surfaces, and in spite of long drying time (5 to 7 hr) it was less time consuming compared to other examination methods. On the other hand, because *B. atrophaeus* samples were on a rough surface, it is difficult to distinguish between the spores and the irregularities on the aluminium discs; it was noted that the spores distributed on the rough surfaces were in the same direction as the surface grooves. The other limitation of this technique is that the detecting efficiency is low when the density of spores $<10^3$ CFU/mL. This method gave improved understanding of the spore distribution over the surface. Future suggestions to make the visualisation of the samples relatively simple could include labelling the spore samples with fluorescent ester dyes. Combined with this approach, image processing software is needed to speed up the identification and counting procedures. Work would need to address the spectral content of the fluorescence signal and identify whether the signal is emanating from the spore or other contaminants in the sample. For example, it is not unknown for spores to be carried by water droplets, on fabric or dust. The spore carrier will also have a fluorescent signal. Such work would be important in clean rooms and hospital environments where real time detection of contaminants provide a significant advantage to cleanliness and reduced risk of infection.

The second method of detection was with the fluorescence measurements via LED excitation of the *Bacillus atrophaeus*, fluorescence spectra of the *Bacillus atrophaeus* with the excimer laser and chlorophyll fluorescence of microalgae in water. The results showed that these methods can be used an alternative method to the conventional counting techniques offering the potential for improved performance and counting accuracy. The same high power Luxeon LED (450 nm) to the LED used herein was used for fluorescence excitation of biofluorophores by Kurilcik *et al.* (2006). For future work, LEDs and excimer laser emissions could be used for production of fluorescence from airborne microorganisms, with appropriate detection systems produced.

The third method was a direct microscopy technique, using the flow chamber. The counting of microalgae culture was accomplished by passing the microalgae in liquid culture through a small flow chamber positioned under the microscopic objective. The results demonstrated that this method enables counting of microorganisms easily and rapidly in their natural environment. The limitation of the flow chamber depends on the depth of the slide, so an objective with large depth of field is needed. Flow cytometry is a standard technique for cell counting. Future work will focus on using the flow cytometry for microorganism quantification and identification.

With the techniques developed and suggested, there is a distinction between microscopic based techniques that provide a high degree of accuracy and recognition over small volumes. However some applications require analysis of much larger volumes. Detection of spores in clean rooms or hospital operating theatres is much harder problem. It would be interesting to scale up some of the technologies researched in this thesis to apply them to much larger volumes and greater throughput. It is likely that sensitivity to detection will be reduced and hence a larger number of microorganisms would be needed before detection was possible.

Chapter 4: The excimer laser was able to kill spores and bacteria rapidly. Exposing microorganisms seeded on agar plates to laser radiation is an established method for determining the biocidal capacity of a laser. It is a simple procedure, provides relatively rapid results, allows quantitative assessment of the laser's efficacy and is reproducible. In the present case, excimer laser radiation at 248 nm was used to inactivate *E. coli* vegetative cells and *B. atrophaeus* spores on LB agar plates. The same wavelength to our laser for inactivation of *B. atrophaeus* spores on packaging boards was used in (Warriner *et al.*, 2000). Images of the areas of clearing and the region between the areas of clearing were analysed and this provided an accurate method of determining the laser inactivation efficiency. The antimicrobial activity of the *KrF* excimer laser was highly effective and, over the range investigated, the area of clearing increased linearly (after the second pulse) for treatment against *E. coli* at a rate of 16.95 mm²/pulse. The area of clearing against *B. atrophaeus* was not linear and much smaller than that observed against *E. coli* (11.9 mm²/pulse for 10 pulses).

In this study, the decontamination methods of airborne microorganisms in a glass and a stainless system were investigated. The *KrF* laser radiation was effective in destruction of

the DNA of *B. atrophaeus*, as high inactivation was obtained and no growth was observed after the treatment. The percentage of killing increased significantly with increasing the length of the booster, as the residency time of the spores interacting with the laser beam increased. Fluent modelling allowed spore distributions analysis dependency on the flow shaping. The inactivation was investigated using the pulse repetition frequency PRF either 20 Hz or 100 Hz. Spetlikova *et al.* (2010) reported that a higher pulse repetition frequency gave faster inactivation. Li *et al.* (2010) investigated the effect of the UV-LED radiation on the *E. coli* biofilm, and reported that the PRF of 100 Hz gave the highest disinfection of the microorganisms. Although, this frequency is not standard for all cases, further investigation is needed (Wengraitis *et al.*, 2013). Further work should be done to optimise the micro-organisms' path to allow optimal laser killing inside the chamber of the glass booster. In conjunction with optimising the flow, optical components could be used to expand the beam over the cross sectional area of the booster cavity. The length of the booster can be extended to increase the inactivation efficiency of the microorganisms. The effect of the plasma on decontamination should be investigated and compare with UV light. The risk of outbreaks of the Ebola virus and warning that the virus could mutate to become airborne would be desirable (Buckwalter-Poza 2014), further research into the inactivation of viruses can be investigated using the laser based system for effective inactivation of surfaces. Of course the system is relevant for any airborne microorganisms, but the system needs further evaluation to identify its true potential. The impact of the spores on the free-plasma electrodes was evaluated, but greater analysis of the effect of the plasma on spores could be done. It is known that the spores bounce along the electrodes when the plasma is off, but there behaviour is not known with the plasma operating. Perhaps debris of the spores could be detected along the length of the electrode after treatment.

Various aspects of the system can be modelled mathematically. Developing such models of the laser – spore or laser – microorganism interaction would help elucidate the killing mechanism and allow the process to be more easily identified and hence optimised.

Chapter 5: Production of biofuel from microalgae may significantly impact the world's climate and food security, where some microalgae have been eaten for centuries and biolipids can be extracted and converted into biofuel. Third generation biodiesel production from microalgae is a potential replacement for a petroleum fuel, and is essentially carbon neutral. In this study algal cultivation, harvesting and oil extraction were investigated, where these processes form the basis of a microalgal biorefinery. The

effect of environmental conditions on the growth of the microalgal species *Nannochloropsis oculata* and *Chlorella vulgaris* were studied. The air flow speed was effective on the cell growth, as increasing the velocity (i.e circulation) increased the number of cells, probably due to even illumination and sufficient gas exchange. The optimal growth was obtained with salinity concentration of 30 ppt, while the lowest growth was observed with no salt (the control sample). The effect of nutrients on *N. oculata* growth showed that increasing the nutrients increased the cell size but did not increase the cell density. Lipid production should be quantified with nutrient and CO_2 supply.

The flow chamber system can be directly coupled to a photobioreactor allowing instantaneous measurements of the cell size, allowing some prediction to be made over the best time to harvest the microalgae. Lipid detection systems would provide information on optimal growth conditions and harvest times. Future research could also investigate suspended tokens or discs to grow algal biofilms and investigate the various related parameters to optimise algal densities, such as immersion period and other growth parameters.

The centrifuging technique was very effective at harvesting the microalgae, but further investigation between the centrifugal parameters and cell recovery is needed and to identify less expensive, alternative methods. The filtration by vacuum (using filter membranes) and by gravity (using cloth) was investigated. Both methods produced high cell recovery and are inexpensive. The vacuum filtration is preferred due to the relative ease and rapidity of the process, around 2 min, but the cloth filtration was more suitable for higher concentrations of microalgae. Additional evaluation of the flocculation ability of albumin, gelatine and bentonite is needed to obtain faster sedimentation rates at a relatively low cost. Further investigation on the energy required for the microalgal growth and harvesting techniques is essential to identify commercially viable strategies.

Lipid extraction from microalgae was investigated with organic solvents. The results showed that the algal dried biomass contains about 11-19 % oil. The effect of mechanical blending on the cellular disruption and lipid release was investigated. The mechanical solid shear was effective in the rupturing of *N. oculata* wall, and the disruption rate increased with time. However further experiments on the microalgal biomass production and lipid content should be investigated under controlled environmental conditions, with the objective to reduce the required energy for the processes. A system to monitor temperature was partially developed as a step towards this goal. A Fluent model was developed to

assess the temperature distribution of a PBR. Instrumentation to measure the real time growth of microalgae in the 6 tube PBR would allow greater data collection rates and faster experimentation towards optimal growth conditions. Further research on sustainably producing the biofuel from microalgae is needed which will ultimately lead to work on a larger commercial scale, where the concept of microalgal biorefineries can be developed to solve the global problems of energy and food security.

Appendices

Appendix A: Laser marker (Violino2)

i. Detailed description specification

Laser output characteristics	
Emission Wavelength	1064 nm
Pump Source Wavelength	808 nm
Gain Medium	Nd:YV04
Q-Switch Frequency	10 - 200 KHz (programmable)
Pulse Width	10 - 35 ns
Pulse Energy	up to 0.4 mJ
Avg Output Power	10W cw
Transverse Mode	Low order mode
Peak Power	up to 50 kW
Beam Diameter 1/e2 (unfocused)	5 mm
Beam Divergence	< 0.5 mrad
Beam Symmetry	Circular
Beam Polarity	Linear (> 100:1)
Power supply unit	
Dimensions (W x D x H)	7" x 19.75" x 17.5" (18 x 50 x 49 cm)
Weight	57 lbs (26 kg)
Electrical Connection	220 VAC-4A
Electrical Consumption	800 W max
Cooling	Air with thermo-electric
Laser resonator	
Dimensions	f85 mm x 402 mm
Dimensions with Scan 4 Head (W x H x L)	4.8" x 7" x 23"
Weight without Scanning Head	13 lbs (6 kg)
Weight with Scanning Head	22 lbs (10 kg)
Red Diode Beam for Positioning	635 nm Class 3A
Scanning head	
Focal Length	6" (160 mm)
Working Field Size	4.3" x 4.3" (110 x 110 mm)
Frontal Distance	185 mm
Resolution (16 bit)	1.7 μm
Focal Spot Diameter	30-50 μm
Marking Speed (roman-s character .04" high 1.2 mm)	250 Char/Sec

ii. Laser marking operational procedure

1. Start the EHT (extreme high tension) power.
2. Wait until the status screen shows ready.
3. Remove the cap from the lens.
4. On the control box, turn key to start position, and check the red laser beam for alignment showing.
5. Start the computer and select laser editor (Smartists 4) program.
6. Switch on fume extractor.
7. Edit drawing file and test the specimen drawing with the red beam.
8. Alter Z axis until red laser has minimum diameter i.e. the laser be in good focus on the specimen.
9. Shut protective doors.
10. Safety goggles or face mask suitable for the wave length should be worn within sight of laser marking.
11. Switch key to on position in the control box and press enable switch/ indicator.
12. Start program to start the marking.
13. Don't move the specimen when the laser marker is work, the eye damage could result from the right reflections from any surface in the path of the beam.
14. After marking or when the program stopped disable the laser by using the enable switch/ indicator in the control box.
15. Switch the key to off position and switch off the laser marker and the PC.
16. Put the safety label in the area when the laser marking under progressing to warn who enter to the area.

Appendix B: GAM EX50 - KrF excimer laser operational procedure

Operation of this laser requires the presence of at least one trained personnel. At least one of the authorised keyholders should be made aware of the laser being used, experiments to be done and the protocol being implemented. This laser is a Class IV laser; with the beam contained within the protective enclosure it is a Class I laser. Always operate the laser with the correct safety eyewear on and as a Class I laser.

1. Before starting the laser, check that the laser is connected to the UPS (Uninterruptible power supply) which generates a mains isolated voltage and frequency, and check the voltage is set to 230 V at 50 Hz.
2. There are three switches on the laser all of which must be turned on. This includes one turn key switch, one flip/lever switch, and an emergency stop switch (which usually remains on).
3. Switch on the computer (which drives the laser) and open the laser operation program called “EX50”.
4. Once the program starts, it will automatically induce a warm up of the laser which takes around 8 min.
5. Once the laser has warmed up and no errors are observed on the screen, check that the gas pressure and temperature are at the correct operational region of the laser: Gas pressure ~2400 torr, and operational temperature 20 ± 4 °C.
6. Once the parameters are checked and cleared take off the silver end cap of the laser at the output coupler of the laser. Make sure the connecting tube to the enclosure is safely secured.
7. Set the desired parameters of the laser on the computer which include: continuous operation or defined number of pulses (in which case the number of pulses), the PRF and continuous voltage mode (in which case the voltage input) or continuous energy mode (in which case the energy output).
8. Once you have finished using the laser, close the program down by going to “file” and “exit”. The laser will then go into a cool down mode. Leave the laser cooling by itself for 20 min plus/minus 5 min. Then switch off the lever/flip switch and the turn key.

Appendix C: Microscope calibration

Calibration of the objective lens of microscope was done by using a graticule (Pyser-SGI, UK). A graticule is a microscopic slide with divisions (100 μm , 10 divisions). The following procedure was followed for calibrating the graticule for the 10X objective:

- Place a graticule on the microscope stage and focus the objective on it then take the photograph. Export the photographs to NI vision software.
- Select two points on the graticule as shown in Figure C.1

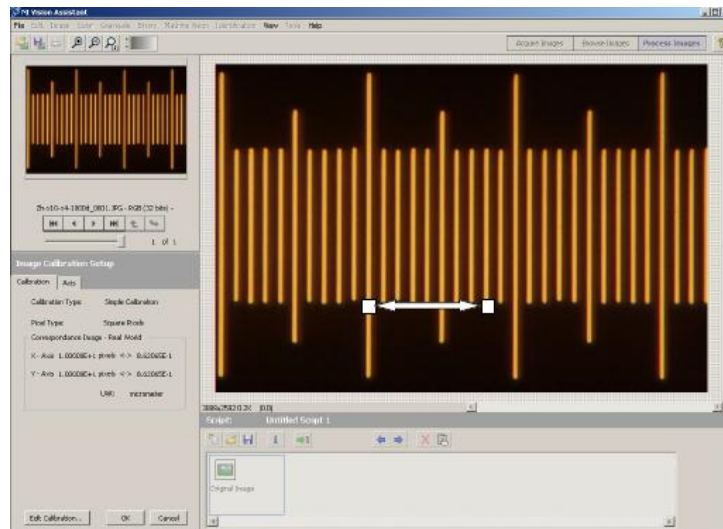


Figure C.1 Calibration the image with graticule

- Calculate the distance between these two lines, for example the distance covered 8 divisions so the full length is $8 \times 10 \mu\text{m} = 80 \mu\text{m}$. Write this value in the calibration scale.
- In the NI vision software, use image calibration unit: simple calibration. The software will convert the value from pixel coordinates to real-world coordinates i.e. μm , and this value represents the calibration factor C_f for the specific objective.
- Repeat the calibration procedure for the other objectives of the microscope.

Appendix D: Prepare Agar plate

- 500 mL LB Agar bottle
 - Petri dishes
 - Hot water bath
 - Bunsen burner
1. Warm the agar bottle after loosening the cap in the hot water bath (around 50°C) until it becomes liquid.
 2. Open the cap and pass the neck of the bottle over a Bunsen flame for sterilizing.
 3. Open the Petri dish lid as little as possible and pour the agar until it just covers the dish bottom ($\sim 15 \text{ mL}$), if there are bubbles on the surface remove these by rapidly passing the Bunsen flame over the plate.
 4. Cover the dish immediately and let the agar solidify at room temperature (about 10-20 min). Store the agar plates upside down under refrigerated conditions.

Appendix E: Microalgal aseptic handling procedure

To avoid contamination of the microalgal cultures (*N. oculata* and *Chlorella vulgaris* in this research), the following protocols were followed:

- Latex gloves were worn and changed frequently during the experiment, and a laboratory coat was worn. The working area was inside the fume cupboard.
- The working surfaces were sprayed with ethanol (70% ethanol and 30% distilled water) and wiped with a clean paper towel.
- Disposable microscopic slides and pipette tips were used.
- Bunsen burners were used to flame sterilize equipment during the inoculation process i.e. the equipment (outer surfaces of flasks, loop and forceps) was flamed before and after its use.
- All the equipments (PBR, glassware, tubing with valves etc) used in the microalgae growth experiments were sterilized in trigene disinfectant (Trigene, Medichem International Ltd, UK) with 1 part to 200 parts of water and wiped with a sterile brush, and then rinsed with distilled water. In some cases for larger volumes, washes were done with running tap water, where contamination was less of an issue and repeated several times.
- A Whatman polycap capsule air filter was used to filter the air supply fed into the PBR. Hands were washed before and after the experiments with the antibacterial soap (Kimcare general 6331, Kimberly-Clark Ltd, UK).

Appendix F: Serial dilution protocol of *Bacillus atrophaeus*

The serial dilution of microorganisms and spreading the diluted microorganisms on the nutrient plate is an ideal and the simplest method for counting live microorganisms. The number of microorganisms is very high in the original sample, so when sampling or spreading the samples directly without dilution the colonies will grow next to or on top of each other and they are too numerous to count (TNTC). The microorganisms should be reduced (diluted) to allow accurate enumeration.

The diluted protocol was done by preparing a number of sterile universal flasks filled with 9 mL of sterile distilled water. Then 1 mL of the original sample of *B. atrophaeus* spores was withdrawn using a pipette and added to 9 mL of the first flask, this would produce a 10-fold dilution (10^{-1}). The new culture solution was mixed to obtain an even mixture, then 1 mL of this culture was withdrawn and put into another universal flask containing 9 mL of

sterile distilled water, this would produce a 100-fold dilution (10^{-2}), this was repeated until the required dilution was reached i.e. a countable number of microorganisms colonies is obtained in this case. The steps of the dilution protocol are shown in Figure F.1. It should be noted that the spore samples were provided by Dr Bill Whyte and were kept under refrigerated conditions to maintain them as spores.

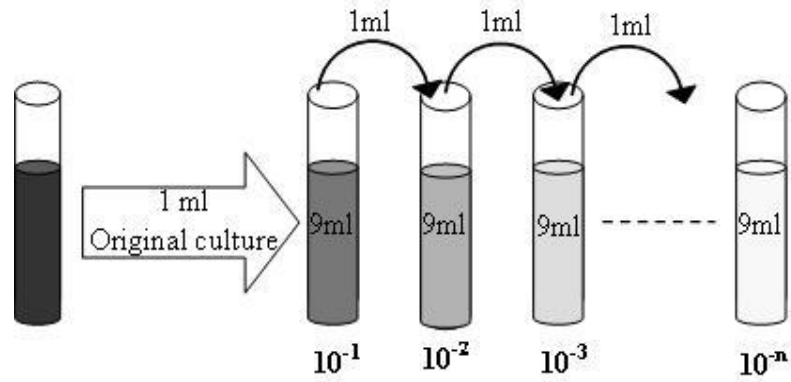


Figure F.1 Protocol of serial dilutions

References

- Alexander, C., H. S. Andersson, L. I. Andersson, R. J. Ansell, N. Kirsch, I. A. Nicholls, J. O'Mahony and M. J. Whitcombe** (2006). "Molecular imprinting science and technology: a survey of the literature for the years up to and including 2003." *Journal of Molecular Recognition* **19**(2): 106-180.
- Alfajara, C. G., K. Nakano, N. Nomura, T. Igarashi and M. Matsumura** (2002). "Operating and scale-up factors for the electrolytic removal of algae from eutrophied lakewater." *Journal of Chemical Technology & Biotechnology* **77**(8): 871-876.
- Amrania, H., A. P. McCrow, M. R. Matthews, S. G. Kazarian, M. K. Kuimova and C. C. Phillips** (2011). "Ultrafast infrared chemical imaging of live cells." *Chemical Science* **2**(1): 107-111.
- Anders, M. I. Ralf and C. David** (2007). "Micro- and macro-algae: utility for industrial applications." *cpl press* **1**.
- Andersen, R. A.** (2005). Algal culturing techniques: 5. Sterilization and sterile technique. Amsterdam, Elsevier, Academic Press
- Babalola, O.** (2003). "Molecular techniques: An overview of methods for the detection of bacteria." *African Journal of Biotechnology* **2**(12): 710-713.
- Baker, N.** (2008). "Chlorophyll fluorescence: a probe of photosynthesis in vivo." *Annu. Rev. Plant Biol.* **59**: 89-113.
- Baker, N. R. and E. Rosenqvist** (2004). "Applications of chlorophyll fluorescence can improve crop production strategies: an examination of future possibilities." *Journal of Experimental Botany* **55**(403): 1607-1621.
- Bancroft, K., E. T. Nelson and G. W. Childers** (1989). "Comparison of the presence-absence and membrane filter techniques for coliform detection in small, nonchlorinated water distribution systems." *Applied and environmental microbiology* **55**(2): 507-510.
- Bauman, R. W., E. Machunis-Masuoka and J. E. Montgomery** (2012). Microbiology: With Diseases by Body System, Benjamin Cummings.
- Bhave, R., T. Kuritz, L. Powell and D. Adcock** (2012). "Membrane-Based Energy Efficient Dewatering of Microalgae in Biofuels Production and Recovery of Value Added Co-Products." *Environmental Science & Technology* **46**(10): 5599-5606.
- Bougaran, G., C. Rouxel, N. Dubois, R. Kaas, S. Grouas, E. Lukomska, J.-R. Le Coz and J.-P. Cadoret** (2012). "Enhancement of neutral lipid productivity in the microalga *Isochrysis affinis Galbana* (T-Iso) by a mutation-selection procedure." *Biotechnology and Bioengineering* **109**(11): 2737-2745.
- Bowe, G.** (2007). An Overview of Counting Methods of Algae. Water Quality Measurements Series, John Wiley & Sons, Ltd.: 71-82.

Brennan, L. and P. Owende (2010). "Biofuels from microalgae_A review of technologies for production, processing, and extractions of biofuels and co-products." *Renewable and Sustainable Energy Reviews* **14**(2): 557-577.

Brown, D. M., E. Thrush and M. E. Thomas (2011). "Chamber lidar measurements of biological aerosols." *Appl. Opt.* **50**(5): 717-724.

Brown, T. A. (2000). *Essential Molecular Biology: A Practical Approach*, Oxford University Press Inc. 2nd edition.

Buckwalter-Poza, R. (2014). "The Scariest Virus: Ebola Is Back, and It's Worse Than Ever. Pacific Standard." from <http://www.psmag.com/navigation/health-and-behavior/scariest-virus-ebola-back-worse-ever-87348/>.

Buhr, T. L., D. C. McPherson and B. W. Gutting (2008). "Analysis of broth-cultured *Bacillus atrophaeus* and *Bacillus cereus* spores." *Journal of Applied Microbiology* **105**(5): 1604-1613.

Busscher, H. J., J. Noordmans, J. Meinders and H. C. van der Mei (1991). "Analysis of the spatial arrangement of microorganisms adhering to solid surfaces - Methods of presenting results." *Biofouling* **4**(1-3): 71-79.

Cardoso, C. L., C. B. Muraro, V. L. Siqueira and M. Guilhermetti (1998). "Simplified technique for detection of significant bacteriuria by microscopic examination of urine." *J Clin Microbiol* **36**(3): 820-823.

Carrera, M., R. O. Zandomeni and J. L. Sagripanti (2008). "Wet and dry density of *Bacillus anthracis* and other *Bacillus* species." *Journal of Applied Microbiology* **105**(1): 68-77.

Carvalho, A. P., L. A. Meireles and F. X. Malcata (2006). "Microalgal Reactors: A Review of Enclosed System Designs and Performances." *Biotechnology Progress* **22**(6): 1490-1506.

Cavalié, T., H. Feuchtgruber, E. Lellouch, M. de Val-Borro, C. Jarchow, R. Moreno, P. Hartogh, G. Orton, T. K. Greathouse, F. Billebaud, M. Dobrijevic, L. M. Lara, A. Gonzalez and H. Sagawa (2013). "Spatial distribution of water in the stratosphere of Jupiter from Herschel HIFI and PACS observations." *A&A* **553**: A21.

CDC (2013). "Estimating Foodborne Illness: An Overview." Centers for Disease Control and Prevention. USA. from <http://www.cdc.gov/foodborneburden/estimates-overview.html>.

Charvalos, E. and A. Karoutis (2001). "Antimicrobial activity of argon fluoride (ArF) excimer laser on gram-negative bacteria." *Applied Microbiology and Biotechnology* **56**(1): 243-248.

Chen, C.-Y., K.-L. Yeh, R. Aisyah, D.-J. Lee and J.-S. Chang (2010). "Cultivation, photobioreactor design and harvesting of microalgae for biodiesel production: A critical review." *Bioresource Technology* **102**(1): 71-81.

- Chen, M.-F., W.-T. Hsiao, W.-L. Huang, C.-W. Hu and Y.-P. Chen** (2009). "Laser coding on the eggshell using pulsed-laser marking system." *Journal of Materials Processing Technology* **209**(2): 737-744.
- Chisti, Y.** (2007). "Biodiesel from microalgae." *Biotechnology Advances* **25**(3): 294-306.
- Choi, S. K., J. Y. Lee, D. Y. Kwon and K. J. Cho** (2006). "Settling characteristics of problem algae in the water treatment process." *Water science and technology : a journal of the International Association on Water Pollution Research* **53**(7): 113-119.
- Clavin, W. and J. D. Harrington** (2013). "Planck Mission Brings Universe Into Sharp Focus." Retrieved 2013, from <http://www.jpl.nasa.gov/news/news.php?release=2013-109&rn=news.xml&rst=3739#1>.
- Cohen, T., J. Starosvetsky, U. Cheruti and R. Armon** (2010). "Whole Cell Imprinting in Sol-Gel Thin Films for Bacterial Recognition in Liquids: Macromolecular Fingerprinting." *International Journal of Molecular Sciences* **11**(4): 1236-1252.
- Cole, J. A. and M. H. Tinker** (1996). "Laser speckle spectroscopy—a new method for using small swimming organisms as biomonitors." *Bioimaging* **4**(4): 243-253.
- Connelly, J., Schultz, M. & Flack, K.** (2006). "Velocity-defect scaling for turbulent boundary layers with a range of relative roughness." *Experiments in Fluids* **40**(2): 188-195.
- Coward, T., J. G. M. Lee and G. S. Caldwell** (2013). "Development of a foam flotation system for harvesting microalgae biomass." *Algal Research* **2**(2): 135-144.
- Cracolici, M. and T. Uberti** (2009). "Geographical distribution of crime in Italian provinces: a spatial econometric analysis." *Jahrbuch fur Regionalwissenschaft* **29**(1): 1-28.
- Craythorn, J. M., A. G. Barbour, J. M. Matsen, M. R. Britt and R. A. Garibaldi** (1980). "Membrane filter contact technique for bacteriological sampling of moist surfaces." *Journal of clinical microbiology* **12**(2): 250-255.
- Csordas, A. and J.-K. Wang** (2004). "An integrated photobioreactor and foam fractionation unit for the growth and harvest of *Chaetoceros* spp. in open systems." *Aquacultural Engineering* **30**(1-2): 15-30.
- Dahorte, N. B. and S. P. Harimkar** (2008). *Laser fabrication and machining of materials*, Springer-Verlag.
- Danielli, A., A. Arie, N. Porat and M. Ehrlich** (2008). "Detection of fluorescent-labeled probes at subpicomolar concentrations by magnetic modulation." *Opt. Express* **16**(23): 19253-19259.
- Danquah, M. K., L. Ang, N. Uduman, N. Moheimani and G. M. Forde** (2009). "Dewatering of microalgal culture for biodiesel production: exploring polymer flocculation and tangential flow filtration." *Journal of Chemical Technology & Biotechnology* **84**(7): 1078-1083.
- Das, P., S. S. Aziz and J. P. Obbard** (2011). "Two phase microalgae growth in the open system for enhanced lipid productivity." *Renewable Energy* **36**(9): 2524-2528.

Dassey, A. J. and C. S. Theegala (2013). "Harvesting economics and strategies using centrifugation for cost effective separation of microalgae cells for biodiesel applications." *Bioresource Technology* **128**(0): 241-245.

Davidson, M. W. and M. Abramowitz (2011). "Optical microscopy. Last accessed August 2014." from <http://www.olympusmicro.com/primer/opticalmicroscopy.html>.

Davitt, K. M. (2006). Ultraviolet Light Emitting Diodes and Bio-aerosol Sensing, Brown University. **Ph.D thesis**.

De la Jara, A., H. c. Mendoza, A. Martel, C. Molina, L. Nordström, V. De la Rosa and R. Daaz (2003). "Flow cytometric determination of lipid content in a marine dinoflagellate, *Cryptocodinium cohnii*." *Journal of Applied Phycology* **15**(5): 433-438.

De Oliveira, R. R. L., D. A. C. Albuquerque, T. G. S. Cruz, F. M. Yamaji and F. L. Leite (2012). Measurement of the Nanoscale Roughness by Atomic Force Microscopy: Basic Principles and Applications, InTech Europe. Federal University of Sao Carlos, Campus Sorocaba. Brazil.

Dehbi, A. (2008). "A CFD model for particle dispersion in turbulent boundary layer flows." *Nuclear Engineering and Design* **238**(3): 707-715.

Demirbas, A. and M. F. Demirbas (2010). Algae Energy: Algae as a New Source of Biodiesel, Springer.

Desai, M. J. and D. W. Armstrong (2003). "Separation, identification, and characterization of microorganisms by capillary electrophoresis." *Microbiology and molecular biology reviews : MMBR* **67**(1): 38-51, table of contents.

Dickert, F., P. Lieberzeit and O. Hayden (2003). "Sensor strategies for microorganism detection - from physical principles to imprinting procedures." *Analytical and Bioanalytical Chemistry* **377**(3): 540-549.

Donard, O. F. X., M. Lamotte, C. Belin and M. Ewald (1989). "High-sensitivity fluorescence spectroscopy of mediterranean waters using a conventional or a pulsed laser excitation source." *Marine Chemistry* **27**(12): 117-136.

Doucha, J., F. e. Straka and K. LÁvanskÁ (2005). "Utilization of flue gas for cultivation of microalgae *Chlorella* sp.) in an outdoor open thin-layer photobioreactor." *Journal of Applied Phycology* **17**(5): 403-412.

Duong, V. T., Y. Li, E. Nowak and P. M. Schenk (2012). "Microalgae Isolation and Selection for Prospective Biodiesel Production." *Energies* **5**(6): 1835-1849.

Dusser, B., Z. Sagan, D. Bruneel, M. Jourlin and E. Audouard (2007). "Laser deep marking of metals and polymers: potential interest for information coding." *Journal of Physics: Conference Series* **77**(1): 012002.

Feng, W., T. Wee Beng, Z. Yong, F. Xianping and W. Minquan (2006). "Luminescent nanomaterials for biological labelling." *Nanotechnology* **17**(1): R1.

Fernandes, D. R. P., N. S. Yokoya and Y. Yoneshigue-Valentin (2011). "Protocol for seaweed decontamination to isolate unialgal cultures." *Brazilian Journal of Pharmacognosy* **21**: 313-316.

Fernandez-Jaramillo, A. A., C. Duarte-Galvan, L. M. Contreras-Medina, I. Torres-Pacheco, R. d. J. Romero-Troncoso, R. G. Guevara-Gonzalez and J. R. Millan-Almaraz (2012). "Instrumentation in Developing Chlorophyll Fluorescence Biosensing: A Review." *Sensors* **12**(9): 11853-11869.

Flint, S. H., J. D. Brooks and P. J. Bremer (2000). "Properties of the stainless steel substrate, influencing the adhesion of thermo-resistant *streptococci*." *Journal of Food Engineering* **43**(4): 235-242.

Fluent_Guide (2009). FLUENT 6.3 User's Guide, Fluent Inc. UK.

Folwaczny, M., T. Liesenhoff, N. Lehn and H.-H. Horch (1998). "Bactericidal action of 308 nm excimer-laser radiation: An in vitro investigation." *Journal of endodontics* **24**(12): 781-785.

Foss-Smith, P. and I. Watson (2008). Decontamination Apparatus and Method. Fluid decontamination apparatus and method of fluid decontamination. Nviro Cleantech (Cayman Islands) Limited. University Court of The University of Glasgow. United Kingdom. GB2465173A.

Foss-Smith, P. and I. Watson (2008). Electrode, Decontamination Apparatus and Method. Roughened electrode for decontamination processes. Nviro Cleantech (Cayman Islands) Limited. University Court of The University of Glasgow. United Kingdom. GB2465174A.

Fuster-Valls, N., M. HernÁindez-Herrero, M. MarÁn-de-Mateo and J. J. RodrÁguez-Jerez (2008). "Effect of different environmental conditions on the bacteria survival on stainless steel surfaces." *Food Control* **19**(3): 308-314.

Goetz, A. and N. Tsuneishi (1951). "Application of the molecular filter membrane to the bacteriological analysis of water." *American Water Works Association* **43**(12): 943-984.

Gouveia, L. (2011). Microalgal biomass harvesting. Microalgae as a Feedstock for Biofuels, SpringerBriefs in Microbiology. **19**: 33.

Gowen, A. A., C. P. O'Donnell, P. J. Cullen and S. E. J. Bell (2008). "Recent applications of Chemical Imaging to pharmaceutical process monitoring and quality control." *European Journal of Pharmaceutics and Biopharmaceutics* **69**(1): 10-22.

Griffiths, M. and S. Harrison (2009). "Lipid productivity as a key characteristic for choosing algal species for biodiesel production." *Journal of Applied Phycology* **21**(5): 493-507.

Grill, A. (2013). "Using Big Data to fight crime and predict what products consumers might purchase in the future. London Calling Social Business." from <http://londoncalling.co/2013/04/using-big-data-to-fight-crime-and-predict-what-products-consumers-might-purchase-in-the-future/>.

Gu, B. (2004). Latest development in chip scale package laser marking and micro laser marking. Electronics Manufacturing Technology Symposium, 2004. IEEE/CPMT/SEMI 29th International.

Gu, B. (2006). Review - 40 years of laser-marking - industrial applications, SPIE.

Habash, M. and R. Johns (2009). "Comparison study of membrane filtration direct count and an automated coliform and Escherichia coli detection system for on-site water quality testing." *J Microbiol Methods* **79**(1): 3-3.

Hankamer, B., F. Lehr, J. Rupprecht, J. H. Mussnug, C. Posten and O. Kruse (2007). "Photosynthetic biomass and H₂ production by green algae: from bioengineering to bioreactor scale-up." *Physiologia Plantarum* **131**(1): 10-21.

Hansatech (2007). Operations manual. Handy PEA. Hansatech Instruments Ltd. England.

Harith, Z., F. Yusoff, M. Mohamed, M. Shariff, M. Din and A. Ariff (2009). "Effect of different flocculants on the flocculation performance of flocculation performance of microalgae, *Chaetoceros calcitrans*, cells." *African Journal of Biotechnology* **8**(21): 5971-5978.

Heimbuch, B. K., K. R. Kinney and R. K. Nichols (2009). "The dry aerosol deposition device (DADD): an instrument for depositing microbial aerosols onto surfaces." *Journal of Microbiological Methods* **78**: 255-259.

Hilbert, L. R., D. Bagge-Ravn, J. Kold and L. Gram (2003). "Influence of surface roughness of stainless steel on microbial adhesion and corrosion resistance." *International Biodeterioration & Biodegradation* **52**(3): 175-185.

Ho, J. (2002). "Future of biological aerosol detection." *Analytica Chimica Acta* **457**(1): 125-148.

Hu, Q., M. Sommerfeld, E. Jarvis, M. Ghirardi, M. Posewitz, M. Seibert and A. Darzins (2008). "Microalgal triacylglycerols as feedstocks for biofuel production: perspectives and advances." *The Plant Journal* **54**(4): 621-639.

Ibidi (2010). Catalog. μ -Slide I Luer. Germany.

Issarapayup, K., S. Powtongsook and P. Pavasant (2009). "Flat panel airlift photobioreactors for cultivation of vegetative cells of microalga *Haematococcus pluvialis*." *Journal of Biotechnology* **142**(3-4): 227-232.

Ivnitski, D., I. Abdel-Hamid, P. Atanasov and E. Wilkins (1999). "Biosensors for detection of pathogenic bacteria." *Biosensors and Bioelectronics* **14**(7): 599-624.

Jannasch, H. W. (1958). "Studies on planktonic bacteria by means of a direct membrane filter method." *Journal of general microbiology* **18**(3): 609-620.

Janssen, M. (2002). Cultivation of microalgae: effect of light/dark cycles on biomass yield, Ponsen & Looijen BV, Wageningen. The Netherlands.

Jeon, Y.-C., C.-W. Cho and Y.-S. Yun (2005). "Measurement of microalgal photosynthetic activity depending on light intensity and quality." *Biochemical Engineering Journal* **27**(2): 127-131.

Jesus, B., R. G. Perkins, C. R. Mendes, V. Brotas and D. M. Paterson (2006). "Chlorophyll fluorescence as a proxy for microphytobenthic biomass: alternatives to the current methodology." *Marine Biology* **150**(1): 17-28.

Kamps, B. and C. Hoffmann (2013). SARS reference. Online book. www.SARSreference.com.

Karube, I., T. Takeuchi and D. J. Barnes (1992). Biotechnological reduction of CO₂ emissions. *Modern Biochemical Engineering*, Springer Berlin Heidelberg. **46**: 63-79.

Katsuda, T., A. Lababpour, K. Shimahara and S. Katoh (2004). "Astaxanthin production by *Haematococcus pluvialis* under illumination with LEDs." *Enzyme and Microbial Technology* **35**(1): 81-86.

Keller, M. D., W. K. Bellows and R. R. L. Guillard (1988). "Microwave treatment for sterilization of phytoplankton culture media." *Journal of Experimental Marine Biology and Ecology* **117**(3): 279-283.

Khalida, Z., A. Youcef, B. Zitouni, Z. Mohammed and P. Radovan (2012). "Use of chlorophyll fluorescence to evaluate the effect of chromium on activity photosystem ii at the alga *scenedesmus obliquus*." *International Journal of Research & Reviews in Applied Sciences* **12**(2): 304.

Kitchens, C. (2013). "Identifying Changes In The Spatial Distribution Of Crime: Evidence From A Referee Experiment In The National Football League " *Economic Inquiry*. Blackwell Publishing Ltd doi: **10.1111/ecin.12016**.

Kochevar, I. E. (1992). "Biological effects of excimer laser radiation." *Proceedings of the IEEE* **80**(6): 833-837.

Koibuchi, H., S. Hayashi, K. Kotani, Y. Fujii, K. Konno, Y. Hirai and N. Taniguchi (2009). "Comparison of methods for evaluating bacterial contamination of ultrasound probes." *Journal of Medical Ultrasonics* **36**(4): 187-192.

Kuchenmuller, T., S. Hird, C. Stein, P. Kramarz, A. Nanda and A. H. Havelaar (2009). "Estimating the global burden of foodborne diseases--a collaborative effort." *Euro surveillance : bulletin europeen sur les maladies transmissibles = European communicable disease bulletin* **14**(18).

Kurilcik, N., P. Vitta, A. Žukauskas, R. Gaska, A. Ramanavičius, A. Kaušaitė and S. Juršėnas (2006). "Fluorescence detection of biological objects with ultraviolet and visible light-emitting diodes." *Optica Applicata* **36**(2-3).

Laakso, P., H. Pantsar and V. Mehtälä (2008). Marking decorative features to stainless steel with fiber laser, The International Laser Users Council (ILUC). Advanced Laser Applications Conference and Exposition, Oct 1-3, 2008, Minneapolis, MN, USA, 29-36.

Lakowicz, J. R. (2009). Principles of fluorescence spectroscopy, Springer London, Limited.

- Laurinavichene, T. V., A. S. Fedorov, M. L. Ghirardi, M. Seibert and A. A. Tsygankov** (2006). "Demonstration of sustained hydrogen photoproduction by immobilized, sulfur-deprived *Chlamydomonas reinhardtii* cells." *International Journal of Hydrogen Energy* **31**(5): 659-667.
- Leamy, H. J.** (1982). "Charge collection scanning electron microscopy." *Journal of Applied Physics* **53**(6): R51-R80.
- Lee, B.-S., Y.-W. Lin, J.-S. Chia, T.-T. Hsieh, M.-H. Chen, C.-P. Lin and W.-H. Lan** (2006). "Bactericidal effects of diode laser on *Streptococcus mutans* after irradiation through different thickness of dentin." *Lasers in Surgery and Medicine* **38**(1): 62-69.
- Lee, J.-Y., C. Yoo, S.-Y. Jun, C.-Y. Ahn and H.-M. Oh** (2010). "Comparison of several methods for effective lipid extraction from microalgae." *Bioresource Technology* **101**(1, Supplement): S75-S77.
- Leonard, P., S. Hearty, J. Brennan, L. Dunne, J. Quinn, T. Chakraborty and R. OKennedy** (2003). "Advances in biosensors for detection of pathogens in food and water." *Enzyme and Microbial Technology* **32**(1): 3-13.
- Li, J., K. Hirota, H. Yumoto, T. Matsuo, Y. Miyake and T. Ichikawa** (2010). "Enhanced germicidal effects of pulsed UV-LED irradiation on biofilms." *Journal of Applied Microbiology* **109**(6): 2183-2190.
- Li, Q., P. K. Dasgupta, H. Temkin, M. H. Crawford, A. J. Fischer, A. A. Allerman, K. H. A. Bogart and S. R. Lee** (2004). "Mid-ultraviolet Light-Emitting Diode Detects Dipicolinic Acid." *Applied Spectroscopy* **58**(11): 1360-1363.
- Lindh, W. Q., M. S. Pooler, C. D. Tamparo and B. M. Dahl** (2010). *Delmar's Comprehensive Medical Assisting: Administrative and Clinical Competencies*, Delmar, Cengage learning, USA.
- Lippemeier, S., R. Hintze, K. Vanselow, P. Hartig and F. Colijn** (2001). "In-line recording of PAM fluorescence of phytoplankton cultures as a new tool for studying effects of fluctuating nutrient supply on photosynthesis." *European Journal of Phycology* **36**(1): 89-100.
- Lisita, A., E. E. Sano and L. Durieux** (2013). "Identifying potential areas of *Cannabis sativa* plantations using object-based image analysis of SPOT-5 satellite data." *International Journal of Remote Sensing* **34**(15): 5409-5428.
- Liu, H.** (2008). *Pathogenic bacterial sensors based on carbohydrates as sensing elements. Principles of Bacterial Detection: Biosensors, Recognition Receptors and Microsystems*. Springer Science+Business and Media, LLC.
- Lou, M. S., J. C. Chen and C. M. Li** (1999). "Surface roughness prediction technique for CNC end-milling, ." *Journal of Industrial Technology* **15**(1).
- Madigan, M., J. Martinko and J. Parker** (2011). *Brock Biology of Microorganisms*, Pearson Education; 13 edition. USA.

- Malik, M.** (2013). "Cosmology with the Cosmic Microwave Background." *International Journal of Astronomy* **2**(2): 17-22.
- Masojidek, J., A. Vonshak and G. Torzillo** (2010). Chlorophyll Fluorescence Applications in Microalgal Mass Cultures. Chlorophyll a Fluorescence in Aquatic Sciences: Methods and Applications, Springer Netherlands. **4**: 277-292.
- Mathew Mate, C.** (2008). Tribology on the small scale: a bottom up approach to friction, lubrication, and wear. Mesoscopic Physics and Nanotechnology, Oxford University Press.
- Mayer-Schonberger, V. and K. Cukier** (2013). Big Data: A Revolution That Will Transform How We Live, Work, and Think, Houghton Mifflin Harcourt.
- McAllister, E. W., L. C. Carey, P. G. Brady, R. Heller and S. G. Kovacs** (1993). "The role of polymeric surface smoothness of biliary stents in bacterial adherence, biofilm deposition, and stent occlusion." *Gastrointestinal Endoscopy* **39**(3): 422-425.
- McMillan, J. R., I. A. Watson, M. Ali and W. Jaafar** (2013). "Evaluation and comparison of algal cell disruption methods: Microwave, waterbath, blender, ultrasonic and laser treatment." *Applied Energy* **103**(0): 128-134.
- Melo, O. T. and C. R. Phillips** (1974). "Aerosol-size spectra by means of membrane filters. Theoretical study." *Environmental Science & Technology* **8**(1): 67-71.
- Mendoza Guzman, H., A. Jara Valido, L. Carmona Duarte and K. Freijanes Presmanes** (2011). "Analysis of interspecific variation in relative fatty acid composition: use of flow cytometry to estimate unsaturation index and relative polyunsaturated fatty acid content in microalgae." *Journal of Applied Phycology* **23**(1): 7-15.
- Meral, G., F. Tasar, S. Kocagöz and C. Sener** (2003). "Factors affecting the antibacterial effects of Nd:YAG laser in vivo." *Lasers in Surgery and Medicine* **32**(3): 197-202.
- Mertz, J.** (2010). Introduction to Optical Microscopy. Colorado, Roberts and Company Publishers.
- Milledge, J.** (2011). "Commercial application of microalgae other than as biofuels: a brief review." *Reviews in Environmental Science and Biotechnology* **10**(1): 31-41.
- Mine, T.** (2010). Laser and Plasma Air Decontamination. Department of Mechanical Engineering., University of Glasgow, Glasgow. **PhD. Thesis.**
- Miura, k. and S. Yamamoto** (2013). "Histological imaging from speed-of-sound through tissues by scanning acoustic microscopy (SAM)." Protocol Exchange. from <http://dx.doi.org/10.1038/protex.2013.040>.
- Moelsund, T. B.** (2012). Introduction to Video and Image Processing: Building Real Systems and Applications, Springer.
- Molina Grima, E., E. H. Belarbi, F. G. Aciñ Fernã;ndez, A. Robles Medina and Y. Chisti** (2003). "Recovery of microalgal biomass and metabolites: process options and economics." *Biotechnology Advances* **20**(7-8): 491-515.

- Muller-Feuga, A.** (2000). "The role of microalgae in aquaculture: situation and trends." *Journal of Applied Phycology* **12**(3/5): 527-534.
- Murphy, K. R., K. D. Butler, R. G. M. Spencer, C. A. Stedmon, J. R. Boehme and G. R. Aiken** (2010). "Measurement of Dissolved Organic Matter Fluorescence in Aquatic Environments: An Interlaboratory Comparison." *Environmental Science & Technology* **44**(24): 9405-9412.
- Nascimento, I., S. Marques, I. Cabanelas, S. Pereira, J. Druzian, C. de Souza, D. Vich, G. de Carvalho and M. Nascimento** (2013). "Screening Microalgae Strains for Biodiesel Production: Lipid Productivity and Estimation of Fuel Quality Based on Fatty Acids Profiles as Selective Criteria." *BioEnergy Research* **6**(1): 1-13.
- Ng, T. W. and S. C. Yeo** (2001). "Aesthetic laser marking assessment using luminance ratios." *Optics and Lasers in Engineering* **35**(3): 177-186.
- Nigam, P. S. and A. Singh** (2011). "Production of liquid biofuels from renewable resources." *Progress in Energy and Combustion Science* **37**(1): 52-68.
- Noelia Isabel, S., M. Maribel, A. Cristina, B. Javier, C. González-Navarro and V. Raquel** (2013). "Optimization of denaturing high performance liquid chromatography technique for rapid detection and identification of acetic acid bacteria of interest in vinegar production." *Acetic Acid Bacteria* **2**(s1:e5).
- Novaes Jr, A., S. d. S. Sérgio Luis, M. d. B. Raquel Rezende, Y. P. Karina Kimiko, I. Giovanna and P. Adriano** (2010). "Influence of Implant Surfaces on Osseointegration." *Braz Dent J* **21**(6): 471-481.
- Obata, M., T. Toda and S. Taguchi** (2009). "Using chlorophyll fluorescence to monitor yields of microalgal production." *Journal of Applied Phycology* **21**(3): 315-319.
- Olympus** (2010). Laboratory Biological Microscopes. Hamburg, Germany
- Osaki, M. and A. Kanagawa** (1990). "Performance of High Efficiency Particulate Air Filters." *Journal of Nuclear Science and Technology* **27**(9): 875-882.
- Papageorgiou, G. and Govindjee** (2004). "Chlorophyll Fluorescence: A Signature of Photosynthesis. Kluwer Academic Publishers. Printed in The Netherlands.": 1-42.
- Parr** (instruction manual 2013). Instrument Company publication 1341. (2009). Oxygen bomb calorimeter 1341. Operating Instruction Manual 204M. USA.
- Pena, A., Z. Wang, D. Whitehead, R. Lloyd and L. Li** (2010). "Laser generation of nano-bumps below 2 nm height on silicon for debris-free marking/patterning." *Journal of Physics D: Applied Physics* **43**(11): 115302.
- Perner, P., O. Salvetti, P. Coltelli, M. Evangelisti, V. Evangelista and P. Gualtieri** (2007). Real-Time Measurement and Analysis of Translational and Rotational Speeds of Moving Objects in Microscope Fields. Advances in Mass Data Analysis of Signals and Images in Medicine, Biotechnology and Chemistry, Springer Berlin Heidelberg. **4826**: 128-135.

- Peterkin, P. I. and A. N. Sharpe** (1980). "Membrane filtration of dairy products for microbiological analysis." *Applied and Environmental Microbiology* **39**(6): 1138-1143.
- Petrusevski, B., G. Bolier, A. N. Van Breemen and G. J. Alaerts** (1995). "Tangential flow filtration: A method to concentrate freshwater algae." *Water Research* **29**(5): 1419-1424.
- Photon_Control** (2009). Photon Control_SPM002 Compact Spectrometer. User guide. Canada.
- Powers, L. S. and C. R. Lloyd** (2004). Method and apparatus for detecting the presence of microbes and determining their physiological status. US, Microbiosystems, Limited Partnership. US **2003/0138875 A1**: 1-6.
- Pratt, W. K.** (2007). Digital Image Processing: PIKS Scientific Inside, John Wiley & Sons.
- Prestel, H., A. Gahr and R. Niessner** (2000). "Detection of heavy metals in water by fluorescence spectroscopy: On the way to a suitable sensor system." *Fresenius' Journal of Analytical Chemistry* **368**(2-3): 182-191.
- Prochazkova, G., I. Safarik and T. Branyik** (2013). "Harvesting microalgae with microwave synthesized magnetic microparticles." *Bioresource Technology* **130**(0): 472-477.
- Pulz, O. and W. Gross** (2004). "Valuable products from biotechnology of microalgae." *Applied Microbiology and Biotechnology* **65**(6): 635-648.
- Purchas, D.** (1996). Handbook of Filter Media, Elsevier Science, 1st edition. UK.
- Qi, J., K. L. Wang and Y. M. Zhu** (2003). "A study on the laser marking process of stainless steel." *Journal of Materials Processing Technology* **139**(1-3): 273-276.
- Raahave, D.** (1975). "EXPERIMENTAL EVALUATION OF THE VELVET PAD RINSE TECHNIQUE AS A MICROBIOLOGICAL SAMPLING METHOD." *Acta Pathologica Microbiologica Scandinavica Section B Microbiology* **83B**(5): 416-424.
- Ramanujam, N.** (2006). Fluorescence Spectroscopy In Vivo. Encyclopedia of Analytical Chemistry, John Wiley & Sons, Ltd.
- Rattray, N. J. W., W. A. Zalloum, D. Mansell, J. Latimer, C. H. Schwalbe, A. J. Blake, E. V. Bichenkova and S. Freeman** (2012). "Fluorescent probe for detection of bacteria: conformational trigger upon bacterial reduction of an azo bridge." *Chemical Communications* **48**(51): 6393-6395.
- Rehse, S. J., H. Salimnia and A. W. Miziolek** (2012). "Laser-induced breakdown spectroscopy (LIBS): an overview of recent progress and future potential for biomedical applications." *Journal of Medical Engineering & Technology* **36**(2): 77-89.
- Renaud, S. and D. Parry** (1994). "Microalgae for use in tropical aquaculture II: Effect of salinity on growth, gross chemical composition and fatty acid composition of three species of marine microalgae." *Journal of Applied Phycology* **6**(3): 347-356.

- Reyes-Prieto, A. and D. Bhattacharya** (2007). "Phylogeny of Calvin cycle enzymes supports Plantae monophyly." *Molecular Phylogenetics and Evolution* **45**(1): 384-391.
- Richards-Kortum, R. and E. Sevick-Muraca** (1996). "QUANTITATIVE OPTICAL SPECTROSCOPY FOR TISSUE DIAGNOSIS." *Annual Review of Physical Chemistry* **47**(1): 555-606.
- Rideout, D.** (2013). "Rough Talk: Understanding Surface Metrology Tools. Quality Digest Magazine." from <http://www.qualitydigest.com/inside/twitter-ed/rough-talk-understanding-surface-metrology-tools.html>.
- Rullgard, H., L. G. Öfverstedt, S. Masich, B. Daneholt and O. Öktem** (2011). "Simulation of transmission electron microscope images of biological specimens." *Journal of Microscopy* **243**(3): 234-256.
- Sakuraoka, A. and L. Madsen** (2001). "Removal of Heat-Resistant Bacterial Spores by Filters: Implications for Filter Use in Soft Drink Production. ." *Scientific & Technical Report. USA*.
- Samadder, S. R., P. Ziegler, T. M. Murphy and N. M. Holden** (2010). "Spatial Distribution of Risk Factors for Cryptosporidium Spp. Transport in an Irish Catchment." *Water Environment Research* **82**(8): 750-758.
- Sarasanandarajah, S.** (2007). Multiwavelength Fluorescence Studies of Bacillus Bacterial Spores: A Thesis Submitted in Partial Fulfilment of the Requirements for the Degree of Doctor of Philosophy in Medical Physics at the University of Canterbury, Christchurch, New Zealand, University of Canterbury. Ph. D Thesis.
- Scallan, E., R. M. Hoekstra, F. J. Angulo, R. V. Tauxe, M. A. Widdowson, S. L. Roy, J. L. Jones and P. Griffin** (2011). "Foodborne Illness Acquired in the United States_Major Pathogens." *Emerging Infectious Diseases* **17**(1): 7.
- Schenk, P., S. Thomas-Hall, E. Stephens, U. Marx, J. Mussnug, C. Posten, O. Kruse and B. Hankamer** (2008). "Second Generation Biofuels: High-Efficiency Microalgae for Biodiesel Production." *BioEnergy Research* **1**(1): 20-43.
- Schiller, J.** (2009). 21st Century Cosmology. pp. 105-110. Booksurge, USA.
- Schloter, M., B. Abmus and A. Hartmann** (1995). "The use of immunological methods to detect and identify bacteria in the environment." *Biotechnology Advances* **13**(1): 75-90.
- Sezonov, G., D. Joseleau-Petit and R. D'Ari** (2007). "Escherichia coli Physiology in Luria-Bertani Broth." *J. Bacteriol* **189**(23): 8746-8749.
- Shahzad, A., G. Kohler, M. Knapp, E. Gaubitzer, M. Puchinger and M. Edetsberger** (2009). "Emerging applications of fluorescence spectroscopy in medical microbiology field." *Journal of Translational Medicine* **7**(1): 99.
- Shamsoddini, A., J. C. Trinder and R. Turner** (2013). "Pine plantation structure mapping using WorldView-2 multispectral image." *International Journal of Remote Sensing* **34**(11): 3986-4007.

- Sikorska, E., I. V. Khmelinskii, M. Sikorski, F. Caponio, M. T. Bilancia, A. Pasqualone and T. Gomes** (2008). "Fluorescence spectroscopy in monitoring of extra virgin olive oil during storage." *International Journal of Food Science & Technology* **43**(1): 52-61.
- Sivaprakasam, V., A. Huston, C. Scotto and J. Eversole** (2004). "Multiple UV wavelength excitation and fluorescence of bioaerosols." *Opt. Express* **12**(19): 4457-4466.
- Solarox_Manual** (2011). "Falko Glanert. SOLAROX (KSQ350, KSQ700, KSQ1000, KS1400). Winger Electronics GmbH & Co. KG. www.led1.de."
- Sousa, C., P. Teixeira and R. Oliveira** (2008). "Influence of surface properties on the adhesion of *Staphylococcus epidermidis* to acrylic and silicone." *International Journal of Biomaterials* **2009**(Article ID 718017): 9 pages.
- Spetlikova, E., H. Shejbalova, P. Lukws and M. Clupek** (2010). "Role of UV Radiation, Solution Conductivity and Pulse Repetition Frequency in the Bactericidal Effects During Pulse Corona Discharges." *WDS'10 Proceedings of Contributed Papers, Part II*, 96–100.
- Stanghellini, M. E. and S. L. Rasmussen** (1989). "Root print: a technique for the determination of the in situ spatial distribution of bacteria on the rhizoplane of field-grown plants." *Phytopathology* **79**(10): p. 1131-1134.
- Strasser, R. J., A. Srivastava, M. Tsimilli-Michael, M. Yunus, U. Pathre and P. Mohanty** (2000). The fluorescence transient as a tool to characterize and screen photosynthetic samples. *Probing Photosynthesis: Mechanism, Regulation and Adaptation*. London, Taylor and Francis: 445-483.
- Suchar, V. A. and P. Chigbu** (2006). "The effects of algae species and densities on the population growth of the marine rotifer, *Colurella dicentra*." *Journal of Experimental Marine Biology and Ecology* **337**(1): 96-102.
- Suggett, D. J., O. Práčil, M. A. Borowitzka, J. Ā. MasojĀdek, A. Vonshak and G. Torzillo** (2010). Chlorophyll Fluorescence Applications in Microalgal Mass Cultures. *Chlorophyll a Fluorescence in Aquatic Sciences: Methods and Applications*, Springer Netherlands. **4**: 277-292.
- Sutherland, K.** (2008). *Filters and Filtration Handbook*, Elsevier Science. 5th edition
- Sutton, S.** (2006). *Pharmaceutical Microbiology Forum Newsletter*, SelectScience Ltd, UK.
- Sweetman, L. J., L. J. Alcock, J. D. McArthur, E. M. Stewart, G. Triani, M. in het Panhuis and S. F. Ralph** (2013). "Bacterial Filtration Using Carbon Nanotube/Antibiotic Buckypaper Membranes." *Journal of Nanomaterials* **2013**: 11.
- Talebzadeh, N., P. R. Morrison and M. P. Fried** (1994). "Comparative cell targeting in vitro using the CO₂ laser." *Lasers in Surgery and Medicine* **14**(2): 164-167.
- Tam, S. C., Y. M. Noor, L. E. N. Lim, S. Jana, L. J. Yang, M. W. S. Lau and C. Y. Yeo** (1993). "Marking of leadless chip carriers with a pulsed Nd : YAG laser." *ARCHIVE: Proceedings of the Institution of Mechanical Engineers, Part B: Journal of Engineering Manufacture 1989-1996 (vols 203-210)* **207**(32): 179-192.

Tang, H., T. Cao, X. Liang, A. Wang, O. S. Salley, J. McAllister and K. Y. SimonNg (2009). "Influence of silicone surface roughness and hydrophobicity on adhesion and colonization of *Staphylococcus epidermidis*." *Journal of Biomedical Materials Research Part A* **88A**(2): 454-463.

TBH (Company, Straubenhardt, Germany 2013). "Extraction and Filtration Technology: Particle sizes." from <http://www.tbh-online.com/needtoknow/particlesizes.html>.

Thomas, T. R. (1999). *Rough surfaces*, Imperial College Press.

Tide, C., S. R. Harkin, G. G. Geesey, P. J. Bremer and W. Scholz (1999). "The influence of welding procedures on bacterial colonization of stainless steel weldments." *Journal of Food Engineering* **42**(2): 85-96.

Torzillo, G., P. Accolla, E. Pinzani and J. i. Masojidek (1996). "In situ monitoring of chlorophyll fluorescence to assess the synergistic effect of low temperature and high irradiance stresses in *Spirulina* cultures grown outdoors in photobioreactors." *Journal of Applied Phycology* **8**(4-5): 283-291.

Tsen, S.-W., T. Wu, J. Kiang and K.-T. Tsen (2012). "Prospects for a novel ultrashort pulsed laser technology for pathogen inactivation." *Journal of Biomedical Science* **19**(1): 62.

Turnbull, P. C. (1996). *Medical Microbiology*, Chapter 15: *Bacillus*. Baron S., editor, The University of Texas Medical Branch at Galveston, 4th edition

Udart, M., K. Stock, R. Graser and R. Hibst (2011). "Inactivation of bacteria by high-power 940nm laser irradiation." *Medical Laser Application* **26**(4): 166-171.

Uduman, N., Y. Qi, M. K. Danquah, G. M. Forde and A. Hoadley (2010). "Dewatering of microalgal cultures: A major bottleneck to algae-based fuels." *Journal of Renewable and Sustainable Energy* **2**(1): 012701-15.

Uduman, N., Y. Qi, M. K. Danquah and A. F. A. Hoadley (2010). "Marine microalgae flocculation and focused beam reflectance measurement." *Chemical Engineering Journal* **162**(3): 935-940.

Valette, S., P. Steyer, L. Richard, B. Forest, C. Donnet and E. Audouard (2006). "Influence of femtosecond laser marking on the corrosion resistance of stainless steels." *Applied Surface Science* **252**(13): 4696-4701.

Vermeulen, N., W. Keeler, K. Nandakumar and K. Leung (2008). "The bactericidal effect of ultraviolet and visible light on *Escherichia coli*." *Biotechnology and Bioengineering* **99**(3): 550-556.

Verran, J. and R. D. Boyd (2001). "The relationship between substratum surface roughness and microbiological and organic soiling: A review." *Biofouling* **17**(1): 59-71.

Verran, J., A. Packer, P. Kelly and K. A. Whitehead (2010). "The retention of bacteria on hygienic surfaces presenting scratches of microbial dimensions." *Letters in Applied Microbiology* **50**(3): 258-263.

- Vijayaraghavan, K. and K. Hemanathan** (2009). "Biodiesel Production from Freshwater Algae." *Energy & Fuels* **23**(11): 5448-5453.
- Vonshak, A., G. Torzillo and L. Tomaseli** (1994). "Use of chlorophyll fluorescence to estimate the effect of photoinhibition in outdoor cultures of *Spirulina platensis*." *Journal of Applied Phycology* **6**(1): 31-34.
- Vorburger, T. V. and J. Raja** (1990). "Surface finish metrology tutorial." *National institute of standards and technology*.
- Wang, B., Y. Li, N. Wu and C. Lan** (2008). "CO₂ bio-mitigation using microalgae." *Applied Microbiology and Biotechnology* **79**(5): 707-718.
- Ward, G. D., I. A. Watson, D. E. S. Stewart-Tull, A. C. Wardlaw and C. R. Chatwin** (1996). "Inactivation of bacteria and yeasts on agar surfaces with high power Nd: YAG laser light." *Letters in Applied Microbiology* **23**(3): 136-140.
- Warriner, K., G. Rysstad, A. Murden, P. Rumsby, D. Thomas and W. M. Waites** (2000). "Inactivation of *Bacillus subtilis* spores on packaging surfaces by u.v. excimer laser irradiation." *Journal of Applied Microbiology* **88**(4): 678-685.
- Watson, I. A.** (2007). Proposal submitted to Nvirocleantech.
- Watson, I. A., G. D. Ward, R. K. Wang, J. H. Sharp, D. M. Budgett, D. E. Stewart-Tull, A. C. Wardlaw and C. R. Chatwin** (1996). "Comparative bactericidal activities of lasers operating at seven different wavelengths." *Journal of Biomedical Optics* **1**(4): 466-472.
- Webber, J. S., A. G. Czuhanych and L. J. Carhart** (2007). "Performance of Membrane Filters Used for TEM Analysis of Asbestos." *Journal of Occupational and Environmental Hygiene* **4**(10): 780-789.
- Weibel, D. B., A. Lee, M. Mayer, S. F. Brady, D. Bruzewicz, J. Yang, W. R. DiLuzio, J. Clardy and G. M. Whitesides** (2005). "Bacterial Printing Press that Regenerates Its Ink: Contact-Printing Bacteria Using Hydrogel Stamps." *Langmuir* **21**(14): 6436-6442.
- Wengraitis, S., P. McCubbin, M. M. Wade, T. D. Biggs, S. Hall, L. I. Williams and A. W. Zulich** (2013). "Pulsed UV-C Disinfection of *Escherichia coli* With Light-Emitting Diodes, Emitted at Various Repetition Rates and Duty Cycles." *Photochemistry and Photobiology* **89**(1): 127-131.
- Whatman** (Manual 2010). Membrane filtration guidance manual. United States Environmental Protection Agency.
- Whitehead, K. A., J. Colligon and J. Verran** (2005). "Retention of microbial cells in substratum surface features of micrometer and sub-micrometer dimensions." *Colloids and Surfaces B: Biointerfaces* **41**(2-3): 129-138.
- Whitehead, K. A. and J. Verran** (2006). "The Effect of Surface Topography on the Retention of Microorganisms." *Food and Bioproducts Processing* **84**(4): 253-259.

Wilks, M., T. Vollmer, K. Kleesiek and J. Dreier (2013). Detection of Bacterial Contamination in Platelet Concentrates Using Flow Cytometry and Real-Time PCR Methods. *PCR Detection of Microbial Pathogens*, Humana Press. **943**: 91-103.

Wolochow, H. (1958). "The membrane filter technique for estimating numbers of viable bacteria: some observed limitations with certain species." *Applied microbiology* **6**(3): 201-206.

Xuewu, L. and B. Kloareg (1992). "Explant exenisation for tissue culture in marine macroalgae." *Chinese Journal of Oceanology and Limnology* **10**(3): 268-275.

Yang, C., Q. Hua and K. Shimizu (2000). "Energetics and carbon metabolism during growth of microalgal cells under photoautotrophic, mixotrophic and cyclic light-autotrophic/dark-heterotrophic conditions." *Biochemical Engineering Journal* **6**(2): 87-102.

Yasa, E. and J. Kruth (2009). An Experimental study of Process Parameters in Laser Marking. 5th International Conference and Exhibition on Design and Production of Machines and Dies/Molds

Yongho, S. and J. Wonho (2008). "Atomic force microscopy and spectroscopy." *Reports on Progress in Physics* **71**(1): 016101.

Yue, W. and C. Bai (2013). "Improved Design of Automatic Luminometer for Total Bacteria Number Detection Based on ATP Bioluminescence." *Journal of Food Safety* **33**(1): 1-7.

Yunker, P. J., T. Still, M. A. Lohr and A. G. Yodh (2011). "Suppression of the coffee-ring effect by shape-dependent capillary interactions." *Nature* **476**(7360): 308-311.

Zacharias, M. (2012). Ecophysiological studies of selected macro- and microalgae: production of organic compounds and climate change interactions. Botany and Plant Science. School of Natural Sciences. NUI Galway. Ireland. **PhD. Thesis**.

Zhao, C., M. Burchardt, T. Brinkhoff, C. Beardsley, M. Simon and G. Wittstock (2010). "Microfabrication of Patterns of Adherent Marine Bacterium *Phaeobacter inhibens* Using Soft Lithography and Scanning Probe Lithography." *Langmuir* **26**(11): 8641-8647.